

ADVERTIMENT. L'accés als continguts d'aquesta tesi queda condicionat a l'acceptació de les condicions d'ús establertes per la següent llicència Creative Commons:  <https://creativecommons.org/licenses/?lang=ca>

ADVERTENCIA. El acceso a los contenidos de esta tesis queda condicionado a la aceptación de las condiciones de uso establecidas por la siguiente licencia Creative Commons:  <https://creativecommons.org/licenses/?lang=es>

WARNING. The access to the contents of this doctoral thesis it is limited to the acceptance of the use conditions set by the following Creative Commons license:  <https://creativecommons.org/licenses/?lang=en>

PhD Thesis

Alpha-synuclein and neuromelanin interplay: unravelling its role in the pathophysiology of Parkinson's disease

Alba Nicolau Vera

**Director: Dr. Miquel Vila Bover
Tutor: Dr. Joan Xavier Comella Carnicé**

**PhD in Neurosciences
Institut de Neurociències
Universitat Autònoma de Barcelona**

Barcelona, 2025

“Above all, don’t fear difficult moments. The best comes from them.”

- Rita Levi-Montalcini

CONTENTS

LIST OF CONTENTS

INTRODUCTION	2
1. Parkinson's disease	2
1.1 Brief history	2
1.2 Physiopathology.....	4
1.2.1 DA depletion.....	4
1.2.2 Lewy pathology.....	5
1.2.3 Neuromelanin.....	7
1.2.4 Neuroinflammation.....	7
1.2.5 Oxidative stress	7
1.3 Epidemiology.....	8
1.4 Symptomatology.....	8
1.5 Etiology	9
1.5.1 Genetic factors.....	9
1.5.2 Non-genetic factors	10
1.6 Biomarkers.....	11
1.6.1 α Syn	11
1.6.2 DOPA-decarboxylase	13
1.6.3 Mitochondrial markers.....	13
1.6.4 Neuroinflammatory markers.....	13
1.7 Current pharmacological treatments	13
1.8 PD experimental animal models	14
1.8.1 Neurotoxic models	14
1.8.2 Genetic models.....	15
1.8.2.1 Autosomal dominant gene models.....	15
1.8.2.2 Autosomal recessive gene models	16
2. Neuromelanin	17
2.1 Origin and distribution	17
2.2 Synthesis of melanin and NM.....	18
2.3 Function.....	20
2.4 NM and its relevance to PD hallmarks	21
2.4.1 NM and aging	21
2.4.2 NM and Lewy pathology	23
2.4.3 NM and neuroinflammation.....	23
2.4.4 Selective vulnerability of NM-containing neurons in PD	24
2.4.5 Altered DA metabolism	25
2.5 Novel NM-producing PD models	26
2.5.1 TYR-overexpressing NM-producing rats.....	26
2.5.2 SH-SY5Y neuroblastoma cells inducible for TYR expression: TR5TY6 cells	28

2.5.3 TYR transgenic mouse model.....	28
2.6 Therapeutic modulation of NM levels	30
2.6.1 TFEB.....	30
2.6.2 VMAT2	31
3. Alpha-synuclein.....	32
3.1 Discovery.....	32
3.2 Structure.....	32
3.3 Distribution	33
3.3.1 Tissue expression	33
3.3.2 Cellular localization	33
3.4 Physiological functions	33
3.4.1 Synaptic roles	33
3.4.1.1 Regulation of synaptic vesicle pooling.....	34
3.4.1.2 Neurotransmission	34
3.4.1.3 Membrane curvature and vesicle fusion.....	35
3.4.1.4 Regulation of DA release	35
3.4.2 Nuclear roles	35
4. Alpha-synuclein relevance to Parkinson's disease pathogenesis	36
4.1 Pathological conformations	36
4.2 Toxic functions	37
4.2.1 Defects in synaptic vesicle cycle.....	37
4.2.2 Defects in the nucleus	38
4.3 Post-translational modifications	38
4.3.1 Phosphorylation	39
4.3.2 Ubiquitination	40
4.3.3 Nitration and oxidation.....	40
4.3.4 Acetylation	40
4.3.5 Glycation	41
4.3.6 Truncation.....	41
4.4 α Syn levels and species in PD pathology	41
4.4.1 α Syn and aging	41
4.4.2 α Syn burden and its implications for PD.....	41
4.4.3 α Syn levels in biospecimens	42
4.4.3.1 Brain.....	42
4.4.3.2 CSF	43
4.4.3.3 Blood	43
4.4.3.4 Skin	43
4.5 α Syn prion-like properties	44
4.5.1 Braak's hypothesis and α Syn-based PD staging.....	44
4.5.2 Cell-to-cell transmission of α Syn	45

4.5.2.1 Prion-like spreading.....	45
4.5.2.2 Mechanisms of release and uptake.....	46
4.5.3 α Syn strain variability and its influence on pathogenic spread.....	48
4.6 Impaired α Syn degradation in PD	48
4.7 Summary of the α Syn pathological roles	49
4.8 α Syn as a therapeutic target.....	50
4.9 α Syn-based PD rodent models	51
4.9.1 Viral vector-mediated α Syn overexpression	51
4.9.2 Transgenic-mediated α Syn overexpression	52
4.9.3 Injection of α Syn PFFs and pathological extracts.....	52
5. Alpha-synuclein and neuromelanin interactions and their contribution to Parkinson's disease pathology	53
5.1. α Syn redistribution to NM granules.....	53
5.2 NM accumulation drives endogenous α Synucleinopathy	54
5.3 α Syn is dispensable for NM-linked PD pathology.....	55
5.4 α Syn, NM and oxidative stress.....	56
HYPOTHESES AND OBJECTIVES	59
Specific aim 1: To evaluate the contribution of α Syn to NM-linked PD pathology	59
Rationale.....	59
Hypothesis.....	59
Objectives	59
Specific aim 2: To evaluate the impact of NM-mediated oxidative stress on α Syn pathology and spreading	60
Rationale.....	60
Hypothesis.....	60
Objectives	60
MATERIALS AND METHODS	62
1. Animals	62
1.1 Rats	62
1.2 Mice.....	62
1.2.1 tgNM mouse colony.....	62
1.2.2 Genotyping.....	62
2. Viral vector production.....	63
3. PD patient-derived α SYN PFFs	63
4. Stereotaxic surgery	65
4.1 Rats	65
4.2 Mice.....	65
5. Histological procedures.....	65
5.1 Brain processing	65
5.1.1 Intracardiac perfusion	65

5.1.2 Tissue fixation	66
5.1.3 Brain sectioning.....	66
5.2 Immunohistochemistry	66
5.2.1 Paraffin-embedded brain slices.....	66
5.2.2 Free-floating brain cryosections	67
5.2.3 Slide mounting	67
5.3 Immunofluorescence	68
5.4 Haematoxylin-Eosin	68
5.5 Proximity-ligation assay.....	68
6. GFP and α SYN-GFP TR5TY6 cell lines	69
6.1 Lentiviral particles	69
6.2 GFP and α SYN-GFP TR5TY6 cell lines generation	69
6.3 GFP and α SYN-GFP TR5TY6 experiments	70
6.4 Western blot	71
6.5 Immunocytochemistry.....	71
6.6 Real-Time quantitative PCR (qPCR).....	71
6.7 TYR activity assay.....	72
7. Image analysis.....	73
7.1 Cell counting.....	73
7.1.1 Artificial intelligence-based quantifications.....	73
7.1.2 Manual quantification.....	76
7.2 Intracellular NM quantification.....	76
7.2.1 H&E-stained sections	76
7.2.2 Bright-field images.....	76
7.2.3 Confocal images.....	76
7.3 Extracellular NM quantification.....	77
7.3.1 H&E-stained sections	77
7.3.2 TH-immunostained cryosections.....	77
7.4 Quantification of neuropathological inclusions	77
7.5 Quantification of neuroinflammation parameters	77
7.6 Optical densitometry	77
7.7 p α Syn pathology quantification and brain distribution.....	78
7.7.1 Early (3.5 mpi) time-point.....	78
7.7.2 Late (8 mpi) time-point.....	80
8. Behavioural tests	82
8.1 Cylinder test.....	82
8.2 Beam traversal test.....	82
8.3 Olfaction test.....	82
8.4 Fecal pellet output test.....	83
8.5 Step down test	83

8.6 Tail suspension test.....	83
9. Chromatographic determination of dopamine metabolites.....	83
9.1 Brain collection.....	83
9.2 Calibration curves and sample preparation	83
9.3 UPLC-MS/MS analysis	84
10. Statistical analyses	85
11. Buffers and antibodies.....	86
RESULTS	90
1. Chapter I. Effects of α SYN overexpression on NM-associated PD pathology.....	90
1.1 Experimental design	90
1.2 Enhanced intracellular NM levels in α SYN-expressing NM-producing animals.....	91
1.3. Increased α Syn pathology in α SYN-expressing NM-producing animals.....	92
1.4. Enhanced nigrostriatal degeneration in α SYN-overexpressing NM-producing animals.....	95
1.5. Impaired DA vesicular uptake in α SYN-overexpressing NM-producing animals	98
1.6 Sustained TYR expression in α SYN-overexpressing NM-producing animals.....	99
1.7 Development of a novel α SYN-overexpressing NM-producing <i>in vitro</i> model	100
1.8. Increased intracellular NM levels in α SYN-overexpressing NM-producing cells.....	101
1.9. Increased TYR activity and expression levels in α SYN-overexpressing NM-producing cells	102
2. Chapter II. Impact of NM-associated pathology on α Syn aggregation and propagation in PD	104
2.1 Experimental design	104
2.2 Local accumulation of endogenous p α Syn in the STR of α SYN PFF-injected wt and tgNM mice .	105
2.3 Widespread accumulation of endogenous p α Syn across interconnected rostral and caudal regions in α SYN PFF-injected wt and tgNM mice	107
2.4 Effects of NM-induced oxidative environment on α SYN PFF-induced p α Syn pathology	108
2.4.1. α SYN PFF-injected wt and tgNM mice at 3,5 mpi	108
2.4.2. α SYN PFF-injected wt and tgNM mice at 8mpi.....	112
2.5 Nigrostriatal integrity in α SYN PFF-injected wt and tgNM mice	116
2.6 Intracellular NM levels in SNpc neurons from α SYN PFF-injected tgNM mice	118
2.7 Lack of behavioural alterations in α SYN PFF-injected wt and tgNM mice.....	119
2.7.1. Motor tests	119
2.7.2 Non-motor tests.....	120
DISCUSSION.....	125
1. Chapter I. Effects of α SYN overexpression on NM-associated PD pathology.....	127
1.1 NM levels	127
1.2 α Syn levels and species.....	127
1.3 Neuropathological inclusions	128
1.4 Nigrostriatal degeneration.....	129
1.5 Molecular mechanisms underlying α Syn and NM interplay	130
2. Chapter II. Impact of NM-associated pathology on α Syn aggregation and propagation in PD	137
2.1 Properties and origins of the injected material	137

2.2 α Syn pathology and spreading	138
2.3 α Synucleinopathy and neurodegeneration	139
2.4 Behavioural phenotypes.....	140
3. Contributions of this thesis to PD research	143
CONCLUSIONS.....	146
1. Chapter I. Effects of α SYN overexpression on NM-associated PD pathology.....	146
2. Chapter II. Impact of NM-associated pathology on α Syn aggregation and propagation in PD	146
REFERENCES	148

LIST OF TABLES

Table 1. Clinical history of PD341 patient.....	63
Table 2. RT-qPCR genes.....	72
Table 3. MRM acquisition settings.....	85
Table 4. Recipes for the buffers used in this study.....	86
Table 5. Overview of the primary antibodies used in immunohistochemistry (IHC), immunofluorescence (IF), immunocytochemistry (ICC) and WB.....	87
Table 6. Overview of the secondary antibodies used in immunohistochemistry (IHC), immunofluorescence (IF), immunocytochemistry (ICC) and WB.....	88

LIST OF FIGURES

Figure 1. Key findings in the history of PD.....	3
Figure 2. Neuropathology of PD.....	4
Figure 3. Lewy pathology in PD.....	5
Figure 4. α Syn aggregation gives rise to LB formation.....	6
Figure 5. New model of LB formation based on crowded organelles and lipid membranes.....	7
Figure 6. Clinical symptoms associated with PD progression.....	9
Figure 7. Summary of genetic variants in PD grouped by allele frequency and associated risk.....	10
Figure 8. Schematic representation of the α Syn SAA.....	12
Figure 9. α Syn SAA kinetic curves in positive and negative samples.....	12
Figure 10. Cytotoxic effects driving neurodegeneration in neurotoxic PD models.....	15
Figure 11. Pathological effects identified in genetic PD models.....	17
Figure 12. Human midbrain showing dark pigmentation of the SN.....	18
Figure 13. Melanin and NM biosynthesis.....	19
Figure 14. Dual roles of NM.....	21
Figure 15. Progressive accumulation of NM in the human brain.....	22
Figure 16. NM developmental stages.....	23
Figure 17. LBs surrounded by NM granules.....	23
Figure 18. Selective vulnerability of neuronal populations in PD.....	25
Figure 19. Age-dependent human-like NM production in rat SNpc triggers PD pathology.....	27
Figure 20. NM production in TR5TY6 cells upon TYR induction.....	28
Figure 21. The tgNM mouse exhibits bilateral NM accumulation across all catecholaminergic brain regions.....	29
Figure 22. Progressive multisystem PD-like features in tgNM mice.....	30
Figure 23. Therapeutic modulation of NM levels.....	31
Figure 24. α Syn structure.....	32
Figure 25. α Syn physiological functions at synapses.....	34
Figure 26. α Syn physiological and pathological conformations.....	36
Figure 27. Effects of pathological α Syn on the synaptic vesicle cycle.....	37
Figure 28. Summary of currently known PTMs of α Syn.....	39
Figure 29. Summary of total, phosphorylated, oligomeric and aggregated α Syn levels in PD compared to healthy controls (HC) observed in brain, CSF, blood and skin samples.....	44
Figure 30. Braak's PD staging.....	45
Figure 31. Mechanisms of α Syn transfer between neurons.....	47
Figure 32. Impaired α Syn degradation in PD.....	49
Figure 33. Pathological roles of α Syn.....	50
Figure 34. Principal alterations in α Syn-based PD rodent models.....	53
Figure 35. α Syn redistribution to NM granules.....	54
Figure 36. NM accumulation drives PD-related inclusion formation and α Synucleinopathy in TYR-injected rats, TYR-injected non-human primates, and tgNM mice.....	55

Figure 37. α Syn is dispensable for NM-associated PD pathology.....	56
Figure 38. Oxidative stress in PD..	57
Figure 39. PD-derived amplified α SYN PFFs characterisation..	64
Figure 40. Workflow of GFP and α SYN-GFP TR5TY6 experiments.....	70
Figure 41. Four TH/NM object categories recognized by the AI-assisted algorithm..	74
Figure 42. Main steps of AI-based cell counting.....	75
Figure 43. Workflow for p α Syn pathology quantification and distribution in PFF-injected wt and tgNM mice at 3.5 mpi.....	79
Figure 44. p α Syn pathological severity score.....	80
Figure 45. Workflow for p α Syn pathology quantification and distribution in PFF-injected wt and tgNM mice at 8 mpi.....	81
Figure 46. Overexpression of α SYN and/or TYR in the nigrostriatal pathway of rats.....	90
Figure 47. Intracellular NM levels in TYR- and α SYN+TYR-injected rats..	91
Figure 48. Total and phosphorylated α Syn expression in α SYN-expressing NM-producing rats.....	93
Figure 49. α Syn oligomerization in α SYN-expressing NM-producing rats.....	93
Figure 50. Neuropathological PD-like inclusions in α SYN-expressing NM-producing rats.....	94
Figure 51. Nigrostriatal degeneration in α SYN-expressing NM-producing rats.....	97
Figure 52. Neuronophagia associated with cell death in α SYN-expressing NM-producing rats..	97
Figure 53. DA synaptic vesicular system in α SYN-expressing NM-producing rats..	99
Figure 54. TYR expression in α SYN-expressing NM-producing rats.....	100
Figure 55. α SYN overexpression in a TYR-inducible TR5TY6 neuroblastoma cell line.....	101
Figure 56. Intracellular NM levels in α SYN-overexpressing NM-producing cells..	102
Figure 57. TYR expression and activity in α SYN-overexpressing NM-producing cells.....	103
Figure 58. Experimental design of PD-derived α SYN PFFs injections into wt and tgNM animals..	105
Figure 59. p α Syn and α SYN immunolabeling in the STR of control- and PFF-injected wt and tgNM mice at 3.5 (left) and 8 mpi (right).....	106
Figure 60. p α Syn immunolabeling in the PFC and SN of PFF-injected wt and tgNM mice at 3.5 (left) and 8 mpi (right).....	107
Figure 61. Quantification of the extent and type of p α Syn pathology in PFF-injected wt and tgNM mice at 3.5 mpi.....	108
Figure 62. Quantification of total p α Syn pathology throughout the mouse brain in PFF-injected wt and tgNM mice at 3.5 mpi, from anatomical level 1 (a) to 12 (l)..	110
Figure 63. Anatomical distribution of p α Syn pathology in PFF-injected wt and tgNM at 3.5 mpi..	111
Figure 64. Quantification of total p α Syn pathology throughout the mouse brain in PFF-injected wt and tgNM mice at 8 mpi, from anatomical level 1 (a) to 12 (l)..	113
Figure 65. Anatomical distribution of p α Syn pathology in PFF-injected wt and tgNM at 8 mpi..	115
Figure 66. Nigrostriatal integrity in PFF-injected wt and tgNM mice.....	118
Figure 67. Intracellular NM levels in BSA- and PFF-injected tgNM mice..	118
Figure 68. Motor function in BSA- and PFF-injected wt and tgNM mice.....	120
Figure 69. Fecal output and olfactory function in BSA- and PFF-injected wt and tgNM mice.....	122
Figure 70. Aversive memory function in BSA- and PFF-injected wt and tgNM mice.....	122
Figure 71. Depressive-like behaviour in BSA- and PFF-injected wt and tgNM mice..	123

Figure 72. Histopathological features associated with α SYN+TYR co-injection.....	130
Figure 73. DA synthesis, vesicular uptake, metabolism and oxidation in a schematic human DA neuron..	131
Figure 74. TYR overexpression in rats results in NM production..	132
Figure 75. α SYN overexpression drives DA leakage and enhances NM build-up.....	134
Figure 76. α SYN overexpression promotes TYR expression and drives DA leakage, thereby increasing NM production..	136
Figure 77. Histopathological features associated with α SYN-PFF-injected tgNM versus wt mice..	142

LIST OF ABBREVIATIONS

6-OHDA	6-hydroxydopamine
AADC	DOPA-decarboxylase
AAV	Adeno-associated viral vector
ABC	Avidin-biotin-peroxidase complex
AI	Artificial intelligence
ALDH	Aldehyde dehydrogenase
BBB	Blood-brain barrier
BF	Bright-field
BSA	Bovine serum albumin
cDNA	Complementary DNA
CNS	Central nervous system
CSF	Cerebrospinal fluid
CT	Cycle threshold
d	Days
DA	Dopamine or dopaminergic
DA-d4	Dopamine-d4 hydrochloride
DAT	Dopamine transporter
DCT	DOPAchrome tautomerase
DHI	5,6-dihydroxyindole
DHICA	5,6-dihydroxyindole-2-carboxylic acid
DI	Discrimination index
DJ-1	Protein deglycase DJ-1
DLB	Dementia with Lewy bodies
DMNX	Dorsal motor nucleus of the vagus
DNA	Deoxyribonucleic acid
DOPA	Dihydroxyphenylalanine
DOPAC	3,4-dihydroxyphenylacetic acid
DOPAL	3,4-dihydroxyphenylacetaldehyde
DOX	Doxycycline
e.g.	exempli gratia (example given)
FA	Formic acid

FC	Fold change
FF	Free-floating
g	g-force
GFP	Green fluorescent protein
h	hours
H&E	Haematoxylin and eosin
i.e.	id est (that is)
ICC	Immunocytochemistry
IF	Immunofluorescence
IHC	Immunohistochemistry
IS	Internal standard
KO	Knockout
LB	Lewy body
LC	Locus coeruleus
L-DOPA	L-3,4-dihydroxyphenylalanine or Levodopa
LOD	Limit of detection
LOQ	Limit of quantification
LRRK2	Leucine-rich repeat kinase 2
m	Months
MAO	Monoamine oxidase
MB	Marinesco body
Min	Minutes
mpi	months post-injection
MPP+	1-methyl-4-phenylpyridinium
MPTP	1-methyl-4-phenyl-1,2,3,6-tetrahydropyridine
MRI	Magnetic resonance imaging
MSA	Multiple system atrophy
NGS	Normal goat serum
NM	Neuromelanin
Nurr1	Nuclear receptor related 1
°C	Degree Celsius
OD	Optical densitometry

PB	Phosphate buffer
PBS	Phosphate buffer saline
PD	Parkinson's disease
PFC	Prefrontal cortex
PFFs	Pre-formed fibrils
PINK1	PTEN induced kinase 1
PLA	Proximity ligation assay
PMCA	Protein misfolding cyclic amplification
PRKN	E3-ubiquitin-protein ligase Parkin
PTM	Post-translational modification
p α Syn	Phosphorylated-S129-alpha-synuclein
RA	Retinoic acid
rAAV	Recombinant adeno-associated viral vector
RNA	Ribonucleic acid
ROS	Reactive oxygen species
RT	Room temperature
RT-qPCR	Real-time quantitative PCR
RT-QuIC	Real-time Quaking-induced conversion
s	Seconds
SAA	Seed amplification assay
SEM	Standard error of the mean
SN	Substantia nigra
SNARE	Soluble N-ethylmaleimide-sensitive factor attachment protein receptor
SNpc	Substantia nigra pars compacta
SNpr	Substantia nigra pars reticulata
STR	Striatum
TBS	Tris buffered saline
TFEB	Transcription factor EB
Tg	Transgenic
TH	Tyrosine hydroxylase
ThT	Thioflavin
TPA	12-O-tetradecanoylphorbol-13-acetate

TYR	Human tyrosinase
Tyr	Tyrosinase
TYRP1	Tyrosinase-related protein-1
TYRP2	Tyrosinase-related protein-2
UAB	Universitat Autònoma de Barcelona
UPLC	Ultra-Performance Liquid Chromatography–Tandem Mass Spectrometry
UPS	Ubiquitin-proteasome system
VAMP2	Vesicle-associated membrane protein 2
VMAT2	Vesicular monoamine transporter 2
vMB	Ventral midbrain
VTa	Ventral tegmental area
w	Weeks or weight
WB	Western blot
wt	Wild-type
α Syn	Alpha-synuclein
α SYN	Human alpha-synuclein
λ	Wavelength

ABSTRACT

ABSTRACT

Parkinson's disease is neuropathologically characterised by the preferential degeneration of neuromelanin-containing neurons, particularly those located in the substantia nigra, and the presence of alpha-synuclein-containing Lewy bodies within affected neurons. In contrast to humans, neuromelanin does not naturally accumulate in most animals, including rodents, which has hindered the exploration of this brain pigment's role and its interplay with alpha-synuclein in the disease process. To overcome this limitation, our group has recently developed the first experimental *in vivo* rodent models exhibiting age-dependent human-like neuromelanin production and accumulation within neurons vulnerable to Parkinson's disease. This was achieved through the overexpression of tyrosinase, a key enzyme involved in melanogenesis, leading to neuromelanin levels comparable to those observed in elderly humans. In these models, age-related intracellular neuromelanin accumulation compromised neuronal function when levels exceeded a certain pathogenic threshold, triggering key features of Parkinson's disease. Notably, this pathogenic threshold was also observed in *post-mortem* brains of Parkinson's disease patients. Currently, the factors that may accelerate neuromelanin accumulation beyond this threshold in Parkinson's disease patients remain unknown.

In this thesis, we assessed the role of increased alpha-synuclein levels on neuromelanin-associated Parkinson's disease pathology. Remarkably, increased alpha-synuclein levels, as seen in Parkinson's disease patients, accelerated neuromelanin build-up and exacerbated neuromelanin-associated Parkinson's disease pathology. Molecular studies revealed that alpha-synuclein overexpression promotes neuromelanin accumulation by: (i) permeabilizing dopamine-containing synaptic vesicles, causing the leakage of vesicular dopamine into the cytosol where it can oxidise into neuromelanin and (ii) regulating tyrosinase expression. Furthermore, it was investigated whether the oxidative environment associated with neuromelanin production can, in turn, influence alpha-synuclein pathology and spreading induced by patient-derived pre-formed fibrils. Our findings showed that alpha-synuclein pathology and spreading were not significantly enhanced in neuromelanin-producing animals.

Altogether, this thesis provides novel insights into Parkinson's disease pathophysiology, highlighting a complex pathological interplay between alpha-synuclein and neuromelanin. These findings establish a path for a deeper understanding of the molecular mechanisms underlying the disease and may offer new potential opportunities for the development of therapeutic strategies.

INTRODUCTION

INTRODUCTION

1. Parkinson's disease

1.1 Brief history

Parkinson's disease (PD) was first described over two centuries ago, in 1817, by the physician James Parkinson in his work *An Essay on the Shaking Palsy*¹ (Figure 1). He defined the condition as a nervous disorder marked by involuntary trembling of the limbs at rest, reduced muscular strength, and a flexed posture. Parkinson also noted that patients frequently displayed a propulsive, hurried gait, referred to as festination. In 1872, Jean-Martin Charcot advanced our understanding of the disease when he identified bradykinesia as a key feature of PD and classified the condition into two main forms: the tremorous type and the rigid/akinetic type²⁻⁴. Charcot was also the first to propose naming the illness "Parkinson's disease" in recognition of James Parkinson's contributions. Charcot's investigations into the physiopathology of PD were continued by his students, notably Georges Marinesco and Edouard Brissaud. In the 1890s, Marinesco, in collaboration with pathologist Paul Oscar Blocq, discovered that a tuberculoma affecting a brain region named the substantia nigra (SN) caused parkinsonism symptoms in a patient suffering from tuberculosis^{5,6}. Later, Brissaud proposed that the SN played an essential role in regulating muscle tone and that damage to this structure was responsible for the development of PD⁷. In 1912, Fritz Jakob Heinrich Lewy identified intracellular inclusions as a characteristic of PD⁸, which Konstantin Nikolaevich Tetriakoff later named "Lewy bodies" (LB)s in 1919⁹. In his doctoral thesis, Tetriakoff also reported a significant loss of neuromelanin (NM)-containing pigmented neurons in the SN, which was visible to the naked eye, in the brains of PD patients^{9,10}. These two neuropathological findings are now recognized as key hallmarks of the disease¹¹. Almost 40 years later, in 1957, Nobel laureate Arvid Carlsson discovered dopamine (DA) as a neurotransmitter in the brain¹², which in 1960 led Oleh Hornykiewicz to associate PD with a severe depletion of DA in the striatum (STR) and link this finding to the motor deficits observed in PD patients¹³. In 1967, George Constantin Cotzias used L-3,4-dihydroxyphenylalanine or levodopa (L-DOPA) to treat PD symptoms, restoring DA levels and alleviating PD-related symptoms¹⁴. While PD was considered a non-genetic disorder until then, the 1997 discovery by Mihael H. Polymeropoulos and colleagues of a missense mutation in the gene encoding α -synuclein (α Syn) (*SNCA*) that was responsible for causing dominantly inherited PD challenged this view¹⁵. In the same year, Maria Grazia Spillantini and colleagues identified α Syn as a key marker of LBs¹⁶.

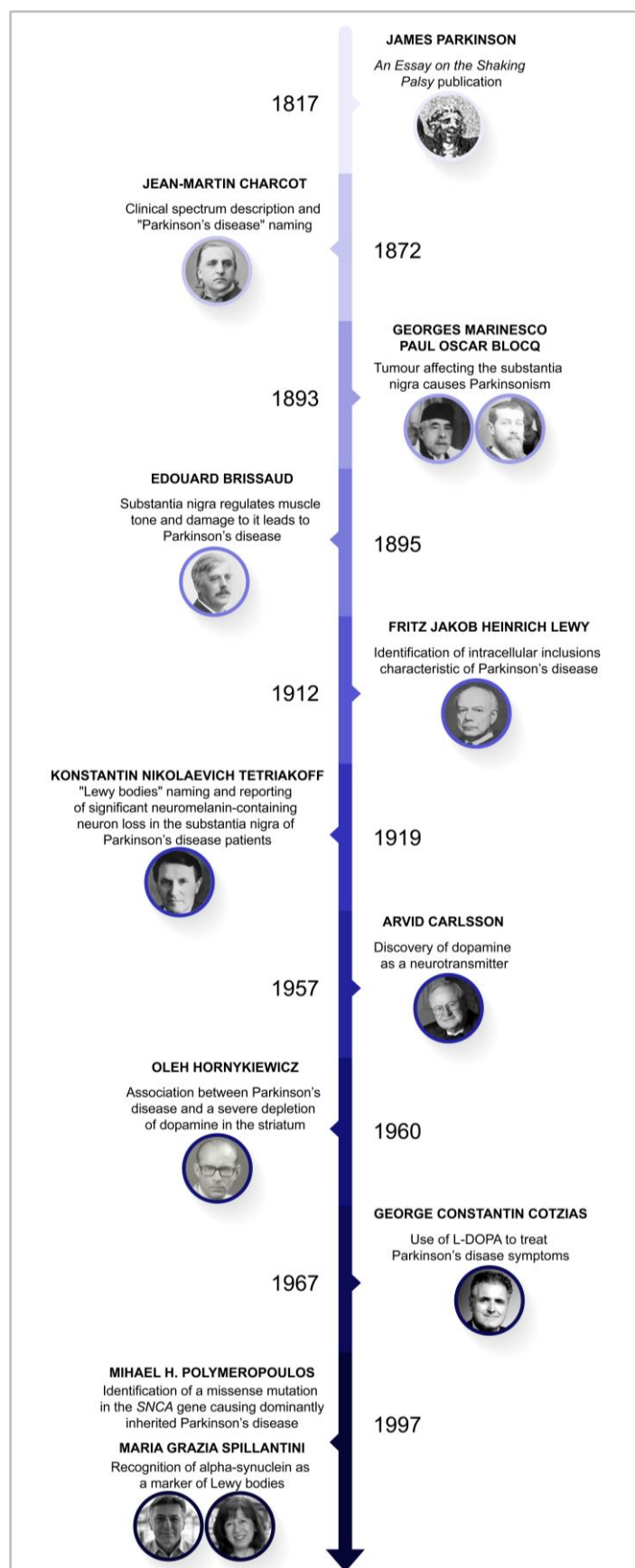


Figure 1. Key findings in the history of PD. Timeline highlighting crucial discoveries related to PD from 1817 to 1919. Images adapted from references^{17–27}.

1.2 Physiopathology

PD is a complex neurodegenerative disease encompassing movement deficits and non-motor symptoms. Neuropathologically, it is mainly characterised by the loss of NM-containing DA neurons in the substantia nigra pars compacta (SNpc) and by the presence of intracellular LB aggregates in affected neurons¹¹.

1.2.1 DA depletion

Degeneration in the SNpc leads to a significant depletion of DA in the STR, which is the primary synaptic target of SNpc axons forming the nigrostriatal pathway^{28,29} (Figure 2). This pathway is crucial for facilitating voluntary movement and motor control³⁰. A reduction in SNpc DA levels is closely associated with motor deficits including decreased movement (akinesia), slow movement (bradykinesia), muscular rigidity, gait instability and tremor at rest³¹.

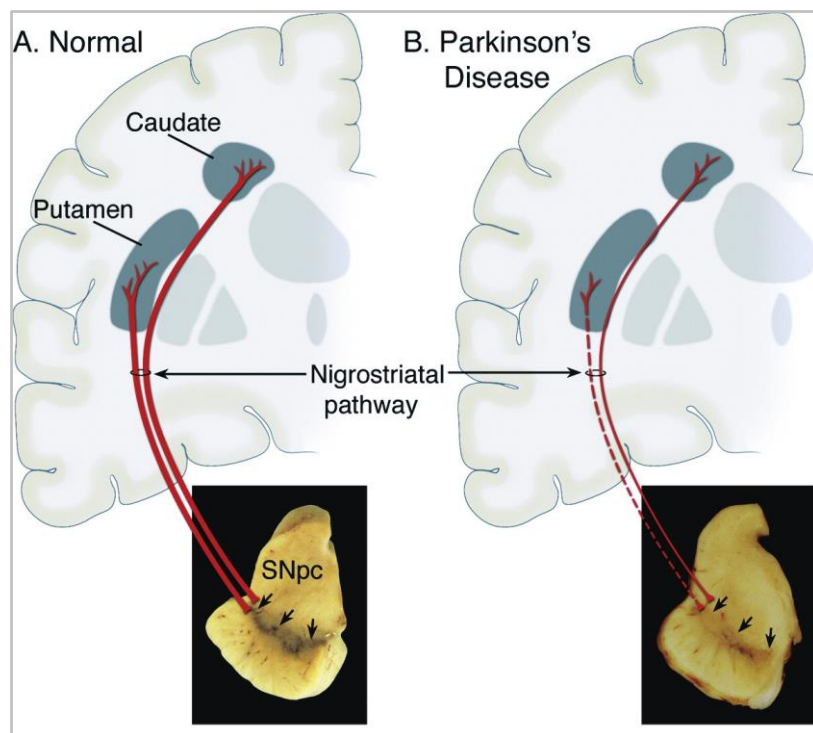


Figure 2. Neuropathology of PD. (a) Schematic representation of the common nigrostriatal pathway (in red). The SNpc (black arrows) is composed of DA neurons whose cell bodies reside in this region. These neurons project (red lines) to the basal ganglia, forming synapses in the STR (including the putamen and caudate nucleus). The scheme illustrates the normal pigmentation of the SNpc, which is due to NM present within dopaminergic neurons. (b) Schematic representation of the diseased nigrostriatal pathway (in red). In PD, a marked loss of DA neurons triggers nigrostriatal pathway degeneration. The image shows depigmentation of the SNpc due to this cell loss. Image adapted from reference³⁰.

1.2.2 Lewy pathology

Lewy pathology refers to pathological inclusions found in nerve cell bodies, known as LBs, and in nerve cell processes, termed Lewy neurites¹⁰. This pathology is a defining diagnostic hallmark of PD, consistently observed in the brains of affected individuals^{32,33}. In the SN, LBs typically appear as eosinophilic, rounded inclusions encircled by a characteristic halo within the neuronal soma³² (Figure 3). On the other hand, Lewy neurites represent abnormal aggregates within neuronal processes and contribute to axonal dysfunction and neurodegeneration³⁴ (Figure 3).

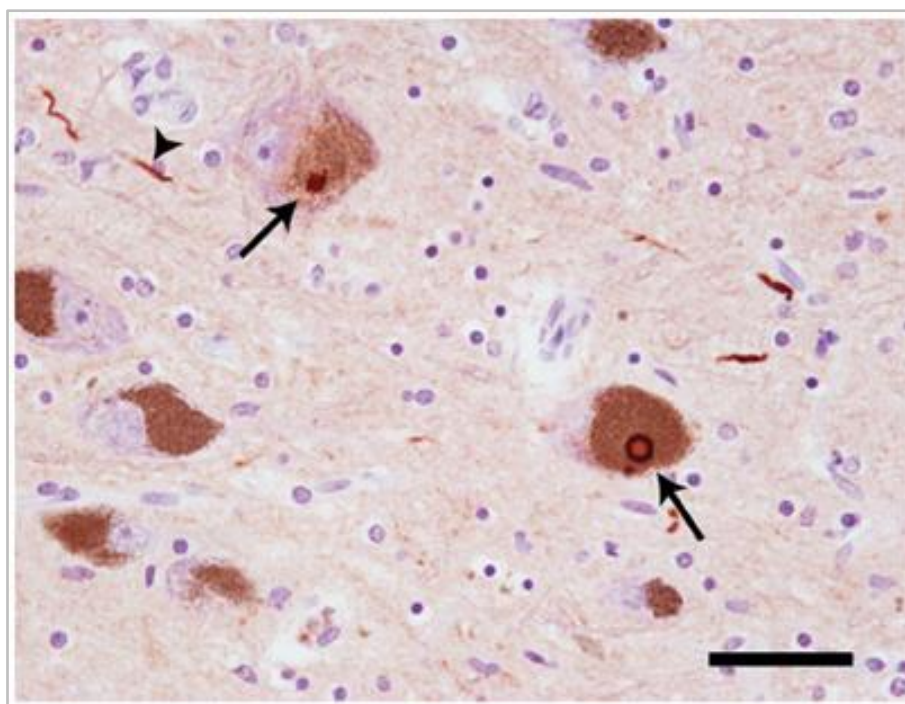


Figure 3. Lewy pathology in PD. Photomicrograph of a *post-mortem* brain section containing the SN from a patient with PD. The section has been stained with an antibody against α Syn and shows LBs (arrows) and Lewy neurites (arrowhead). Scale bar, 50 μ m. Image from reference³⁵.

α Syn protein is widely recognized as a major component of both LBs and Lewy neurites, and plays a central role in their formation¹⁰. Electron microscopy studies showed that LBs are composed of unbranched α Syn filaments³⁶, which ultimately adopt a cross- β structure³⁷. Traditionally, the mechanism of LB formation is considered to begin from cytosolic natively unfolded α Syn monomers which, under uncertain conditions, misfold into β -sheet-rich oligomers (Figure 4). These oligomers then assemble into higher-order protofibrils and fibrils exhibiting different conformations (i.e. fibrils or ribbons) with distinct biochemical properties. α Syn fibrils aggregate to form insoluble LB inclusions³⁸.

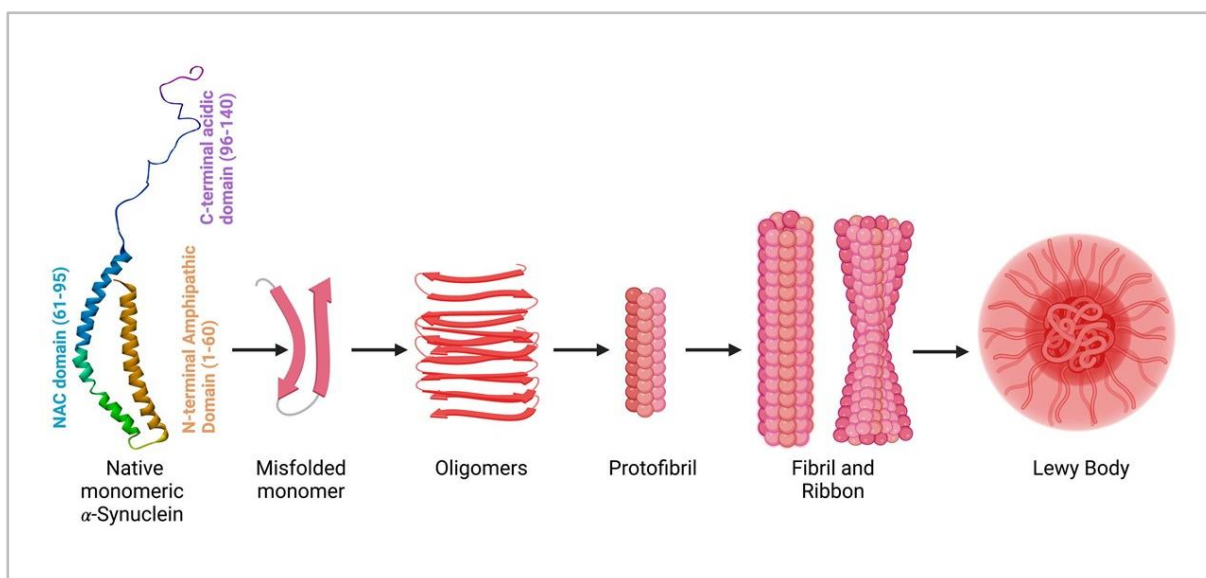


Figure 4. α Syn aggregation gives rise to LB formation. Native monomeric α Syn misfolds into β -sheet-rich oligomers that then assemble into protofibrils and fibrils exhibiting different conformations (such as fibrils and ribbons) which aggregate to ultimately form LB inclusions. Image adapted from reference³⁸.

In 2019, Shahmoradian et al. used advanced microscopy techniques to show that LBs are composed not only of α Syn but also densely packed organelles and lipid membranes³⁹. They proposed a model in which α Syn, in its healthy membrane-bound state, interacts with trafficking lipid vesicles. Under certain pathological conditions, α Syn may drive excessive clustering of these vesicles^{39,40} (Figure 5). If these lipid-protein aggregates are not properly dissociated, they eventually become insoluble and form the characteristic LB inclusions. Concurrently, or as an alternative process, high local concentrations of α Syn bound to vesicle clusters can promote amyloid fibril formation, contributing to late-stage LB development.

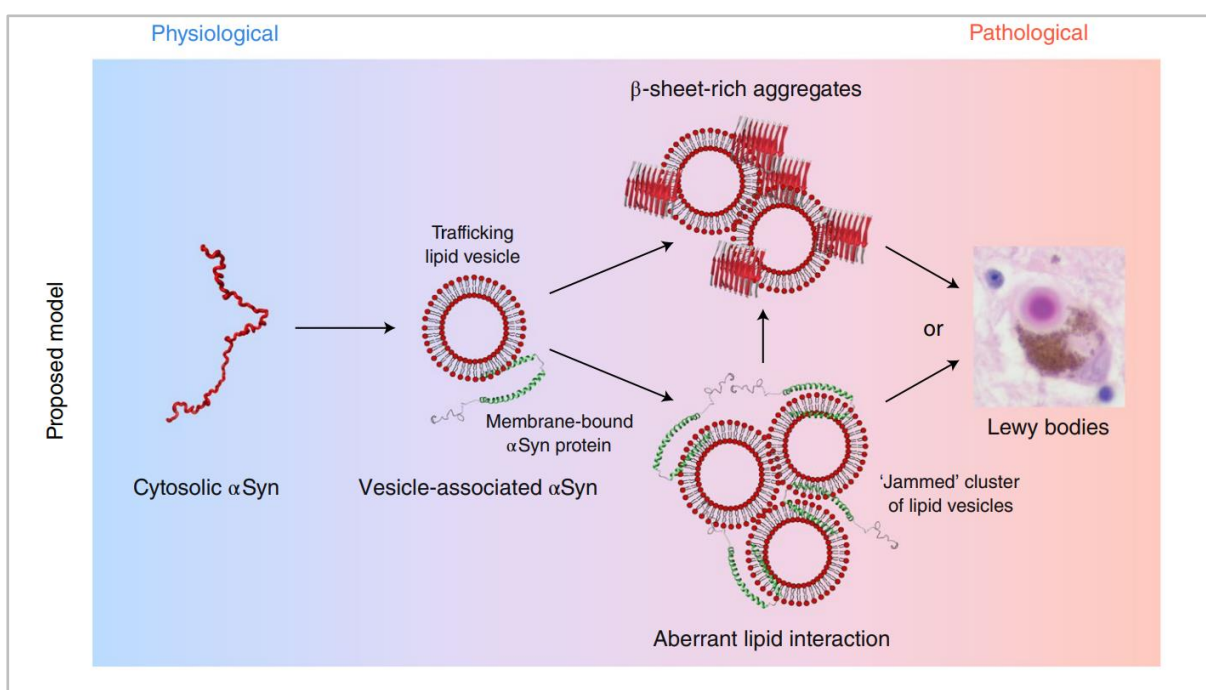


Figure 5. New model of LB formation based on crowded organelles and lipid membranes. In the pathological state of PD, the normal physiological interaction between α Syn and trafficking vesicles becomes disrupted. This disruption results in an excessive aggregation of vesicles mediated by α Syn. If these lipid-protein aggregates fail to dissociate, they eventually become insoluble and are recognized as classical LB. Additionally, the accumulation of α Syn at high local concentrations bound to these vesicle clusters can lead to the formation of amyloid fibrils in later stages of LB development. Image adapted from reference⁴⁰.

All these observations are consistent with the fact that LBs are positive for ubiquitin and p62, two markers of protein degradation and cellular stress responses⁴¹. Both markers reflect activation of the ubiquitin-proteasome system (UPS) and the autophagy-lysosome pathway, which are essential for degrading damaged proteins⁴². When these systems are disrupted, misfolded proteins like α Syn and other cellular components accumulate, contributing to the formation of LBs.

In contrast to cytoplasmic LBs, Marinesco bodies (MB)s are spherical eosinophilic intraneuronal bodies found in pigmented neurons of the SN and locus coeruleus (LC) in non-diseased human brains⁴³. Similar to LBs, MBs are immunopositive for ubiquitin and p62^{41,43}. They are associated with normal aging, being rare or absent in children and increasing in frequency with age⁴⁴. Interestingly, their prevalence is significantly reduced in PD, correlating with a reduced neuronal density in the SN.

1.2.3 Neuromelanin

The loss of NM-containing neurons in the SNpc is a critical feature of PD, given that these neurons are essential for DA production. The selective vulnerability of NM-containing neurons in PD has led to speculation regarding the role of NM in the disease's pathology. The presence of NM, a hallmark of these vulnerable neurons, suggests it may function as a contributing factor to their susceptibility. Various studies indicate that NM accumulation could influence oxidative stress and neuroinflammation, processes implicated in PD neurodegeneration^{45,46}. The specific role of NM in the context of PD will be further explored in the following sections of this introduction (section 2.4).

1.2.4 Neuroinflammation

Histological analyses along with studies of peripheral blood and cerebrospinal fluid (CSF) from PD patients, indicate significant alterations in inflammatory markers and immune cell populations⁴⁷. Numerous inflammatory manifestations have been identified in PD patients including: (i) intestinal dysbiosis and inflammation; (ii) pro-inflammatory cytokines; (iii) innate and adaptive immune cell activation; (iv) peripheral immune cell infiltration on the central nervous system (CNS) and (v) neuroinflammation.

1.2.5 Oxidative stress

Oxidative stress plays a pivotal role in the PD neurodegenerative cascade. It refers to an imbalance between the production of reactive oxygen species (ROS) and the body's ability to eliminate them through antioxidant defences⁴⁸. In PD, this imbalance is exacerbated by

several factors including mitochondrial dysfunction, impaired dopamine metabolism, neuroinflammation and the accumulation of misfolded proteins that ultimately contribute to the degeneration of DA neurons.

1.3 Epidemiology

PD is currently the most common neurodegenerative movement disorder and the second most common neurodegenerative disease after Alzheimer's disease^{49,50}. The estimated prevalence of PD is approximately 0.3% in the general population, rising to 1% in individuals over 60 years of age and 3% in those over 80, underscoring aging as a significant risk factor for developing the disease⁴⁹. Indeed, the prevalence of PD has doubled in the past 25 years, with an estimated 8.5 million individuals affected worldwide in 2019, a trend that correlates with the aging global population⁵¹. Incidence rates of PD vary between 8 and 18 cases per 100,000 person-years worldwide, indicating a substantial public health challenge that demands further research and new therapeutic strategies.

1.4 Symptomatology

Loss of DA neurons in the SNpc leading to reduced DA levels in the STR is the fundamental mechanism underlying the primary motor features of PD. The key motor signs essential for a clinical diagnosis of idiopathic PD include resting tremor, bradykinesia, rigidity and loss of postural reflexes⁵². Motor symptoms typically begin unilaterally, and this asymmetry tends to persist throughout the disease's progression. In addition to motor features, many PD patients also experience non-motor symptoms such as sleep disorders, constipation, hyposmia, depression and anxiety. Although the diagnosis often occurs upon the onset of motor symptoms, it is believed that non-motor symptoms may appear earlier, during the prodromal phase of PD (Figure 6). The onset of motor symptoms typically includes bradykinesia, rigidity or tremor alongside other symptoms like apathy or mild cognitive impairment, which characterise the early stages of the disease. As PD progresses, fluctuations and dyskinesias may occur, with late-stage symptoms including postural instability, gait disorders, dysphagia and dementia. Notably, non-motor symptoms become increasingly prevalent and pronounced throughout the course of the illness, although they can vary widely in intensity across all stages of PD.

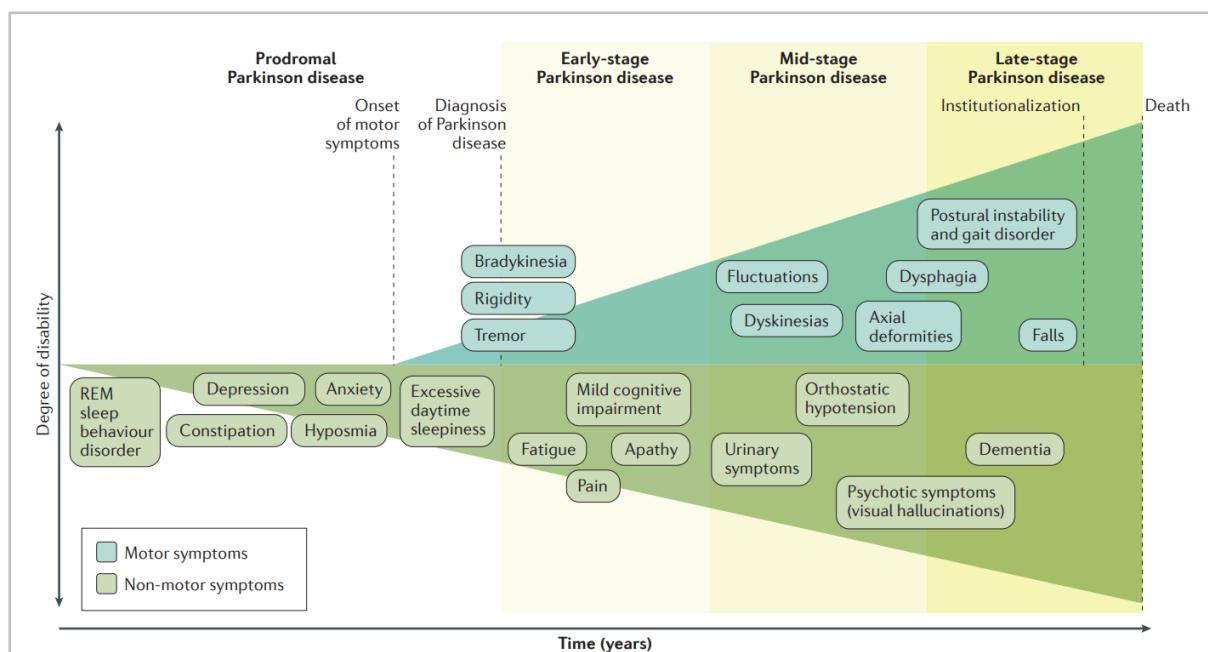


Figure 6. Clinical symptoms associated with PD progression. Clinical diagnosis of PD typically occurs with the onset of motor symptoms (early-stage PD) but is usually preceded by a prodromal phase characterised by a variety of non-motor symptoms (prodromal PD). The combination of non-motor symptoms with the motor impairments promotes disease progression and symptoms such as motor fluctuations, dyskinesias, postural instability and dementia appear in mild and advanced PD stages. Image from reference⁵²

1.5 Etiology

1.5.1 Genetic factors

Although 85-90% of PD cases are idiopathic, 10-15% of them report a family history, with about 5% exhibiting Mendelian inheritance⁵³. Genetic variations linked to PD vary in both frequency and risk⁵⁴ (Figure 7). On one side, there are rare genetic variants that are pathogenic, meaning they are sufficient to cause the disease. These monogenic forms of PD have been identified through linkage analysis in affected families, with key genes such as *SNCA*, *PARK7*, and *PRKN* playing a prominent role. In particular, missense mutations in the α Syn gene (*SNCA*), along with various genomic duplications and triplications, have been identified in individuals with dominantly inherited PD⁵². Conversely, genome wide association studies have identified numerous common genetic variants that each contribute a small amount to the risk of developing PD. Between these common variants and rare pathogenic mutations are intermediate-risk variants, such as those found in the *GBA* and *LRRK2* genes, which are less common but still represent a significant influence on disease susceptibility.

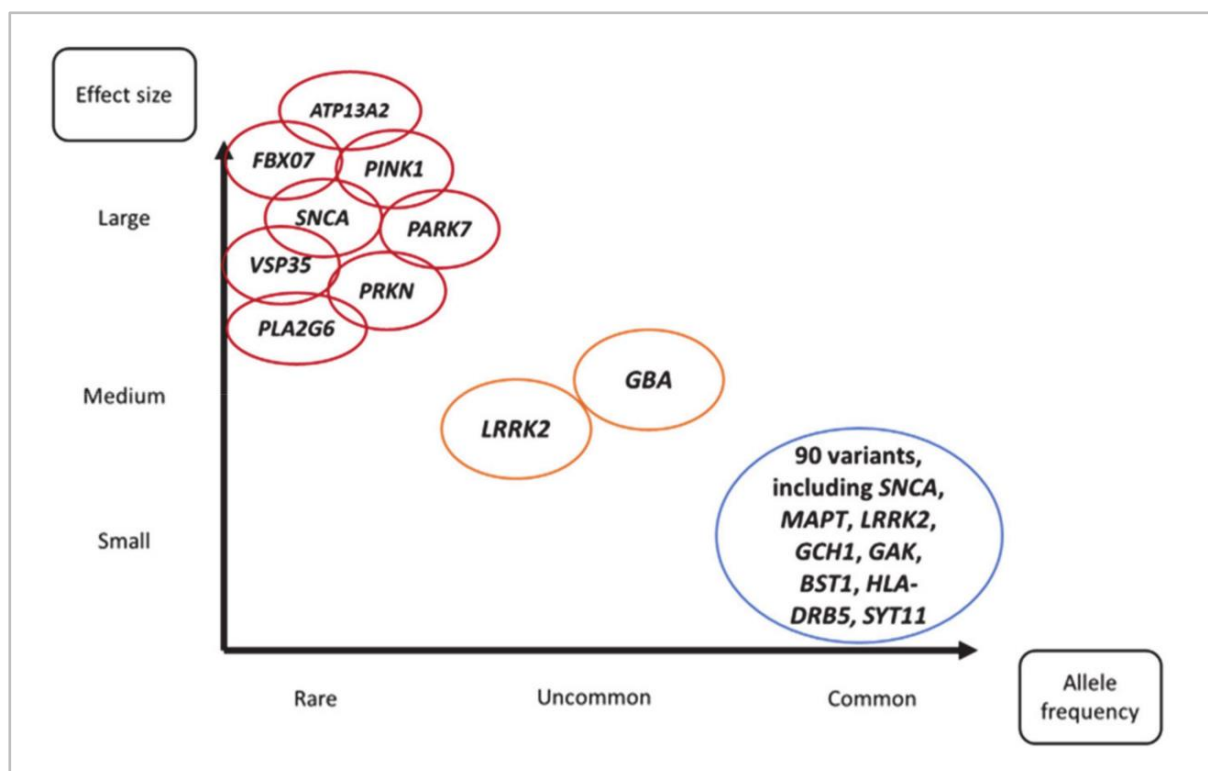


Figure 7. Summary of genetic variants in PD grouped by allele frequency and associated risk. In the left part, rare variants in pathogenic genes are graphed. In the right part, common genetic variants that individually contribute a small amount to the risk of developing PD are shown. In the middle of the spectrum, variants that are uncommon (but not rare) and represent an intermediate risk are illustrated. Image from reference⁵⁴.

Among the monogenic variants associated with PD, many are involved in critical processes such as mitochondrial function, lysosomal activity, and the formation and trafficking of synaptic vesicles⁵⁴.

1.5.2 Non-genetic factors

The fact that 85-90% of PD cases are idiopathic suggest an important role of non-genetic and environmental factors in PD pathogenesis. Aging is widely recognized as a major risk factor, with most PD cases emerging after the age of 60⁴⁹. Additionally, gender plays an important role as the risk of developing PD is twice as high in men as in women¹¹. Several environmental risk factors have also been identified, including exposure to pesticides, heavy metals, viral infections, gut microbiome alterations, prior head trauma and air pollution⁵⁵. Moreover, studies have found positive associations between PD risk and other complex conditions such as bipolar disorder and schizophrenia.

1.6 Biomarkers

The clinical diagnosis of PD relies on identifying hallmark motor symptoms based on the Parkinson's disease Society Brain Bank criteria¹¹. Neuroimaging techniques are commonly employed during the diagnostic process to assess SNpc neurodegeneration. However, these tools are unable to distinguish PD from other disorders linked to SNpc cell loss, such as progressive supranuclear palsy or multiple system atrophy (MSA). Several challenges underline the need for a more accurate diagnostic approach: (i) PD often manifests with a non-motor phase prior to motor symptoms⁵²; (ii) a definitive neuropathological diagnosis is currently only available through *post-mortem* brain examination⁵⁶; (iii) when confirmed by *post-mortem* analysis, the clinical diagnosis of PD is only about 80% accurate⁵⁶; and (iv) PD can be difficult to differentiate from other parkinsonian disorders, particularly in the early stages⁵⁶. Therefore, there is an urgent need for a reliable biomarker that can provide an accurate and differential diagnosis of PD.

Significant advances have taken place in recent years in the search for PD biomarkers, with promising developments in various sample types including CSF, serum, genetic markers and imaging.

1.6.1 α Syn

In past years, numerous studies have aimed to quantify total and oligomeric α Syn levels in various biosamples from both healthy controls and PD patients using biochemical techniques such as Enzyme-linked immunosorbent assay (ELISA). However, these assays have yielded inconsistent results, with low-to-moderate sensitivity and specificity. Key factors contributing to this variability include differences in antibodies, calibration standards and quantification methods⁵⁷.

Recently, a new technique based on α Syn self-aggregation properties has emerged^{57–59}. Two techniques can be used for measuring the self-replication nature of prion-like proteins: protein misfolding cyclic amplification (PMCA) and Real-time Quaking-induced conversion (RT-QuIC). These approaches have demonstrated nearly 100% sensitivity and specificity when applied to human prion disorders⁵⁷. The primary difference between these methods relies on their approach to breaking down oligomers: PMCA uses sonication, while RT-QuIC employs shaking. Despite this distinction, the underlying principle of both techniques is the same. To prevent confusion, the consensus term now used is the α Syn seed amplification assay (SAA). Several studies confirmed excellent sensitivity and specificity of α Syn SAA in differentiating healthy controls from clinically established PD patients^{58–63}. Briefly, exogenous α Syn recombinant monomers are added to the analysed sample together with non-fluorescent thioflavin (ThT)⁶⁴ (Figure 8). If the sample has the capacity to seed the exogenous monomeric α Syn, oligomers are formed and subsequently elongated into fibrils. These longer fibrils are then fragmented into shorter, reactive oligomers, which can further act as seeds amplifying the aggregation process. When ThT binds to amyloid fibrils, it emits a strong fluorescent signal that is monitored, reflecting the seeding capacity of the sample (Figure 8). This approach has

been extensively demonstrated to be capable of discriminating between a healthy control and a PD patient⁵⁹ (Figure 9).

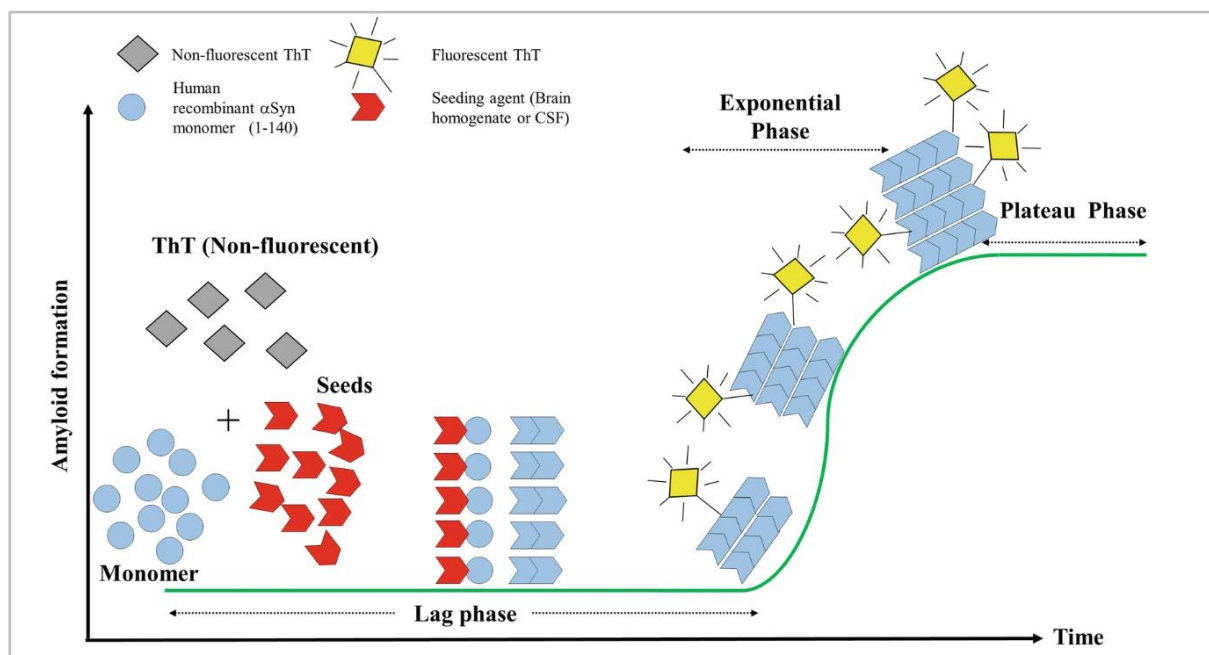


Figure 8. Schematic representation of the α Syn SAA. Seeds in the sample trigger the aggregation of exogenous monomeric α Syn, forming misfolded oligomers that then elongate into fibrils. After fibril detection, a shaking event breaks the longer fibrils into shorter, reactive oligomers, which further act as a seed and thereby amplify the seeding process. The typical shape of the kinetic curve is shown during the aggregation process. Image from reference ⁶⁴.

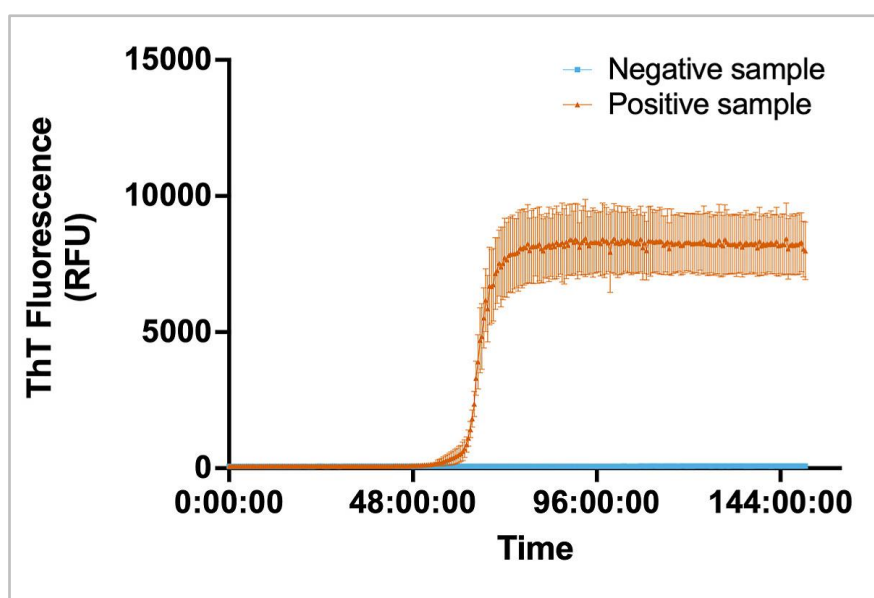


Figure 9. α Syn SAA kinetic curves in positive and negative samples. ThT fluorescence curve of an α Syn SAA in CSF of a negative healthy control (negative sample) and PD (positive sample). Kinetic curves represent the mean of three replicates, including standard deviation. RFU, relative fluorescent units. Image adapted from reference⁵⁹.

1.6.2 DOPA-decarboxylase

DOPA-decarboxylase (AADC) is an essential enzyme for DA metabolism and NM biosynthesis⁶⁵. Although further investigations are needed, studies have reported elevated levels of AADC in both CSF and plasma of PD patients. This elevation has been proposed as a potential biomarker for DA neuron loss^{57,66}.

1.6.3 Mitochondrial markers

As previously discussed, mitochondrial dysfunction plays a significant role in the pathogenesis of PD. In particular, levels of the mitochondrial marker DJ-1 in CSF have been found to be lower in PD patients compared to healthy controls, and these levels correlate with the severity of the disease⁵⁷. However, the presence of similar DJ-1 levels in other parkinsonian syndromes limits the utility of this approach as a definitive diagnostic marker.

1.6.4 Neuroinflammatory markers

Neuroinflammation is another key contributor to the pathophysiology of PD, for which inflammatory mediators are being investigated as candidates' biomarkers for PD. To date, neutrophil-to-lymphocyte ratios (NLRs) and glial fibrillary acidic protein (GFAP) have attracted researchers' attention⁵⁷. Recent publications suggest the potential of these biomarkers to distinguish between healthy controls and PD patients. Nevertheless, there is considerable overlap in individual values and other studies have reported inconsistent results regarding their significance.

1.7 Current pharmacological treatments

At present, there is no cure for PD. For over 50 years, the gold standard treatment has been the administration of the DA precursor L-DOPA, which aims to restore striatal DA levels. While this therapy can temporarily alleviate motor deficits, it often leads to motor response fluctuations and drug-induced dyskinesia after 2-5 years of treatment⁵². Moreover, L-DOPA has a short half-life, and variability in gastrointestinal absorption and BBB transport results in inconsistent drug delivery. To mitigate these shortcomings, researchers are actively developing novel sustained-release formulations of L-DOPA.

Other strategies to restore DA levels include treatment with catechol-O-methyltransferase inhibitors (which redirect L-DOPA metabolism to alternative pathways and thereby enhance its bioavailability), monoamine oxidase type B inhibitors (which increase synaptic DA concentrations), and DA agonists^{52,67}.

Given that PD is a multifaceted disorder characterised not only by motor symptoms but also a range of non-motor symptoms influenced by various neurotransmitter systems, non-dopaminergic approaches are also essential. For example, cholinesterase inhibitors

may be beneficial for PD patients experiencing cognitive dysfunction due to impairments in the cholinergic system^{52,67}.

1.8 PD experimental animal models

As stated above, PD is a complex disorder with no cure, has limited biomarkers, and an incompletely deciphered aetiology. It is thus crucial to develop an appropriate and accurate model reflecting both the pathological and clinical features of the disease, encompassing dysfunctions both in dopaminergic and non-dopaminergic systems, which contribute to motor and non-motor symptoms.

Considering the multifactorial nature of PD and the continuous discoveries about its underlying mechanism, no existing model fully captures all the pathological and clinical features of the disease. PD animal models can be classified into neurotoxic and genetic groups. Neurotoxic models rely on inducing acute neurodegeneration in the nigrostriatal system, mimicking the hallmark loss of DA neurons in the SNpc. In contrast, genetic models, while highly variable in their phenotypes, may not always replicate SNpc neurodegeneration. However, they still provide critical insights into the molecular mechanisms underlying PD pathophysiology, offering valuable clues for understanding disease progression and therapeutic targets.

1.8.1 Neurotoxic models

The most commonly used neurotoxic PD models include the 1-methyl-4-phenyl-1,2,3,6-tetrahydropyridine (MPTP), 6-hydroxydopamine (6-OHDA), paraquat and rotenone models^{68–70}. These compounds exert their cytotoxic effects predominantly on the mitochondria by inhibiting the mitochondrial respiratory chain, disrupting redox reactions or promoting oxidative stress, ultimately leading to nigrostriatal neurodegeneration. While MPTP and rotenone are able to cross the blood-brain barrier (BBB) easily, 6-OHDA and paraquat cannot and therefore require intracranial administration to induce their neurotoxic effects. It is important to note that although both MPTP and 6-OHDA result in DA neuron loss, they fail to replicate LB-like pathology, though increased α Syn expression has been observed in MPTP-treated mice⁷¹. In contrast, paraquat and rotenone not only cause neuronal damage but also promote the formation of LB-like inclusions^{68,72}.

Pathological effects caused by neurotoxin-induced damage in animal models of PD are summarized in the figure 10 ([Figure 10](#)).

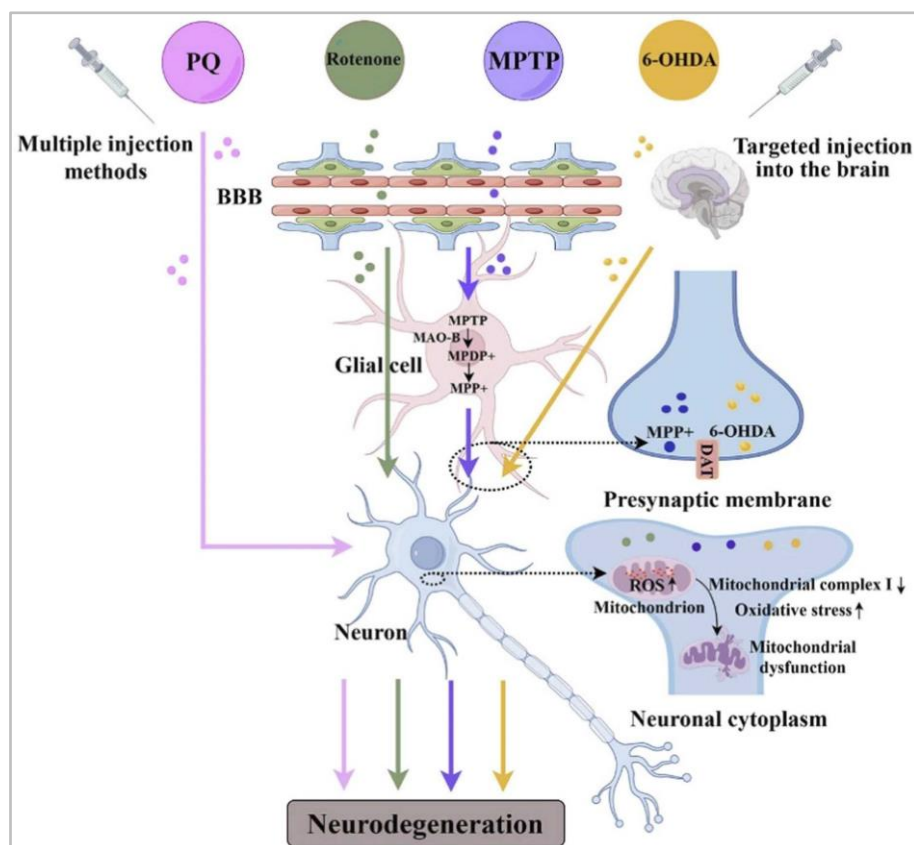


Figure 10. Cytotoxic effects driving neurodegeneration in neurotoxic PD models. After crossing the BBB, MPTP ions are oxidised to MPP⁺, which can be recognized by the dopamine transporter (DAT) and enter into DA neurons, thereby increasing ROS production. 6-OHDA also enters DA neurons via DAT after intracranial injection, where it increases ROS production and inhibits the production of antioxidant enzymes. Rotenone inhibits the activity of mitochondrial complex I, increases ROS production, disrupts DA metabolism and impairs mitochondrial function. Paraquat (PQ) reaches the SNpc after intracranial injection and destroys DA neurons via a cytotoxic mechanism similar to that of MPTP. All these mitochondrial impairments in DA neurons lead to neurodegeneration. Image from reference⁷⁰.

1.8.2 Genetic models

Although familiar PD accounts for only 10-15% of all PD cases⁵³, the role of genetic factors in the pathogenesis of the disease is well-established. Consequently, researchers have developed genetic models of PD by either overexpressing autosomal dominant genes or knocking down autosomal recessive genes associated with the disease⁷⁰. These models help provide insights into the molecular mechanisms underlying both familial and sporadic PD, offering crucial data for understanding its progression and potential therapeutic approaches.

1.8.2.1 Autosomal dominant gene models

Among the autosomal dominant genes linked to PD, *SNCA* and *LRRK2* stand out prominently. The *SNCA* model, focusing on α Syn overexpression, is currently the most widely used transgenic PD model⁷⁰. Given that abnormal α Syn levels and aggregation of

this protein are implicated in PD¹¹, various models have been developed that overexpress either wild-type (wt) α Syn, PD-associated α Syn mutated forms, or fibrillar α Syn⁷⁰. While certain models fail to induce neurodegeneration, others amplify the pathological insult, resulting in DA neuron loss⁶⁹. However, none of these models fully recapitulate the full spectrum of human PD symptoms. Further discussion on α Syn-based PD models follows in subsequent sections.

The *LRRK2* gene encodes the leucine-rich repeat kinase 2 (LRRK2) protein, a cytoplasmic kinase associated with the outer mitochondrial membrane⁶⁹. Pathogenic mechanisms involving *LRRK2* mutations are linked to disrupted autophagy, mitochondrial dynamics, and several other pathways. Interestingly, 21-54% of PD patients carrying a *LRRK2* mutation do not present LB-like pathology, indicating that this mutation may induce neurodegeneration independently of α Syn. In LRRK2-overexpressing models, synaptic dysfunction, impaired DA transmission, and behavioural anomalies are commonly observed, although neurodegeneration in the SNpc is typically absent.

1.8.2.2 Autosomal recessive gene models

Autosomal recessive genes linked to PD have been targeted using knockdown or gene silencing techniques, resulting in the loss of gene function and the development of PD-like phenotypes. Among these genes, *PRKN* (which encodes E3 ubiquitin-protein ligase Parkin, a protein involved in the ubiquitin-proteasome system), *PINK1* (a gene encoding PTEN-induced kinase 1, a protein critical for mitochondrial quality control), and *DJ-1* (which encodes protein deglycase DJ-1, important for oxidative stress response) are the most prominent genes extensively studied in PD research^{69,70}. These models mimic various aspects of the disease and provide critical insights into mitochondrial dysfunction, oxidative stress, and protein degradation pathways associated with PD pathogenesis. *PRKN* is the most commonly mutated gene, accounting for approximately 50% of genetic early-onset PD cases, followed by mutations in *PINK1*, which represent up to 8% of such cases⁶⁹. Both *PRKN* and *PINK1* are critical components of the mitochondrial stress response, believed to operate within the same biological pathway. In mice, the genetic deletion of *PINK1* and *PRKN* results in mitochondrial dysfunction and neuroinflammation; however, this does not lead to hallmark PD features such as α Syn aggregates, behavioural abnormalities, reduced striatal DA levels, or the loss of SNpc dopaminergic (DA) neurons.

DJ-1 protein plays a protective role against oxidative stress⁶⁹. A deficiency in DJ-1 is thought to exacerbate α Syn aggregation and mitochondrial dysfunction, contributing to PD pathology. While DJ-1 knockout (KO) mice exhibit altered DA metabolism, the KO alone is not enough to trigger DA neuron loss or induce PD-like symptoms in young mice⁶⁹. However, in KO older mice, significant DA neuronal loss and motor deficits become apparent. Although DJ-1 alterations may contribute to increased α Syn aggregation, DJ-1 KO mice do not display prominent LB-like pathology⁷³.

Pathological effects caused by genetic animal models of PD are summarized in the figure 11 (Figure 11).

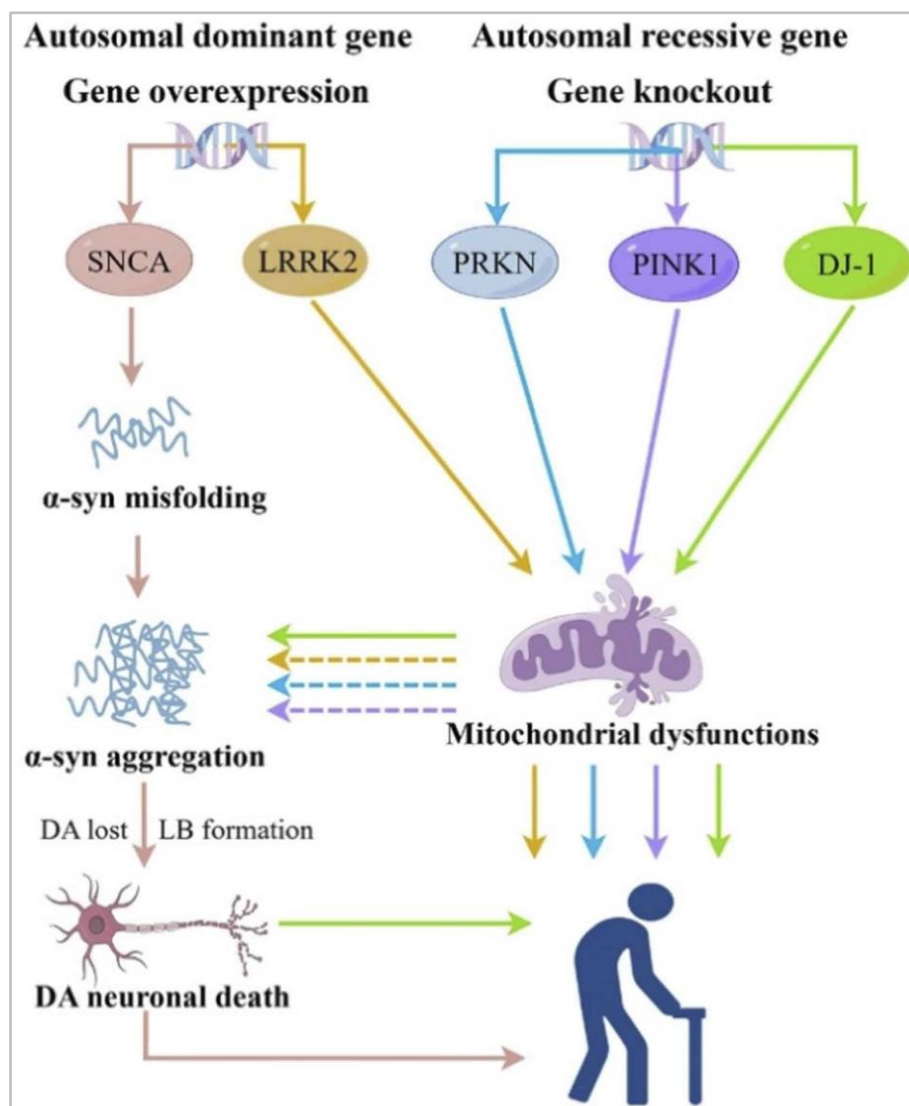


Figure 11. Pathological effects identified in genetic PD models. Mutations in the *SNCA* gene or increased α Syn levels lead to α Syn aggregation, which, if not cleared efficiently, results in the formation of LB and subsequent cellular damage. Mutations in *LRRK2*, *PRKN*, *PINK1*, and *DJ-1* can induce mitochondrial dysfunction, contributing to neurodegeneration and PD symptoms. Additionally, *DJ-1* mutations may exacerbate α Syn aggregation, further promoting the development of PD-related pathology. Image adapted from reference⁷⁰.

2. Neuromelanin

2.1 Origin and distribution

Over a century ago, Tretiakoff was the first to document a significant loss of pigmented neurons in the SN of *post-mortem* brains from PD patients, a change that is visible to the naked eye^{9,10}. This finding remains a critical confirmatory diagnostic criterion for PD to this day⁵². The pigment contained within these neurons, termed NM due to its similarity to cutaneous melanin, is so prevalent in the human SN that it can be observed macroscopically as a darkened area, contributing to the nomenclature of this brain region^{74,75} (Figure 12).

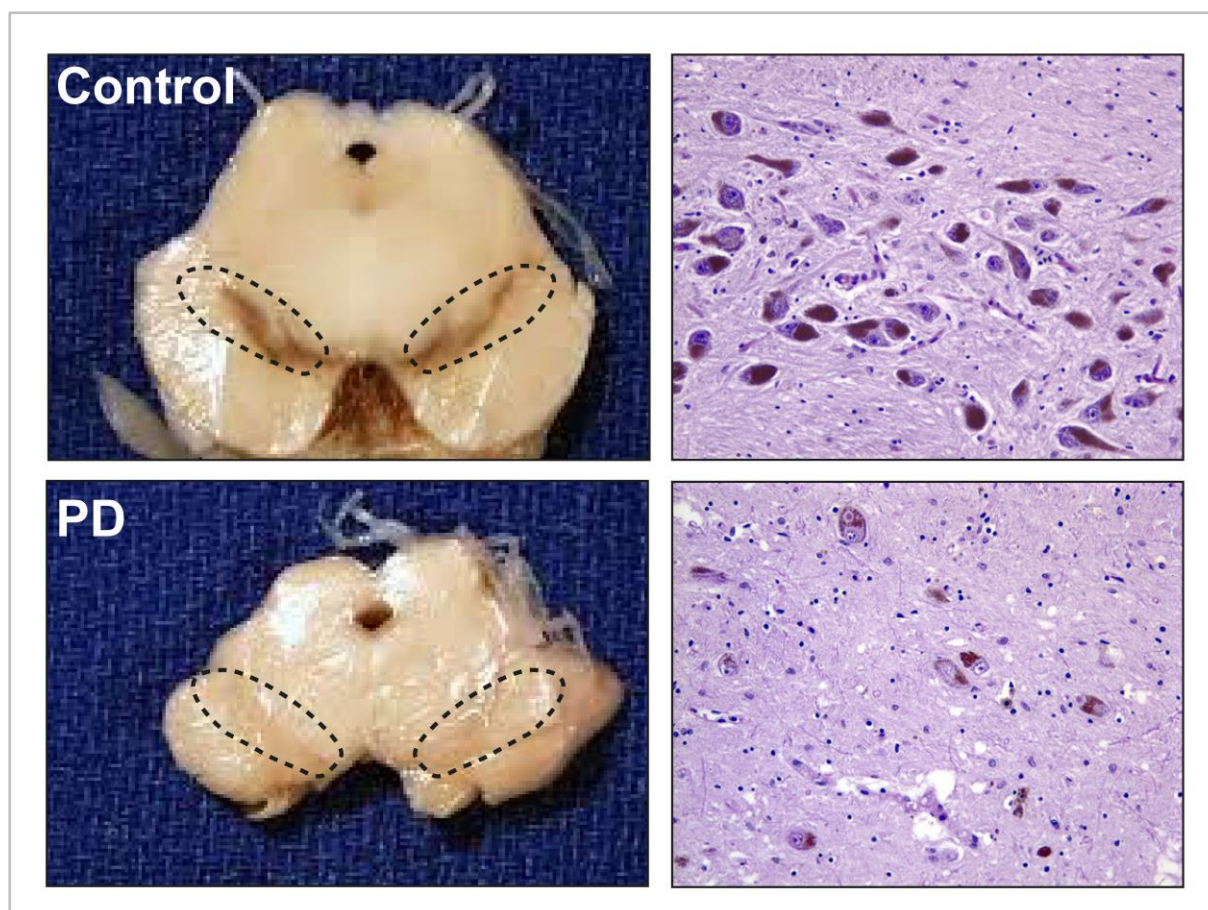


Figure 12. Human midbrain showing dark pigmentation of the SN. *Left*, photographs of transverse sections of human midbrain showing the dark pigmentation of the SN in a neurological control and its loss in PD. *Right*, photomicrographs of NM-containing neurons in the SNpc of a neurological control and its loss in PD. Images adapted from reference⁷⁶.

In addition to the SN, other neurons containing NM that consistently degenerate in PD include the noradrenergic neurons of the LC and the dorsal motor nucleus of the vagus (DMNX)^{77,78}. This degeneration contributes to the characteristic non-motor symptoms of the disease, such as anxiety and depression, sleep disorders and autonomic dysfunction.

Although not visible macroscopically, NM is also present in various regions of the human brain and there seems to be a correlation between catecholaminergic cell groups and pigmentation⁷⁹. The high abundance of NM in the brainstem appears to be unique to humans, although other species, such as monkeys and dolphins, also possess this pigment⁷⁵. In contrast, common laboratory animal species lack NM.

2.2 Synthesis of melanin and NM

The mechanisms underlying the synthesis of NM in the brain remain unclear. In contrast, the pathways for the synthesis of peripheral melanins are well-understood, which may offer insights into potential NM synthesis. In the skin, the biosynthesis of melanin occurs within melanosomes, which are specialized organelles in melanocytes⁸⁰. Two main types of melanin are synthesized: pheomelanin (yellow, red) and eumelanin (brown, black). Their ratio and amounts determine the colour of the skin. Tyrosinase (TYR) is the key

enzyme involved in melanogenesis. TYR catalyses the conversion of tyrosine into dihydroxyphenylalanine (DOPA) and then into DOPAquinone^{80,81} (Figure 13a). From here, two distinct pathways diverge: in the absence of cysteine, DOPAquinone, which is highly reactive, undergoes autooxidation to form DOPAchrome, which rearranges to produce 5,6-dihydroxyindole (DHI) and, to a lesser extent, 5,6-dihydroxyindole-2-carboxylic acid (DHICA). The ratio between these products is regulated by DOPAchrome tautomerase (DCT), also known as tyrosinase-related protein-2 (TYRP2). In humans, TYR also participates in oxidizing DHICA, a step carried out by tyrosinase-related protein-1 (TYRP1) in mice. The oxidation and polymerization of these dihydroxyindoles lead to eumelanin production. Alternatively, when cysteine is present, DOPAquinone reacts with it to form cysteinylquinones, ultimately leading to pheomelanin production. Since TYR catalyses the formation of the common precursor DOPAquinone, it represents the rate-limiting enzyme for both melanin types, whereas TYRP1 and TYRP2 are only involved in eumelanin synthesis.

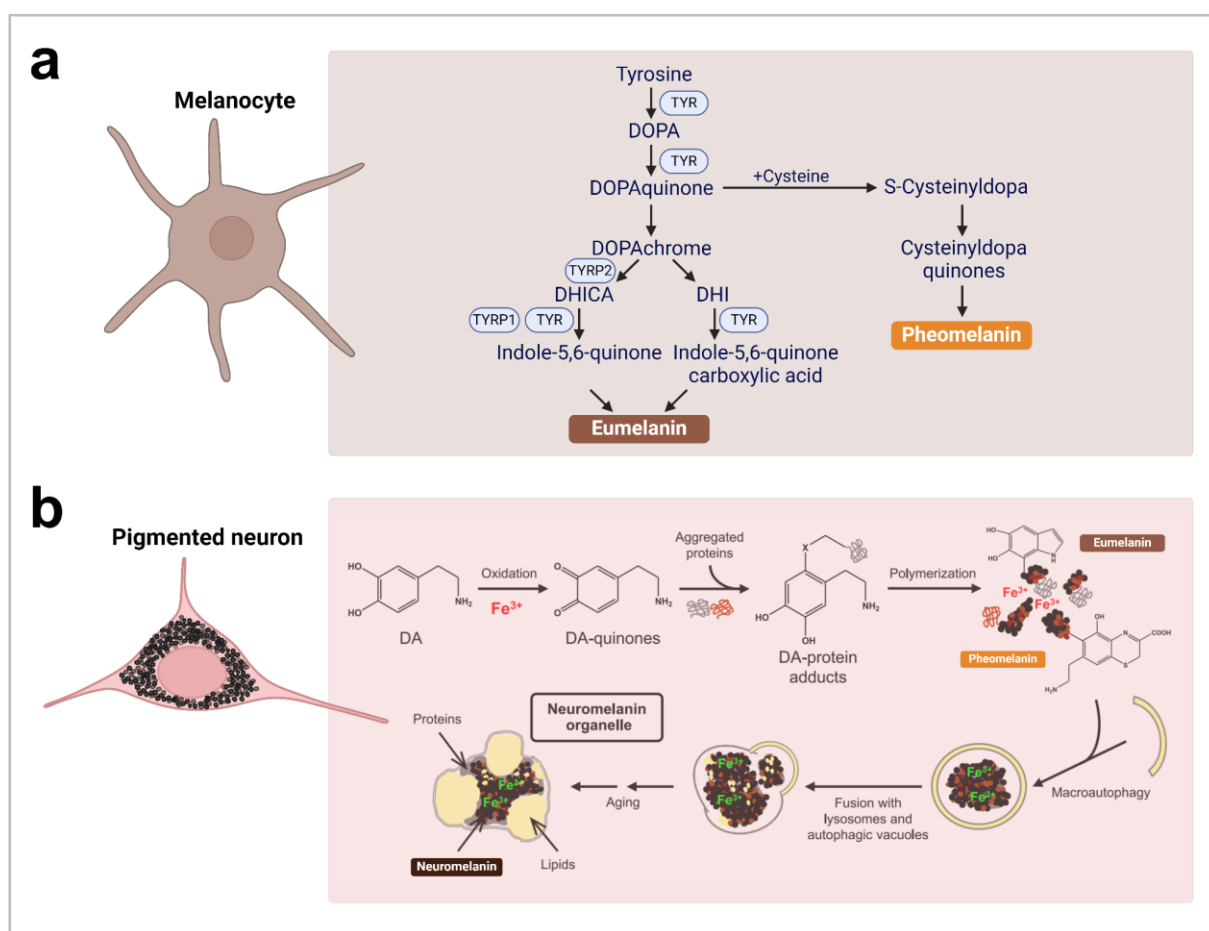


Figure 13. Melanin and NM biosynthesis. (a) Two types of melanin are synthesized in melanocytes: eumelanin and pheomelanin. TYR catalyses tyrosine to DOPA and then to DOPAquinone. In the presence of cysteine, DOPAquinone is converted to cysteinyl-dopa and cysteinyl-dopaquinones which form pheomelanin. In the absence of cysteine, DOPAquinone is highly reactive and undergoes autooxidation to form DOPAchrome, which rearranges to produce DHI and, to a lesser extent, DHICA. The ratio between these products is regulated by TYRP2. In humans, TYR also participates in the oxidation of DHICA, while in mice this process is regulated by TYRP1. DHI is also oxidised by TYR. The oxidation and polymerization of these dihydroxyindoles lead to eumelanin production. (b) In pigmented neurons, NM is hypothesised to originate from the spontaneous autooxidation of DA. Excess DA in the cytosol of pigmented neurons can be oxidised into

quinones by ferric iron. Reactive quinones can bind to aggregated proteins initiating the formation of a melanin-protein component with eumelanin and pheomelanin components that can also bind metals, particularly iron. The resulting undegradable product is taken into autophagic vacuoles, thus forming mature NM granules containing a mixture of NM pigment, metals, lipids and proteins. Illustration created with Biorender.com and images adapted from references^{80,82} respectively.

The question of whether NM biosynthesis is under enzymatic control, similar to that of peripheral melanin production, or whether it simply results from spontaneous autooxidation of catecholamines remains a topic of ongoing debate. Evidence suggest that NM formation *in vitro* can be driven by excess cytosolic catecholamines that are not encapsulated into synaptic vesicles. The addition of L-DOPA in cultures has been shown to promote NM formation, which can be mitigated by increasing DA uptake into vesicles or by using iron chelators⁸³. This indicates that both free cytosolic DA and iron contribute to NM synthesis. The hypothesis that NM synthesis occurs via DA autoxidation is widely accepted (Figure 13b). Excess DA in the cytosol of SN neurons can be oxidised into quinones by ferric iron⁸². These reactive quinones can bind to aggregated proteins in the cytosol, initiating oxidative polymerization and forming NM that binds to both iron and aggregated proteins. The undegradable product is eventually engulfed by autophagic vacuoles, forming mature NM granules that contain a mixture of NM pigment, metals, lipids and proteins.

However, some observations challenge this theory⁷⁵: (i) NM distribution does not align perfectly with the expression of tyrosine hydroxylase (TH), the key enzyme in DA production; (ii) NM is absent in most animal species despite the presence of DA and other catecholamines; (iii) experimentally increasing DA or oxidised DA in rodents does not lead to NM formation.

2.3 Function

NM appears to have a dual role in cellular processes, being both protective and toxic depending on the cellular environment⁸⁴. It has been proposed that NM synthesis *per se* helps prevent the build-up of toxic catecholamine derivatives by incorporating them into the NM polymer (Figure 14). Under normal physiological conditions, NM may act as an antioxidant by binding harmful ions like metals (e.g. iron, zinc, copper) and toxic compounds (e.g. MPTP, paraquat). However, when intracellular iron levels surpass NM's binding capacity, NM can switch to a pro-oxidant role, releasing redox-active iron which promotes oxidative stress. Additionally, while autophagic vacuoles that trap NM via macroautophagy might initially protect neurons from stress, the continuous accumulation of these pigmented vacuoles can disrupt normal cellular degradation pathways and interfere with endocytic and secretory processes, leading to detrimental effects on neuronal survival^{82,84}. Moreover, once NM is released into the extracellular space, it triggers microglial activation and may contribute to chronic inflammation by releasing trapped metals and toxic compounds, further harming surrounding cells⁸⁴.

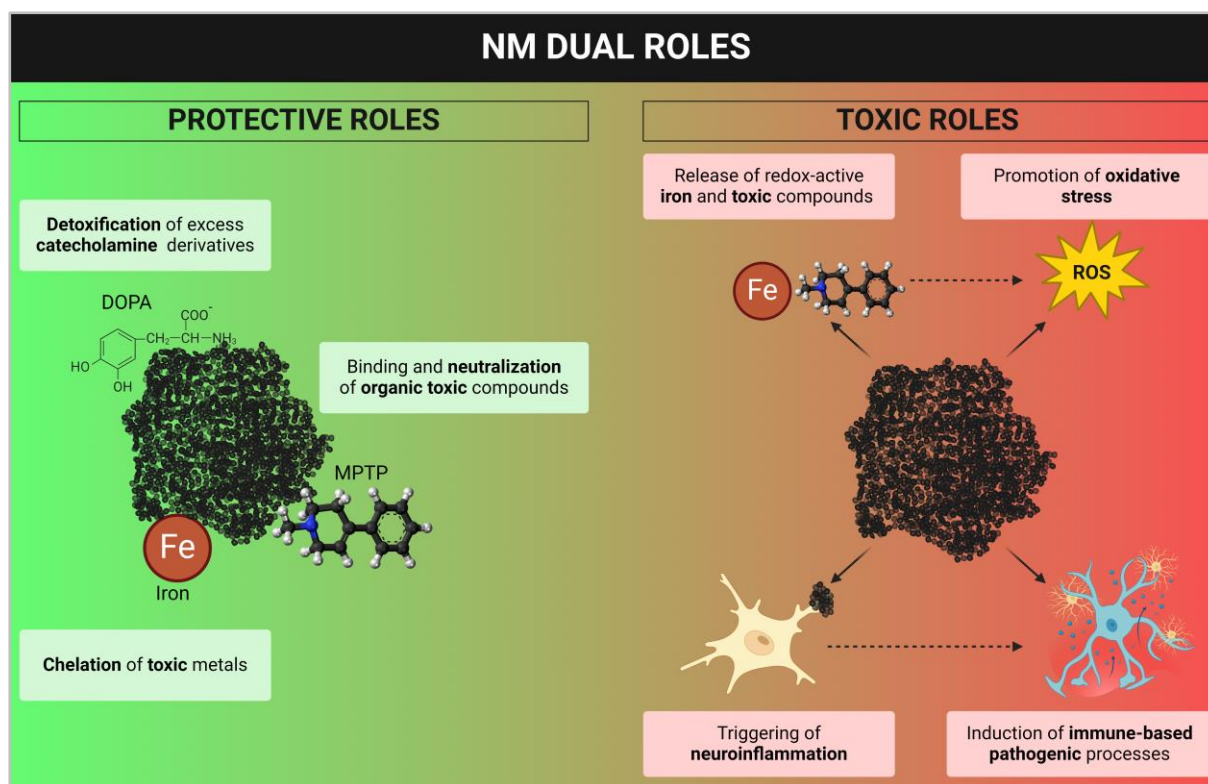


Figure 14. Dual roles of NM. This illustration summarizes both protective and toxic roles of NM. *Left*, protective roles of NM achieved by buffering potentially neurotoxic compounds. *Right*, toxic roles that NM can adopt under pathological conditions. Illustration created with Biorender.com based on information provided in reference⁸⁴.

2.4 NM and its relevance to PD hallmarks

2.4.1 NM and aging

In humans, NM deposition begins around the age of three years⁸⁵ (Figure 15), implying that either the process of autooxidation takes far longer than expected or that the regulatory mechanism for NM synthesis develops later in life. Once pigmentation commences, the proportion of the cellular volume occupied by NM granules increases progressively until approximately 20 years of age, at which point nearly the entire cytoplasm is filled with these granules⁸⁵. After this, the cell volume occupied by NM stabilizes, but the absolute concentration of NM continues to rise with age, increasing linearly into the ninth decade of life. NM levels start at 0.3 to 0.8 $\mu\text{g}/\text{mg}$ tissue between 10 and 20 years of age, peaking at up to 3.7 $\mu\text{g}/\text{mg}$ tissue between the fifth and ninth decades⁸⁶ (Figure 16). This increase is likely due to NM granule aggregation, which concurs with a rise in the optical density of NM and a change in its coloration from yellow-brown to dark brown over time⁸⁵.

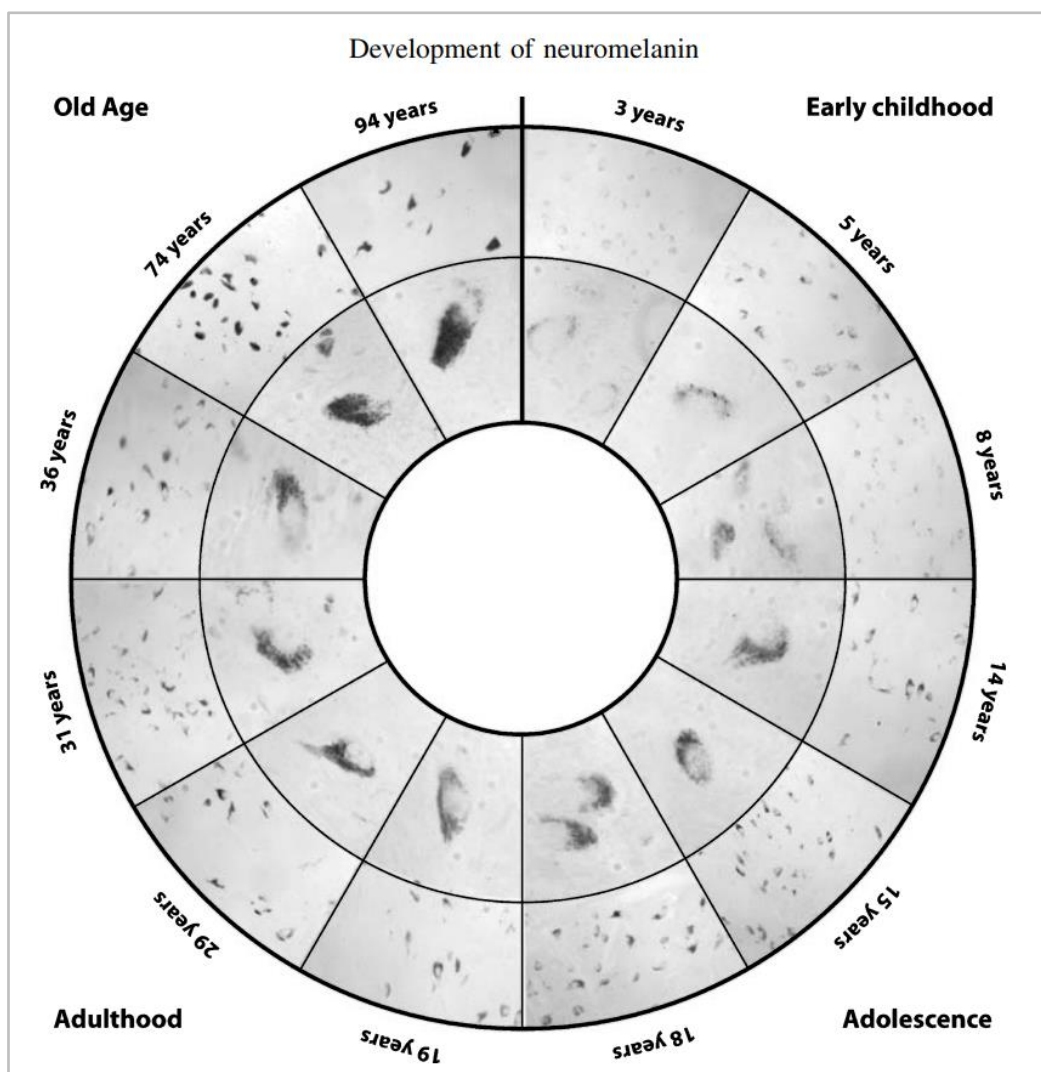


Figure 15. Progressive accumulation of NM in the human brain. This figure shows intermediate and high magnification photomicrographs of representative unstained NM-pigmented neurons from the ventral region of the human SN at various ages. NM first becomes visible at 3 years of age. As individuals age, the OD of NM pigment increases consistently, while the average volume of the NM occupied area peaks around 20 years and then stabilizes. Image from reference⁸⁵.

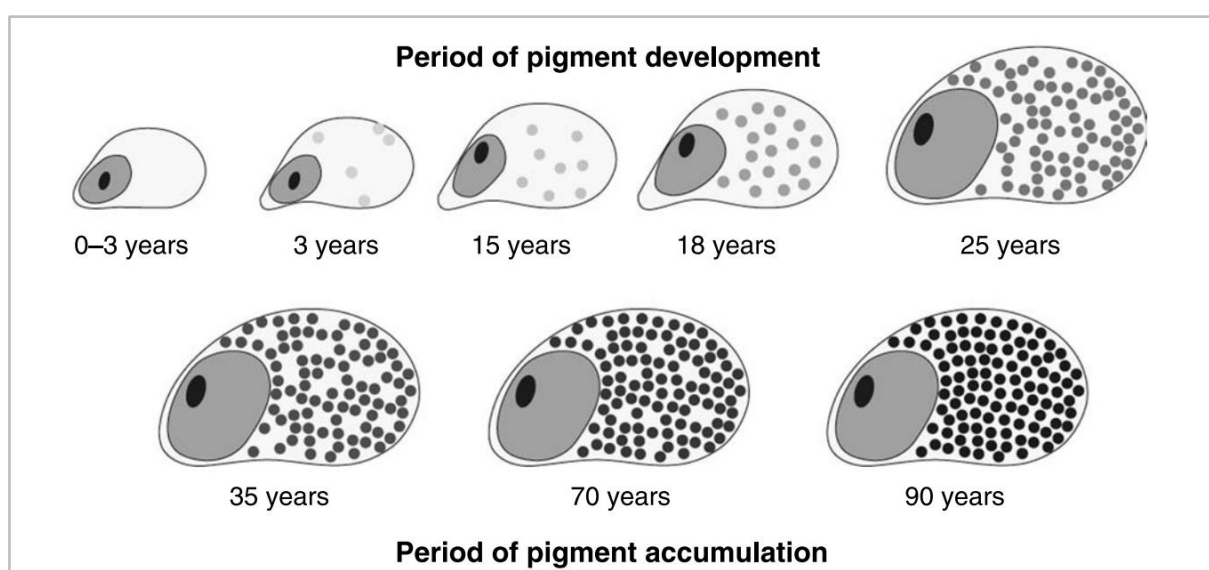


Figure 16. NM developmental stages. The first signs of evident pigmentation occur at around 3 years of age; this is followed by an increase in cell size and the NM occupied area until around 20 years of age. After this moment, the NM occupied area stabilizes but NM pigment darkens over time. Image from reference⁸⁵.

In summary, considering that aging is the primary risk factor for PD, the age-related and progressive accumulation of NM suggest it may play a crucial role in the PD pathogenesis. This is supported by evidence indicating that when NM cannot be effectively degraded and begins to accumulate, it can assume toxic roles contributing to cellular stress as mentioned above.

2.4.2 NM and Lewy pathology

The first ultrastructural characterisation of LB from the SN and LC of PD cases revealed the presence of filamentous structures with a dense central core and lipofuscin positivity suggesting the presence of NM granules and lipid-protein complexes⁸⁷ (Figure 17a). Posterior histological analyses showed that classical brainstem LBs within pigmented neurons typically appear surrounded by NM pigment^{41,88} (Figure 17b).

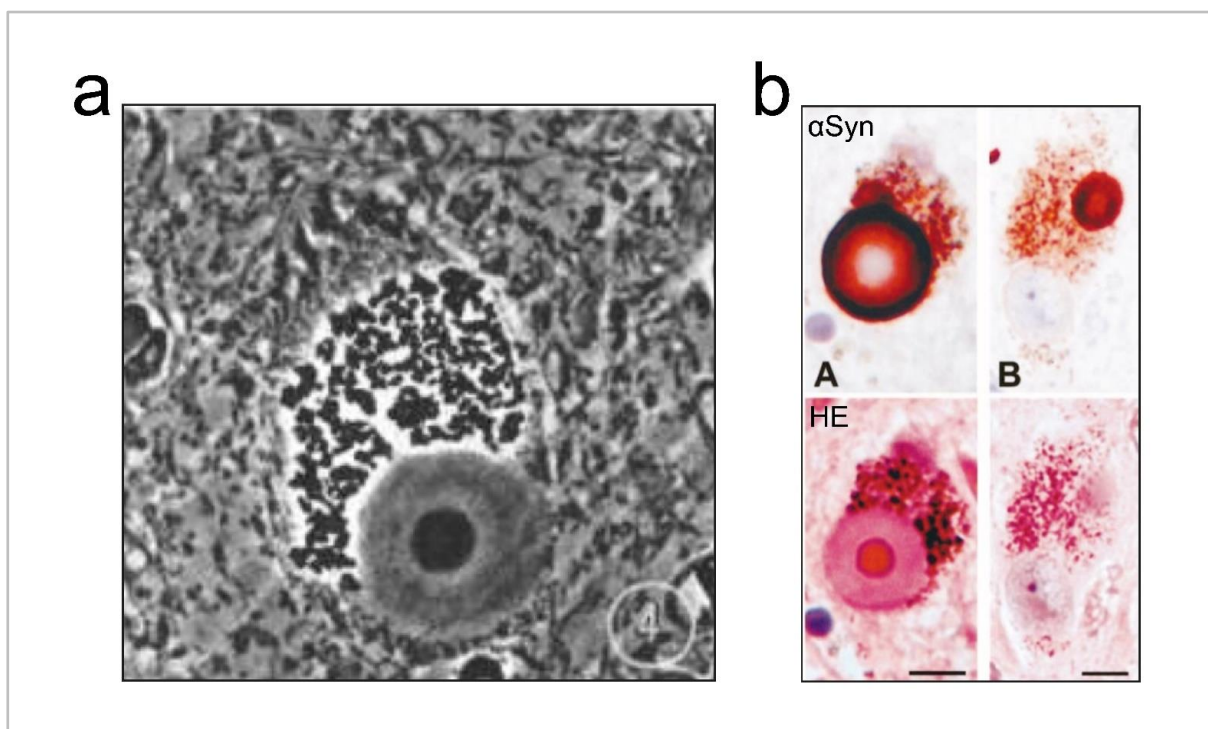


Figure 17. LBs surrounded by NM granules. (a) LB within a nerve cell of the SN of a PD case with a dense core surrounded by NM granules. (b) LBs from different cases stained by either α Syn and haematoxylin-eosin. Scale bars, 10 μ m. Images adapted from references^{41,87} respectively.

2.4.3 NM and neuroinflammation

When pigmented neurons die, NM and its bound components (including toxic molecules and extracellular NM granules) are released into the extracellular space and engulfed by surveillant microglia, which recognize them as cellular debris⁸⁹. Initially, microglia act to clear this debris; however, once their phagocytic capacity is exhausted, they adopt a

proinflammatory phenotype triggering an inflammatory response. In this scenario, proinflammatory cytokines are released, thereby amplifying neuroinflammation leading to damage to surrounding neural structures and transforming astrocytes into a reactive phenotype. These reactive astrocytes may produce interferons, potentially inducing an autoimmune response that further exacerbates neuronal damage. As a result, NM-related neuroinflammation may create a pathogenic feedback loop where NM release perpetuates neuroinflammation, which in turn accelerates cell death.

2.4.4 Selective vulnerability of NM-containing neurons in PD

Although key pathogenic events and hallmarks of PD are well-established, the initial trigger, the chronological sequence of these events and the specific factors contributing to the selective vulnerability of certain neuron populations remain elusive. Notably, neurons with the highest NM levels, such as DA neurons in the SNpc and the ventral tegmental area (VTA), as well as noradrenergic neurons in the LC, are particularly prone to degeneration in PD^{77,90} (Figure 18). Even in the absence of overt PD, NM-containing neurons from apparently healthy aged individuals show early signs of neuronal dysfunction and degeneration compared to young adult brains, including an age-related loss of pigmented neurons in the SNpc and LC, downregulation of phenotypic neuronal markers, α Syn pathology and the presence of extracellular NM^{91–94}. The origins of this selective vulnerability are thought to be multifactorial, including: (i) unique electrophysiological properties, such as calcium-dependent pace-making activity; (ii) elevated oxidative stress; (iii) pathological protein aggregation and (iv) an excessive iron load⁹⁰. Furthermore, NM complexes accumulate reactive toxic compounds derived from DA metabolism, organic molecules, metals (e.g., iron) and misfolded proteins which, under certain conditions, can be released and trigger the production of ROS and immune-mediated pathogenic events.

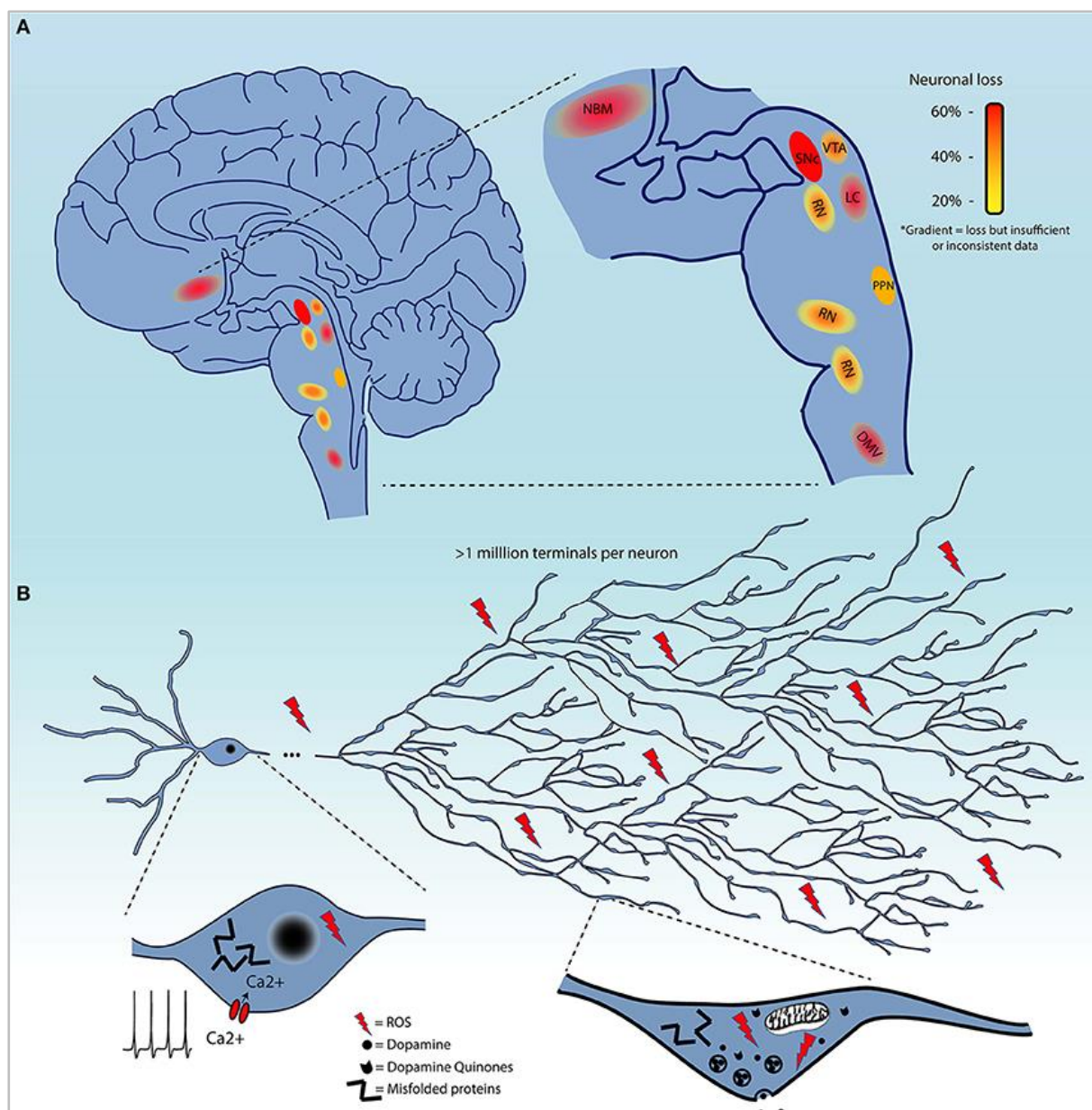


Figure 18. Selective vulnerability of neuronal populations in PD. (a) Schematic representation of brain regions exhibiting cell loss in PD. Regions are color-coded based on evidence of cell loss. Red = 60%, orange = 40%, and yellow = 20%. (b) Summary of the current hypothesis that may explain the origins of the selective vulnerability of neurons in PD, including exceptionally large axonal arbor of PD affected neurons, their electrophysiological properties, high levels of oxidative stress, pathological protein aggregation and reactive dopamine quinones. Image from reference⁹⁰.

2.4.5 Altered DA metabolism

DA levels within SNpc neurons are tightly regulated through a balance of synthesis, storage in synaptic vesicles and metabolism, which ultimately leads to NM formation. During DA metabolism, several reactive intermediates are generated, one of which is 3,4-dihydroxyphenylacetaldehyde (DOPAL), a physiological DA metabolite known to be neurotoxic⁹⁵. Studies have shown that DOPAL injections in the SNpc of rats cause significant neuronal loss, surpassing that induced by DA or its metabolites^{95,96}. In PD

patients, *post-mortem* analysis revealed impaired DOPAL detoxification leading to elevated cytosolic levels that may contribute to DA neuron degeneration⁹⁷. DOPAL's highly reactive nature facilitates protein cross-linking and aggregation⁹⁵. Of particular significance in PD, DOPAL has been shown to trigger the oligomerization of α Syn. In addition to its direct neurotoxic effects, DOPAL disrupts proteostasis by promoting protein aggregation, which leads to the accumulation of ubiquitinated proteins. Furthermore, it can inhibit enzymes by modifying critical active site residues, as well as exacerbate oxidative stress, potentially leading to mitochondrial dysfunction.

2.5 Novel NM-producing PD models

2.5.1 TYR-overexpressing NM-producing rats

Beyond reported findings, NM appears to be linked to PD pathophysiology, either as a vulnerability factor or a triggering event. However, NM has often been neglected in PD animal research because commonly used laboratory species, such as mice and rats, do not naturally produce this pigment^{75,98}. To address this limitation, our group developed the first rodent model mimicking age-dependent human-like NM production and accumulation⁹⁹. This model is based on the unilateral overexpression of the rate-limiting melanogenic enzyme TYR in the rat SNpc, achieved through the use of a viral vector (Figure 19a). Overexpression of TYR in SNpc DA neurons is sufficient to generate macroscopically visible human-like NM (Figure 19b) with properties that closely resemble those found in humans, as confirmed by magnetic resonance imaging (MRI), electron microscopy, and histology. Quantification of intracellular NM levels revealed an age-dependent accumulation, reaching levels comparable to those seen in elderly humans. Notably, once NM build-up exceeded a certain pathogenic threshold, it began to compromise neuronal function, leading to PD-like phenotype. PD-like features included neuroinflammation, lysosomal and autophagy dysfunction, impairment of the UPS, LB-like pathology, increased ROS production, disrupted neurotransmission, and neurodegeneration (Figure 19c). These neuropathological changes led to contralateral forepaw hypokinesia.

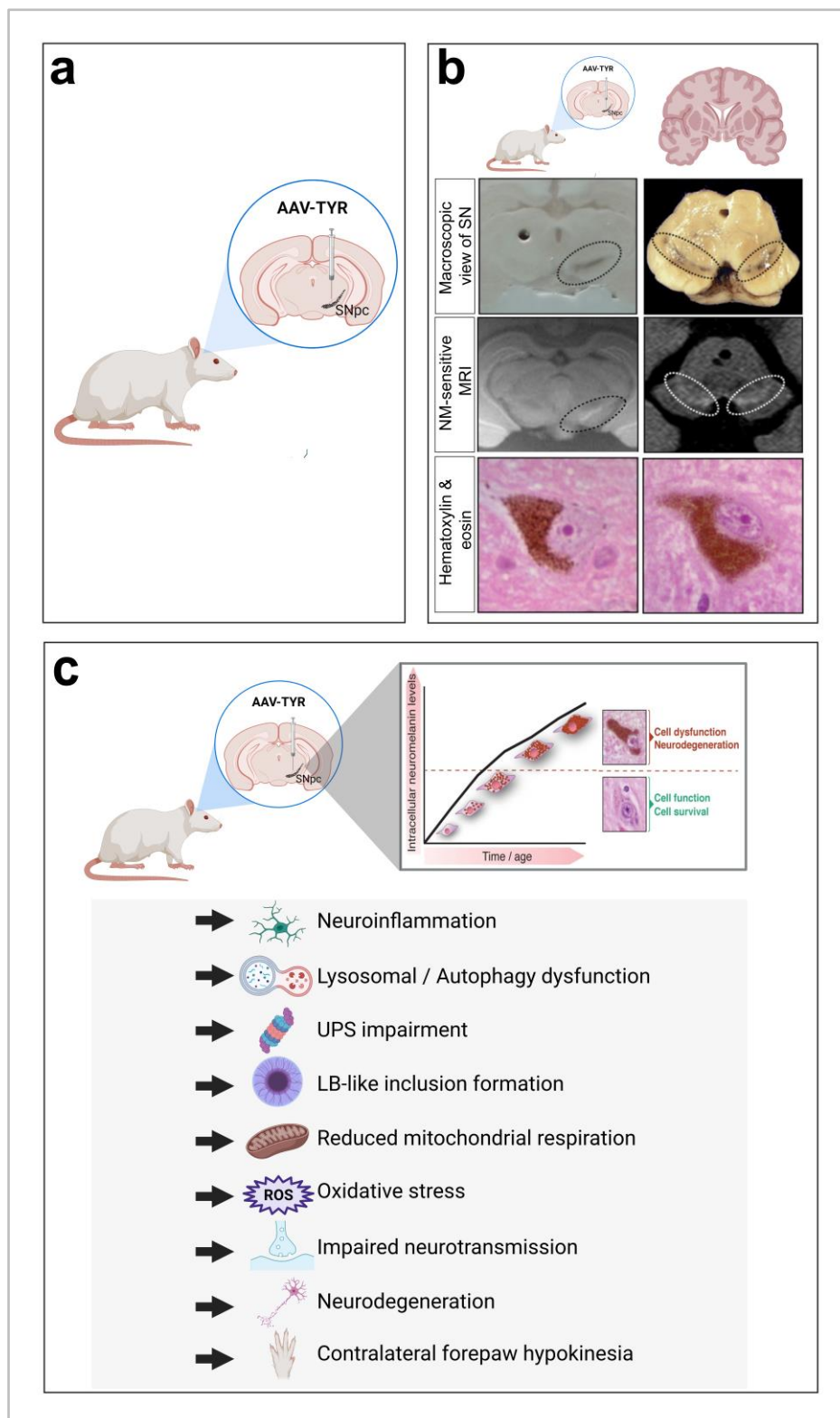


Figure 19. Age-dependent human-like NM production in rat SNpc triggers PD pathology. (a) Schematic representation of unilateral AAV-TYR injection in the area above the rat SNpc. (b) Macroscopic view of SN, NM-sensitive MRI and HE staining showing a pigmented neuron from rat brain (*left*) and human brain (*right*). (c) Upon reaching a pathological threshold, NM accumulation triggers a PD-like phenotype. Illustrations created with Biorender.com based on the information provided in reference⁹⁹.

2.5.2 SH-SY5Y neuroblastoma cells inducible for TYR expression: TR5TY6 cells

The induction of TYR expression in human catecholaminergic neuroblastoma SH-SY5Y cells (TR5TY6 cells) led to a gradual intracellular production and accumulation of NM, similar to what was observed in TYR-injected rats⁹⁹ (Figure 20). By 6 days (d) post-induction, NM had occupied most of the cellular cytoplasm. These NM-producing cells exhibited impaired autophagy, reduced UPS activity, subsequent accumulation of p62 and deposition of oligomeric α Syn, and increased production of ROS. These functional changes ultimately compromised cell viability, as cell death began to occur 6 d after TYR induction.

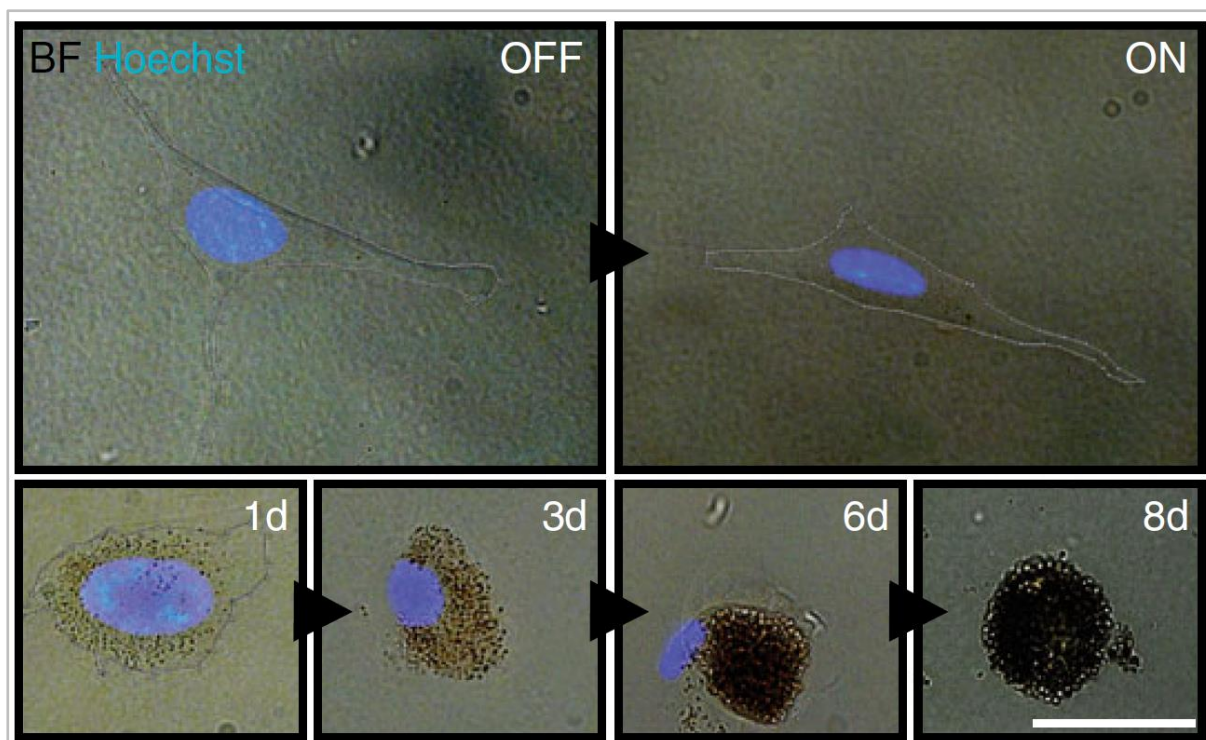


Figure 20. NM production in TR5TY6 cells upon TYR induction. In the absence of TYR induction (OFF), neuroblastoma cells do not produce NM. When TYR expression is induced (ON), NM is progressively produced and accumulates within the cell cytoplasm. There is a positive correlation between the number of days post-induction and the level of intracellular NM, with accumulation increasing over time. Scale bar, 12,5 μ m. Image from reference⁹⁹.

2.5.3 TYR transgenic mouse model

As previously discussed, NM production is not limited to the SNpc; it is produced in all catecholaminergic neurons. In light of this, our group has recently developed a tissue-specific transgenic mouse (termed tgNM) exhibiting an age-dependent, brain-wide distribution of pigmentation across all catecholaminergic regions¹⁰⁰ (Figure 21). This model is based on the constitutive expression of TYR driven by the TH promoter, specifically targeting catecholaminergic neurons. This allows for a more comprehensive study of NM's role in neurodegeneration and PD across different brain regions.

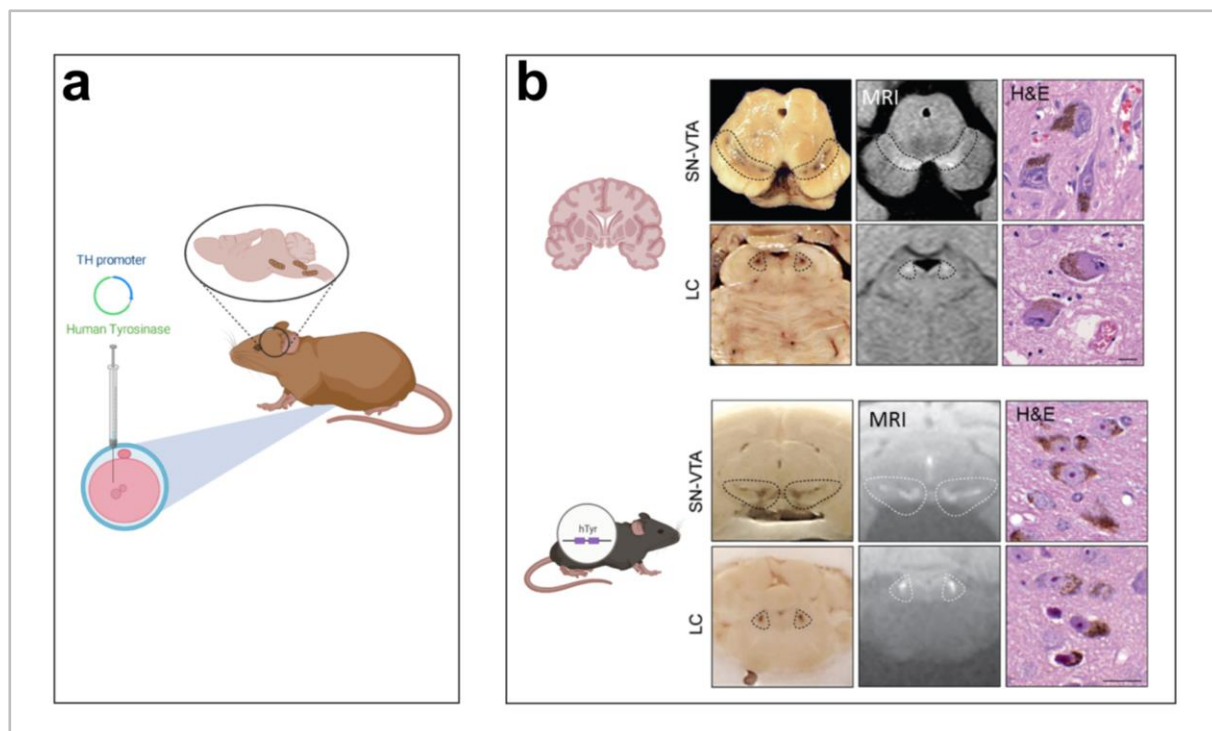


Figure 21. The tgNM mouse exhibits bilateral NM accumulation across all catecholaminergic brain regions. **(a)** Development of the tgNM mouse model based on the constitutive expression of TYR driven by TH promoter, specifically targeting catecholaminergic neurons. **(b)** Bilateral NM accumulation in catecholaminergic regions such as SN and VTA (*top*) and LC (*bottom*) comparing a human brain (*upper panel*) with a tgNM mouse brain (*lower panel*). Scale bars, 20 μm . Illustrations created with Biorender.com based on images provided in reference¹⁰⁰.

TgNM animals exhibited progressive, multisystem PD-like features resembling the prodromal and early stages of PD¹⁰⁰. At early time-points, the animals displayed autonomic dysfunction and non-motor behavioural alterations, with motor symptoms emerging around 12 months (m), mimicking prodromal PD symptomatology (Figure 22). Bilateral NM accumulation in all catecholaminergic regions affected multiple neuronal systems including dopaminergic, noradrenergic, cholinergic and serotonergic pathways. Notably, noradrenergic neurodegeneration in the LC preceded DA dysfunction in the SN and VTA. These animals also exhibited key neuropathological PD-like features in pigmented areas such as LB-like pathology, extracellular NM granules and neuroinflammation.

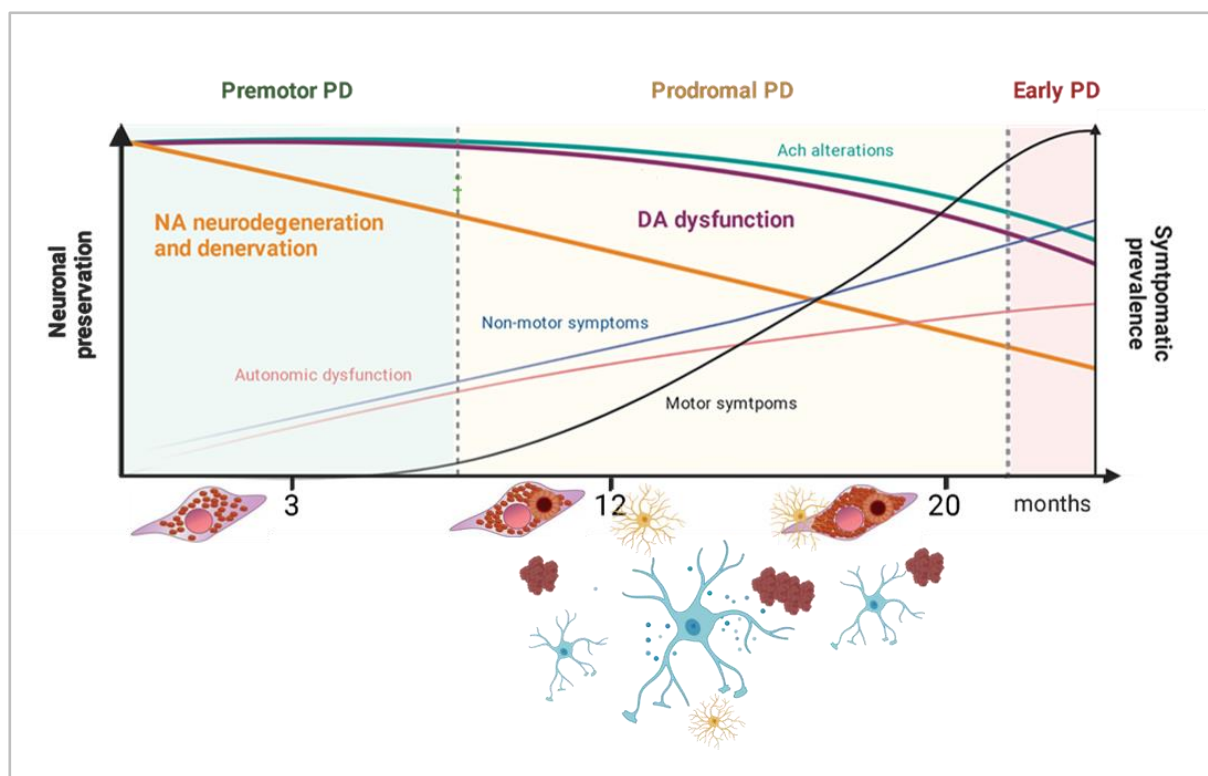


Figure 22. Progressive multisystem PD-like features in tgNM mice. By 3m, tgNM animals exhibit noradrenergic (NA) neurodegeneration and denervation, accompanied by autonomic dysfunction. By 12 m, both non-motor and motor symptoms emerge, along with DA dysfunction and neuropathological PD-like features such as LB-like pathology, extracellular granules and neuroinflammation, which become more pronounced by 20 m. Illustration from reference¹⁰⁰.

2.6 Therapeutic modulation of NM levels

As accumulation of intracellular NM beyond a pathogenic threshold has been implicated in neuronal dysfunction and neurodegeneration, our group has designed therapeutic strategies aimed at reducing intracellular NM to sub-threshold levels. Two promising approaches, involving overexpression of either transcription factor EB (TFEB) or vesicular monoamine transporter 2 (VMAT2), have demonstrated efficacy in alleviating NM-induced PD-like phenotypes in TYR-overexpressing rat models^{99,101} (Figure 23).

2.6.1 TFEB

As the failure of proteostasis is implicated in NM-associated PD pathology, our group investigated the therapeutic potential of TFEB overexpression, a master regulator of autophagy⁹⁹. TFEB enhances lysosome and autophagosome biogenesis, promotes autophagic clearance of cellular debris, facilitates lysosomal exocytosis, and restores proteostasis. Co-injection of AAV-TFEB and AAV-TYR into the rat SNpc significantly increased the expression of lysosomal-associated membrane protein 1 (LAMP1), reduced the formation of inclusion bodies, and decreased intracellular NM levels compared to AAV-TYR alone (Figure 23). These effects prevented nigrostriatal degeneration, reversed

motor impairments, and highlighted the therapeutic potential of TFEB in mitigating NM-induced neurodegeneration.

2.6.2 VMAT2

Considering that NM derives from the oxidation of free cytosolic DA, our group aimed to limit NM accumulation by enhancing DA internalization into synaptic vesicles via VMAT2 overexpression¹⁰¹. This strategy reduces the availability of free cytosolic DA, thereby decreasing the formation of potentially toxic oxidised DA species that contribute to NM synthesis. Co-injection of AAV-VMAT2 and AAV-TYR in rat SNpc led to a significant reduction in NM levels compared to AAV-TYR alone (Figure 23). This decrease was accompanied by reduced inclusion body formation, sustained DA homeostasis, preservation of the nigrostriatal system and improvements in motor function. These findings underscore the protective effects of VMAT2 overexpression in maintaining neuronal integrity and counteracting NM-associated toxicity.

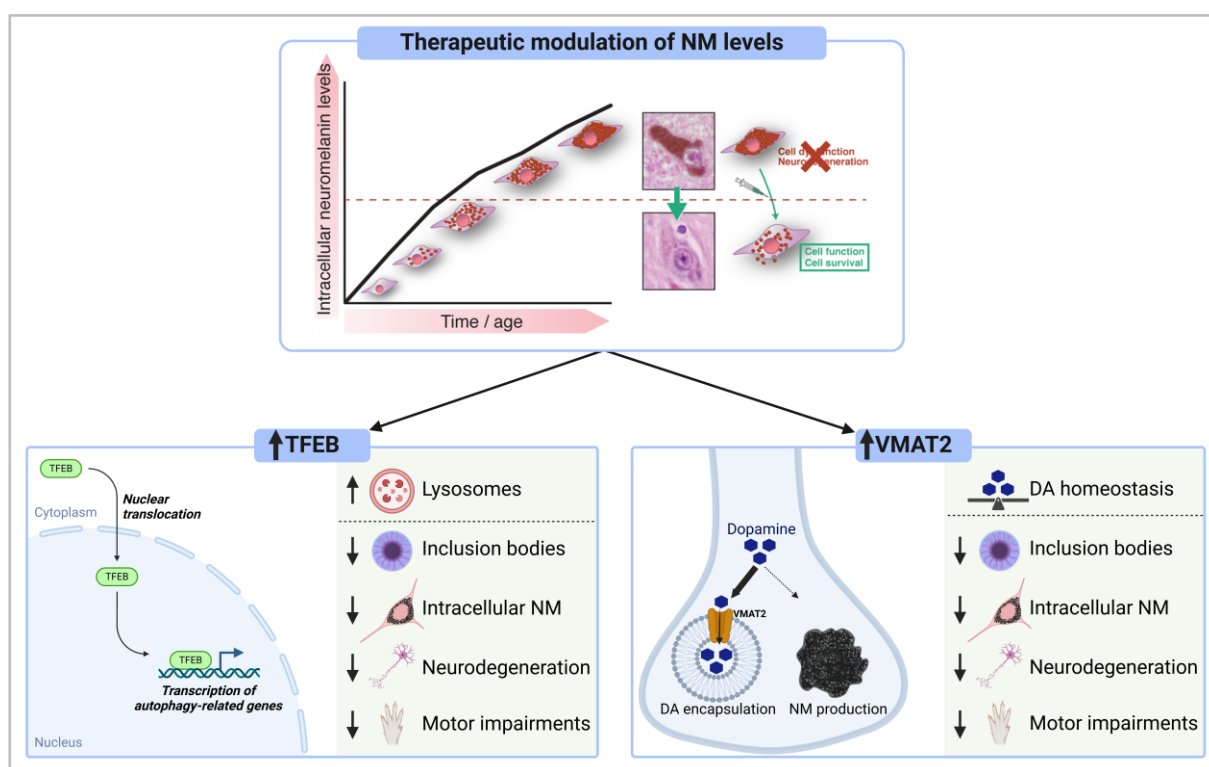


Figure 23. Therapeutic modulation of NM levels. NM accumulation above a pathogenic threshold triggers cell dysfunction and neurodegeneration. Therapies directed to reduce intracellular NM levels aim to preserve cell function and survival. *Left*, TFEB overexpression in NM-producing rats enhances the transcription of autophagy-related genes promoting lysosome biogenesis. This process decreases inclusion body formation and intracellular NM levels, thereby preventing neurodegeneration and motor impairments. *Right*, VMAT2 overexpression in NM-producing rats promotes DA encapsulation into synaptic vesicles, thus reducing cytosolic DA available for oxidation to form NM. Sustained DA homeostasis and reduced NM production decreases inclusion body formation and protects against neurodegeneration and motor impairments. Illustration created with Biorender.com based on the information provided in references^{99,101}.

3. Alpha-synuclein

3.1 Discovery

α Syn was first discovered in the electric ray *Torpedo californica* using an antibody against purified cholinergic vesicles^{102,103}. The protein was initially observed in presynaptic terminals and along the nuclear envelope, leading to its name: “synuclein”, combining “syn” from synaptic vesicles and “nuclein” from the nuclear envelope.

α Syn became a key player in PD research in 1997 when two pivotal discoveries were made¹⁰. First, a missense mutation in the *SNCA* gene encoding α Syn was identified as the cause of autosomal dominant familial PD^{10,15}. Moreover, LBs and Lewy neurites were found to be immunoreactive to α Syn^{10,16}. These findings marked a major breakthrough in our understanding of PD and positioned α Syn at the forefront of PD research. From that point on, α Syn became a major target for research due to its implication in both genetic and sporadic forms of PD, sparking significant interest in its structure, function, and pathological mechanisms in neurodegenerative disorders.

3.2 Structure

The synuclein family is composed of α -, β -, and γ -synucleins, which are soluble proteins. α Syn is a 14 kDa protein composed of 140 amino acids¹⁰⁴ (Figure 24). It is characterised by an amphipathic lysine-rich N-terminus forming an α -helix, which plays a crucial role in modulating its interactions with cellular membranes. The C-terminus, which is disordered and acidic, is involved in regulating α Syn’s nuclear localization as well as its interactions with metals, small molecules and proteins. The central region, known as the non-amyloid- β component (NAC) domain, contains a highly hydrophobic motif critical for α Syn aggregation.

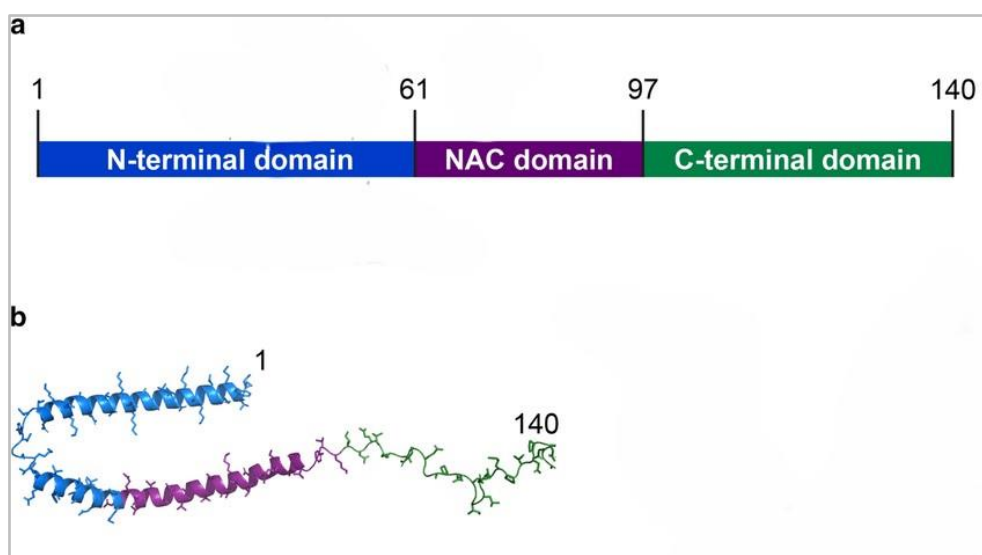


Figure 24. α Syn structure. (a) α Syn is formed by an amphipathic N-terminal domain which forms an α -helix, a highly hydrophobic central region component known as the non-amyloid β component (NAC) domain, and a disordered C-terminal domain. (b) Structural representation of the α Syn monomer. Image from reference¹⁰⁵.

3.3 Distribution

3.3.1 Tissue expression

Within the CNS, α Syn is widely expressed throughout the brain in a developmentally regulated pattern, with particularly high levels in the neocortex, hippocampus, STR, thalamus and cerebellum^{103,106}. Beyond the brain, α Syn is also present in various peripheral tissues including the colon, kidney, testis, muscle, skin and bone marrow¹⁰⁷.

3.3.2 Cellular localization

At a cellular level, native α Syn is present in synaptic terminals, in the nucleus of neuronal cells, mitochondria, endoplasmic reticulum, Golgi apparatus and in the endolysosomal system^{102,108}.

3.4 Physiological functions

3.4.1 Synaptic roles

Due to its affinity for negatively charged phospholipids, α Syn has been reported to interact with a wide range of proteins, enabling it to perform various functions through these interactions. Notably, α Syn interacts with the GTP-binding protein Rab3 on membranes, particularly synaptic vesicles, as well as with soluble N-ethylmaleimide-sensitive fusion factor attachment protein receptors (SNARE) proteins, DJ-1 and TH¹⁰³. However, the precise mechanisms, functions and physiological significance of many of these interactions remain unclear. Current evidence suggests that α Syn's association with cell membranes at the synapse plays key roles in regulating synaptic plasticity, DA homeostasis, and synaptic vesicle trafficking¹⁰⁹. These specific functions, summarized in figure 25, include lipid-related roles such as regulating synaptic vesicle pools through sorting and clustering, remodelling of lipid membranes, and promoting SNARE complex assembly and synaptic vesicle release (Figure 25). Additionally, α Syn is involved in non-lipid-related functions, such as modulating DA synthesis via TH and regulating DA transport.

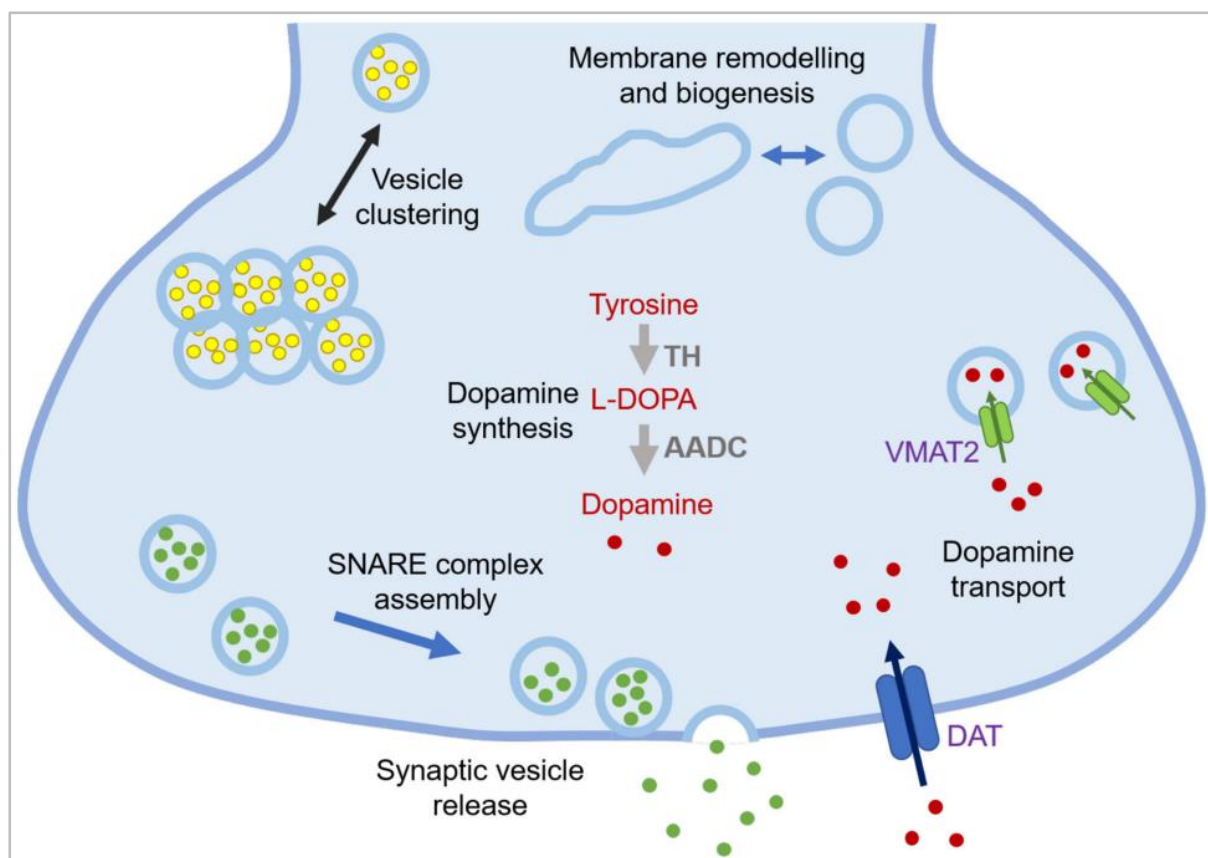


Figure 25. α Syn physiological functions at synapses. The exact physiological functions of α Syn remain to be fully elucidated. α Syn is thought to play roles in membrane remodelling and biogenesis, vesicle clustering, regulation of DA synthesis, SNARE complex assembly and synaptic vesicle release. Image from reference¹⁰⁹.

3.4.1.1 Regulation of synaptic vesicle pooling

α Syn regulates the availability of synaptic vesicles in the reserve pool^{103,110}. It interacts with vesicle-associated proteins as previously mentioned, such as Rab3, which are crucial for vesicle docking and priming at the active zone of the synapse. By clustering and organizing vesicles, α Syn maintains a balance between vesicle storage and release, ensuring that a sufficient pool of readily available vesicles is maintained for efficient neurotransmission.

3.4.1.2 Neurotransmission

Neurotransmission relies on a precisely coordinated sequence of events at the nerve terminal. When an action potential reaches the presynaptic terminal, synaptic vesicles docked at the plasma membrane fuse to release neurotransmitters, enabling the signal to be transmitted to the next neuron¹¹⁰. This fusion process is driven by the formation of the SNARE complex, which consists of synaptobrevin-2 (VAMP2) on the synaptic vesicle and syntaxin-1 and SNAP-25 on the presynaptic membrane. α Syn interacts with VAMP2, stabilizing vesicles and facilitating assembly of the SNARE complex, which ultimately promotes synaptic vesicle fusion with the presynaptic membrane.

3.4.1.3 Membrane curvature and vesicle fusion

As a lipid-binding protein, α Syn plays a crucial role in inducing membrane curvature, which converts larger vesicles into highly curved membrane tubules and smaller vesicles¹⁰³. This ability to reshape membranes is essential for both vesicle formation and fusion. α Syn's role in creating curvature facilitates the fusion of synaptic vesicles with the presynaptic membrane during neurotransmitter release and supports the formation of new vesicles during endocytic recycling, thereby ensuring synaptic transmission.

3.4.1.4 Regulation of DA release

In DA neurons, α Syn is critical for modulating DA levels and release, thus ensuring a correct physiological balance. Excessive DA production can lead to ROS generation during metabolism, which can be detrimental to neurons. To counteract this, α Syn regulates DA synthesis by inhibiting the expression and activity of TH by decreasing its phosphorylation state and stabilizing its dephosphorylated, inactive form^{103,111,112}. In addition to regulating TH, α Syn also influences VMAT2, which is responsible for packaging DA into synaptic vesicles. Studies have shown that KO of α Syn triggers an increased density of VMAT2 molecules per vesicle, indicating an enhanced capacity for DA transport. Conversely, α Syn overexpression inhibits VMAT2 activity, further underscoring its critical role in maintaining DA homeostasis.

3.4.2 Nuclear roles

Although the nuclear role of α Syn remains poorly understood, emerging evidence highlights its involvement in modulating (i) DNA and histones, (ii) transcription factors and (iii) immediate early gene responses¹¹³. α Syn influences gene expression by altering post-translational modifications of DNA and histones through multiple mechanisms. It can either increase gene expression by inducing DNA hypomethylation or repress gene expression through reduced histone acetylation or modifications in histone methylation, with the latter occurring in a retinoic acid (RA)-dependent manner^{113,114}.

As part of synaptic plasticity, α Syn contributes to gene regulation through nuclear translocation of nuclear receptors and transcription factors. It has been shown to bind RA, thereby facilitating its nuclear translocation to regulate transcription factors¹¹³. By activating RA receptor and peroxisome proliferator-activated receptor- γ (PPAR γ), several genes, including *PINK1* and genes involved in fatty acid metabolism, become upregulated. Conversely, α Syn downregulates nuclear receptor related 1 (Nurr1), leading to reduced expression of genes critical for DA biosynthesis, including *TH* and *AADC* as well as genes linked to mitochondrial biogenesis and antioxidant responses.

Additionally, cytosolic α Syn interacts with transcription factors involved in mitogen-activated protein kinase (MAPK) signalling, resulting in the downregulation of specific gene response elements¹¹³.

4. Alpha-synuclein relevance to Parkinson's disease pathogenesis

4.1 Pathological conformations

In its physiological state, α Syn exists in a dynamic equilibrium between a soluble unfolded monomeric form and a membrane bound state, where its secondary structure can adopt either a single elongated α -helix or a broken α -helix depending on the membrane curvature¹⁰³ (Figure 26). However, under pathological conditions, α Syn transitions to a β -sheet-rich amyloid conformation. This misfolded form is closely associated with α Syn aggregation and is believed to exhibit neurotoxic properties.

While the precise nature of the neurotoxic species remains to be fully elucidated, it is widely hypothesised that misfolded α Syn forms β -sheet-rich oligomers, often referred to as protofibrils¹⁰³. These oligomers are highly unstable and can either redissolve or mature into elongated and structured amyloid fibrils, which eventually deposit in LBs¹⁰⁹. Although the mechanisms of LB formation and maturation are yet to be established, it is thought that this process may involve not only α Syn amyloid deposition but also interactions between α Syn and lipid membranes.

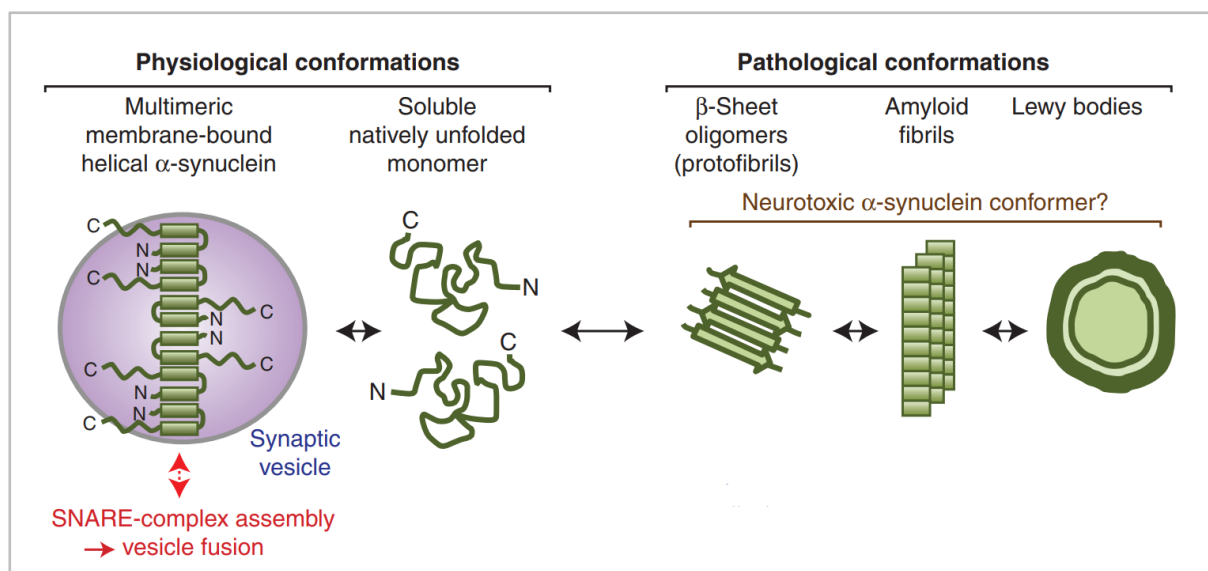


Figure 26. α Syn physiological and pathological conformations. Soluble α Syn is natively unstructured and monomeric. Upon binding to highly curved membranes, such as synaptic vesicles, α Syn undergoes a conformational change, folding into an amphipathic α -helix. This conformational change is associated with multimerization and plays a crucial role in mediating α Syn's function as a chaperone for the SNARE complex. Under pathological conditions, soluble α Syn can form β -sheet-rich oligomers, known as protofibrils, which subsequently convert into amyloid fibrils that ultimately accumulate in LB. Image adapted from reference¹⁰³.

4.2 Toxic functions

α Syn aggregation under pathological conditions may contribute to PD pathogenesis and progression in two key ways. First, the recruitment of physiologically active α Syn into pathological aggregates diminishes its normal function, leading to a loss-of-function mechanism¹¹⁵. Second, these toxic aggregates disrupt essential cellular processes, impairing cellular homeostasis and triggering gain-of-toxic function mechanisms.

4.2.1 Defects in synaptic vesicle cycle

With regard to α Syn's role in regulating synaptic vesicle pools and neurotransmission, studies have shown that α Syn overexpression reduces the size of the reserve pool and decreases the number of docked vesicles, suggesting that elevated α Syn levels, even without overt toxicity, lead to defects in synaptic vesicle recycling^{110,116}. Moreover, antibody-mediated disruption of α Syn results in a dose-dependent reduction of synaptic vesicles in the reserve pool, along with depletion of the docked readily available vesicles pool^{110,117}. Additionally, α Syn oligomers may form pores in synaptic vesicle membranes, thereby increasing membrane permeability¹¹⁸. Taken together, these findings indicate that α Syn regulates vesicle recycling and docking in a dose-dependent manner, where both α Syn loss-of-function and gain-of-toxic-function can impair vesicle dynamics (Figure 27). Under pathological conditions, the accumulation of misfolded α Syn or the sequestration of functional α Syn into aggregates leads to impaired synaptic vesicle clustering and reduced SNARE complex assembly. This disruption of the synaptic vesicle cycle compromises neurotransmission and contributes to long-term neuronal dysfunction and degeneration.

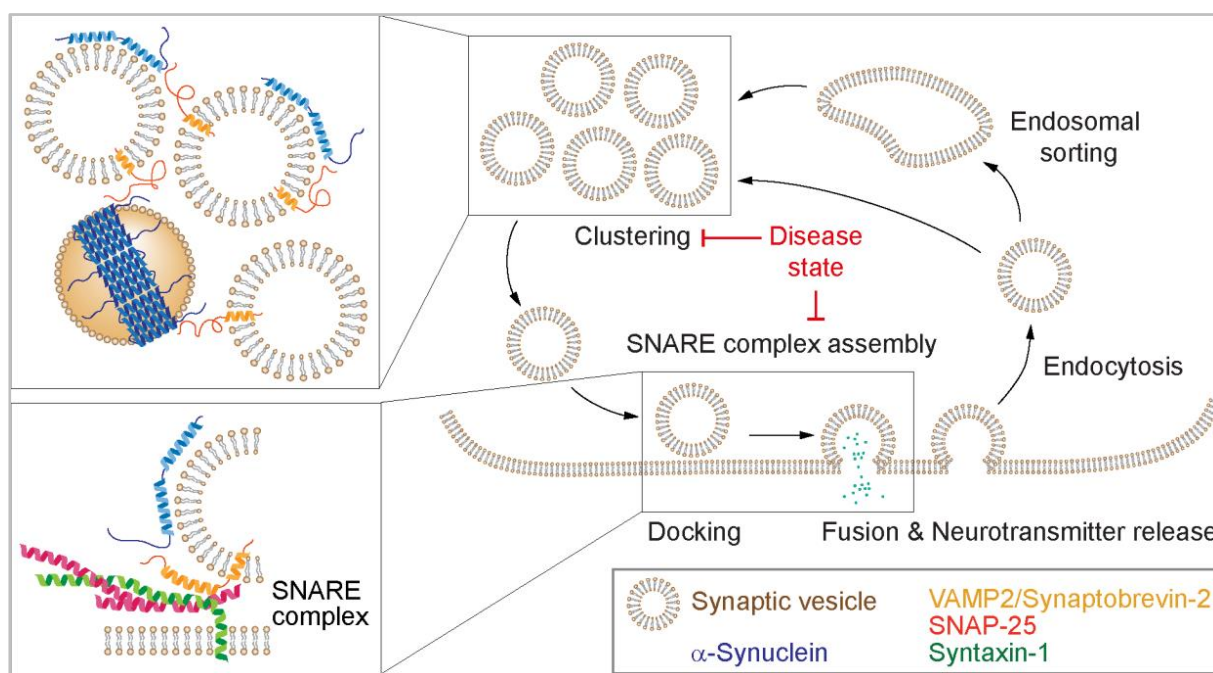


Figure 27. Effects of pathological α Syn on the synaptic vesicle cycle. Upon the arrival of an action potential at the presynaptic terminal, docked synaptic vesicles fuse with the plasma membrane, releasing neurotransmitters to enable propagation of the signal. This fusion is driven by formation of the SNARE complex (syntaxin-1 and SNAP-25) on the presynaptic membrane and VAMP2 on the synaptic vesicle. After

neurotransmitter release, vesicle components are recycled via endocytosis to maintain the vesicle cycle. α Syn binds to synaptic vesicle membranes and interacts with VAMP2, promoting the clustering of synaptic vesicles (*top inset*) and facilitating SNARE complex assembly (*bottom inset*). Under pathological conditions, either the presence of misfolded α Syn or the depletion of functional α Syn due to its recruitment into aggregates impairs synaptic vesicle clustering and disrupts SNARE complex formation, thereby impairing neurotransmission. Image from reference¹¹⁰.

4.2.2 Defects in the nucleus

Overexpression of the soluble form of α Syn increases its presence in the nucleus, with p α Syn at serine 129 promoting this nuclear localization^{113,114}. However, the pathological cytoplasmic aggregation of α Syn reduces its nuclear translocation, leading to a loss of its physiological nuclear functions. This deficiency may contribute to DNA damage, triggering pro-apoptotic signalling pathways and compounding neuronal vulnerability.

Interestingly, α Syn exhibits an autogenous feedback mechanism by binding its own mRNA, which may play a critical role in regulating its localization and protein levels¹¹³. This feedback mechanism could influence the balance between nuclear and cytoplasmic α Syn, potentially exacerbating dysregulation in disease states.

Furthermore, aggregated α Syn can sequester DNA methyltransferases in the cytoplasm, disrupting normal DNA methylation patterns and impairing gene regulation¹¹⁹. In addition, α Syn overexpression has been shown to induce cellular senescence accompanied by activation of the p53 pathway and DNA damage responses¹²⁰.

4.3 Post-translational modifications

α Syn undergoes various post-translational modifications (PTM)s, mostly within its C-terminal tail, including phosphorylation, ubiquitination, nitration, oxidation, acetylation, glycation and truncation¹⁰⁹. These PTMs can alter the protein's charge and structure, affecting its binding affinities with other proteins and lipids and potentially contributing to α Syn-mediated neurotoxicity. A summary of the known PTMs of α Syn is shown in Figure 28 ([Figure 28](#)).

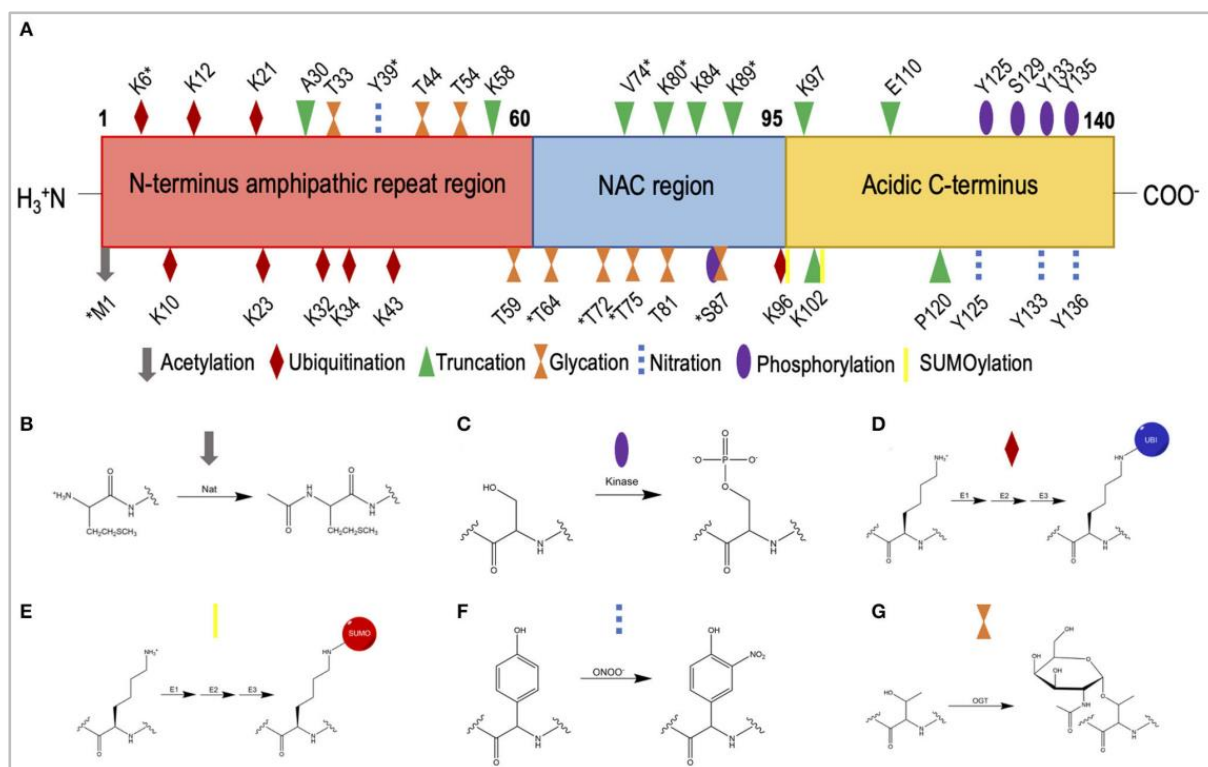


Figure 28. Summary of currently known PTMs of α Syn. (a) PTM sites labelled in the amino acid sequence of α Syn; *indicates PTMs within low-solubility areas identified using CamSol method. (b) N-terminal acetylation carried out by N-acetyltransferases (Nat). (c) Phosphorylation, which occurs via the action of a kinase on serine and tyrosine residues; in this example the phosphorylation of a serine residue is shown. (d) Ubiquitination, where ubiquitin is added to lysine residues catalysed by the sequential action of E1 (ubiquitin-activating enzyme), E2 (ubiquitin-conjugating enzyme) and E3 (ubiquitin ligase). (e) SUMOylation, where small ubiquitin-like modifier (SUMO) is added to lysine residues via a thioester bond catalysed by the sequential action of E1 (SUMO-activating enzyme), E2 (SUMO-conjugating enzyme), and E3 (SUMO ligase). (f) Nitration, where tyrosine residues are nitrated. (g) O-GlcNAcylation, where O-GlcNAc transferase (OGT) catalyses the addition of N-acetylglucosamine (GlcNAc) to the hydroxyl group of serine and threonine residues; in this example the O-GlcNAcylation of a threonine residue is shown. Image from reference¹⁰⁹.

4.3.1 Phosphorylation

α Syn physiologically undergoes cycles of phosphorylation and dephosphorylation *in vivo*, with serine and tyrosine residues being the most common phosphorylation sites¹⁰⁹ (Figure 28). Among these, phosphorylation at serine 129 (pS129) and serine 87 (pS87) are particularly relevant in the context of PD, as they are enriched in LBs. Remarkably, pS129 has long been associated with PD, with levels increasing from approximately 5% in healthy brains to nearly 90% in LBs. Despite this strong correlation, whether pS129 precedes or follows LB formation, inhibits or promotes α Syn aggregation, and enhances or reduces α Syn affinity for lipid membranes remains to be elucidated. Recent studies suggest that pS129 may play a role in α Syn's physiological regulation^{121,122}. Increased neuronal activity triggers α Syn phosphorylation at S129, which in turn facilitates the interaction of α Syn with VAMP2, thus promoting synaptic vesicle clustering, limiting vesicle mobility, and reducing the availability of vesicles for recycling at the plasma

membrane. This process may serve as a homeostatic mechanism, attenuating neurotransmitter release in response to excessive neuronal activity.

The link between pS129 α Syn (p α Syn) and PD pathology is further supported by the former's enrichment in LBs and its disruption in PD-linked mutations. For example, mutations in *PARK6*, which encodes the protein kinase PINK1, one of the key regulators of α Syn phosphorylation, represent the second most common cause of autosomal recessive familial PD¹⁰⁹. Additionally, pS129 α Syn levels in CSF were found to be significantly elevated in PD patients compared to controls and are correlated with disease progression and duration. However, whether pS129 promotes or mitigates α Syn aggregation remains a subject of debate. Some studies suggest that pS129 makes α Syn more prone to aggregation^{123–125} while others suggest that pS129 α Syn is preferentially targeted for ubiquitination and degradation via the UPS, reducing phosphorylated soluble α Syn levels as it is cleared during the aggregation process¹²⁶. Alternatively, pS129 may represent a protective cellular response to aggregation, promoting native protein-protein interactions to help restore normal function¹²².

4.3.2 Ubiquitination

Ubiquitination marks α Syn for degradation through the UPS. The colocalization of α Syn with ubiquitin in LBs suggests that ubiquitinated α Syn is sequestered in pathological inclusions¹⁰³. Several E3 and E4 ligases have been identified as responsible for tagging α Syn for degradation. In PD, dysfunction in the UPS likely impairs the clearance of ubiquitinated α Syn contributing to its accumulation and the formation of LBs¹⁰⁹. Mutations in the *Parkin* gene, encoding an E3 ligase, can lead to familial PD¹⁰⁹. Moreover, *Parkin* gene therapy is effective against α Syn-mediated toxicity and neuronal loss¹²⁷.

4.3.3 Nitration and oxidation

Oxidative stress is a major factor in the pathogenesis of PD. ROS and nitric oxide derivatives can lead to nitration of tyrosine residues in α Syn, an irreversible PTM¹²⁸. Nitrated α Syn is enriched in LBs compared to healthy brains, indicating a pathological role¹⁰⁹. Nitrated tyrosine residues are highly reactive and can promote cross-linking through the formation of dityrosine bonds contributing to α Syn oligomerization. In fact, nitrated α Syn has been shown to induce cytotoxicity in neuroblastoma cells and in the SN of rats. Additionally, nitrated α Syn has a reduced affinity for phospholipid vesicles compared to its wt form, which may impair its normal membrane-binding function and contribute to neurodegeneration.

4.3.4 Acetylation

N-terminal acetylation is a highly prevalent modification in α Syn, with over 80% of α Syn molecules constitutively acetylated at their N-terminus¹⁰⁹. This modification involves the addition of an acetyl group to the amine group at the N-terminus, which results in the loss

of a positive charge in a region that is otherwise poorly soluble. Since phospholipids are generally negatively charged, this modification enhances α Syn's ability to form α -helices, increases its affinity for membrane binding, and makes it more resistant to aggregation. As a result, N-terminal α Syn acetylation is observed in both healthy individuals and PD patients¹⁰³.

4.3.5 Glycation

Glycated products and α Syn colocalize in the brains of PD patients, suggesting that the glycation of α Syn may serve as a pathological hallmark of LBs¹⁰³. This glycation process leads to cross-linking of recombinant α Syn *in vitro*, accelerating its aggregation and contributing to its cytotoxic effects.

4.3.6 Truncation

Irreversible truncation of α Syn at both the N- and C-termini is a frequent PTM, with over 15% of α Syn found in LBs being truncated¹⁰⁹. Truncation is thought to result from the incomplete degradation of α Syn by various proteases. C-terminal truncation, in particular, plays a significant role in α Syn pathology, as it may enhance the protein's ability to act as an effective seed for further aggregation¹²⁸. Truncated α Syn accelerates the formation of high-molecular-weight aggregates and exacerbates neurotoxicity. Additionally, since α Syn is primarily localized at the presynaptic terminal, it may serve as a substrate for soluble or membrane-associated proteases.

4.4 α Syn levels and species in PD pathology

4.4.1 α Syn and aging

In aged individuals, α Syn levels in the SNpc are nearly twice as high as those found in younger people, a variation that concurs with reduced TH levels, which is critical for DA synthesis¹²⁹. In the elderly without PD, elevated α Syn levels are associated with decreased DA metabolism, two facts that may predispose individuals to PD. This age-associated increase in α Syn, combined with DA reduction, supports the reason why aging is considered the primary risk factor for PD. It is worth noting that the age-associated increase in α Syn levels is not accompanied by a significant increase in *SNCA* mRNA expression, suggesting that the regulation of this protein may occur at translational or degradational levels¹³⁰.

4.4.2 α Syn burden and its implications for PD

Brain regions with low α Syn accumulation rarely exhibit LB pathology, suggesting that a certain α Syn threshold concentration may be required for PD-associated neuropathological inclusions¹²⁹. Supporting this, PD patients with *SNCA* triplication show approximately double α Syn levels compared to controls, displaying significant LB

pathology in the brainstem and cortex along with severe clinical symptoms. Similarly, PD patients with homozygous *SNCA* duplications suffer a more severe disease manifestation compared to those who are heterozygous, further highlighting the link between elevated α Syn levels and the extent of PD pathology.

4.4.3 α Syn levels in biospecimens

Recently, considerable efforts employing diverse techniques have been directed towards measuring α Syn in various biospecimens such as brain homogenates, CSF, blood, saliva, tears, skin, retina, gut mucosa and gonadal tissue¹³¹. Findings to the present time, however, require replication and validation across multiple laboratories and large patient cohorts to reach the clinical setting.

4.4.3.1 Brain

Analyses of *post-mortem* brain samples from individuals with sporadic PD have yielded inconsistent findings regarding α Syn expression levels. Several studies reported significantly increased *SNCA* mRNA levels in the SN of PD patients compared to controls^{132,133}, while others observed decreases^{134,135}. Interestingly, *SNCA* mRNA levels are notably reduced in neurons containing LBs in idiopathic PD cases, preceding complete neurodegeneration¹²⁹. In brain regions affected by LB pathology, both with and without neuronal loss, soluble total α Syn protein levels generally appear unchanged in PD brains relative to age-matched healthy controls^{129,136}. However, emerging evidence indicates a disturbed equilibrium between physiological α Syn conformations in PD. Indeed, studies on *post-mortem* brain tissue revealed a reduction in helical α Syn forms together with increased unfolded forms of the protein which are more susceptible to aggregation¹³⁶. In contrast, p α Syn levels in insoluble brain fractions are significantly elevated in PD brains relative to controls¹³⁷. α Syn proximity ligation assay (PLA) studies revealed that PD brains exhibit higher levels of oligomeric α Syn, often prior to LB formation, compared to age- and sex-matched controls¹³⁸. Additionally, RT-QuIC assays detected greater α SYN seeding activity in PD brain homogenates versus controls, indicating enhanced aggregation potential^{62,139}.

Collectively, these findings suggest that in PD, soluble α Syn undergoes PTMs, such as phosphorylation, that promote its aggregation into insoluble oligomers, eventually forming LBs. This pathological shift from soluble α Syn to aggregated forms may deplete the pool of functional α Syn and, in certain contexts, is accompanied by reduced *SNCA* expression. This points to a state of pathological proteinopenia. The aggregation of α Syn has dual consequences: (i) impaired cellular function due to the reduced availability of functional α Syn and (ii) toxic effects associated with aggregated forms of the protein.

4.4.3.2 CSF

Studies consistently show that PD patients exhibit decreased CSF levels of total α Syn together with increased levels of both phosphorylated and oligomeric α Syn compared to controls^{131,140,141}. In line with this observation, using the oligomeric-to-total α Syn ratio was proposed as a sensitive and specific biomarker to differentiate PD patients from healthy individuals¹³¹. Furthermore, PMCA assays revealed high α Syn seeding capacity in PD patients in contrast to absent α Syn seeding capacity in healthy controls¹⁴².

4.4.3.3 Blood

While studies have not shown conclusive differences in total blood α Syn levels between PD patients and controls, both plasma oligomeric α Syn and p α Syn levels are consistently elevated in PD patients^{131,140}. Additionally, α Syn fibril analysis using RT-QuIC in serum samples was used to successfully differentiate PD patients from controls across various cohorts⁶³.

4.4.3.4 Skin

Various studies have reported significantly increased total α Syn deposition in skin biopsy samples from PD patients compared to healthy controls, with higher levels observed in patients with advanced disease or autonomic dysfunction^{143,144}. A recent study showed that p α Syn was present in skin biopsies from 92.7% of PD patients, contrasting with 3.3% in healthy controls¹⁴⁵. Furthermore, studies analysing α Syn PLA have visualised increased oligomeric α Syn within the synaptic terminals of autonomic fibers in PD patient skin samples relative to controls¹⁴⁶. In parallel, RT-QuIC and PMCA assays both demonstrated enhanced α Syn aggregation in skin biopsies from PD patients¹⁴⁷.

Figure 29 summarizes α Syn levels and species observed in PD across brain, CSF, blood and skin samples ([Figure 29](#)).

PD vs HC	Total α Syn	p α Syn	Oligomeric α Syn	Aggregated α Syn
Brain	Inconsistent results ↑ ↓	↑	↑	↑
CSF	↓	↑	↑	↑
Blood	Inconsistent results	↑	↑	↑
Skin	↑	↑	↑	↑

Figure 29. Summary of total, phosphorylated, oligomeric and aggregated α Syn levels in PD compared to healthy controls (HC) observed in brain, CSF, blood and skin samples. In PD patients, phosphorylated, oligomeric and aggregated α Syn species are elevated in brain, CSF, blood and skin samples relative to HCs. Total α Syn levels in brain tissue homogenates are comparable to HCs, while in CSF, they are reduced. Studies based on findings in blood report inconsistent results for total α Syn, while skin samples generally show an increase in total α Syn. Illustration created with Biorender.com.

4.5 α Syn prion-like properties

4.5.1 Braak's hypothesis and α Syn-based PD staging

In 2003, Braak and colleagues proposed a six-stage model of PD progression based on the predictable spread of α Syn pathology, which appears to initiate in the peripheral nervous system and advances in a caudal-to-rostral pattern to the CNS¹⁴⁸ (Figure 30). Initially, in Stage 1, α Syn-positive inclusions are detected in the olfactory system, the enteric nervous system and the lower brainstem^{10,11,52}. This corresponds with early, non-motor prodromal PD symptoms such as hyposmia and constipation. As α Syn pathology progresses to the pons and spinal cord gray matter in Stage 2, early motor symptoms, such as bradykinesia, begin to appear. In Stage 3, the pathology extends further into the

pons, midbrain, basal forebrain, and limbic system, intensifying motor symptoms and, in some patients, triggering neuropsychiatric manifestations. By Stage 4, the limbic system is increasingly affected, along with the interstitial nucleus, thalamus and temporal cortex, regions that support cognitive and emotional functions. In Stages 5 and 6, α Syn pathology spreads to multiple cortical regions such as the neocortex leading to cognitive impairments commonly observed in advanced PD phases.

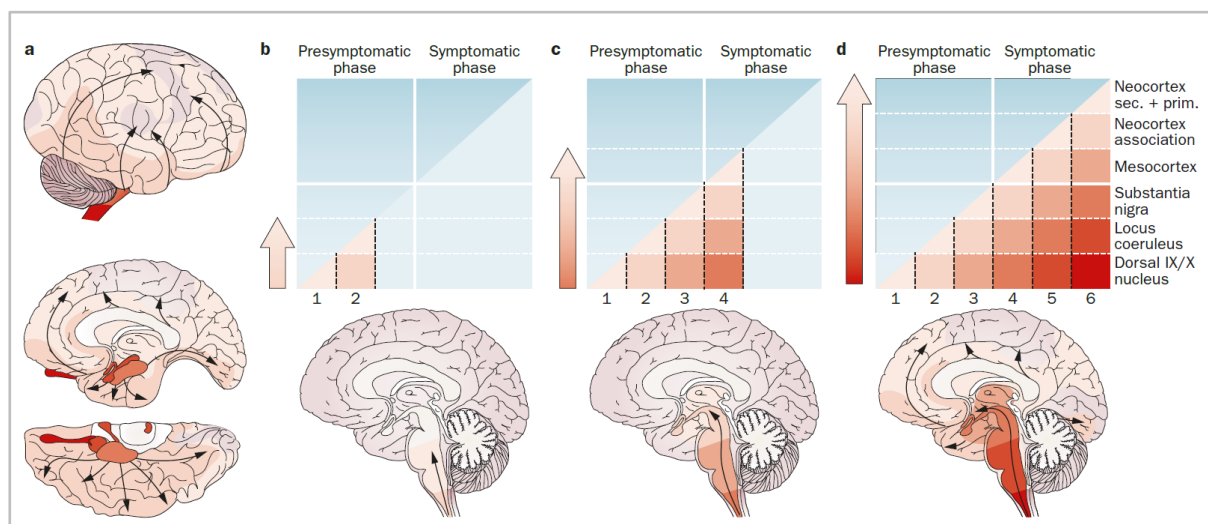


Figure 30. Braak's PD staging. (a) Rostrocaudal progression of pathological α Syn deposition in the brain (arrows). The gradient of red shading is indicative of the severity of the pathology. (b) Brain α Syn deposition correlates with PD symptoms. Stage 1: lesions occur in the olfactory regions and the DMNX. Stage 2: lesions are observed in the pontine tegmentum. Stage 3: lesions reach the pedunculopontine nucleus, the basal forebrain and the SN. Stage 4: lesions extend to the hypothalamus, portions of the thalamus and the anteromedial temporal mesocortex. Stages 5 and 6: lesions spread to neocortical areas followed by first-order association areas and primary sensory fields. Stages 1, 2 and 3 correspond to the presymptomatic phases of PD, during which time non-motor symptoms emerge. The first clinical symptoms of PD typically appear during Stage 3 or early Stage 4. Cognitive deficits associated with late PD arise in Stages 5 and 6. Image from reference¹⁰.

4.5.2 Cell-to-cell transmission of α Syn

4.5.2.1 Prion-like spreading

Braak's hypothesis suggests that a neurotropic agent, possibly a pathogen or fragments of misfolded α Syn may enter the body through the nasal or gastric routes¹⁴⁹. In the nasal pathway, this agent could access the brain by traveling through the olfactory epithelium to the olfactory bulb, while in the gastric route, it might infiltrate the gut and reach the submucous plexus^{149,150}. From there, it can spread along the vagus nerve to the DMNX, ultimately progressing to other regions of the CNS. This theory is supported by studies in which grafts of embryonic DA neurons transplanted into the brains of PD patients developed LBs closely resembling those in the PD brains^{103,151,152}. This suggests that misfolded α Syn from the host was transferred into the transplanted neurons, where it spread in a prion-like manner. Such findings highlight the possibility that misfolded α Syn could propagate through neural networks and thereby contribute to the progressive spread of PD pathology.

4.5.2.2 Mechanisms of release and uptake

α Syn is released from neurons through both passive and active pathways, often via unconventional exocytosis mechanisms^{153,154} (Figure 31). Passive release can occur by diffusion across the cell membrane or through damaged cellular membranes¹⁵⁴. Notably, α Syn aggregates can disrupt lipid membrane integrity, thereby facilitating α Syn release. Active release involves both endoplasmic reticulum(ER)-Golgi-dependent and independent exocytosis. An additional pathway, known as misfolding-associated protein secretion (MAPS) uses the ER-associated deubiquitylase USP19 to export misfolded cytosolic proteins. In this process, misfolded α Syn is recruited to the ER surface for deubiquitylation where it is encapsulated in late endosomes and ultimately secreted into the extracellular space. MAPS contributes to protein homeostasis by removing aberrant proteins through unconventional secretion mechanisms. Exosomes, which are derived from the fusion of multivesicular bodies (MVBs) with the plasma membrane, also play a crucial role in α Syn propagation. These vesicles facilitate intercellular communication by carrying proteins and RNAs; their release is calcium-dependent which links α Syn exocytosis with neuronal activity. Additionally, tunnelling nanotubes provide another route for α Syn transfer between cells.

α Syn can be internalized by neurons through both passive diffusion and active endocytosis mechanisms¹⁵⁴ (Figure 31). Monomeric α Syn easily enters cells via passive diffusion, while direct interaction with lipid and protein components of the plasma membrane allows its non-specific membrane penetration. Additionally, α Syn uptake occurs via various endocytic pathways which are determined by the α Syn conformations. Large aggregates are internalized through actin-dependent phagocytosis, while smaller α Syn species may enter through pinocytosis. Exosome-associated α Syn oligomers show increased uptake by neurons and microglia compared to free α Syn, suggesting that exosomes facilitate the efficient delivery of α Syn into target cells. However, the exact mechanism underlying the internalization of α Syn-carrying exosomes remains to be clarified.

Once internalized by neighbouring cells, α Syn can initiate self-aggregation by recruiting endogenous α Syn monomers, which then serve as seeds for further aggregate expansion.

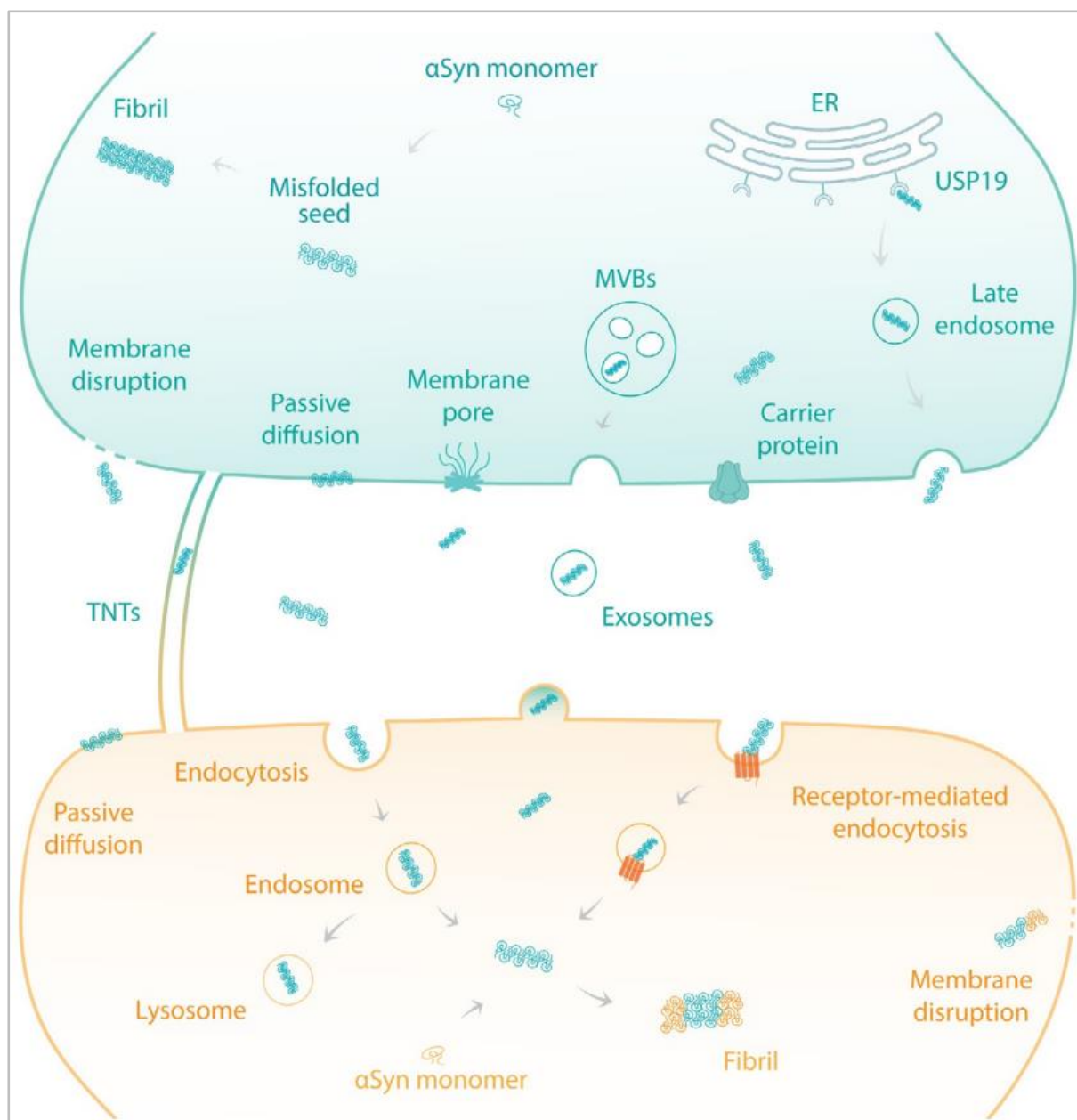


Figure 31. Mechanisms of α Syn transfer between neurons. α Syn can be released by neurons in both monomeric and aggregated forms through multiple pathways. Cells with damaged plasma membranes release α Syn passively. On the other hand, α Syn can also be transferred through specialized structures like tunnelling nanotubes or it can diffuse passively across the plasma membrane. Other active release pathways include exocytosis via pore-like structures, exosome secretion, and carrier-mediated transport. Additionally, α Syn can also be directed to the ER where it is deubiquitylated by USP19, encapsulated into late endosomes and secreted via the MAPS pathway. Once released into the extracellular environment, α Syn aggregates can be internalized by neighbouring cells through direct diffusion across the plasma membrane, endocytosis mechanisms or receptor-mediated endocytosis. Exosome-bound α Syn may enter target cells through vesicle fusion with the plasma membrane. Upon uptake, α Syn seeds can either be processed within endosomes or disrupt the endosomal membrane to access the cytosol. In the cytosol, these seeds recruit endogenous α Syn monomers, triggering aggregation and fibrillization. This aggregation process may ultimately damage the cell membrane, releasing α Syn aggregates back into the extracellular space and perpetuating the toxic cycle of propagation and cell-to-cell transmission. Image from reference¹⁵⁴.

4.5.3 α Syn strain variability and its influence on pathogenic spread

In addition to PD, other neurodegenerative disorders such as dementia with LBs (DLB) and MSA are classified as synucleinopathies due to their shared feature of pathological α Syn aggregation¹⁵⁵. While PD and DLB mainly exhibit intraneuronal α Syn deposits, MSA is characterised by oligodendroglial cytoplasmic inclusions. Despite their shared hallmark of α Syn inclusion pathology, these disorders differ in clinical symptoms and disease progression, which may be influenced by differences in α Syn aggregate structure and behaviour.

It has been proposed that neuronal and oligodendrocyte environments influence α Syn aggregation to adopt distinct structural conformations. For example, research indicates that MSA-derived α Syn and PD-/DLB-derived α Syn have distinct conformational and biological properties¹⁵⁵. In line with this, different buffer conditions generate different α Syn conformers termed “ribbons” and “fibrils” which vary in toxicity, seeding potential and capacity for propagation¹⁵⁶. Interestingly, MSA brain tissue resembles the ribbon-like structure, while PD/DLB samples align with the fibril-like structure¹⁵⁷. Patient-derived α Syn strains also exhibit structural variability concurring with disease type. For instance, MSA-derived α Syn shows a higher proportion of β -sheet structures, which are more toxic and resistant to protease degradation compared to PD and DLB¹⁵⁸. Seeding amplification assays from brain and CSF samples also show that MSA-derived α Syn exhibits faster aggregation kinetics compared to PD, although PD α Syn tends to reach a higher fluorescence plateau suggestive of differences in final aggregate structure and stability. These findings underscore the notion that α Syn strain diversity may drive specific pathological patterns and disease progression in synucleinopathies.

4.6 Impaired α Syn degradation in PD

Under healthy conditions, intracellular α Syn homeostasis is maintained by the UPS and the lysosomal autophagy system, where both chaperone-mediated autophagy and macroautophagy contribute⁵². Extracellular proteases can also cleave α Syn outside cells. Impairment of these systems, however, may lead to pathological α Syn accumulation (Figure 32). Aging, the main risk factor for PD, is associated with a natural decline in UPS and lysosomal autophagy system functions which correlate with α Syn levels in the SN during normal aging. In PD, lysosomal enzyme levels are notably reduced, particularly in neurons containing α Syn inclusions. Moreover, markers of chaperone-mediated autophagy are decreased and autophagosomes accumulate, indicating disrupted autophagy. Furthermore, α Syn has been shown to inhibit UPS function, while accumulated α Syn can obstruct macroautophagy and chaperone-mediated autophagy, creating a vicious cycle of impaired proteostasis and α Syn accumulation. This cycle perpetuates α Syn aggregation which further disrupts cellular degradation systems.

Conversely, α Syn aggregation and mitochondrial dysfunction also create a cycle where each factor amplifies the other’s damaging effects, ultimately leading to cellular stress⁵² (Figure 32). α Syn accumulation in the mitochondria impairs complex I activity, leading to increased oxidative stress. Elevated oxidative stress levels are indeed observed in PD

patients, but whether this stress is a primary cause of neurodegeneration or a secondary effect is not known.

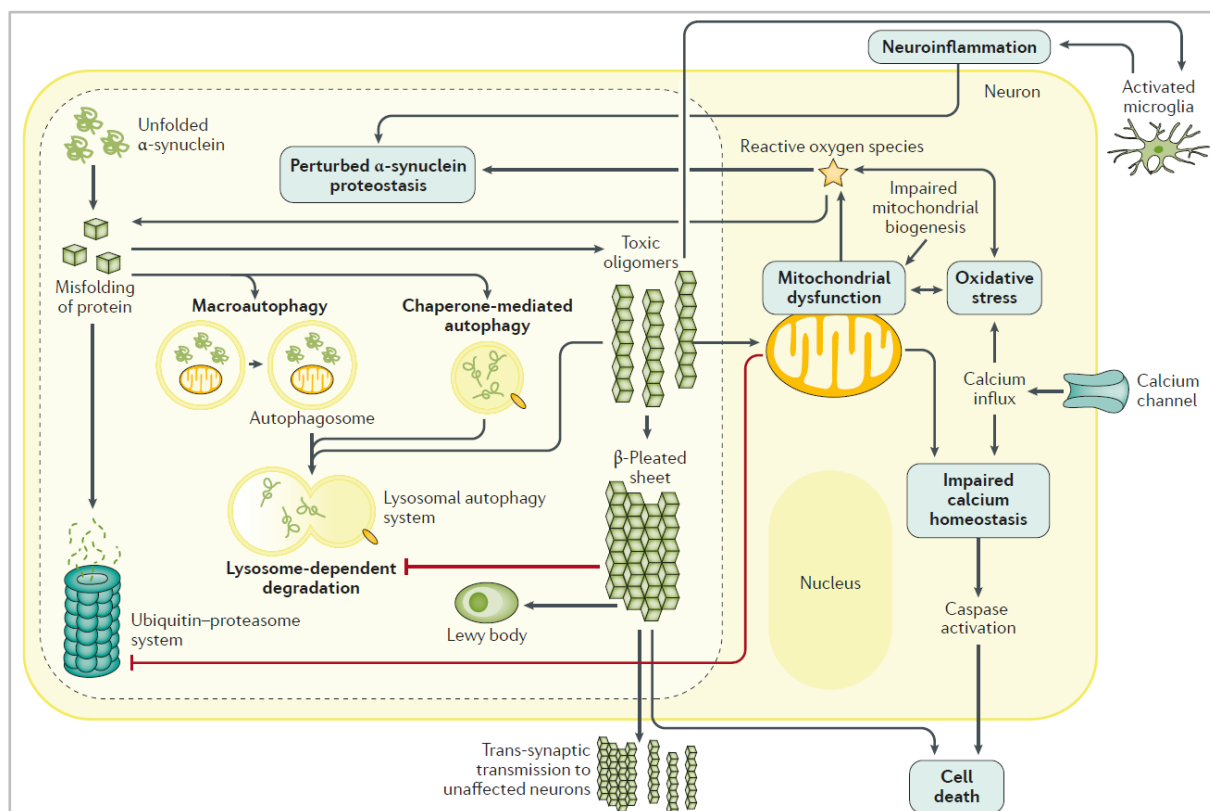


Figure 32. Impaired α Syn degradation in PD. Misfolded α Syn can be degraded through macroautophagy, chaperone-mediated autophagy, and the UPS. When these degradation pathways are compromised, toxic α Syn aggregates accumulate, which in turn inhibit further degradation mechanisms and thus establish a pathological cycle. These aggregates can also accumulate in the mitochondria, disrupting UPS function and promoting mitochondrial dysfunction which generates oxidative stress. The resulting effects contribute to impaired α Syn proteostasis, disrupted calcium homeostasis, and neuroinflammation, thus compromising cell viability. Image from reference⁵².

4.7 Summary of the α Syn pathological roles

Pathological roles of α Syn are illustrated in the figure 33 (Figure 33). At a cellular level, aggregated α Syn disrupts multiple critical functions, including mitochondrial integrity leading to ROS production, impaired axonal transport, compromised autophagy and lysosomal functions, as well as UPS and disturbed calcium homeostasis¹⁵⁰. Recent research has also indicated that α Syn may contribute to DNA damage, possibly due to its nuclear localization and oxidative stress-inducing properties. These molecular alterations compromise cell viability, thereby contributing to neurodegeneration. Furthermore, α Syn release to the extracellular space activates microglia and induces astrogliosis to promote α Syn clearance. This response can ultimately lead to neuroinflammation and demyelination, exacerbating neurodegenerative effects.

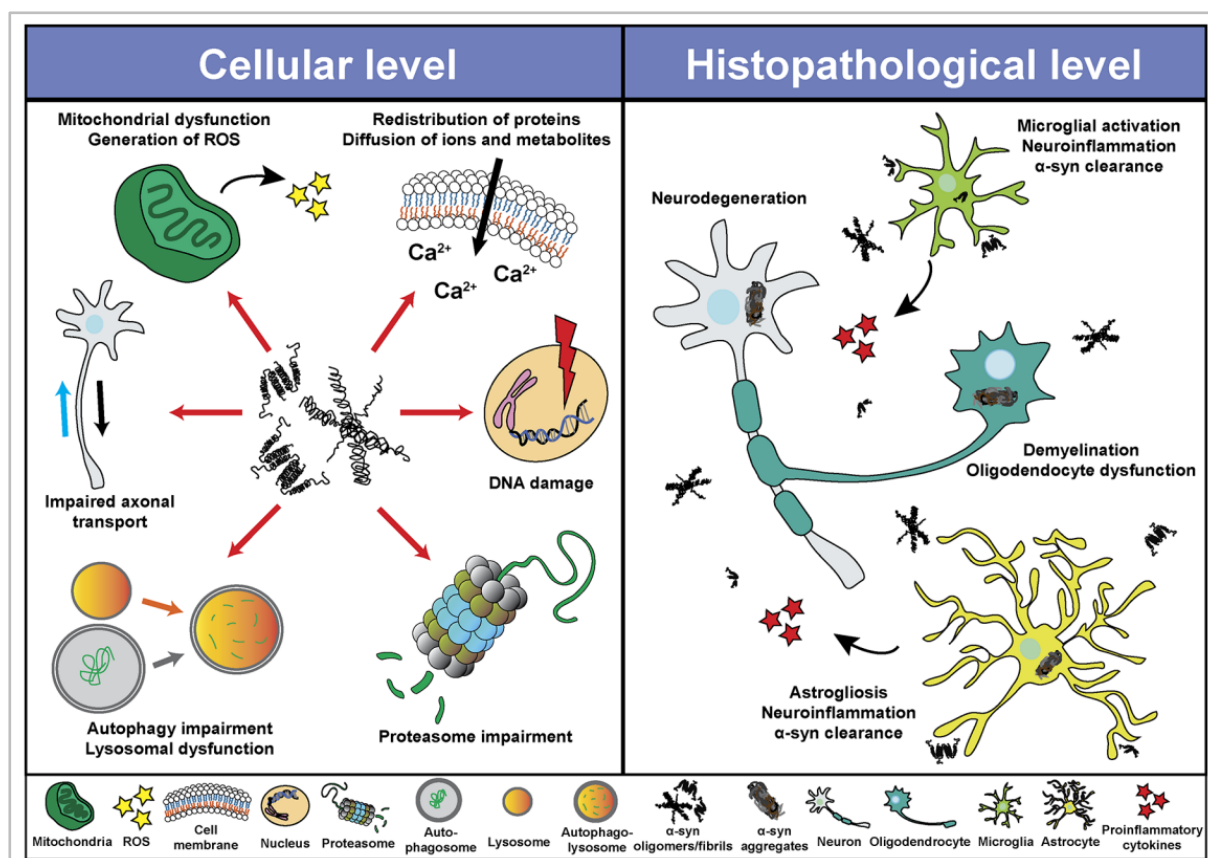


Figure 33. Pathological roles of α Syn. Schematic overview of pathological roles of α Syn, including some cellular processes (*left*) and histopathological events (*right*). Image from reference¹⁵⁰.

4.8 α Syn as a therapeutic target

Mutations in the *SNCA* locus as well as duplications or triplications of its wt form are linked to autosomal dominant PD. Furthermore, α Syn is not only a primary component of LBs, but also plays a key role in the *post-mortem* diagnosis of idiopathic PD and, more recently, the *in vivo* diagnosis of PD through α Syn SAA. These factors together position α Syn as a potential target for therapeutic interventions.

Immunotherapies targeting α Syn have been hypothesised to reduce its aggregation, reduce its prion-like spreading properties and neuroinflammation, and promote intracellular or extracellular clearance¹⁵⁹. Despite initial promise in preclinical models, two recent vaccination clinical trials in early-stage PD (cinpanemab and prasinezumab) yielded negative results^{160–162}. Although both trials confirmed that the antibodies effectively bound native α Syn in human serum, they did not trigger a disease-modifying neuroprotective effect. Several factors likely contributed to these outcomes, including the reliance on clinical scales rather than sensitive biomarkers such as α Syn SAA, the heterogeneity of patient populations, and the timing of therapeutic intervention¹⁶². Specifically, it is increasingly evident that treatment initiated during prodromal stages may be critical to achieving meaningful results.

In parallel, other approaches using novel peptides, antisense oligonucleotides, and exosomes among others have focused on gene-silencing mechanisms targeting *SNCA* expression¹⁵⁹. For instance, the intranasal administration of indatraline-a monoamine uptake inhibitor- conjugated with an antisense oligonucleotide successfully suppressed α Syn mRNA transcription selectively in monoaminergic neurons in a PD mouse model¹⁶³. This intervention was associated with improved DA neurotransmission, underscoring the potential efficacy of gene-silencing approaches.

While targeting α Syn is a promising strategy, several challenges will need to be addressed¹⁵⁹. Physiologically, α Syn plays essential roles in synaptic function and neuronal plasticity, meaning that excessive reductions in α Syn levels could disrupt cellular homeostasis. Moreover, therapeutic agents should cross the BBB, representing a major obstacle for effective delivery. Achieving sustained therapeutic efficacy is another critical concern requiring innovative methodologies to avoid frequent invasive administrations. Finally, immunotherapeutic approaches must be carefully designed to minimize the risk of adverse immune responses.

4.9 α Syn-based PD rodent models

4.9.1 Viral vector-mediated α Syn overexpression

Viral vector approaches are commonly employed to overexpress human α Syn (α SYN) in the SNpc of both rats and mice. Among these vectors, recombinant adeno-associated viral vectors (rAAV) and lentiviral vectors have been widely used, with rAAVs preferred for their efficient transduction, long-term expression and safety profile¹⁶⁴. A major advantage of this model is its ability to replicate the time-course of PD, making it feasible to recreate pre-symptomatic, early symptomatic and advanced phases of the disease. Moreover, rAAV-mediated overexpression allows researchers to selectively express either wt or mutant forms of the protein, offering flexibility in studying specific pathological features. However, observed effects are heterogenous due to multiple factors including viral titer, serotype, promoters and enhancers, and differences in production and purification methods.

rAAV-mediated overexpression of both wt and PD-associated α SYN mutants (i.e., A53T and A30P) generally results in progressive DA neuronal loss in the SNpc, loss of DA terminals in the STR, and decreased striatal DA levels^{165,166}. Nevertheless, the extent of neurodegeneration varies across studies. In terms of α Syn pathology, overexpression results in p α Syn accumulation¹⁶⁶, with some studies reporting proteinase-K-resistant aggregates^{167–169}. However, these aggregates do not replicate the morphological structure of LBs¹⁶⁶. Additionally, while endogenous α Syn expression is achieved within SNpc neurons, there is virtually no evidence of trans-synaptic propagation of α Syn pathology to non-transduced neurons¹⁶⁶, with only some studies suggesting limited α Syn spread from the site of rAAV injection in the vagal complex^{170,171}. In behavioural assessments, rAAV-mediated α SYN overexpression has been shown to induce motor deficits such as apomorphine/amphetamine-induced rotations and forepaw asymmetry^{164,166}. These symptoms emerge several weeks post-injection only in models exhibiting significant DA neuronal loss. α Syn levels achieved with rAAV-mediated overexpression typically exceed

those observed in idiopathic PD cases or in cases of PD associated with *SNCA* gene multiplications. Although dose-dependent effects are present, the model may not fully recapitulate critical aspects of PD pathology, such as the exact LB morphology or overt and widespread neurodegeneration.

4.9.2 Transgenic-mediated α Syn overexpression

Transgenic techniques have been used to create models overexpressing both wt and PD-associated mutant forms of α SYN. These α SYN-overexpressing mice exhibit a range of PD-related features including α Synucleinopathy, neurodegeneration, reductions in striatal DA, and locomotor dysfunction¹⁷². However, these hallmark PD features are often observed inconsistently across lines, with neuronal loss frequently mild or located in regions less directly relevant to PD, such as the spinal cord. While the levels of α SYN overexpression in these models are moderate – though lower than those achieved with rAAV-mediated overexpression – they are more comparable to the α SYN levels observed in human patients. Nonetheless, none of these early transgenic mouse models reliably develop LB pathology. Additionally, α Syn pathology generally does not propagate beyond the initial sites of expression, showing limited evidence of spread to non-transduced neurons outside the dopaminergic system¹⁶⁵.

4.9.3 Injection of α Syn PFFs and pathological extracts

Other strategies are based on the unilateral or bilateral infusion α Syn preformed fibrils (PFFs) of different types or brain tissue homogenates containing LB into different brain regions including the SNpc, STR and the olfactory bulb to investigate α Syn toxicity in terms of seeding and spreading^{166,173}. Exogenous fibrils or brain homogenates act as templates that interact with endogenous α Syn, promoting the formation of new inclusions and spreading α Syn pathology anterogradely and retrogradely through neural pathways. Remarkably, α Syn levels achieved with this model are more physiological than those achieved using overexpression techniques.

PFFs can be generated by incubating either monomeric recombinant α Syn or patient-derived α Syn under established buffer conditions, while LB-containing brain extracts can be sourced from *post-mortem* PD patients or tg mice with α Syn pathology¹⁶⁶. Injecting α Syn PFFs or pathological extracts initiates p α Syn accumulation in neuronal soma and processes and, in some cases, leads to the development of LB-like inclusions. Over time, these aggregates spread from the injection site to connected regions, providing a model for time-dependent α Syn propagation. Studies confirm that unilateral PFF injections can induce contralateral α Syn accumulation. Since α Syn pathology does not develop in α Syn KO mice following PFF injection,¹²⁴ and given that exogenous α Syn cannot be detected in mice injected with LBs into the SNpc at 4 months post-injection (mpi)¹⁷⁴, it is well-established that exogenous fibrils serve as a template for endogenous α Syn aggregation. The accumulation and spread of α Syn pathology in these models result in both neurodegeneration and neuroinflammation. Several studies have reported associated

behavioural changes including impairments in motor coordination and balance, though some research groups have been unable to replicate these findings¹⁷³.

While injections of α Syn PFFs or pathological extracts induce progressive protein aggregation, spreading, neuronal loss and neuroinflammation, variations across studies highlight methodological differences. Indeed, establishing standardized protocols for sample preparation and injection may enhance the reproducibility and robustness of these models across research groups.

Key alterations observed in α Syn-based PD rodent models are outlined in figure 34. (Figure 34).


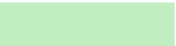


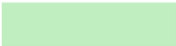
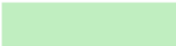
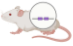
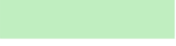


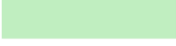
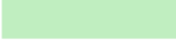

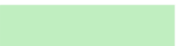
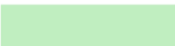
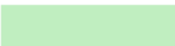
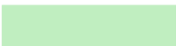
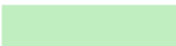
α Syn-based PD rodent models	α Syn aggregation	α Syn propagation	LB pathology	Neurodegeneration	Behavioral changes
 rAAV- α SYN					
 Tg α SYN					
 α Syn PFFs / pathological extracts					

Figure 34. Principal alterations in α Syn-based PD rodent models. PD-related alterations that are reproduced (*in green*) or not reproduced (*in red*) in rAAV, Tg and PFFs/pathological extracts α Syn PD rodent models. Illustration created with Biorender.com.

5. Alpha-synuclein and neuromelanin interactions and their contribution to Parkinson’s disease pathology

5.1. α Syn redistribution to NM granules

In PD-vulnerable regions, neurons exhibit increased NM density, which is associated with a reduction in NM’s lipid component and an increased α Syn concentration around the lipid-rich NM granules¹⁷⁵ (Figure 35). These alterations appear prior to neuronal degeneration, suggesting that α Syn redistribution to the lipid component of NM in early PD stages may predispose neurons to degeneration. Indeed, α Syn is entrapped in NM granules extracted from PD, but not control, brains¹⁷⁶.

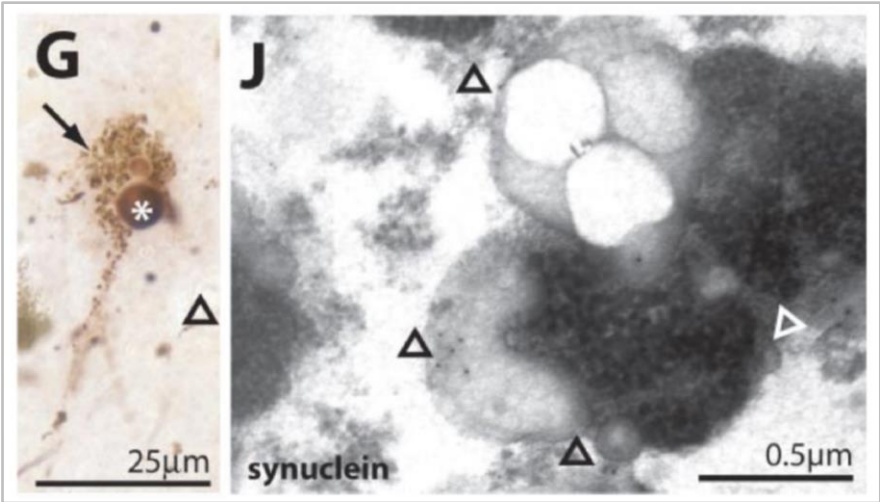


Figure 35. α Syn redistribution to NM granules. (G) High power photomicrographs of a PD neuron with α Syn-immunoreactive LB (asterisk) and NM granules. (J) Immunogold detection of α Syn associated with electron-lucent NM lipid droplets in PD NM-containing neurons (arrowheads indicate 10 nm gold particles). Image adapted from reference¹⁷⁵.

5.2 NM accumulation drives endogenous α Synucleinopathy

Our novel age-dependent NM TYR-injected rat model showed PD-like neuropathological inclusions over time, including both cytoplasmic inclusions resembling LBs and MBs⁹⁹ (Figure 36a). Notably, inclusion formation was confined to NM-containing neurons, peaking at 2 mpi, which coincided with functional changes and preceded neurodegeneration. By 4 m, once neurodegeneration had progressed, inclusions were reduced. These inclusions displayed positivity for p62 and ubiquitin, and in some cases, for α Syn. Consistent with these findings, unilateral TYR injection in non-human primates also induced p62- and ubiquitin-positive LB and MB formation in melanized neurons¹⁷⁷ (Figure 36b). LB inclusions were positive for total α Syn, p α Syn and insoluble α Syn, as they demonstrated resistance to proteinase K treatment.

Furthermore, brain-wide NM accumulation in tgNM, mimicking that seen in human brains, drives the formation of LB and MB inclusions¹⁰⁰ (Figure 36c). Remarkably, over 60% of SNpc p62-positive cytoplasmic inclusions were also immunopositive for α Syn.

Overall, inclusion formation is restricted to melanized neurons with NM accumulation directly driving α Syn accumulation and LB pathology.

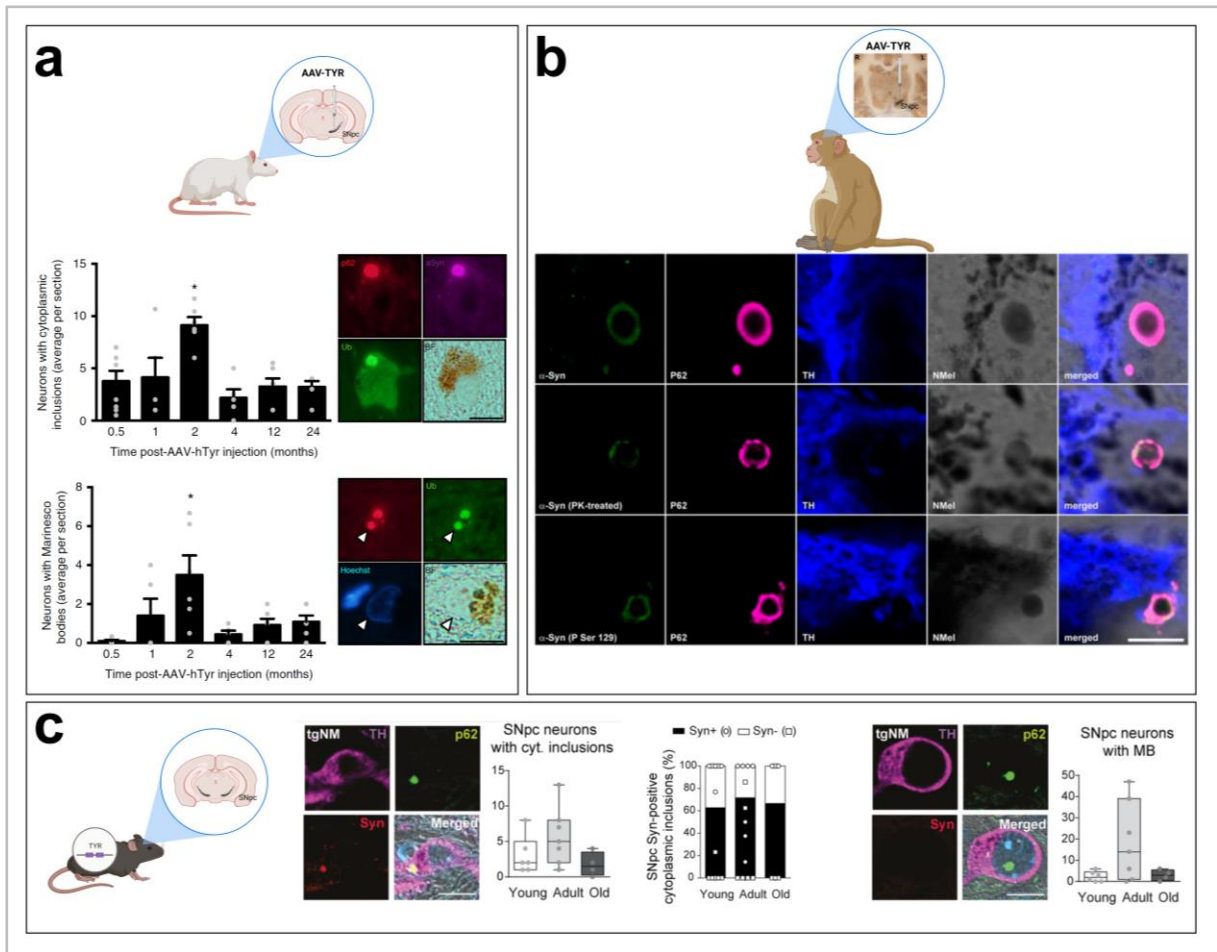


Figure 36. NM accumulation drives PD-related inclusion formation and α Synucleinopathy in TYR-injected rats, TYR-injected non-human primates, and tgNM mice. **(a)** p62-positive cytoplasmic (*top*) and MB (*bottom*) inclusions in TYR-injected rats. p62, red; α Syn, magenta; ubiquitin (Ub), green; NM, brown in bright-field. Scale bars, 12.5 μ m. **(b)** p62-positive cytoplasmic inclusions displaying total α Syn, PK-resistant α Syn, and p α Syn positivity in TYR-injected non-human primates. α Syn, green; p62, magenta; TH, blue; NM, dark grey in bright-field. Scale bar, 5 μ m. **(c)** p62-positive cytoplasmic (*left*) and MB (*right*) inclusions in tgNM mice with over 60% of SNpc p62-positive cytoplasmic inclusions showing positivity for α Syn (*left*). TH, magenta; p62, green; α Syn, red; NM, dark grey in merged. Scale bars, 10 μ m. Illustrations created with Biorender.com and images adapted from references^{99,100,177} respectively.

5.3 α Syn is dispensable for NM-linked PD pathology

Considering the presence of α Syn-positive PD-like inclusions in NM-producing rats, our group investigated whether NM pathology depends on α Syn accumulation. To address this objective, TYR was injected above the SNpc of both wt and α Syn KO mice⁹⁹ (Figure 37). Both groups developed PD-like inclusions although in α Syn KO mice, these p62-positive inclusions lacked α Syn. Likewise, both wt and α Syn KO mice exhibited comparable levels of neurodegeneration on the TYR-injected side relative to the contralateral side. These findings indicate that α Syn is not required for NM-associated PD pathology.

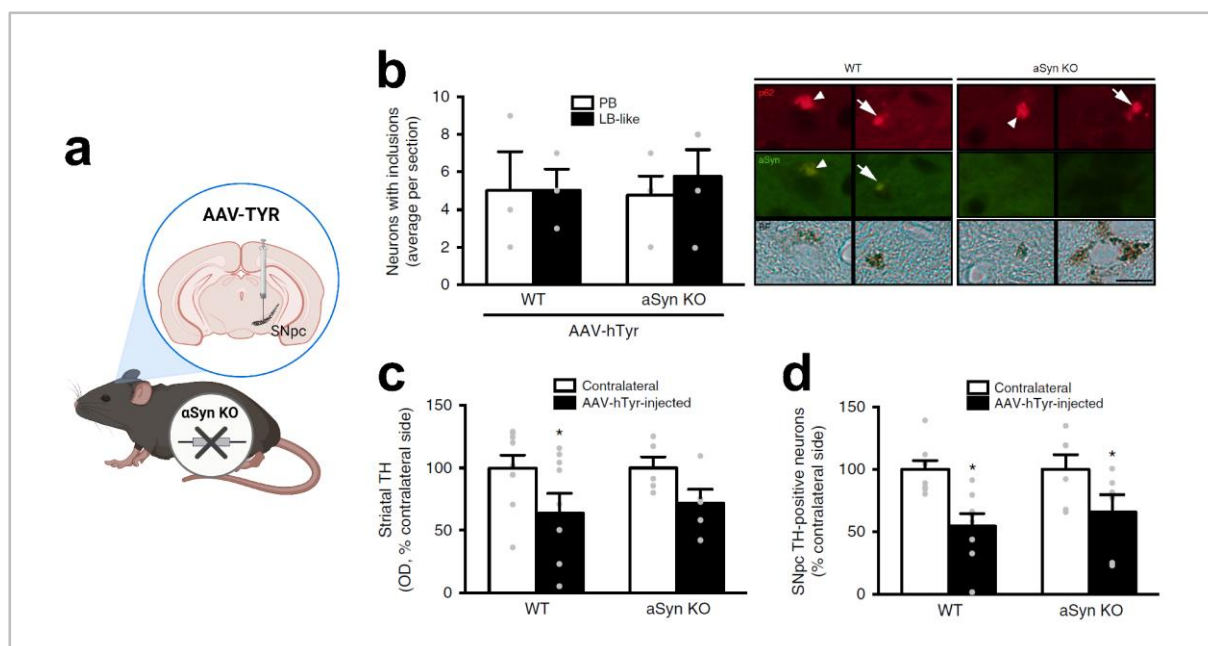


Figure 37. α Syn is dispensable for NM-associated PD pathology. (a) Schematic representation of TYR-injected α Syn KO mouse. (b) Neurons with inclusions in TYR-injected wt and α Syn KO mice. (c) Striatal TH-positive fibers in TYR-injected wt and α Syn KO mice. Scale bar, 12.5 μ m. (d) SNpc TH-positive neurons in TYR-injected wt and α Syn KO mice. Illustration in a created with Biorender.com and images adapted from reference⁹⁹.

5.4 α Syn, NM and oxidative stress

DA can be internalized into synaptic vesicles, metabolized or oxidised to ultimately form NM^{84,178}. In the cytosol, DA undergoes auto-oxidation to produce cytotoxic ROS and electron-deficient DA quinones¹⁷⁸ (Figure 38). ROS generation disrupts mitochondrial respiration and alters the permeability of mitochondrial pores. Additionally, DA quinones can modify PD-related proteins such as α Syn, thereby promoting its aggregation, as well as inactivate the dopamine transporter (DAT) and TH and induce dysfunction in mitochondrial complex I. Along this line, significant increases in cysteinyl adducts of L-DOPA, DA and 3,4-dihydroxyphenylacetic acid (DOPAC) have been observed in the SN of PD patients, supporting the cytotoxic role of DA oxidation in PD pathology^{178,179}.

Aggregated α Syn can selectively oxidise ATP synthase and induce lipid peroxidation in mitochondria, impairing the mitochondrial permeability¹⁸⁰. This cascade results in mitochondrial swelling and eventually cell death. Compromised ATP production and mitochondrial membrane depolarization further increase ROS production, exacerbating cytotoxicity and accelerating neurodegeneration. Supporting these findings, α Syn overexpression in the DMNX neurons generates oxidative stress¹⁸¹. When α Syn overexpression is combined with the ROS-generating agent paraquat, oxidative stress, α Syn aggregation, and neurotoxicity are all enhanced. Increased oxidative stress also aggravates α Syn spreading from the DMNX to more rostral brain regions.

Dysregulation of DA homeostasis and α Syn aggregation also disrupts protein degradation pathways, compounding cytotoxic effects. DA quinones can irreversibly modify UPS

components and autophagy-related proteins, leading to the accumulation of misfolded and aggregated α Syn¹⁷⁸. These toxic oligomers resist proteasomal degradation exacerbating oxidative stress by impeding the clearance of damaged mitochondria and oxidised macromolecules¹⁸², creating a vicious cycle of cellular dysfunction and neurodegeneration. Furthermore, oxidative stress compromises lysosomal membrane integrity, impairing autophagosome function in clearing aggregated α Syn effectively¹⁸³.

This synergistic interaction between oxidative stress, impaired protein degradation, and mitochondrial dysfunction highlights the multifaceted role of DA, NM and α Syn in PD-related neurodegeneration.

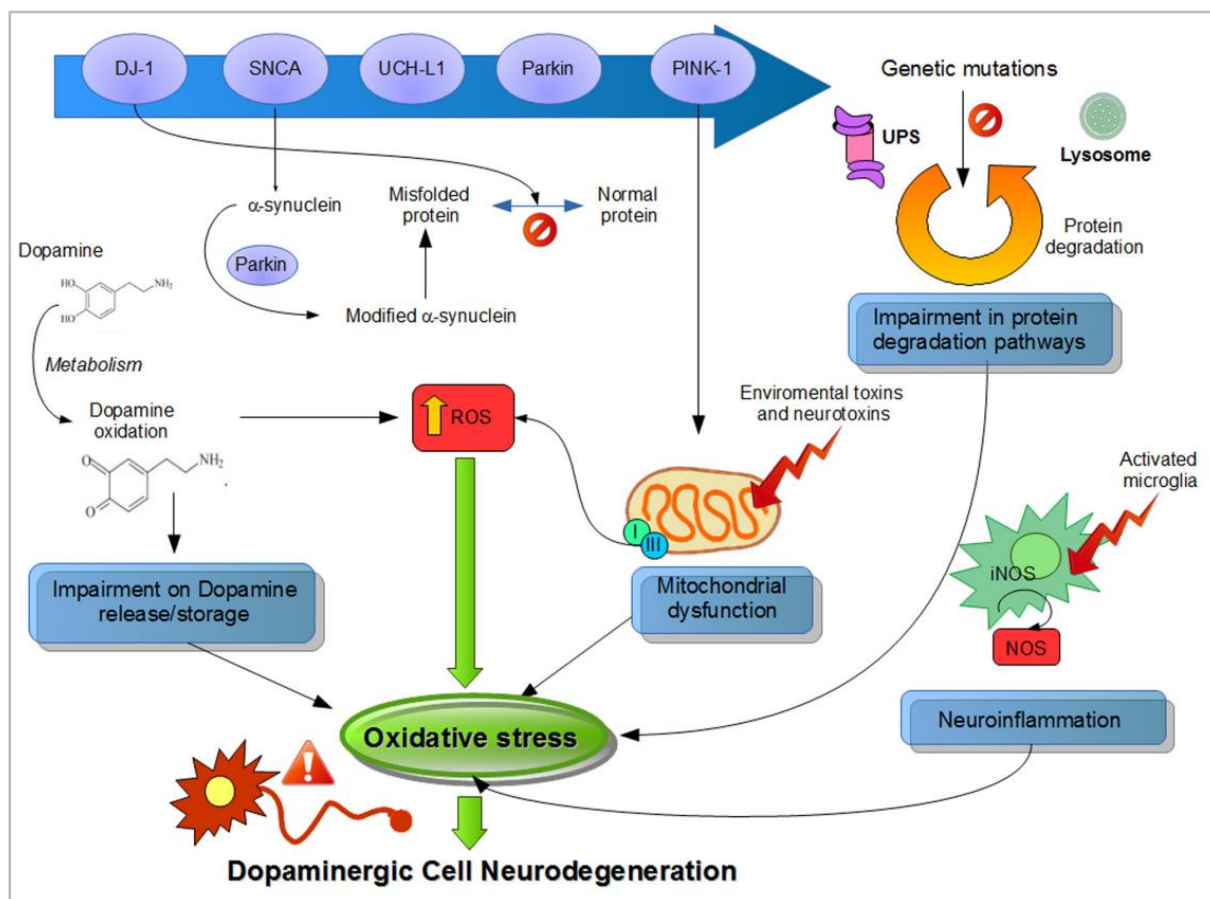


Figure 38. Oxidative stress in PD. DA oxidation produces DA quinones, which contribute to increased ROS levels and modify PD-related proteins like α Syn, promoting its aggregation. Elevated oxidative stress impairs the UPS, disrupting the degradation of aggregated α Syn. This stress also triggers mitochondrial dysfunction, which further exacerbates oxidative damage. In turn, aggregated α Syn can directly impair mitochondrial function, creating a cycle of increasing oxidative stress. Taken together, these cellular processes contribute to heightened oxidative stress and the selective degeneration of DA neurons. Image from reference¹⁷⁸.

HYPOTHESES & OBJECTIVES

HYPOTHESES AND OBJECTIVES

The central hypothesis of this PhD thesis is that α Syn and NM, two key contributors to PD pathogenesis, exert a synergistic pathological effect. The main goal is to describe features of this pathological interplay and elucidate the combined role of α Syn and NM in driving the molecular pathophysiological cascade associated with PD.

To achieve this main objective, two specific aims are outlined.

Specific aim 1: To evaluate the contribution of α Syn to NM-linked PD pathology

Rationale

Elevated α Syn levels are strongly associated with PD. α Syn expression levels are increased in melanized SNpc neurons from PD brains^{133,184} and in DA neurons differentiated from iPSC derived from PD patients¹⁸⁵. Also, *SNCA* genetic duplications and triplications cause familial forms of PD^{10,52,186–188}. While, previous findings from our group indicated that NM-associated PD pathology in TYR-expressing rodents can occur independently of α Syn⁹⁹, progressive NM build-up in these animals triggers endogenous α Syn oligomerization and the formation of LB-like inclusions concomitant to cell dysfunction/degeneration^{99–101}.

In addition to α Syn pathology in the brain, PD patients also exhibit increased α Syn aggregation within skin melanocytes¹⁸⁹. α Syn is also highly expressed in skin biopsies from melanoma patients¹⁹⁰. Patients with PD have an increased risk of melanoma and vice versa¹⁹¹. α Syn can promote ultraviolet-mediated melanin formation *in vitro*¹⁹² and release DA from synaptic vesicles to the cytosol in catecholaminergic neurons¹⁹³.

Hypothesis

Increased α Syn levels, as occur in PD patients, accelerate NM accumulation and enhance NM-associated PD pathology.

Objectives

1. To investigate the impact of α Syn overexpression on NM accumulation.
2. To examine the combined effects of α Syn and NM on:
 - 2.1 α Syn levels and molecular conformations.
 - 2.2 Neuropathological inclusions.
 - 2.3 Nigrostriatal system integrity.
 - 2.4 Neuroinflammation/neuronophagia.

3. To elucidate the molecular mechanisms underlying α Syn and NM pathological interplay:
 - 3.1 To determine the impact of α Syn and NM on DA vesicular uptake and neurotransmission.
 - 3.2 To explore α Syn's role in modulating TYR levels.

Specific aim 2: To evaluate the impact of NM-mediated oxidative stress on α Syn pathology and spreading

Rationale

NM is synthesized through the continuous oxidation of catecholamines^{82,194}. When NM's binding capacity becomes saturated, it shifts to a pro-oxidant state contributing to oxidative stress generation⁸⁴. Progressive NM build-up in NM-producing cells correlates with increased ROS production in these cells⁹⁹. Oxidative stress has been reported to drive α Syn aggregation and facilitate its propagation¹⁰.

Hypothesis

Oxidative stress resulting from DA oxidation into NM aggravates α Syn pathology and promotes its spread, contributing to neurodegenerative processes in PD.

Objectives

1. To confirm the occurrence of p α Syn pathology induced by amplified PD patient-derived α Syn PFFs.
2. To distinguish between exogenous and endogenous origins of PFF-induced p α Syn pathology.
3. To analyse PFF-induced p α Syn spreading across interconnected brain regions.
4. To assess whether NM production amplifies PFF-induced p α Syn pathology and spreading.
5. To study the impact of PFF-induced p α Syn pathology on nigrostriatal system integrity.
6. To evaluate the effects of PFF-induced p α Syn pathology on NM levels.
7. To assess the consequences of PFF-induced p α Syn pathology on motor and non-motor behaviours.

MATERIALS & METHODS

MATERIALS AND METHODS

1. Animals

1.1 Rats

Adult male Sprague-Dawley rats (Charles River), 225–250 g at the time of surgery, were housed two or three per cage with *ad libitum* access to water and food and exposed to a 12 hours (h) light/dark cycle. All experimental and surgical procedures were conducted in strict accordance with the European Directive (2010/63/UE) and Spanish regulations (Real Decreto 53/2013; Generalitat de Catalunya Decret 214/97) regarding the protection of animals used for experimental and other scientific purposes, and approved by the Vall d'Hebron Research Institute (VHIR) Animal Research Ethics Committee (CEEa). Rats were randomly distributed into the different experimental conditions and experimental groups were processed at same time to minimize bias.

1.2 Mice

1.2.1 tgNM mouse colony

Transgenic NM mice (tgNM) were obtained by pronuclear microinjection of the full-length human TYR complementary DNA (cDNA) fused to the rat tyrosine hydroxylase (Th) promoter (Tg-Th-TYR; tgNM) into C57B16-SJL mouse zygotes [Centre for Animal Biotechnology and gene Therapy (CBATEG)]. Mice were backcrossed for 8-10 generations using C57BL/6J mice (Charles River) and maintained in heterozygosis. Animals were housed two to five per cage with *ad libitum* access to water and food and exposed to a 12 h light/dark cycle. All experimental and surgical procedures were conducted in strict accordance with the European Directive (2010/63/UE) and Spanish regulations (Real Decreto 53/2013; Generalitat de Catalunya Decret 214/97) regarding the protection of animals used for experimental and other scientific purposes, and approved by the Vall d'Hebron Research Institute (VHIR) Animal Research Ethics Committee (CEEa). Male and female wt and tgNM mice were randomly distributed into the different experimental conditions and experimental groups were processed at same time to minimize bias.

1.2.2 Genotyping

DNA was routinely extracted from mice ear punches with the AccuStart™ II Mouse Genotyping kit (QuantaBio, #95135) and a PCR was performed by mixing 1 ul of DNA with the primers TYR-Forward (TTCAGACCCAGACTCTTTTCAA), TYR-Reverse (GCTGCTTTCTCTTGTGACGA) at a concentration of 500 nM using a 9800 Fast Thermal Cycler (Applied Biosystems). Amplification product was loaded into 2% agarose gel and visualised using a GelDoc XR (BioRad). Male and female wt and tgNM mice were randomly distributed into the different experimental groups and all animals were processed at once to minimize bias.

2. Viral vector production

rAAV vector serotype 5 expressing α SYN cDNA driven by the chicken beta-actin (CBA) promoter (AAV5-CBA-h α SYN; concentration $1 \cdot 10^{13}$ gc/ml) was obtained at the Michael J. Fox Foundation. rAAV serotype 2/1 expressing hTYR cDNA driven by the cytomegalovirus (CMV) promoter (AAV2/1-CMV-hTYR) was produced at the Viral Vector Production Unit of the Autonomous University of Barcelona (UPV-UAB, Spain). Briefly, rAAV vector expressing hTYR was produced by triple transfection of 2×10^8 HEK293 cells with 250 μ g of pAAV, 250 μ g of pRepCap, and 500 μ g of pXX6 plasmid mixed with polyethylenimine (PEI; branched, MW 25000; Sigma-Aldrich). The UPV-UAB generated a pAAV plasmid containing the ITRs of the AAV2 genome, a multicloning site to facilitate cloning of expression cassettes, and ampicillin resistance gene for selection. 48 h after transfection, cells were harvested by centrifugation [$200 \times g$, 10 minute (min)]; resuspended in 30 ml of 20 mM NaCl, 2 mM MgCl₂, and 50mM Tris-HCl (pH 8.5), and lysed by three freeze–thaw cycles. Cell lysate was clarified by centrifugation ($2000 \times g$, 10 min) and the rAAV particles were purified from the supernatant by iodixanol gradient as previously described¹⁹⁵. The clarified lysate was treated with 50 U/ml of Benzonase (Novagen; 1 h, 37 °C) and centrifuged ($3000 \times g$, 20 min). The vector-containing supernatant was collected and adjusted to 200 mM NaCl using a 5-M stock solution. To precipitate the virus from the clarified cell lysate, polyethylene glycol (Sigma-Aldrich, #PEG8000) was added to a final concentration of 8% and the mixture was incubated (3 h, 4 °C) and centrifuged ($8000 \times g$, 15 min). The AAV containing pellets were resuspended in 20 mM NaCl, 2 mM MgCl₂, and 50mM Tris-HCl (pH 8.5) and incubated for 48 h at 4 °C. The rAAV titration method used was based on the quantitation of encapsulated DNA with the fluorescent dye PicoGreen® as previously described¹⁹⁶, and the following vector concentration was obtained: AAV-hTYR: $2.43 \cdot 10^{12}$ gc/ml.

3. PD patient-derived α SYN PFFs

PD patient-derived α SYN PFFs were provided by Prof. Ronald Melki (*Protein misfolding and aggregation in neurodegenerative diseases group, François Jacob Institute of biology, Paris, France*). Briefly, brain tissue from a PD patient was obtained *post-mortem* through the UK Brain Bank (Imperial College London, UK)¹⁹⁷ (Table 1).

Number	Sex	Age at onset	Duration (years)	Cause of death	Clinical diagnosis	Neuropathological diagnosis
PD341	M	54	14	Parkinson's with dementia	Akinetic-rigid syndrome with progression to PDD, RBD	LBD-Neocortical (α SYN, Braak VI); Tau Braak II, Thal phase 2

Table 1. Clinical history of PD341 patient. Information about sex, age at onset, duration of the disease, cause of death, clinical and neuropathological diagnosis are described. PDD, Parkinson's with dementia; RBD, rapid eye movement sleep behaviour disorder. Table created based on the information provided in reference¹⁹⁷.

Upon removal, one hemibrain was dissected fresh and the tissue blocks were frozen while the other hemibrain was formalin fixed for neuropathological diagnosis. Cingulate cortex was isolated and diluted five times in PMCA buffer (150 mM KCl, 50 mM Tris-HCl pH 7.5) to obtain brain homogenate at 20% (weight:volume). Brain tissue was homogenised by sonication and samples were flash frozen in liquid nitrogen and stored until use at -80 °C. The presence of aggregated α SYN was quantified using a filter retardation assay and western blotting with the 4B12 (Biolegend, cat # 807801) and P-S129 α SYN antibody (mouse 11A5, provided by Elan Pharmaceuticals, Inc., Dublin, Ireland) antibodies (Figure 39). Additionally, the Cisbio fluorescence resonance energy transfer (FRET) assay was also used to quantify aggregated α SYN in patient's brain homogenate following the manufacturer's recommendations. For PD-derived amplified α SYN PFFs, monomeric α SYN (100 μ M) was added to brain homogenate diluted in PMCA buffer to a final concentration of 2% (W:V), equivalent to 6 mg of brain tissue. PMCA amplification was performed in quadruplicates were flash frozen in liquid nitrogen and stored until use at -80°C. *De novo* assembled PD-derived amplified α SYN PFFs (1.4 mg/ml) fibrils were characterised by obtaining their proteolytic pattern after Proteinase K digestion as well as morphology assessment using transmission electron microscopy (TEM) (Figure 39). It is important to note that while the term "PD-derived α SYN PFFs" is used, the inoculum primarily consists of whole brain homogenate, which contains PFFs but is not composed solely of them.

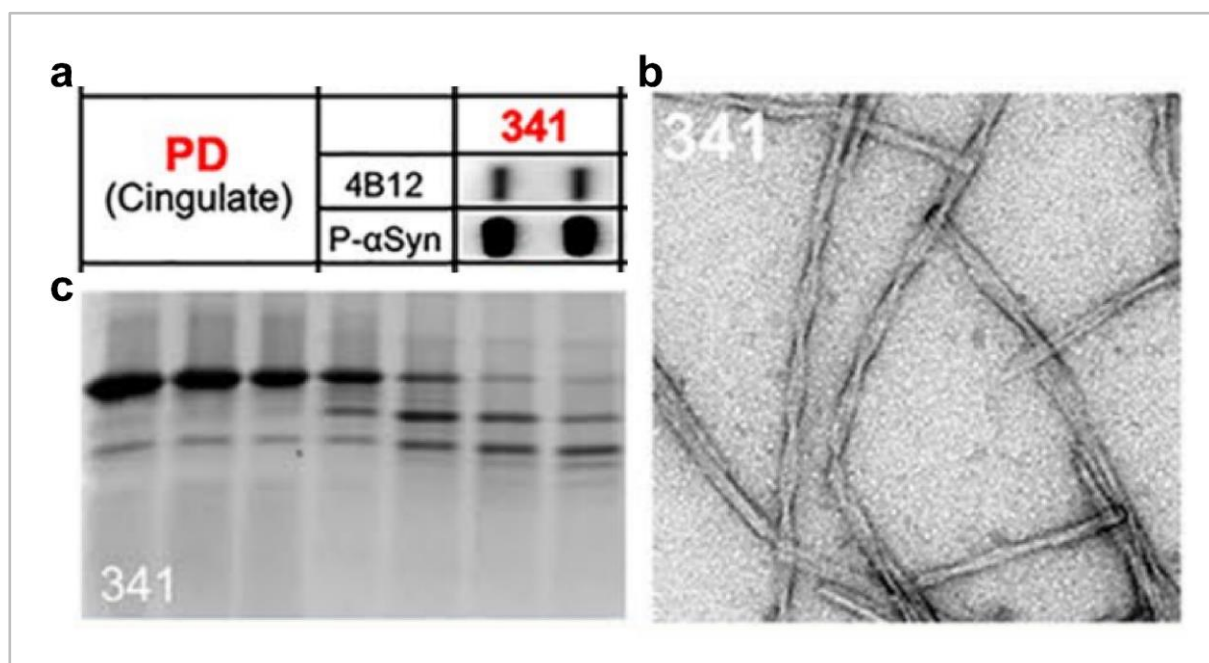


Figure 39. PD-derived non-amplified and amplified α SYN PFFs characterisation. (a) Filter retardation assay showing the amount of aggregated α SYN in brain homogenates using antibodies against total human α SYN (4B12) and phosphorylated α SYN (p- α Syn). (b) Electron micrograph of α SYN assemblies obtained after the 3rd cycle of amplification by PMCA. (c) Proteolytic patterns of α SYN assemblies obtained after the 3rd cycle of amplification by PMCA and Proteinase K digestion. Adapted from reference¹⁹⁷. Panel a shows PD-derived non-amplified α SYN PFFs, while panels b and c illustrate PD-derived amplified α SYN PFFs.

4. Stereotaxic surgery

Before surgery, all surgical instruments were autoclaved and analgesic solution (meloxicam, 0.5 mg/ml) was prepared. All surgical procedures were performed with the animals placed in stereotaxic frame under general anaesthesia with isoflurane (Baxter) (5% for the induction phase and 2% for the maintenance phase). Vector solutions were injected using a 10 µl Hamilton syringe fitted with a glass capillary (Hamilton, #701). In all cases, infusion was performed at a rate of 0.4 µl/min, with the needle remaining in place for an additional 4 min before being slowly retracted. Injection was performed unilaterally on the right side of the brain at the corresponding coordinates relative to bregma according to the stereotaxic atlas of Paxinos and Watson¹⁹⁸. For rats, the craniotomy site was sealed by suturing the scalp with sterile sutures, while for mice, the craniotomy was sealed using bone wax. To reduce pain and inflammation, meloxicam (5 mg/kg) was administered subcutaneously.

4.1 Rats

Rats received 2 µl of either a mixture of 1:1 AAV-αSYN/vehicle, AAV-TYR/vehicle or AAV-αSYN/AAV-TYR right above the SNpc; antero-posterior: -5.2 mm, medio-lateral: -2 mm, dorso-ventral: -7.6 mm.

4.2 Mice

BSA (Bovine serum albumin)-, PD-derived non-amplified αSYN PFFs- and PD-derived amplified αSYN PFFs-injected mice received 1 µl of either BSA in PBS (phosphate buffer saline) (1.4 mg/ml), PD-derived non-amplified αSYN PFFs in PBS (1.4 mg/ml) and PD-derived amplified αSYN PFFs in PBS (1.4 mg/ml) at two rostrocaudal levels of the STR; antero-posterior: 0.5 mm, medio-lateral: -1.75 mm, dorso-ventral: -3 mm (0.5 µl)/-4 mm (0.5 µl).

5. Histological procedures

5.1 Brain processing

5.1.1 Intracardiac perfusion

Animals were deeply anesthetized with sodium pentobarbital (50 mg/kg i.p.) and then perfused through the left ventricle with saline (0.9% [wt/vol]) at room temperature (RT) for 5 min (rats) or 3 min (mice), followed by ice-cold paraformaldehyde fixative solution 4% phosphate buffered (Panreac, #252931.1214) for 15 min (rats) and 8 min (mice), before brains being removed for histology.

5.1.2 Tissue fixation

Brains were post-fixed for 24 h in the same fixative solution. After fixation, rat brains were washed with PBS and processed for paraffin embedding at the VHIR's Drug Delivery and Targeting laboratory facility. Mouse brains were cryoprotected for 24-48 h in 30% sucrose in 0.2 M phosphate buffer (PB) until the tissue sank to the bottom of the tube. Brains were then frozen with pre-cooled 2-methylbutane at a temperature between -30 °C and -40 °C in dry ice for 1 min. Once frozen, brains were stored at -80 °C until sectioning.

5.1.3 Brain sectioning

Paraffin-embedded rat brains were sectioned with a slicing microtome (Leica, Germany) at 5 µm-thickness and sections containing the SN and STR regions were collected in Polysine adhesion slides (Eprelia™, #J2800AMNZ).

Frozen mouse brains were sectioned with a cryostat (Leica, Germany) at a 20 µm-thickness and free-floating sections from the entire brain were collected in a standard 24-well plate in PB supplemented with 0.01% sodium azide (Sigma-Aldrich, #S2002).

5.2 Immunohistochemistry

5.2.1 Paraffin-embedded brain slices

Brain slices were initially deparaffinized and rehydrated. First, slides were incubated at 60 °C for 30 min to melt the paraffin. They were then washed three times of 3 min each with xylene to dissolve and remove paraffin. Following this, tissue slices were rehydrated through a descending ethanol gradient with a 10-min washes in ethanol solutions of 100%, 95% and 70%. Finally, slides were washed twice with 0.1 M Tris buffered saline (TBS) (see details in section 11, [Table 4](#)). Next, slides were incubated in endogenous peroxidase blocking solution [3% H₂O₂ (Panreac, #121076.1211) and 10% methanol in 0.1 M TBS] for 10 min to avoid interference with the peroxidase-based detection system. Slides were then washed three times in 0.1 M TBS for 5 min. To eliminate chemical modifications caused by formalin fixation and unmask epitopes, antigen retrieval was performed by incubating slides in citrate buffer 10 mM at pH 6.0 in a heating water bath at 95 °C for 20 min. Slides were then cooled at RT for 20 min. Tissue sections were permeabilised by washing them twice with 0.1 M TBS containing 0.5% Triton X-100 (Sigma, #T9284) for 5 min each, followed by a third wash with 0.1 M TBS. In order to ensure a constant wet environment, slides were placed in a slide staining tray. Tissue sections were dried with a soft tissue and then circled with a hydrophobic pen (Vector Laboratories, #H-4000). Next, 5% normal goat serum (NGS) (Vector Laboratories, #S-1000-20) in 0.1 M TBS blocking solution was added to each section and incubated for 1 h at RT. Slides were gently dried and incubated with primary antibody diluted in 2% NSG – 0.1 M TBS. Slides were stored at 4 °C for 24 or 48 h depending on the antibody used.

After primary antibody incubation, slides were washed three times with 0.1 M TBS for 5 min and incubated with the corresponding biotinylated secondary antibody diluted in 2% NSG – 0.1 M TBS for 1 h at RT. Avidin-biotin complex (ABC) (Thermo Fisher Scientific, #32050) amplification solution was prepared and left on a shaker for 30 min. Slides were washed again three times with 0.1 M TBS for 5 min and treated with the ABC solution for 1 h at RT. Afterwards, slides were washed three times with 0.1 M TBS for 5 min. Peroxidase activity was developed by using either DAB (Vector Laboratories, #SK-4100; brown staining) or Vector®SG (Vector Laboratories, #SK-4700; dark blue staining) developing solutions, which are light-sensitive. The duration of the colour development depends on the antibody employed, usually taking 5-15 min. Once the desired colour intensity was achieved, the developing solution was removed with a vacuum unit and the slides were washed three times with 0.1 M TBS for 5 min.

5.2.2 Free-floating brain cryosections

Free-floating brain cryosections were washed three times in 0.1 M TBS for 5 min each, and then incubated in endogenous peroxidase blocking solution (3% H₂O₂ and 10% methanol in 0.1M TBS) for 10 min to prevent interference with the peroxidase-based detection system. Sections were then washed three times in 0.1 M TBS for 5 min and blocked with 5% NGS in 0.1 M TBS blocking solution. Following this, cryosections were incubated with primary antibody diluted in 2% NSG – 0.1 M TBS at 4 °C for 24 or 48 h depending on the antibody used. See additional details in section 11, [Table 5](#).

Sections were then washed three times with 0.1 M TBS for 5 min and incubated with the corresponding biotinylated secondary antibody diluted in 2% NSG – 0.1 M TBS for 1 h at RT, see additional details in section 11, [Table 6](#). ABC amplification solution was prepared and left on a shaker for 30 min. Tissue sections were washed again three times with 0.1 M TBS for 5 min and treated with the ABC solution for 1 h at RT. Afterwards, sections were washed three times with 0.1 M TBS for 5 min. Peroxidase activity was developed by using either DAB (for brown staining) or Vector®SG (for dark blue staining) developing solutions, which are light-sensitive. The duration of the colour development depends on the antibody employed, usually taking 5-15 min. Once the desired colour intensity was achieved, the developing solution was removed and the slides were washed three times with 0.1 M TBS for 5 min. Sections were washed with distilled water and mounted in Superfrost Plus Adhesion Microscope slides (Epredia™, #J1800AMNZ).

5.2.3 Slide mounting

Because mounting medium is hydrophobic, sections needed to be dehydrated. To do so, consecutive immersions in ethanol of increasing gradient were performed: a quick rinse in 70%, 15 seconds (s) in 95% and 1 min in 100%. Slides were then incubated in xylene for 1 min. Coverslips, previously rinsed with 70% ethanol, were mounted on the slides with DPX (Sigma-Aldrich, #100579) mounting medium. Any bubbles were removed with tweezers. Slides were left to dry overnight.

5.3 Immunofluorescence

Paraffin-embedded brain slices were initially deparaffinized and rehydrated. First, slides were incubated at 60 °C for 30 min to melt the paraffin. They were then washed three times for 3 min with xylene to dissolve and remove paraffin. Following this, tissue slices were rehydrated through a descending ethanol gradient with 10-min washes in ethanol solutions of 100%, 95% and 70%. Finally, slides were washed twice with 0.1 M PBS (see details in section 11, Table 4). To eliminate chemical modifications caused by formalin fixation an unmask epitopes, antigen retrieval was performed by incubating slides in citrate buffer 10 mM at pH 6.0 in a heating water bath at 95 °C for 20 min. Slides were then cooled at RT for 20 min. Tissue sections were permeabilised by washing them twice with 0.1 M PBS containing 0.5% Triton X-100 (Sigma, #T9284) for 5 min, followed by a third wash with 0.1 M PBS. In order to ensure a constant wet environment, slides were placed in a slide staining tray. Tissue sections were dried with a soft tissue and then circled with a hydrophobic pen (Vector Laboratories, #H-4000). Next, 5% NSG (Vector Laboratories, #S-1000-20) in 0.1 M PBS blocking solution was added to each section and incubated for 1 h at RT. Slides were gently dried and incubated with primary antibodies diluted in 2% NSG – 0.1 M PBS. Slides were stored at 4 °C for 24 h depending on the antibody used. See additional details in section 11, Table 5.

After incubation with the primary antibodies, slides were washed three times with 0.1 M PBS for 5 min. The appropriate Alexa Fluor-conjugated secondary antibodies (Alexa 488, 568, 594 and 647) were then added along with 1:5000 Hoechst 33342 (Thermo Fisher Scientific, #H3570) for nuclear staining, and incubated in 2% NSG – 0.1 M PBS for 1 h at RT. See additional details in section 11, Table 6. Slides were then washed three times with 0.1 M PBS for 5 min and coverslipped using DAKO fluorescent mounting medium (Merck, #F4680).

5.4 Haematoxylin-Eosin

To quantify intra/extra cellular NM in rat paraffin-embedded sections, standard Haematoxylin-Eosin (H&E) staining was performed at VHIR's Drug Delivery and Targeting laboratory facility.

5.5 Proximity-ligation assay

The day before the assay, rabbit anti-alpha-synuclein polyclonal antibody (Merck, #AB5038P) was conjugated with Duolink probes. 2 µl of Conjugation buffer from the Duolink PLUS (Merck, #DUO92009-1KT) or Duolink MINUS (Merck, #DUO92010-1KT) probes were added to 20 µL of rabbit anti-alpha-synuclein polyclonal antibody (Merck, AB5038P) at a concentration of 1 mg/ml. Antibody solution was transferred to one vial of lyophilized oligonucleotides (either PLUS or MINUS) and incubated at RT overnight. 2 µl of Stop Reagent were added to the reaction and incubated at RT for 30 min. Finally, 24 µl of Storage Solution were added and solution was stored at 4 °C.

For the assay, rat paraffin-embedded brain sections were initially deparaffinized and rehydrated (see additional details in 5.2 Immunohistochemistry section). To unmask epitopes, sections were submerged in citrate buffer 10 mM, pH 6 and incubated in water bath at 95°C for 20 min followed by 20 min at RT. Slides were then washed 2 x 5 min in PBS 1x-triton 0.5% buffer followed by 1 x 5 min in PBS 1x buffer. For blocking, tissue sections were dried and circled with a hydrophobic pen (Vector laboratories, #NC9545623). Tissue sections were then incubated in Duolink blocking solution from Duolink PLUS or MINUS (1-2 drops/section). Conjugated primary antibodies (PLUS and MINUS) were diluted at 1:500 with the antibody diluent. Tissue sections were then incubated with the primary antibodies overnight at 4 °C.

The next day, slides were washed 2 x 5 min in 1x Wash Buffer A (Merck, #DUO82049-4L). For ligation, 5x Duolink ligation buffer was diluted in 1:5 high purity water and then mixed to create the ligation buffer. Ligase was then diluted in ligation buffer at 1:40. Tissue sections were then incubated 30 min at 37°C. Slides were washed 2 x 5 min in 1x Wash Buffer A (Merck, DUO82049-4L). For amplification, 5x Duolink amplification buffer was diluted in 1:5 high purity water and then mixed to create the amplification buffer, which is light-sensitive. Polymerase was then diluted in amplification buffer at 1:80. Tissue sections were then incubated 100 min at 37 °C. For final washes, slides were washed 2 x 10 min 1x Wash Buffer B (Merck, #DUO82049-4L) and in 0.01x Wash B for 1 min. Tissue sections were then incubated with Hoechst 33342 (Thermo Fisher Scientific, #H3570) at 1:5000 for 10 min at RT for nuclei visualization. Slides were mounted with DAKO fluorescent mounting medium (Merck, #F4680) and stored at 4 °C.

6. GFP and αSYN-GFP TR5TY6 cell lines

6.1 Lentiviral particles

αSYN (*SNCA*) lentiviral particles tagged with a C-terminal monomeric green fluorescent protein (GFP) tag and a P2A-Puro tag, which allow for puromycin selection (#RC210606L4V), as well as lentiviral control particles including only a C-terminal monomeric GFP tag and a P2A-Puro tag (#PS100093V), were purchased at Origene.

6.2 GFP and αSYN-GFP TR5TY6 cell lines generation

TR5TY6 neuroblastoma cell line, which expresses *TYR* under the transcriptional control of the DOX-inducible Tet-On system, was transduced with either GFP lentiviral particles or αSYN-GFP lentiviral particles at a multiplicity of infection (MOI) of 0.5. Briefly, cells were cultured in low-glucose (1 g/l) Dulbecco's modified Eagle's medium (DMEM, Gibco, #11574446), supplemented with tetracycline-free fetal bovine serum (FBS, Takara Bio, #631101) and the appropriate selection of antibiotics: penicillin/streptomycin (100 I.U./ml of penicillin and 100 µg/ml of streptomycin), blasticidin (7 µg/ml) and zeocin (300 µg/ml), all from Thermo Fisher Scientific. When cells reached a 65-70% confluence, they were transduced with the corresponding lentiviral particles in the presence of polybrene (8 µg/ml), which enhances binding between pseudoviral capsid and the cellular

membrane. After 20 h of incubation, the medium was replaced. On the following day, puromycin (1 µg/ml) was added to the medium to select for successfully transduced cells. From this step, GFP and αSYN-GFP TR5TY6 cell lines were maintained with the aforementioned cell media and puromycin (1 µg/ml). Cell lines were confirmed negative for mycoplasma contamination by routine PCR analysis. Gene overexpression was confirmed by GFP immunofluorescence, western blot (WB) and real-time quantitative PCR (RT-qPCR) analysis.

6.3 GFP and αSYN-GFP TR5TY6 experiments

Both GFP TR5TY6 cells and αSYN-GFP TR5TY6 cells were seeded at 30,000 cells/ml onto 12-mm slides coated with 50 µg/ml poly-D lysine (Sigma-Aldrich, #A-003-M) in 24-well plates for immunocytochemistry analysis and at a 300,000 cells/ml in 10 cm plates for WB and RT-qPCR analysis. 24 h after seeding, cells were differentiated with 10 µM RA (Thermo Fisher Scientific, #207341000) for 3 d, followed by 80 nM 12-O-tetradecanoylphorbol-13-acetate (TPA) (Cell Signalling, #4174S) for an additional 3 d (Figure 40). At this point, the "6 d" group was treated with 2 µg/ml doxycycline (DOX) to induce TYR expression. After three days, the "6 d" and "3 d" groups received DOX treatment (2 µg/ml). Two days later, the "6 d", "3 d" and "1 d" groups were again treated with 2 µg/ml DOX (Figure 40). After 24 h, all groups were harvested.

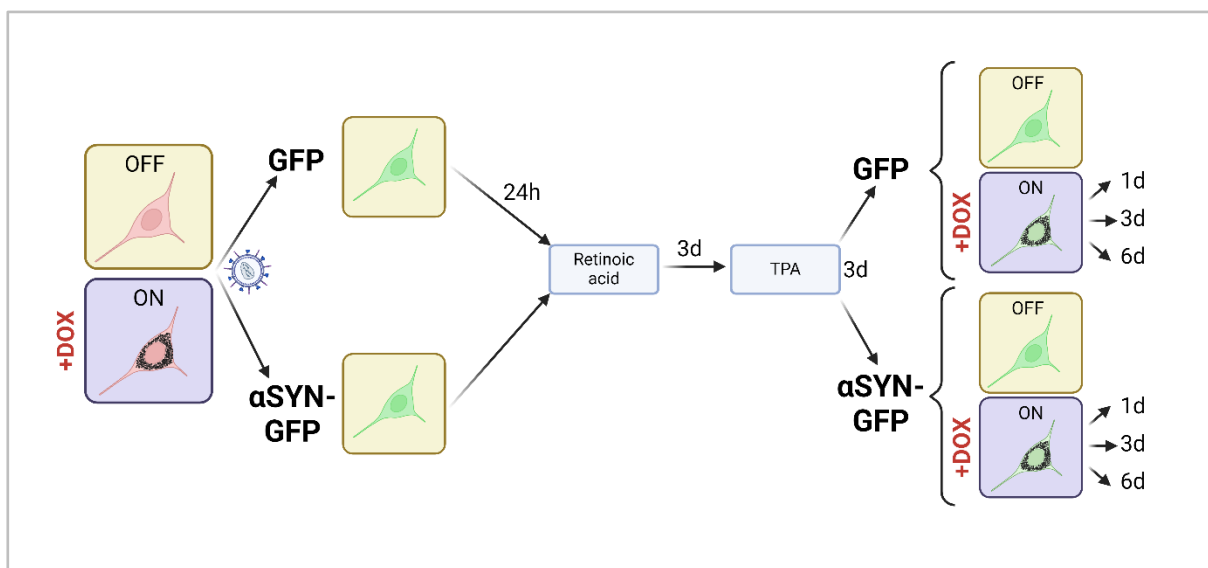


Figure 40. Workflow of GFP and αSYN-GFP TR5TY6 experiments. TR5TY6 neuroblastoma cells, which express TYR under a DOX-inducible system, were transduced with lentiviral particles encoding either GFP or αSYN-GFP and subsequently selected with puromycin to establish stable cell lines. Once stable, cells were seeded and, after 24 h, differentiation was initiated with retinoic acid for 3 d, followed by TPA treatment for an additional 3 d. Following differentiation, four conditions were established for both GFP and αSYN-GFP groups: OFF (no TYR induction); 1 d (1 d post-TYR induction), 3 d (3 d post-TYR induction) and 6 d (6 d post-TYR induction).

6.4 Western blot

Differentiated GFP and α SYN-GFP TR5TY6 cells either not induced (OFF) or induced for 1, 3 and 6 d were homogenized in RIPA buffer supplemented with protease/phosphatase inhibitors (Thermo Fisher Scientific, #78440) and cell extracts clarified by centrifugation at 10,000 x g for 10 min at 4 °C. After this, protein extracts were sonicated and protein concentrations were quantified using the bicinchoninic acid (BCA) method and processed for SDS-PAGE. Proteins were resolved in 12% polyacrylamide gels and transferred onto 0.45 μ m nitrocellulose membranes (Amersham, #GE10600014). Blocking with 5% milk powder in PBS was followed by overnight incubation at 4°C with the primary antibodies. See additional details in section 11, [Table 5](#). Incubation with the secondary antibodies was performed for 1 h at RT. See additional details in section 11, [Table 6](#).

Band densitometry, normalized to β -actin expression, was measured using ImageJ image analysis software.

6.5 Immunocytochemistry

Differentiated GFP and α SYN-GFP TR5TY6 cells either not induced (OFF) or induced for 1, 3 and 6 d were fixed in 3% formaldehyde for 30 min at RT. Following incubation with a blocking solution (powdered milk 0,2%, glycine 0.1 M, Triton X-100 0,01%, NGS 2% and BSA 1% in a 0.1 M PBS solution) for 1 h at RT, the corresponding primary antibodies were used diluted in 0.1% BSA – 0.1 M PBS overnight at 4 °C. See additional details in section 11, [Table 5](#).

Next day, cells were incubated for 1 h at RT with the corresponding secondary antibodies diluted in 0.1% BSA – 0.1 M PBS. See additional details in section 11, [Table 6](#). Afterwards, nuclei were labelled with Hoechst 33342 (Thermo Fisher Scientific, #H3570) diluted in 0.1 M PBS at 1:5000 for 10 min at RT. Coverslips were then mounted using DAKO fluorescent mounting medium and stored at 4 °C. Confocal images were obtained using the LSM 980 with Airyscan 2 confocal and ZEN 3.1 software.

6.6 Real-Time quantitative PCR (qPCR)

RNA was purified from GFP and α SYN-GFP TR5TY6 cells either not induced (OFF) or induced for 1, 3 and 6 d using the miRNeasy tissue/cells advanced mini kit (Qiagen, #217604). RNA concentration was determined using a NanoDrop ND-1000 Spectrophotometer. 100 ng of total RNA were retrotranscribed using High-Capacity cDNA Reverse Transcription Kit (Thermo Fisher Scientific, #4368814). qPCR was performed with 4.5 ng of cDNA per well, combined with Taqman Gene Expression Master Mix (Applied Biosystems, #4369016) and Taqman gene expression assays (*ACTB* and *RPLP0* as housekeeping genes and *SNCA* and *TYR* as target genes) in a LightCycler® 480 multiwell plate (Roche Diagnostics, #4729749001) following standard procedures in LightCycler® 480 Instrument II ([Table 2](#)).

	ID	Gene	Source	Manufacturer	Reference	Dye
Housekeeping genes	<i>ACTB</i>	Actin, beta	Human	Applied Biosystems	Hs99999903_m1	FAM
	<i>RPLP0</i>	Ribosomal protein lateral stalk subunit P0	Human	Applied Biosystems	Hs00420895_gH	FAM
Target genes	<i>SNCA</i>	Synuclein, alpha	Human	Applied Biosystems	#Hs00240907_m1	FAM
	<i>TYR</i>	Tyrosinase	Human	Applied Biosystems	Hs00165976_m1	FAM

Table 2. RT-qPCR genes. Information about housekeeping and target genes used in RT-qPCR analyses including the ID, gene, source, manufacture, reference and dye.

Cycle threshold (CT) for each target gene was normalized for the geometric mean of the two housekeeping genes. Water was included in the reaction as a non-template (negative control). The relative expression was calculated using the comparative method (Δ CT-method). Relative quantities (RQ, Δ CT²) were calculated normalizing CTs to endogenous controls and fold changes (FC, Δ CT²) were calculated normalizing CTs to endogenous controls and to experimental control expression (i.e. GFP OFF cells).

6.7 TYR activity assay

Differentiated GFP and α SYN-GFP TR5TY6 cells either not induced (OFF) or induced for 1, 3 and 6 d were homogenized in RIPA buffer supplemented with protease/phosphatase inhibitors and cell extracts clarified by centrifugation at 10,000 x g for 10 min at 4 °C. After this, protein extracts were sonicated and protein concentrations were quantified using the BCA method. The final reaction volume was set to 200 μ l and sodium phosphate buffer (NaPB) at pH 6.8 was prepared in advance. Briefly, 22 μ l of cell lysate were added to 158 μ l of NaPB in a 96-well standard plate. For the negative control (blank), 180 μ l of NaPB was added. As a positive control, 10 μ l of mushroom Tyr (Sigma-Aldrich, #T3824-25100) at 0.5 mg/ml was added to 170 μ l of NaPB. Additionally, an extra negative control was created where mushroom Tyr activity was inhibited by pre-incubating the enzyme with 20 μ l of 4-Butylresorcinol (Sigma-Aldrich, #49707) (10 mM) before adding 10 μ l of mushroom Tyr and 150 μ l of NaPB. Each condition was replicated four times. The plate was incubated at 37 °C for 30 min. After incubation, 20 μ l of light-sensitive L-DOPA (5 mM) was added to each well. Absorbance was measured at λ =484 nm using a Varioskan LUX multimode microplate reader using the SkanIt Software 6.1. Readings were taken every 5 min over a 220-min period, with constant agitation at 37 °C. Absorbance measures were normalized to protein concentration.

7. Image analysis

All quantifications were performed by an investigator blinded to the experimental cell groups.

7.1 Cell counting

7.1.1 Artificial intelligence-based quantifications

TH, α SYN and p α Syn-immunostained sections were scanned with Olympus Slideview VS200 slide scanner and the Olyvia 3.3 software. For TH immunostaining, either 5 μ m-thick rat SNpc brain sections were collected every 17th section, yielding 10-12 sections per animal, or 20 μ m-thick mouse SNpc brain sections were collected every 6th section, resulting in a similar number of 10-12 sections per animal. For α SYN and p α Syn immunostaining, four representative 5 μ m-thick rat brain sections spanning the entire SNpc were selected. A specific artificial intelligence (AI)-assisted algorithm was implemented for the quantification of Vector[®]SG-immunostained neurons (including TH-, α SYN- and p α Syn-positive neurons) using the Olympus VS200 Desktop 3.3 software. The algorithm was trained to identify four categories of objects within the desired region of interest (ROI): TH⁺NM⁻, TH⁺NM⁺, TH⁻NM⁺ neurons and extracellular NM (Figure 41 and Figure 42). Additionally, the algorithm was also capable to recognize α SYN and p α Syn-positive neurons.

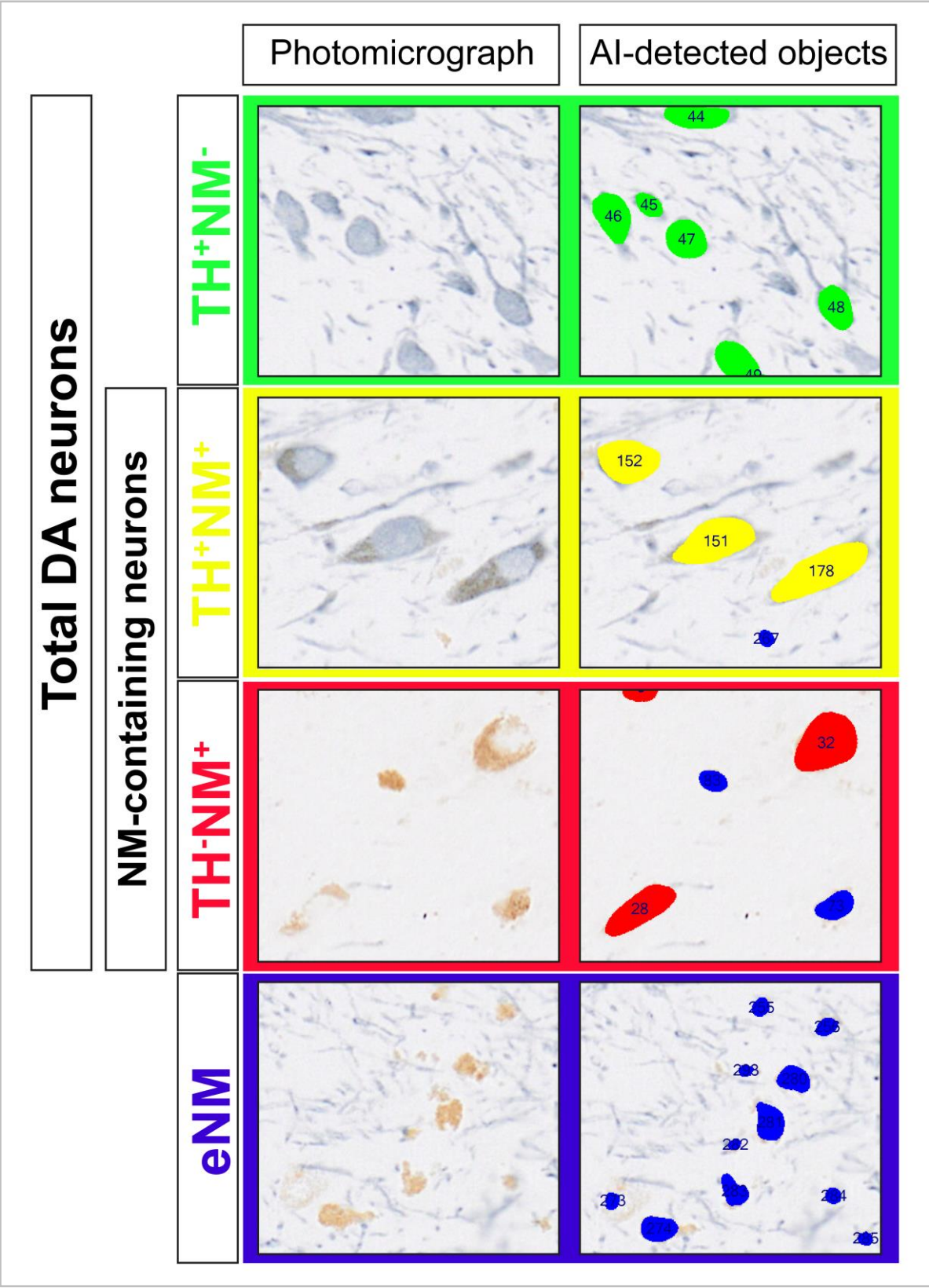


Figure 41. Four TH/NM object categories recognized by the AI-assisted algorithm. AI-assisted algorithm was trained to recognize Vector@SG-immunostained neurons distinguishing between TH⁺NM⁻, TH⁺NM⁺, TH⁻NM⁺ neurons and extracellular NM (eNM).

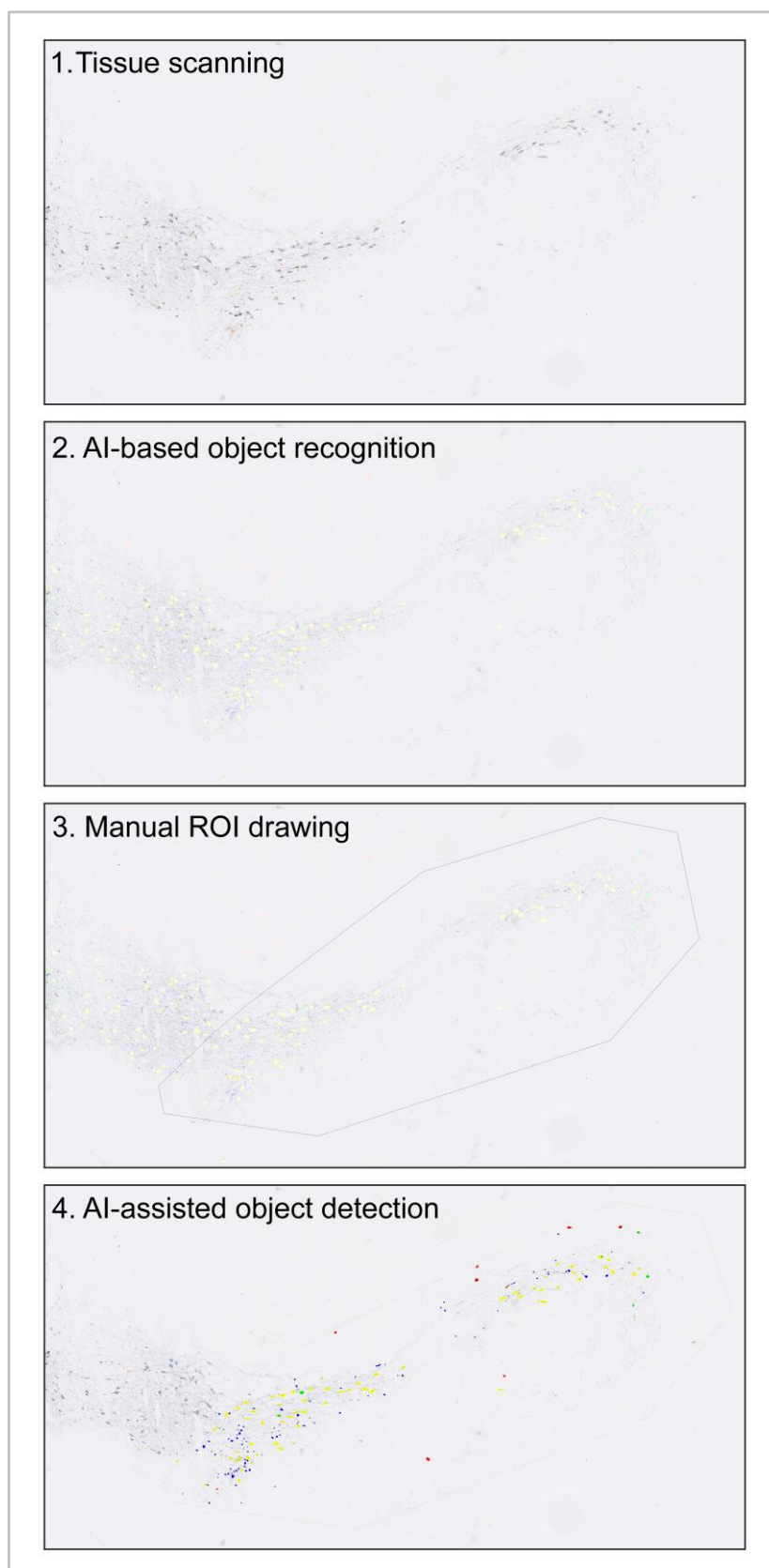


Figure 42. Main steps of AI-based cell counting. First, immunostained tissue sections were scanned using high-resolution imaging. The AI algorithm was then applied to automatically detect and classify all objects within the tissue. ROIs were manually defined, and the AI-detected objects within the selected ROIs were quantified for analysis.

7.1.2 Manual quantification

5µm-thick rat paraffin-embedded SN sections immunostained for TYR were scanned using the Olympus Slideview VS200 slide canner and the Olyvia 3.3 software, with one representative section selected per animal. TYR-positive neurons were manually quantified with QuPath and data was normalized to the total SN area to minimize bias.

7.2 Intracellular NM quantification

7.2.1 H&E-stained sections

5µm-thick rat paraffin-embedded H&E-stained sections representative from SN were selected (one representative section per animal) and all neurons per section were analysed. Catecholaminergic neurons were identified by the visualization of unstained NM brown pigment. H&E-stained sections were scanned using the Olympus Slideview VS200 slide scanner and the Olyvia 3.3 software. Quantifications were performed using QuPath for image visualization and ImageJ for analysis. Optical densitometry (OD) was used to assess intracellular NM density by measuring pixel brightness values of NM-containing cells (excluding the nucleus) and correcting for non-specific background staining, as in reference⁹⁹. The NM occupied area was calculated as the percentage of intracellular NM area relative to the total cytosolic area.

7.2.2 Bright-field images

For mouse brain analysis, 20 µm-thick cryopreserved sections from SN were selected, with one representative section per animal. All neurons within each section were analysed, with catecholaminergic neurons identified by the presence of brown NM pigment. The unstained bright-field (BF) sections were scanned using the Olympus Slideview VS200 slide scanner and visualised with Olyvia 3.3 software. An AI-assisted algorithm in the Olympus VS200 Desktop 3.3 software was applied for quantifying intracellular NM. Since the nuclei were unstained, only the pixel brightness of the NM pigment was measured. OD was used to assess intracellular NM density by measuring the brightness values of the NM pigment and correcting for non-specific background staining, as in reference¹⁰⁰.

7.2.3 Confocal images

Confocal images were obtained from Hoechst-stained GFP and αSYN-GFP TR5TY5 cells using the LSM 980 with Airyscan 2 confocal and ZEN 3.1 software. Quantifications were performed using QuPath for image visualization and ImageJ for analysis. OD was used to assess intracellular NM density by measuring pixel brightness values of NM-containing cells (excluding the nucleus) and correcting for non-specific background staining. The NM occupied area was calculated as the percentage of intracellular NM area relative to the total cytosolic area.

7.3 Extracellular NM quantification

7.3.1 H&E-stained sections

Serial H&E-stained, 5 μm -thick sections of the rat SN were collected, with one section every 34th, resulting in 5–6 sections per animal encompassing the entire SN, corresponding to half of the full SN series. Extracellular NM was identified by the presence of compacted brown NM granules/debris outside neurons. The stained sections were scanned using the Olympus Slideview VS200 slide scanner and visualised with Olyvia 3.3 software. Quantifications were performed using QuPath software, where extracellular NM granules were manually identified and counted.

7.3.2 TH-immunostained cryosections

For mouse brain analysis, extracellular NM granules/debris were quantified in TH-immunostained sections using an AI-assisted algorithm, as described in section 7.1 (Cell counting).

7.4 Quantification of neuropathological inclusions

Four representative 5 μm -thick rat brain sections covering the entire SNpc were selected for immunofluorescence staining with anti-p62 and anti-TH antibodies. Confocal images were captured using the LSM 980 with Airyscan 2, and quantifications were carried out using ZEN 3.1 software. Both p62-positive cytoplasmic and nuclear inclusions were quantified, and their presence within NM/TH-positive or negative neurons was recorded.

7.5 Quantification of neuroinflammation parameters

5 μm -thick rat paraffin-embedded sections of the SN stained for microglial/macrophage glycoprotein CD68 were scanned using the Olympus Slideview VS200 slide scanner and the Olyvia 3.3 software, with one representative SN section selected per animal. An AI-assisted algorithm in the Olympus VS200 Desktop 3.3 software was implemented for quantifying CD68-positive cells. Data was normalized to the total SN area to minimize bias.

7.6 Optical densitometry

The integrity of striatal DA fibers and the αSYN overexpression levels were evaluated by quantifying striatal TH or αSYN immunosignal, respectively, by OD. Serial coronal sections covering the whole STR (10 sections/animal for 5 μm -thick sections and 4 sections/animal for 20 μm -thick sections) were selected. TH/ αSYN -immunostained 5 μm -thick paraffin-embedded sections (rats) and 20 μm -thick free-floating cryosections (mice) were scanned with an Olympus Slideview VS200 slide scanner and visualised using QuPath software. Quantification was performed using Image J. Striatal densitometry values were corrected for non-specific background staining by subtracting densitometric

values obtained from the cortex within the same images. Data are expressed as OD or absorbance, calculated based on the logarithmic intensity of light transmission through the material using the formula: $-\log_{10} = \frac{\text{Striatum intensity}}{\text{Cortex intensity}}$.

7.7 pαSyn pathology quantification and brain distribution

pαSyn pathology and brain distribution were quantified in PFF-injected mice at 3.5 and 8 mpi in 20 μm-thick cryosections spanning the whole mouse brain, with each section stained for pαSyn. High-resolution photomicrographs were captured using an Olympus Slideview VS200 slide scanner and the Olyvia 3.3 software.

7.7.1 Early (3.5 mpi) time-point

First, pαSyn-positive elements were categorized in: (i) Lewy neurites, (ii) dystrophic Lewy neurites, (iii) aggregates or (iv) pαSyn-positive (either NM⁺ or NM⁻) cells (Figure 43). For quantification, 12 representative anatomical coronal sections from each mouse brain were selected. These sections were manually quantified using QuPath software, distinguishing between the different pαSyn-positive elements.

To represent the distribution of pαSyn pathology, the average total pαSyn accumulation at each anatomical level, including all pαSyn-positive elements from each animal, was calculated for both wt and tgNM mice. The anatomical level showing the highest pαSyn pathology was set to 100% and all the other data were normalized to a 0-100% scale. Different colour gradients were assigned for every 10% increment, and anatomical coronal sections from the Paxinos and Franklin atlas¹⁹⁹ were coloured using Adobe Illustrator according to this scale.

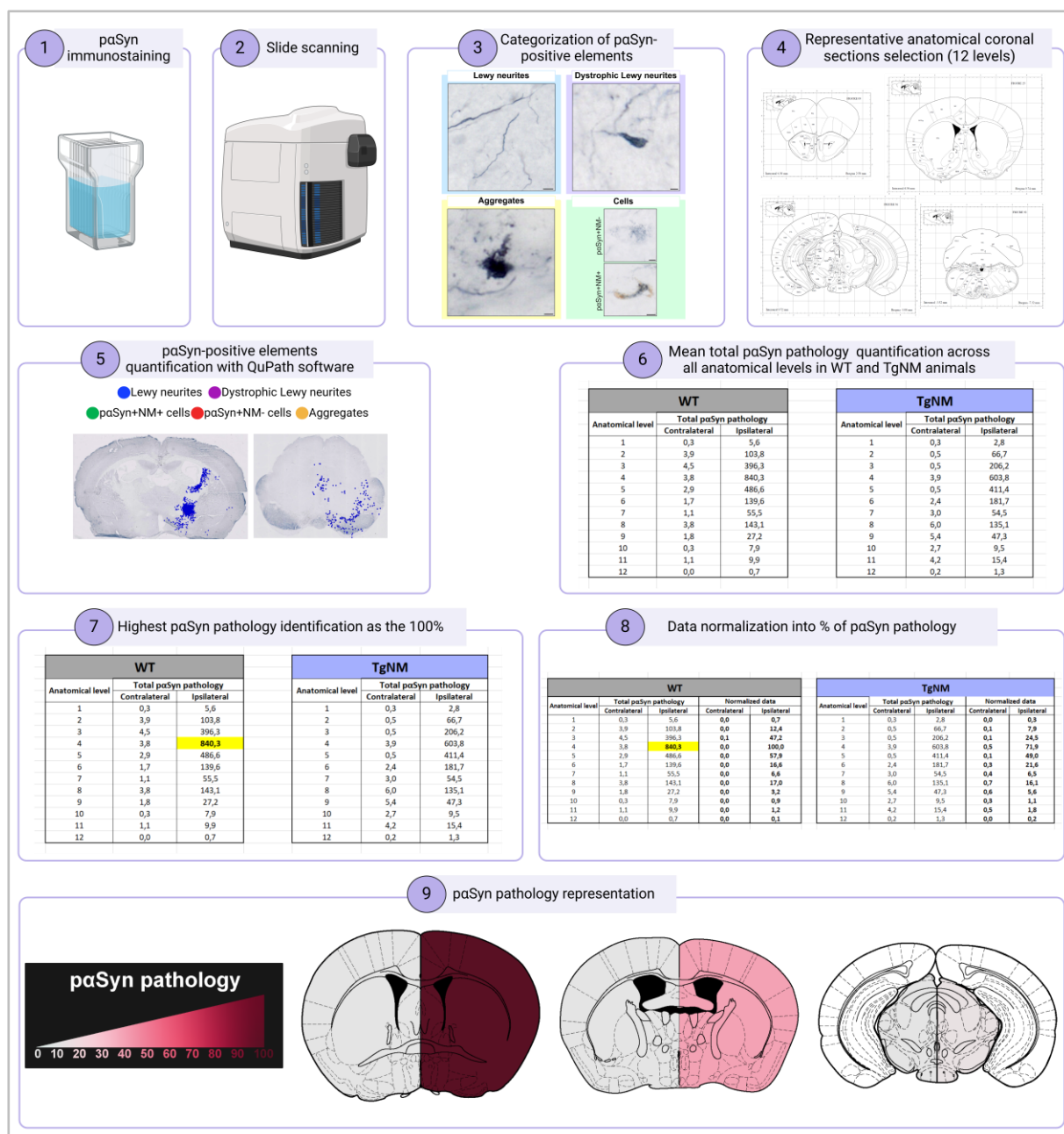


Figure 43. Workflow for pαSyn pathology quantification and distribution in PFF-injected wt and tgNM mice at 3.5 mpi. Brain sections spanning the entire mouse brain from PFF-injected wt and tgNM mice at 3.5 mpi were stained for pαSyn and scanned. pαSyn-positive structures were categorized into four types: (i) Lewy neurites, (ii) dystrophic Lewy neurites, (iii) aggregates or (iv) pαSyn-positive (NM+/NM-) neurons. Twelve representative anatomical coronal sections were selected per animal and manually quantified in QuPath, distinguishing among the different pαSyn-positive elements. For both wt and tgNM mice, the average total pαSyn accumulation at each anatomical level was calculated. The level with the highest pαSyn pathology was set at 100%, and all other values were normalized to a 0-100% scale. A colour gradient was applied in 10% increments, with anatomical sections from the Paxinos and Franklin atlas¹⁹⁹ coloured in Adobe Illustrator to visually illustrate pαSyn pathology distribution.

7.7.2 Late (8 mpi) time-point

Given the extensive p α Syn pathology at this time-point, manual quantification (as in the early time-point) proved unfeasible. Instead, a severity scoring system was developed, ranging from 0 (no pathology) to 5 (extensive pathology) (Figure 44).

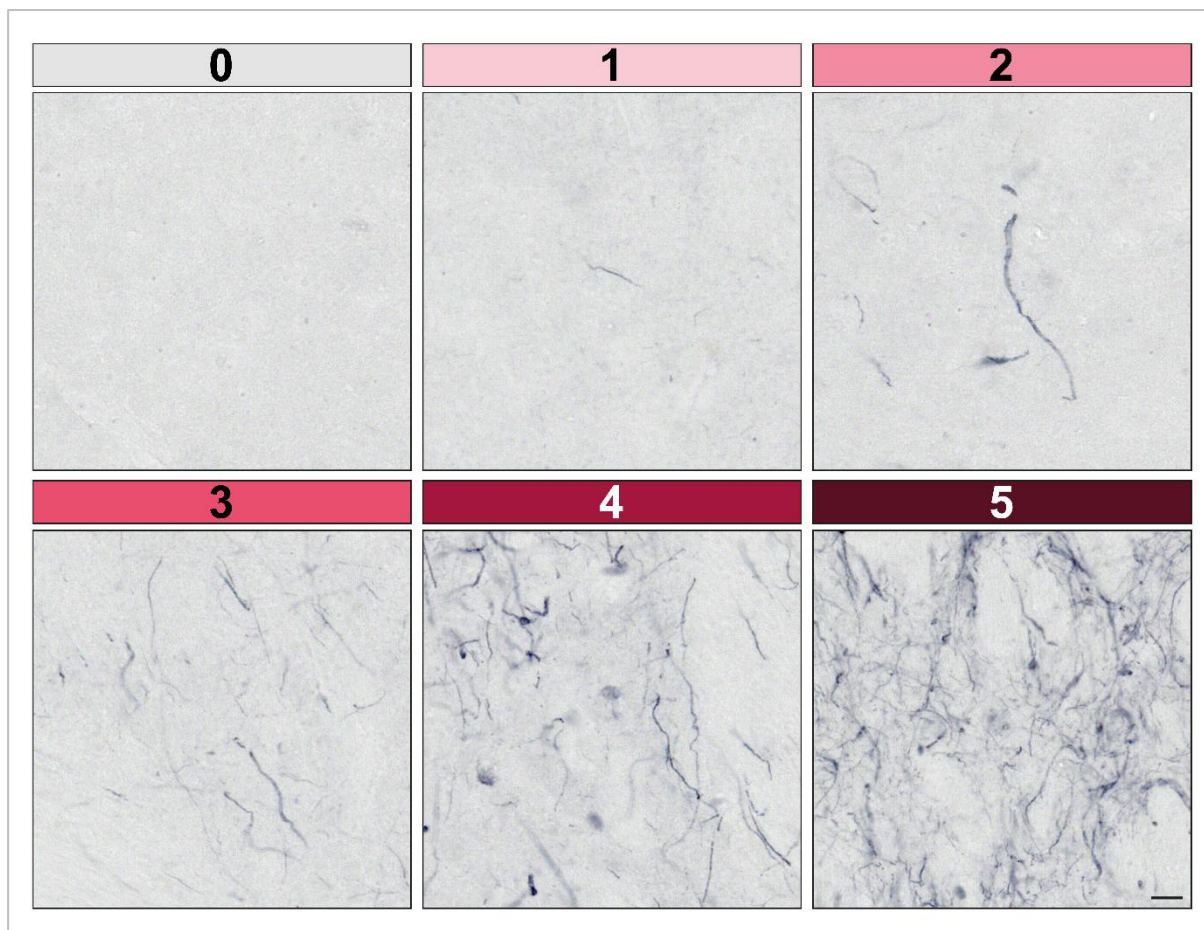


Figure 44. p α Syn pathological severity score. p α Syn pathology classification from 0 (no pathology) to 5 (massive pathology). Scale bar, 10 μ m.

The same 12 representative anatomical coronal sections from each mouse brain were selected as in 3.5 mpi time-point (Figure 45). Each nucleus within these coronal sections was assigned a unique letter code. Photomicrographs of tissue sections were superimposed onto the corresponding Paxinos and Franklin atlas¹⁹⁹ coronal sections in Adobe Illustrator to enable precise regional quantification using the severity scoring system. The mean severity score for each nucleus was calculated for both wt and tgNM animals. Different colour gradients were assigned to each score, and the Paxinos and Franklin atlas¹⁹⁹ coronal sections were colour-coded accordingly to visually represent the distribution of p α Syn pathology.

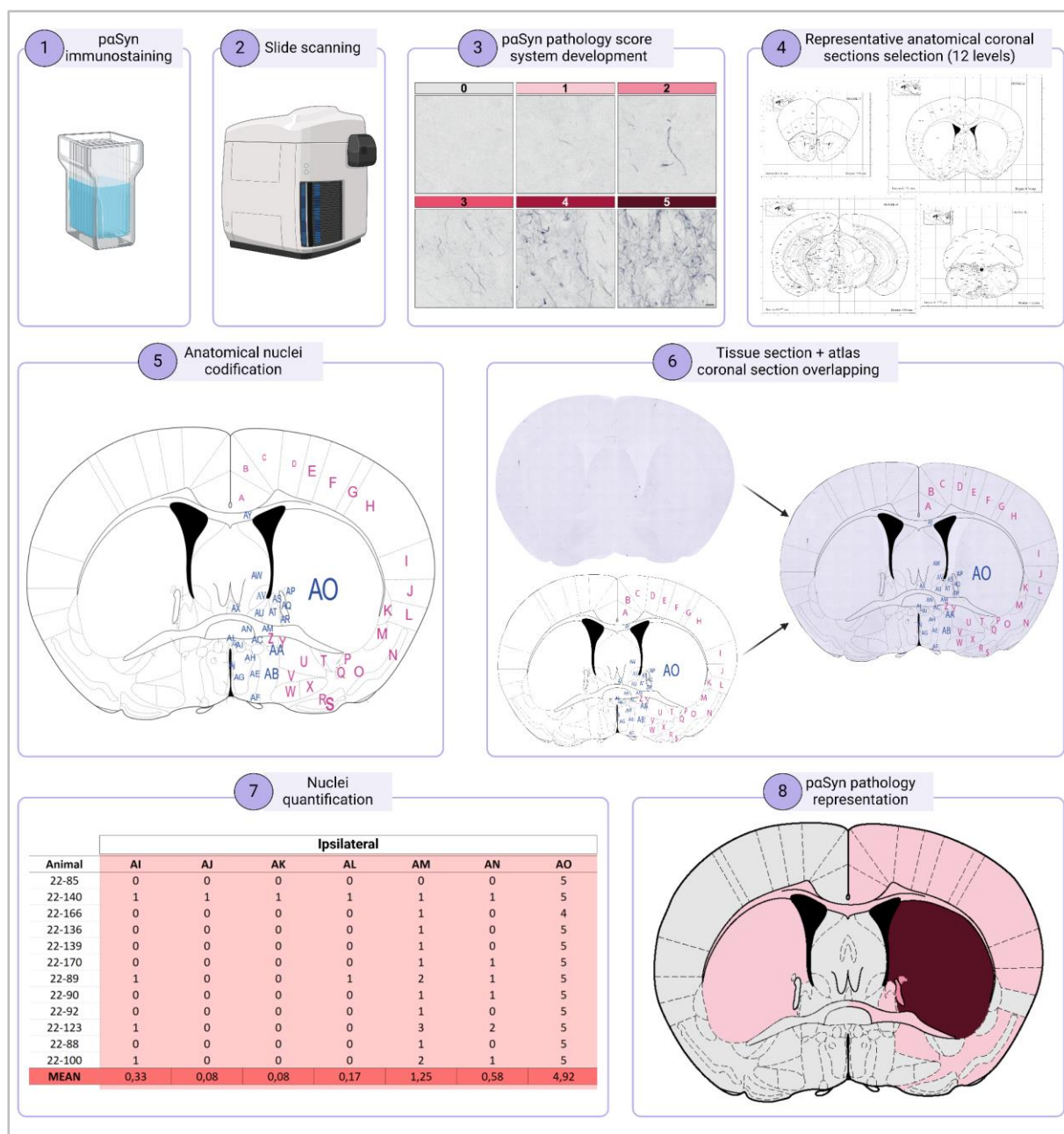


Figure 45. Workflow for pαSyn pathology quantification and distribution in PFF-injected wt and tgNM mice at 8 mpi. Brain sections spanning the entire mouse brain from PFF-injected wt and tgNM for pαSyn and scanned. A pαSyn pathological severity score system ranging from 0 (no pathology) to 5 (massive pathology) was developed. Twelve representative anatomical coronal sections were selected per mouse, with each nucleus assigned a unique letter code. Tissue photomicrographs were superimposed into corresponding Paxinos and Franklin atlas¹⁹⁹ coronal sections in Adobe Illustrator for precise scoring. Mean severity scores were calculated for each nucleus in both wt and tgNM animal groups. A colour gradient was applied to each score, and atlas sections were colour-coded accordingly to visually illustrate the intensity and distribution of pαSyn pathology.

8. Behavioural tests

All behavioural analyses were performed at the same time of the day (8 am-1 pm) during the light cycle by an investigator blinded to the experimental groups. The battery of motor and non-motor behavioural tests was performed over one and a half weeks prior to euthanasia, beginning with the less stressful tests and progressing to more stressful ones (i.e., cylinder test, olfaction test, fecal pellet output test, step down test and tail suspension test). A minimum of 48 h was ensured between the step down and tail suspension tests. Mice were habituated to the testing room for at least 1 h before each session. All equipment was cleaned with 70% ethanol after each test session to avoid olfactory cues.

8.1 Cylinder test

Mice were tested for left and right (i.e. contra- and ipsilateral) forepaw use with the cylinder test. Animals were individually placed in an open-top glass cylinder and the total number of left and right forepaw touches performed within 5 min was counted. Data are represented as use of contralateral forepaw (as % of total forepaw use) and number (n°) of total forepaw uses.

8.2 Beam traversal test

Mice were placed at the beginning of an elevated horizontal beam bar (40 cm) to evaluate their fine motor skills and coordination. The time taken by each mouse to traverse the beam was recorded, with a maximum cut-off of 60 s. If a mouse fell, the maximum time of 60 s was assigned. Mice that failed to complete the task _ either by not crossing or moving backward _ were excluded from the analysis. Two trials per mouse were performed. Mice at 3.5 mpi (corresponding to 6 m of age) were tested on a thinner beam, while those at 8 mpi (corresponding to 11.5 m of age) were tested on a thicker beam, as the older animals were unable to cross the thinner beam due to their body weight. Data are represented as the time to cross the beam (s).

8.3 Olfaction test

Animals were initially habituated to the presence of a cotton swab without any scent for 10 min. Following this, they were exposed to a cotton swab with water, then to a cotton swab impregnated with lemon essence (Essenciales) and finally to one impregnated with banana essence (Essenciales), with each exposure lasting 3 min. The discrimination index (DI) was calculated according to the formula: $(\text{Time exploring lemon or banana essence} - \text{Time exploring water}) / (\text{Time exploring lemon or banana essence} + \text{Time exploring water})$. Data are represented as the DI for either lemon or banana.

8.4 Fecal pellet output test

Mice were placed in individual cages and the number of fecal pellets evacuated was counted every 5 min during 1 h. Data are represented as the total n° of fecal pellets in 1h and the cumulative n° of fecal pellets in 1h.

8.5 Step down test

For the step down (or passive avoidance) test, the Step Down for Mice vibrating platform (#40570, Ugo Basile instrument) was used. The apparatus consists of a platform inside a mouse cage connected to a controllable high precision electric shocker. During the training session, mice were individually placed in the platform and received an electric shock of 0.6 mA when stepping down the platform. After 24 h, during the test session, mice were placed back on the same platform, and the time spent on the platform was measured, with the net remaining uncharged this time. Data are presented as the latency to step down during the test session (s) and the ratio of the latency to step down in the test session to that in the training session (s). This ratio normalizes for inter-individual variability in curiosity and activity levels among the mice.

8.6 Tail suspension test

Mice were suspended by their tails with a tape into a suspension bar, ensuring they could not escape, grip nearby surfaces or climb their tails. The latency to the first immobility and the total immobility time were recorded over a 6 min period. Data are presented as the latency (s) and the total immobilization time (s).

9. Chromatographic determination of dopamine metabolites

9.1 Brain collection

For Ultra-Performance Liquid Chromatography–Tandem Mass Spectrometry (UPLC-MS/MS) analyses, brain samples were obtained from 24 Sprague-Dawley male rats that were stereotaxically injected in the right SNpc with either AAV- α SYN/vehicle, AAV-TYR/vehicle or AAV- α SYN/AAV-TYR, following above-mentioned procedures. Contra- and ipsilateral ventral midbrain (vMB) hemiregions were quickly dissected out, frozen on dry ice and stored at -80 °C until analysed.

9.2 Calibration curves and sample preparation

UPLC-MS/MS analysis of vMB rat samples was performed using our previously validated method²⁰⁰ with modifications. A stock solution of the internal standard (IS), dopamine-1,1,2,2-d4 hydrochloride (DA-d4) (Sigma-Aldrich, #73483), was prepared in 25mM formic acid (FA) and stored and -80 °C until use. DA and L-DOPA solutions were freshly

prepared, mixed and serially diluted with 25 mM FA to create a concentration series for calibration curves. The IS was added to the mixture at a final concentration of 500 nM.

To generate calibration curves and quality control samples, vMB hemiregions from three animals were pooled and homogenized in 4 ml of 250 mM FA. Homogenates were divided into 120 μ l aliquots, followed by the addition of 40 μ M of the mixture. Samples were then centrifuged at 20,000 \times g for 10 min at 4 °C, and 120 μ l of the supernatant combined with an equal volume of 25 mM FA, was transferred to an Ostro® protein precipitation and phospholipid removal plate (Waters, #186005518) and filtered. Finally, 7 μ l were injected in the UPLC-MS/MS system. For brain samples, calibration levels spanned a linear range of 1–3000 nM for each metabolite (DA and L-DOPA), maintaining the IS concentration at 500 nM.

On the day of analysis, frozen brain samples were homogenized in 300 μ l of 250 mM FA. A 10 μ l aliquot was taken and diluted 1:10 with FA for protein quantification using the BCA method. IS was then added to samples at a final concentration of 500nM. Samples were centrifuged at 20,000 \times g for 10 min at 4 °C, and the resulting supernatant was filtered using the Ostro®. Finally, 7 μ l of the processed sample was injected in the UPLC-MS/MS system for analysis.

9.3 UPLC-MS/MS analysis

An Acquity UPLC system coupled to a Xevo TQ-S triple quadrupole mass spectrometer with an electrospray ionization interface was utilized. Instrument control, data acquisition, and analysis were conducted using MassLynx v4.1 software. Chromatographic separation was achieved using an Acquity™ HSS T3 column (1.8 μ m, 2.1 \times 100 mm) (Waters, #186003539) paired with an Acquity™ HSS T3 VanGuard pre-column (100 Å, 1.8 μ m, 2.1 \times 5 mm) (Waters, #186003976). The column was maintained at 40 °C, while the autosampler was held at 6 °C. The mobile phase consisted of solvent A (methanol 100%) and solvent B (25 mM Fa in water), delivered at a flow rate of 0.4 ml/min with the following gradient profile: 0.5% B maintained for 0.5 min, 8% B at 2.6 min, 55% B at 2.9 min, 60% B at 3.3 min, 80% B at 4.3 min, 90% B at 4.4 min and maintained for 0.5 min, and 0.5% B at 5 min followed by 1 min of equilibration. The mass spectrometer detector operated under the following parameters: source temperature 150 °C, desolvation temperature 450 °C, cone gas flow 50 l/h, desolvation gas flow 1100 l/h and collision gas flow 0.15 ml/min. Argon was employed as the collision gas. The capillary voltage was set at 0.5 kV. The electrospray ionization source was alternated between positive and negative ion modes, depending on the analyte. Multiple Reaction Monitoring (MRM) acquisition settings for the targeted metabolites are summarized in [Table 3](#). Samples were considered acceptable if their concentrations were between the limit of detection (LOD) and the limit of quantification (LOQ) or exceeded the LOQ. Concentrations below the LOD were reported as the LOD value. DA vesicular uptake was calculated as DA:L-DOPA ratio²⁰¹.

Analyte	Transition (m/z)	Retention time (min)	Dwell time (ms)	Cone voltage (V)	Collision energy (eV)	Capillary voltage (kV)
DA-4d (IS)	157.83>9.8	1.44	52	10	20	0.5
DA	153.93 > 90.57	1.46	52	10	20	0.5
L-DOPA	198,1 > 152.1	1.48	52	15	15	0.5

Table 3. MRM acquisition settings. MRM acquisition settings for DA-4d, DA and L-DOPA analytes.

10. Statistical analyses

Statistical analyses were performed with GraphPad Prism software (v8, Graphpad Softaw Inc, USA). No statistical methods were used to pre-determine sample size but sample sizes are equivalent to those reported in previous similar publications. Data are presented as histogram bars, with all values expressed as the mean \pm standard error of the mean (SEM). Outlier values were identified by ROUT test and excluded from the analyses when applicable.

Normality of data distribution was assessed using the Shapiro-Wilk test. For comparisons between two groups, an unpaired t-test was used for normally distributed data, while the Mann-Whitney test was applied for non-parametric data. For comparisons among three groups or more involving a single variable, a one-way ANOVA followed by Holm-Sidak's post-hoc test was performed for normal data, or a Kruskal-Wallis test with Dunn's post-hoc for non-parametric data. For comparisons involving two variables, a two-way ANOVA followed by Tukey's post-hoc test was applied. For comparisons involving three variables, a three-way ANOVA followed by Tukey's post-hoc test was used. In all analyses, the null hypothesis was rejected at the 0.05 level.

11. Buffers and antibodies

The buffer recipes used in this study are summarized in [Table 4](#).

Buffer	Recipe	
Phosphate buffer (PB) 0.2M (1l)	Sodium phosphate dibasic (Na_2HPO_4)	21.3g
	Sodium phosphate monobasic (H_2NaPO_4)	6.4g
	H_2O	1000ml
Tris buffered saline (TBS) 1M at pH 7,4 (1l)	Tris-base ($\text{C}_4\text{H}_{11}\text{NO}_3$)	121.1g
	Sodium chloride (NaCl)	90g
	H_2O	1000ml
Phosphate buffered saline (PBS) 1M at pH 7,4	Sodium phosphate dibasic (Na_2HPO_4)	17.8g
	Potassium phosphate dibasic (KH_2HPO_4)	2.4g
	Sodium chloride (NaCl)	90g
	H_2O	1000ml
Sodium phosphate buffer (NaPB) at pH 6,8 (1l)	4 Sodium phosphate dibasic (Na_2HPO_4)	5.325g
	1 Sodium phosphate monobasic (H_2NaPO_4)	1.725g
	H_2O	1000ml

Table 4. Recipes for the buffers used in this study.

The primary antibodies used in this study, along with their specifications, are summarized in Table 5.

Primary antibody	Host	Manufacturer	Technique	Brain region	Dilution	Incubation
Anti- α Syn	Mouse	BD Biosciences, #610786	WB		1:1000	24h
Anti- α SYN	Rat	Enzo, #ALX-804-258-LC05	IHC (paraffin)	SN and STR	1:1000	24h
			IHC (FF)	Whole brain	1:1000	24h
			IF (paraffin)	SN	1:100	24h
			WB		1:1000	24h
			ICC (cells)		1:500	24h
Anti-p α Syn	Rabbit	Abcam, #51253	IHC (paraffin)	SN	1:500	24h
			IHC (FF)	Whole brain	1:1000	24h
Anti- β -actin	Mouse	Sigma-Aldrich, #A5441	WB		1:10,000	24h
Anti-CD68	Mouse	BIO-RAD, #MCA341R	IHC (paraffin)	SN	1:100	24h
Anti-p62	Guinea pig	Progen, #GP62-C	IF (paraffin)	SN	1:500	24h
			ICC (cells)		1:500	24h
Anti-TH	Rabbit	Calbiochem, #657012	IHC (paraffin)	SN	1:20,000	48h
				STR	1:3,500	48h
			IHC (FF)	SN	1:20,000	48h
				STR	1:5,000	48h
			IF (paraffin)	SN	1:1000	24h
Anti-TYR	Mouse	Epredia™, #MS-800-P1	IHC (paraffin)	SN	1:750	24h
			ICC (cells)		1:500	24h
Anti-TYR	Rabbit	Santa Cruz, #sc-15341	WB		1:1000	24h
Anti-VAMP2	Mouse	Thermo Fisher Scientific, #MA5-38260	IF (paraffin)	SN	1:500	24h

Table 5. Overview of the primary antibodies used in immunohistochemistry (IHC), immunofluorescence (IF), immunocytochemistry (ICC) and WB. The table provides detailed technical information for each antibody including host species, manufacturer's reference, application technique, brain region, dilution and incubation duration. FF, free-floating.

Details of the secondary antibodies used are summarized in Table 6.

Technique	Secondary antibody	Host	Manufacturer	Dilution
IHC	Biotinylated anti-rabbit	Goat	Vector laboratories, #BA1000	1:1000
	Biotinylated anti-mouse	Goat	Vector laboratories, #BA9200	1:1000
	Biotinylated anti-rat	Goat	Vector laboratories, #BA9400	1:1000
IF	Alexa fluor 488 anti-guinea pig	Goat	Gibco, #A11073	1:1000
	Alexa fluor 488 anti-mouse	Goat	Gibco, #A11001	1:1000
	Alexa fluor 647 anti-rabbit	Donkey	Life technologies, #A31573	1:1000
	Alexa fluor 647 anti-rat	Chicken	Gibco, #A21472	1:1000
ICC	Alexa fluor 568 anti-mouse	Goat	Life technologies, #A11004	1:1000
	Alexa fluor 647 anti-rat	Chicken	Gibco, #A21472	1:1000
WB	Anti-mouse IgG HRP	Goat	Merck, #NXA931	1:1000
	Anti-rabbit IgG HRP	Goat	Invitrogen, #31460	1:1000

Table 6. Overview of the secondary antibodies used in immunohistochemistry (IHC), immunofluorescence (IF), immunocytochemistry (ICC) and WB. The table provides detailed technical information for each antibody including host species, manufacturer reference and dilution.

RESULTS

RESULTS

1. Chapter I. Effects of α SYN overexpression on NM-associated PD pathology

1.1 Experimental design

To assess whether increased α Syn levels may hasten NM-associated PD pathology *in vivo*, adult male rats received a single unilateral stereotaxic injection of either an AAV expressing human α SYN (AAV- α SYN), human TYR (AAV-TYR), or both (AAV- α SYN + AAV-TYR) above the right SNpc (Figure 46a). Rats were euthanised at (i) 8 weeks (w) post-AAV (i.e. preceding NM-linked cell death according to a previously validated AAV-TYR rat model from this laboratory)⁹⁹; (ii) 16 w post-AAV (at which time-point animals start exhibiting nigrostriatal dysfunction and incipient degeneration); or (iii) 60 w post-AAV (once nigrostriatal degeneration is fully established in these animals). Ipsilateral α SYN overexpression was verified by immunohistochemistry using an antibody specific for human α SYN in the STR of 8 w α SYN-injected and α SYN+TYR-co-injected animals (Figure 46b). Furthermore, levels of TYR overexpression were assessed by immunohistochemistry in the SNpc of 8 w TYR-injected and α SYN+TYR-co-injected animals (Figure 46c).

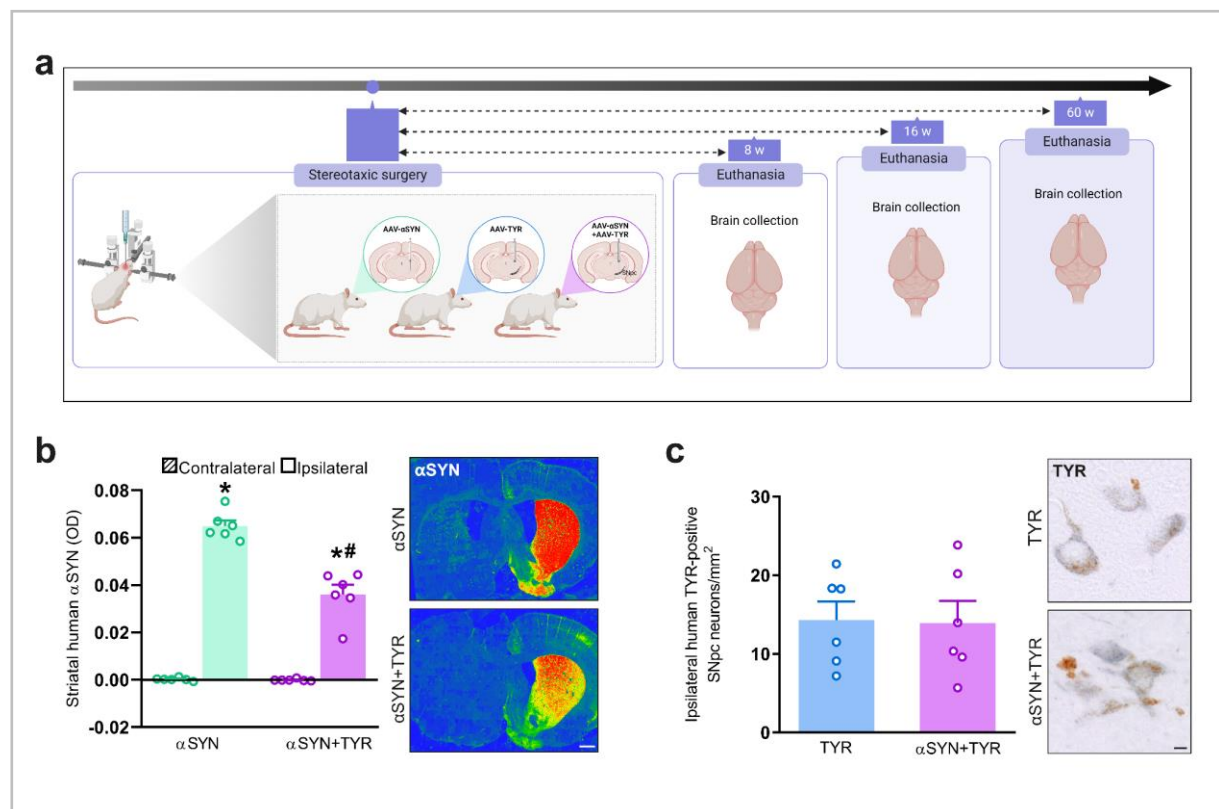


Figure 46. Overexpression of α SYN and/or TYR in the nigrostriatal pathway of rats. (a) Schematic representation of the experimental design. (b) *Left*, OD of striatal α SYN in α SYN- and α SYN+TYR-injected rats at 8 w. * $p < 0.05$ compared to respective contralateral measurement; # $p < 0.05$ compared to ipsilateral α SYN level. A two-way ANOVA followed by Tukey's post-hoc test was used to assess statistical significance. $n = 6$ animals per group. *Right*, representative photomicrographs of striatal α SYN immunolabeling. Scale bar,

1 mm. (c) *Left*, quantification of ipsilateral TYR-positive SNpc neurons in TYR- and α SYN+TYR-injected rats at 8 w. Mann-Whitney test. n=6 animals per group. *Right*, representative photomicrographs of ipsilateral SNpc TYR-immunolabeling (TYR-positive neurons in blue; unstained NM in brown). Scale bar, 5 μ m. Drawing in a was created with Biorender.com.

1.2 Enhanced intracellular NM levels in α SYN-expressing NM-producing animals

NM accumulation in the AAV-TYR rat model progresses over time, ultimately leading to a PD-like phenotype characterised by motor deficits and neuropathological alterations such as intracellular inclusions or TH phenotypic downregulation and nigrostriatal degeneration⁹⁹. To determine the potential effects of α SYN upregulation on NM-linked PD pathology, we first assessed NM levels in α SYN-overexpressing AAV-TYR rats. The intracellular NM density and NM-occupied cell area were quantified in H&E-stained SNpc sections from TYR- and α SYN+TYR-injected animals at 8, 16 and 60 w post-AAV (Figure 47). Compared to TYR-injected animals, α SYN+TYR-co-injected rats exhibited a significant increase in intracellular NM density and NM-occupied area over time, reaching statistical significance from 16w onwards (Figure 47). These results suggest that α SYN overexpression boosts intracellular NM accumulation in TYR melanized rats.

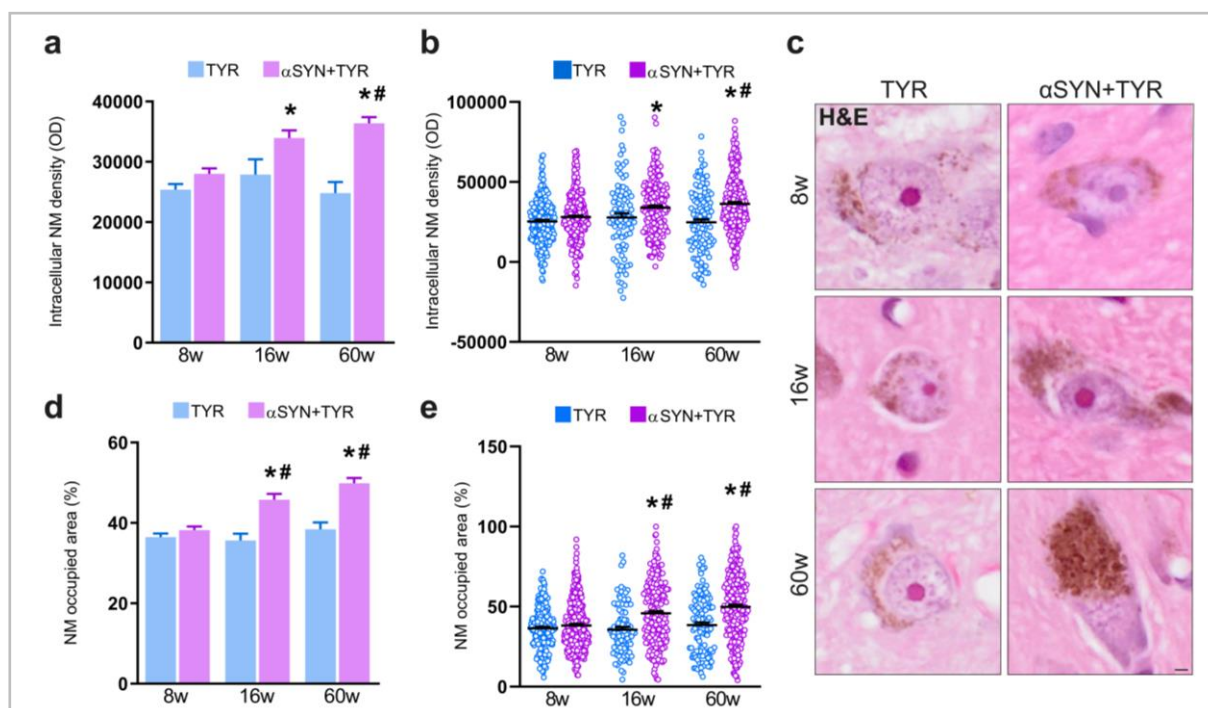


Figure 47. Intracellular NM levels in TYR- and α SYN+TYR-injected rats. (a & b) Quantification of intracellular NM levels by OD in ipsilateral SNpc DA neurons from TYR- and α SYN+TYR-injected rats at 8, 16 and 60 w. *p<0.05 compared to α SYN+TYR at 8 w. #p<0.05 compared to TYR at 60 w. (c) Representative photomicrographs from H&E-stained brain sections showing progressive NM accumulation (brown) within ipsilateral SNpc DA neurons in TYR- and α SYN+TYR-injected rats at 8, 16 and 60 w. Scale bar, 2 μ m. (d & e) Percentage of neuronal cytosolic area occupied by NM in ipsilateral SNpc DA neurons in TYR- and α SYN+TYR-injected rats at 8, 16 and 60 w. *p<0.05 compared to α SYN+TYR at 8 w. #p<0.05 compared to respective TYR. In all panels, statistical significance was assessed with a two-way ANOVA followed by Tukey's post-hoc test. n=89-294 neurons per group.

1.3. Increased α Syn pathology in α SYN-expressing NM-producing animals

Nigral overexpression of total human-specific α SYN was assessed by counting ipsilateral α SYN-positive SNpc neurons in α SYN- and α SYN+TYR-injected rats at 8, 16 and 60 w post-AAV (Figure 48a). Within each experimental group, the number of nigral α SYN-positive neurons was roughly constant over time. However, α SYN+TYR co-injected animals displayed fewer α SYN-positive SNpc neurons than α SYN-injected animals at all time-points examined. Phosphorylation of α Syn (p α Syn) has been associated with its aggregation and accumulation into LB insoluble protein deposits and is largely considered to be an index of pathological α Syn^{109,125}. Here, p α Syn at serine 129 was analysed by quantifying ipsilateral p α Syn-positive SNpc neurons in the three animal groups at 8, 16 and 60 w (Figure 48b). Using an antibody that detects both human and murine p α Syn, TYR-injected animals did not exhibit p α Syn-positive SNpc neurons at any time-point. In contrast, all α SYN-injected animals exhibited p α Syn-positive nigral neurons. Similar to the total α SYN analyses above, the number of p α Syn-positive neurons was lower in α SYN+TYR-injected rats at 16 and 60 w compared to respective α SYN-injected animals. In all α SYN-injected groups, the number of p α Syn-positive neurons was systematically lower than the number of total α SYN-positive neurons.

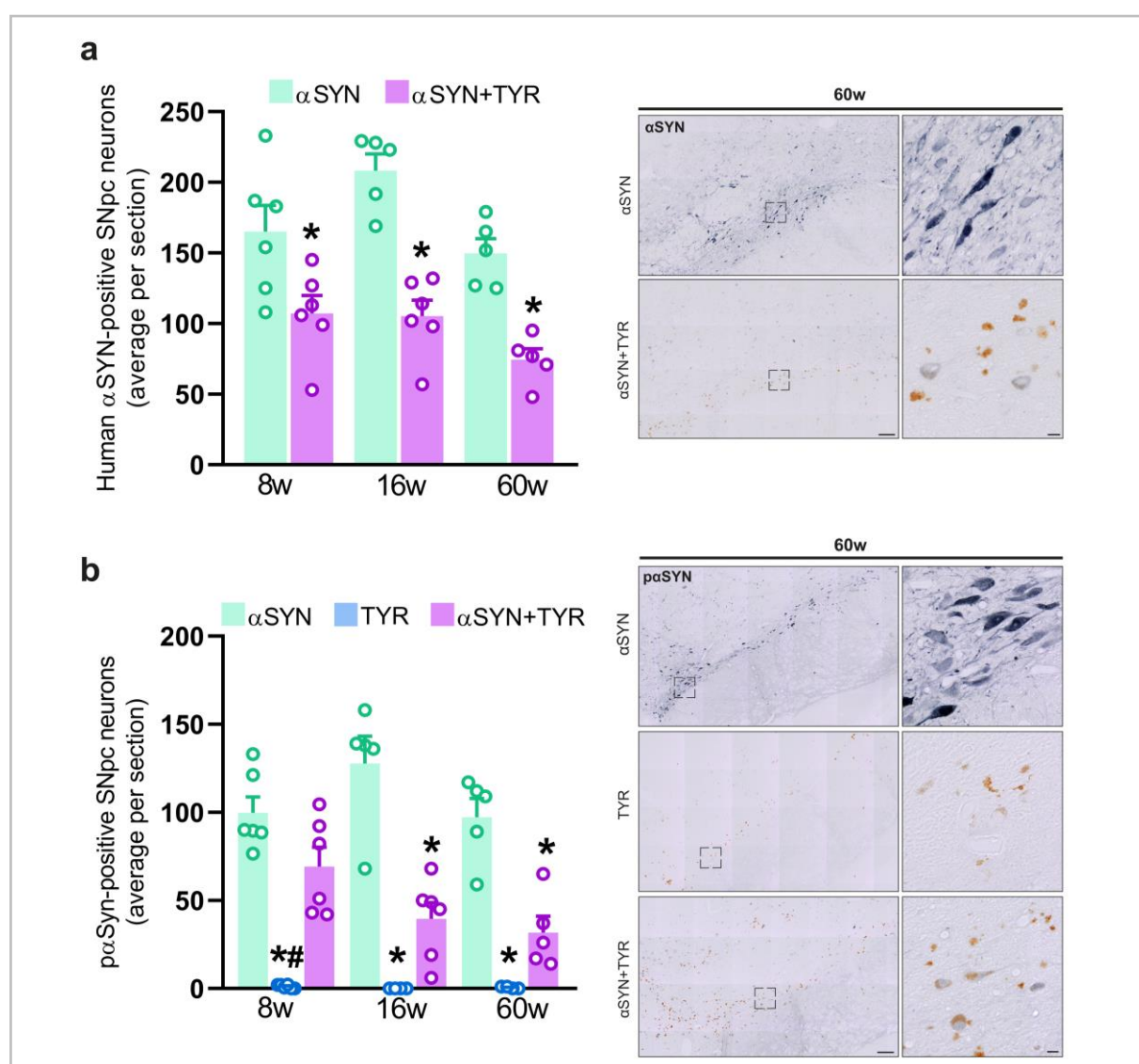
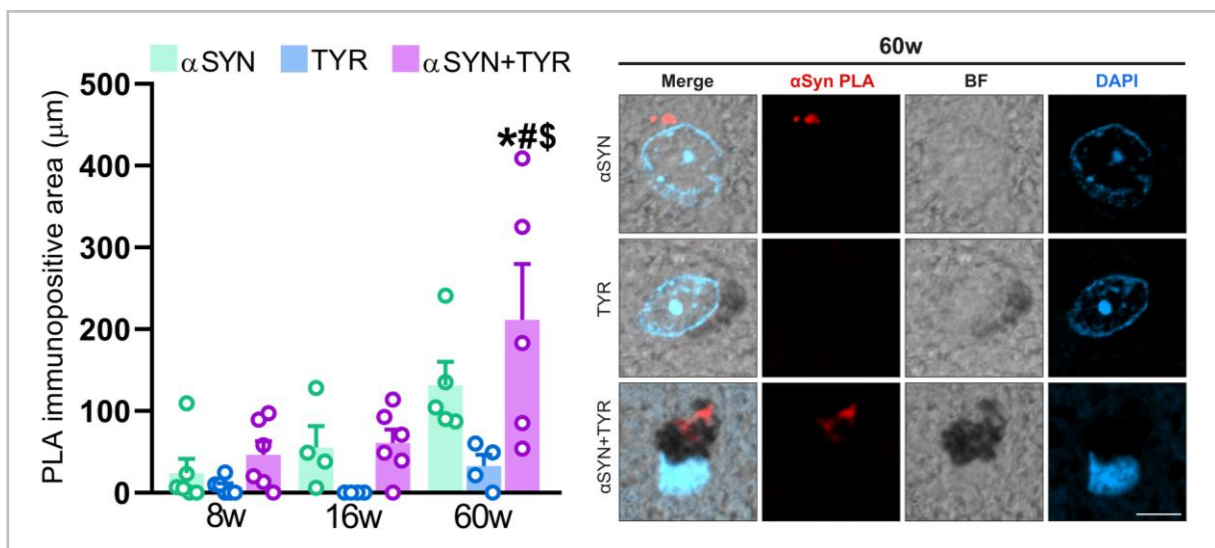


Figure 48. Total and phosphorylated α Syn expression in α SYN-expressing NM-producing rats. **(a)** *Left*, quantification of human α SYN-positive SNpc neurons in α SYN- and α SYN+TYR-injected rats at 8, 16 and 60 w. * $p < 0.05$ compared to respective α SYN levels. *Right*, representative photomicrographs of ipsilateral α SYN immunolabeling at 60 w. Scale bars, 10 μ m. **(b)** *Left*, quantification of p α SYN-positive SNpc neurons in α SYN, TYR- and α SYN+TYR-injected rats at 8, 16 and 60 w. * $p < 0.05$ compared to respective α SYN levels. # $p < 0.05$ compared to α SYN+TYR levels at 8 w. *Right*, representative photomicrographs of ipsilateral p α Syn immunolabeling at 60 w. Scale bars, 10 μ m. In a & b, a two-way ANOVA followed by Tukey's post-hoc test was used to assess statistical significance. $n = 4-6$ animals per group.

Given that α Syn oligomers are considered to be noxious intermediaries in PD-related neurodegeneration¹³⁸, α Syn oligomeric species were quantified by means of a PLA. At 60 w, α SYN+TYR-co-injected animals manifested the highest α SYN PLA immunopositive area compared to the other experimental groups and time-points (Figure 49).



As a PD-relevant neuropathological hallmark in the AAV-TYR rat model, animals showed LB-like cytoplasmic inclusions as well as MB-like nuclear inclusions, an aging hallmark specific to NM-containing neurons. Both types of inclusions peaked at 8 w preceding neuronal death as previously described⁹⁹. Similar to inclusions identified in human *post-mortem* aged and PD brains, these inclusions were immunopositive for p62, a prevalent constituent of neuropathological inclusions⁴¹. Here, the number of p62-positive cytoplasmic and nuclear inclusions was determined in the SN from α SYN-, TYR- and α SYN+TYR-injected animals at 8, 16 and 60 w (Figure 50). Very few p62-positive cytoplasmic or nuclear inclusions were observed in any of the α SYN-injected animals. In TYR-injected animals, p62 cytoplasmic inclusions peaked at 8 w and then decreased substantially, which is consistent with the abovementioned previous results (Figure 50a). In contrast, α SYN+TYR-co-injected rats showed a more sustained accumulation of p62

cytoplasmic inclusions before levels decreased by 60 w. Regarding MB-like inclusions, a progressive accumulation of intranuclear p62 inclusions was observed exclusively in α SYN+TYR-co-injected animals (Figure 50b). Notably, in all experimental groups, p62-positive inclusion formation, either cytoplasmic or nuclear, was restricted to melanized neurons.

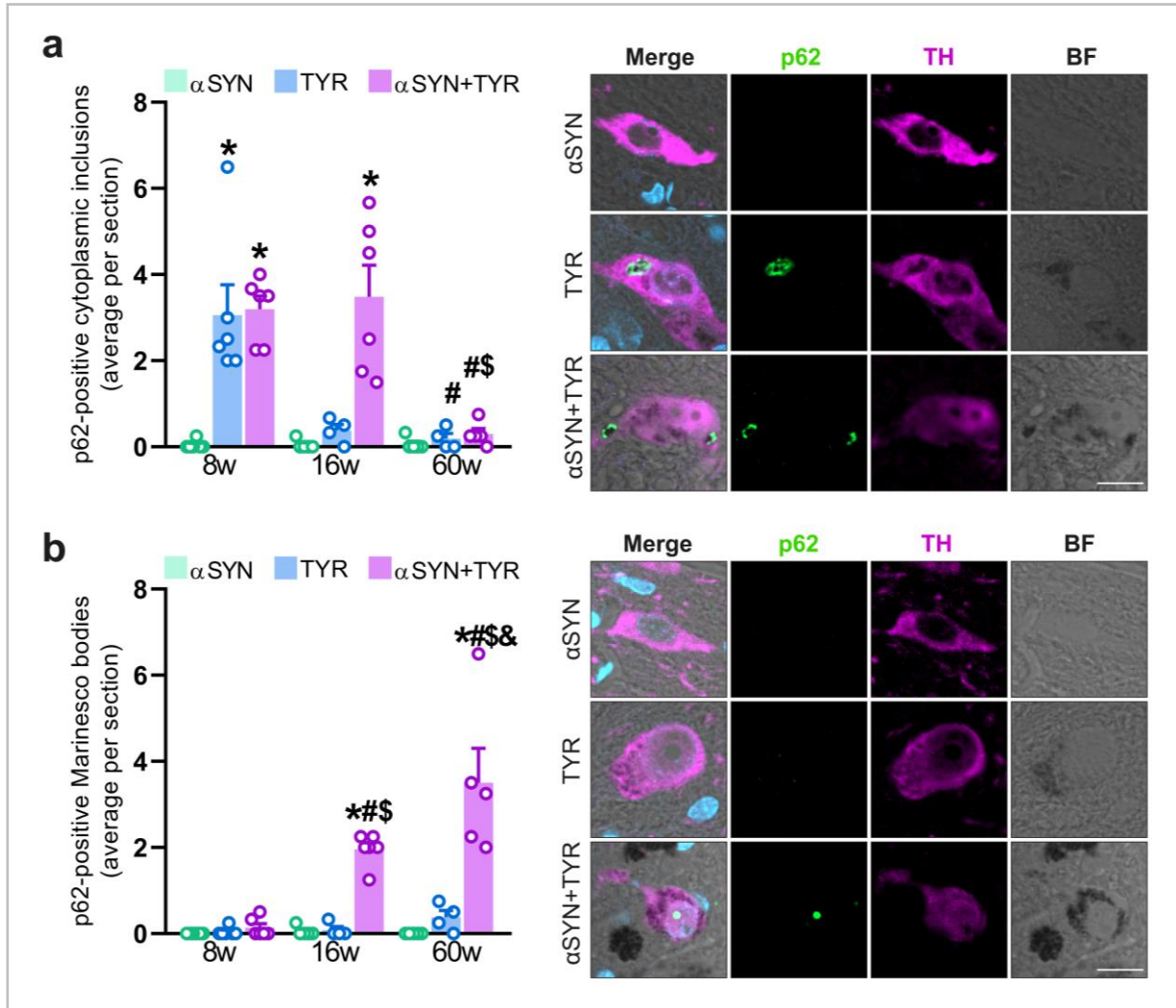


Figure 50. Neuropathological PD-like inclusions in α SYN-expressing NM-producing rats. **(a)** *Left*, quantification of p62-positive cytoplasmic SNpc inclusions in α SYN-, TYR- and α SYN+TYR-injected rats at 8, 16 and 60 w. *p<0.05 compared to respective α SYN. #p<0.05 compared to respective 8 w. \$p<0.05 compared to α SYN+TYR at 16 w. *Right*, representative photomicrographs of ipsilateral p62-positive cytoplasmic inclusions. p62, green; TH, magenta; DAPI, blue; NM, dark grey in BF. Scale bar, 10 μ m. **(b)** *Left*, quantification of p62-positive nuclear SNpc inclusions in α SYN-, TYR- and α SYN+TYR-injected rats at 8, 16 and 60 w. *p<0.05 compared to respective α SYN. #p<0.05 compared to respective TYR. \$p<0.05 compared to α SYN+TYR at 8 w. &p<0.05 compared to α SYN+TYR at 16 w. *Right*, representative photomicrographs of ipsilateral MB. p62, green; TH, magenta; DAPI, blue; NM, dark grey (BF). Scale bar, 10 μ m. In a & b, a two-way ANOVA followed by Tukey's post-hoc test was used to assess statistical significance. n=4-6 animals per group.

1.4. Enhanced nigrostriatal degeneration in α SYN-overexpressing NM-producing animals

Next, the impact of α SYN overexpression on NM-linked neurodegeneration was assessed in α SYN-, TYR- and α SYN+TYR-injected rats at 8, 16 and 60 w post-AAV. First, TH-positive fibers in the STR of these animals were quantified by OD (Figure 51a). In α SYN-injected animals, ipsi- versus contralateral striatal TH levels were maintained at ~60-80% over time. In contrast, TYR-injected animals exhibited a significant decrease in nigrostriatal TH fibers at 16 and 60 w compared to 8 w animals. This decrease was further enhanced in α SYN+TYR-injected rats at 60 w compared to TYR-injected animals. Since a heightened striatal loss was observed in α SYN+TYR animals at 60 w, SNpc TH-positive cell bodies were quantified at this time-point (Figure 51b). Both TYR- and α SYN+TYR-injected rats exhibited a significant loss of TH-positive neurons in the ipsilateral SNpc, either compared to their respective contralateral SNpc or to the ipsilateral SNpc of α SYN animals. As observed in PD brains, NM-producing rats also display a phenotypic loss of TH expression within NM-laden neurons, indicative of early-stage neuronal dysfunction/degeneration^{94,99}. Here, TH downregulation was determined by assessing the percentage of TH-immunonegative neurons within the total population of NM-containing neurons (Figure 51c). Both TYR and α SYN+TYR animals exhibited a similar degree of TH downregulation. To distinguish between the effects of α SYN on TH downregulation and on actual cell death, the total number of SNpc DA neurons (including TH⁺NM⁻, TH⁺NM⁺ and TH⁻NM⁺ neurons) was assessed, with a significant decrease in ipsilateral SNpc DA neurons seen exclusively in α SYN+TYR-injected rats, thus indicating that increased α SYN levels in NM-accumulating animals exacerbate nigrostriatal cell death.

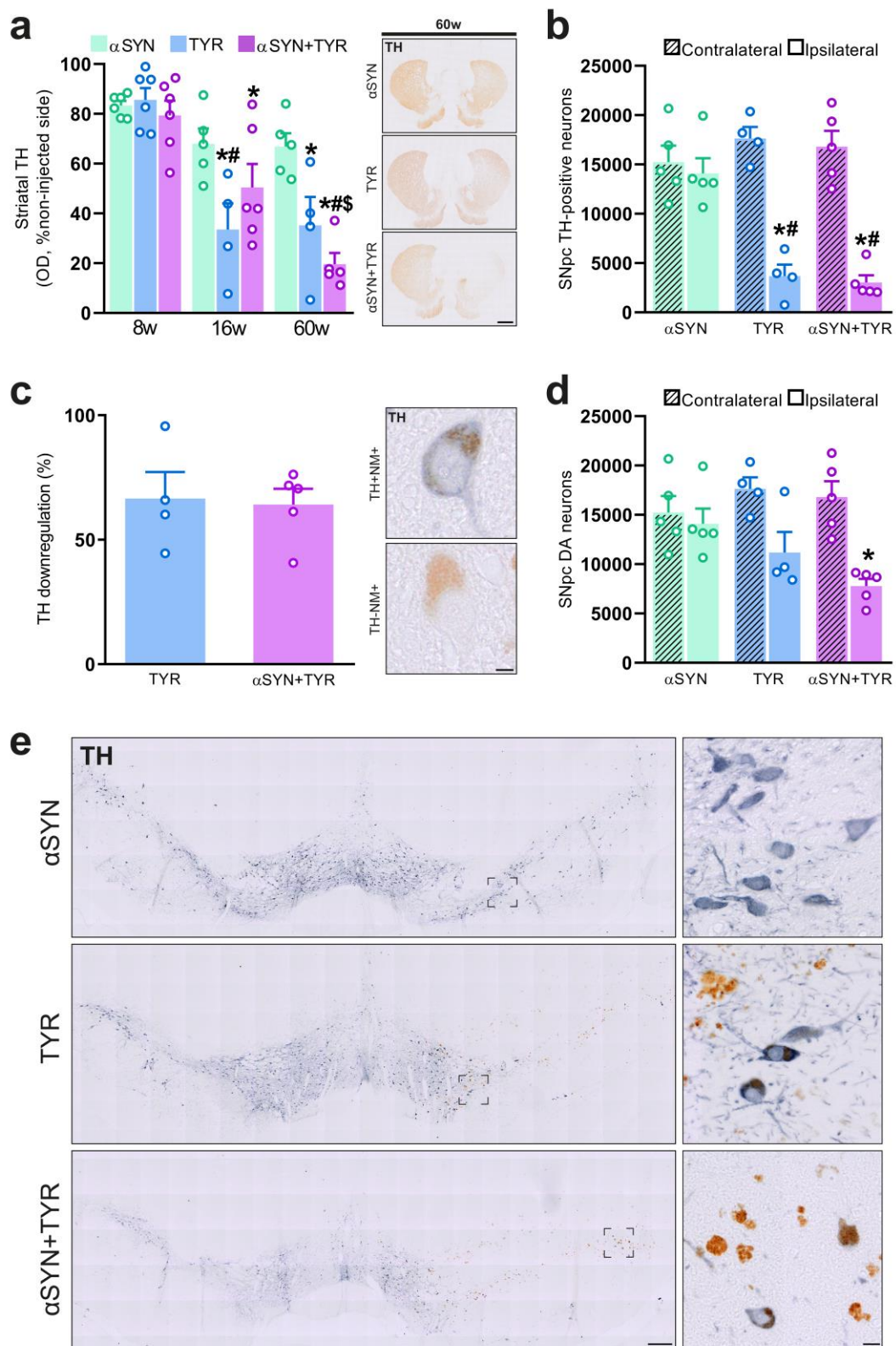


Figure 51. Nigrostriatal degeneration in α SYN-expressing NM-producing rats. (a) *Left*, OD quantification of striatal TH fibers in α SYN-, TYR- and α SYN+TYR-injected rats at 8, 16 and 60 w. * $p < 0.05$ compared to respective 8 w. # $p < 0.05$ compared to respective α SYN. \$ $p < 0.05$ compared to ipsilateral α SYN+TYR 16 w. A two-way ANOVA followed by Tukey's post-hoc test was used to assess statistical significance. $n = 4-6$ animals per group. *Right*, representative photomicrographs of striatal TH immunolabeling at 60 w. Scale bar, 1 mm. (b) Quantification of SNpc TH-positive neurons in α SYN-, TYR- and α SYN+TYR-injected rats at 60 w. * $p < 0.05$ compared to ipsilateral α SYN. # $p < 0.05$ compared to respective contralateral side. A two-way ANOVA followed by Tukey's post-hoc test was used to assess statistical significance. $n = 4-5$ animals per group. (c) *Left*, TH-NM⁺ neurons versus total NM⁺ neurons (including TH-NM⁺ and TH-NM⁻ neurons) as an index of TH downregulation in TYR- and α SYN+TYR-injected rats at 60 w. Mann-Whitney test was used. $n = 4-5$ animals per group. *Right*, representative photomicrographs of TH-NM⁺ neuron and TH-NM⁻ neuron. (d) Quantification of total SNpc DA neurons in α SYN-, TYR- and α SYN+TYR-injected rats at 60 w. * $p < 0.05$ compared to contralateral α SYN+TYR. A two-way ANOVA followed by Tukey's post-hoc test was used to assess statistical significance. $n = 4-5$ animals per group. (e) Representative photomicrographs of TH immunolabeling in SNpc (TH, blue; unstained NM, brown). Scale bar, 200 μ m (*left*) and 10 μ m (*right*).

When a NM-containing neuron dies, its NM contents remain in the extracellular space where they are engulfed by activated microglia/macrophages. This phenomenon, known as neuronophagia, is commonly seen in *post-mortem* aged and PD brains⁹³. Extracellular NM debris were quantified in H&E-stained SNpc sections from TYR- and α SYN+TYR-injected animals at 60 w (Figure 52a). Co-injected animals showed an increase in extracellular NM debris compared to TYR-injected animals, consistent with enhanced nigrostriatal cell death in these animals (see above). In turn, increased extracellular NM debris in these animals was associated with increased macrophage activation as assessed by immunohistochemistry with the macrophage marker CD68 (Figure 52b). Overall, α SYN overexpression in NM-producing animals exacerbates nigrostriatal cell loss and increases parameters associated with cell death-induced neuronophagia.

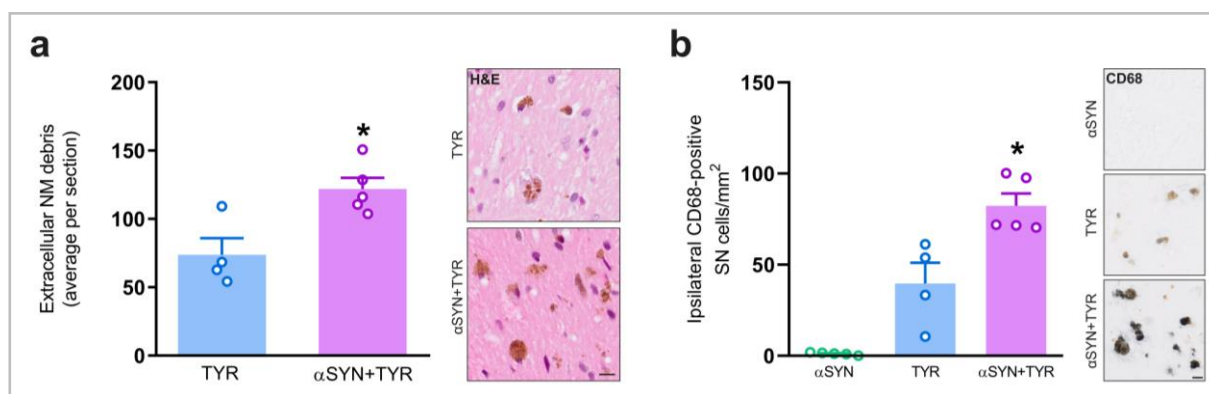


Figure 52. Neuronophagia associated with cell death in α SYN-expressing NM-producing rats. (a) *Left*, quantification of extracellular NM debris in TYR- and α SYN+TYR-injected rats at 60 w. * $p < 0.05$ compared to TYR. Mann-Whitney test. $n = 4-5$ animals per group. *Right*, representative photomicrographs of ipsilateral extracellular NM debris. Scale bar, 10 μ m. (b) *Left*, quantification of ipsilateral CD68-positive SNpc cells in α SYN-, TYR- and α SYN+TYR-injected rats at 8, 16 and 60 w. * $p < 0.05$ compared to α SYN. A Kruskal-Wallis test followed by Dunn's post-hoc test was used to assess statistical significance. $n = 4-5$ animals per group. Scale bar, 10 μ m.

1.5. Impaired DA vesicular uptake in α SYN-overexpressing NM-producing animals

As outlined in the introduction, α Syn plays key physiological roles at the synapse, including regulation of synaptic vesicle pools through sorting and clustering, remodelling of lipid membranes, and facilitating SNARE complex assembly to promote neurotransmitter release¹⁰⁹. Vesicle-associated membrane protein 2 (VAMP2) together with syntaxin-1A (SYX-1A) and synaptosome-associated protein 25 (SNAP25) constitute the SNARE complex, which is essential for priming synaptic vesicles and enabling their fusion with the plasma membrane²⁰². In particular, VAMP2 is the most prevalent synaptic vesicle-associated protein in the brain²⁰³. Interestingly, the α Syn C-terminal domain has been shown to interact with the N-terminal amino acids of VAMP2, a crucial step required for vesicle clustering and binding to the plasma membrane^{204–206}. Upon oligomerisation, α Syn gains several pathological functions including membrane permeabilization and disruption^{193,207,208}.

Here, to investigate the potential mechanisms by which α SYN overexpression results in increased intracellular NM levels (section 1.2 above), we hypothesised that α Syn oligomerization linked to NM production may induce synaptic vesicle permeabilization, thus increasing the pool of free cytosolic DA that can oxidise into NM¹⁰¹. To evaluate the integrity of the DA vesicular system, DA vesicular uptake was first studied by using UPLC-MS/MS (Figure 53a-b). In particular, an index of SN DA vesicular uptake was calculated in terms of the DA:L-DOPA ratio²⁰¹ in vMB tissue samples from α SYN-, TYR- and α SYN+TYR-injected rats. In α SYN-injected rats, α SYN overexpression by itself did not modify DA vesicular uptake (Figure 53b). In contrast, TYR-injected animals showed decreased DA vesicular uptake, indicating that DA is less efficiently internalized and more prone to oxidation, as previously described⁹⁹. Notably, α SYN+TYR co-injection further reduced DA vesicular uptake compared to α SYN- and TYR-injected rats (Figure 53b). As α Syn facilitates synaptic vesicle maturation and fusion with the plasma membrane by interacting with VAMP2, VAMP2 levels were examined in α SYN-, TYR- and α SYN+TYR-injected animals at 8, 16 and 60 w (Figure 53c). Double immunofluorescence for VAMP2 and α SYN revealed a high number of co-localizing VAMP2/ α SYN-positive SNpc neurons in α SYN-injected animals, compatible with soluble α SYN overexpression increasing α SYN-VAMP2 interactions to promote synaptic vesicle maturation and function. In contrast, the reduced DA uptake in α SYN+TYR co-injected animals was associated with a drastic reduction of VAMP2-positive neurons aligning with an increased α Syn aggregation in this group. As a consequence, α Syn's interaction with VAMP2 is prevented, thereby disrupting vesicle fusion with the plasma membrane and contributing to DA cytosolic leakage via vesicle membrane permeabilization. Although VAMP2-positive neurons were scarce in the α SYN+TYR group, their presence suggests some residual soluble α SYN in these cells. In the TYR-injected animals, VAMP2-positive neurons were not detected, similar to what was observed under baseline conditions (i.e., on the contralateral sides; data not shown), indicating that without α SYN's stabilizing influence, VAMP2 levels are insufficient for reliable detection by immunofluorescence.

Taken together, these results suggest that α Syn oligomerization linked to NM accumulation may permeabilise DA synaptic vesicles, thus releasing DA into the cytosol where it can oxidise to NM and thereby prevent vesicle fusion with the plasma membrane.

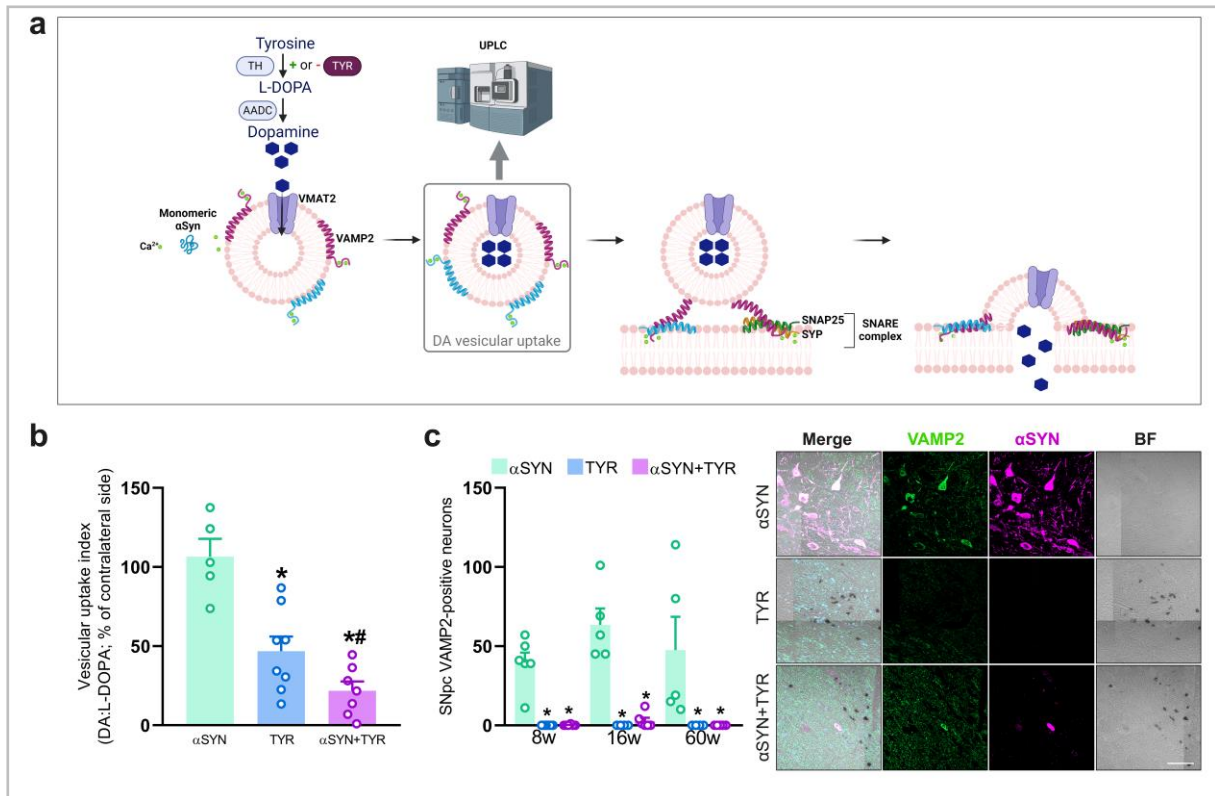


Figure 53. DA synaptic vesicular system in αSYN-expressing NM-producing rats. **(a)** Schematic representation of the DA vesicular system. **(b)** UPLC-MS/MS quantification of ipsi- vs contralateral DA vesicular uptake index, calculated as the DA:L-DOPA ratio. * $p < 0.05$ compared to αSYN. # $p < 0.05$ compared to TYR. A one-way ANOVA was used followed by Holm-Sidak's post-hoc test. $n = 5-8$ animals per group. **(c)** *Left*, quantification of ipsilateral SNpc VAMP2-positive neurons at 8, 16 and 60 w. * $p < 0.05$ compared to αSYN. A two-way ANOVA followed by Tukey's post-hoc test was used to assess statistical significance. $n = 4-6$ animals per group. *Right*, representative photomicrographs of ipsilateral VAMP2- and αSYN-positive neurons. VAMP2, green; αSYN, magenta; DAPI, blue; NM, dark grey (BF). Scale bar, 50 μm. Drawing in **a** was created with Biorender.com.

1.6 Sustained TYR expression in αSYN-overexpressing NM-producing animals

Given that (i) αSYN is upregulated in skin biopsies both from PD patients and melanoma^{147,189,190,209}, that (ii) there is a reciprocal increased risk between PD and melanoma^{210,211}, that (iii) αSYN can modulate melanin levels in melanoma cells¹⁹² and that (iv) αSYN can localize to the nucleus in DA neurons and drive transcriptional changes^{114,212}, we next checked whether the putative modulation of TYR expression by αSYN could potentially contribute to the increased NM levels and pathology observed in αSYN+TYR-injected animals. To do so, SNpc TYR-positive neurons were quantified in TYR- and αSYN+TYR-injected animals at 8, 16 and 60 w (Figure 54). In TYR-injected rats, the number of TYR-positive neurons decreased over time while αSYN+TYR-co-injected rats exhibited sustained TYR expression (Figure 54).

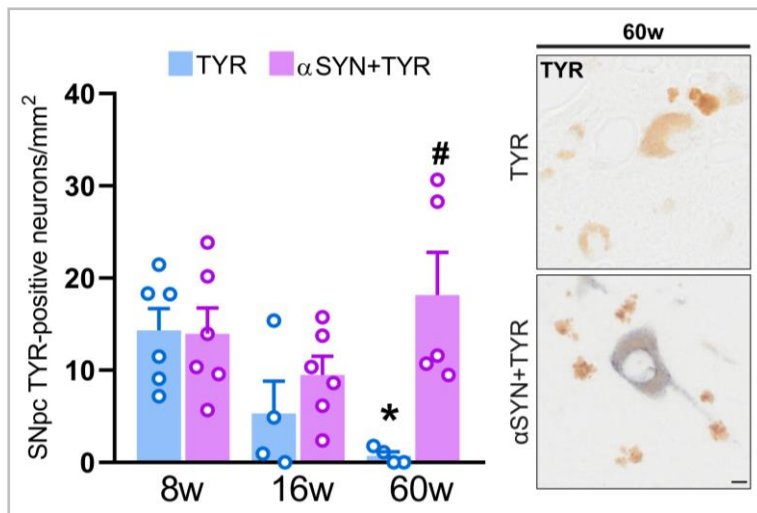


Figure 54. TYR expression in α SYN-expressing NM-producing rats. *Left*, quantification of SNpc TYR-positive neurons in TYR- and α SYN+TYR-injected animals at 8, 16 and 60 w. * $p < 0.05$ compared to TYR 8 w. # $p < 0.05$ compared to TYR 60 w. A two-way ANOVA followed by Tukey's post-hoc test was used to assess statistical significance. $n = 4-6$ animals per group. *Right*, representative photomicrographs of TYR-immunostained SNpc neurons at 60 w. Scale bar, 5 μ m.

1.7 Development of a novel α SYN-overexpressing NM-producing *in vitro* model

To thoroughly investigate TYR modulation linked to α Syn overexpression, a novel α Syn overexpressing NM-producing *in vitro* model was generated based on a TYR-inducible TR5TY6 neuroblastoma cell line. Upon TYR induction by DOX treatment, TR5TY6 cells begin producing NM, with most of the cytoplasm occupied by the pigment within 6 d post-induction⁹⁹. Taking advantage of this cellular model, α SYN-GFP and a corresponding GFP control were overexpressed in non-induced (OFF) and non-differentiated TR5TY6 cells using lentiviral particles (Figure 55a). Both GFP and α SYN-GFP lentiviral particles contained a puromycin resistance gene allowing for the selection of GFP- or α SYN-GFP-infected cells through puromycin treatment. Once the new cell line was stable, GFP- and α SYN-GFP-overexpressing cells were differentiated with RA, and TYR expression was induced with DOX. Cells were collected at three different time-points (1, 3 and 6 d) post-induction (ON), and α SYN overexpression was confirmed by assessing gene expression and protein levels (Figure 55b-d). GFP OFF and α SYN-GFP OFF were also generated as control groups. α SYN-GFP-infected cells exhibited markedly elevated levels of *SNCA* mRNA expression compared to GFP control cells (Figure 55b), while α Syn immunoblot experiments revealed multiple bands exclusively in α SYN-GFP-infected cells at OFF, and at the 1- and 3-d post-induction time-points (Figure 55c). Considering the molecular weights of 14 kDa for α SYN and 27 kDa for GFP, α SYN-GFP protein should weigh around 41 kDa, which was consistent with the more intense band observed. The higher molecular weight band may correspond to a dimerized form of the protein, while the smaller band potentially results from cleavage of the α SYN-GFP protein, thus creating a fragment to which the primary antibody can still bind. It is worth noting that overall protein levels were virtually undetectable at 6 d due to significant cell death, as indicated by β -actin levels, but a faint band corresponding to α SYN-GFP protein remains visible. The increased α SYN protein levels in α SYN-GFP cells were further validated by immunocytochemistry as shown in Figure 55d.

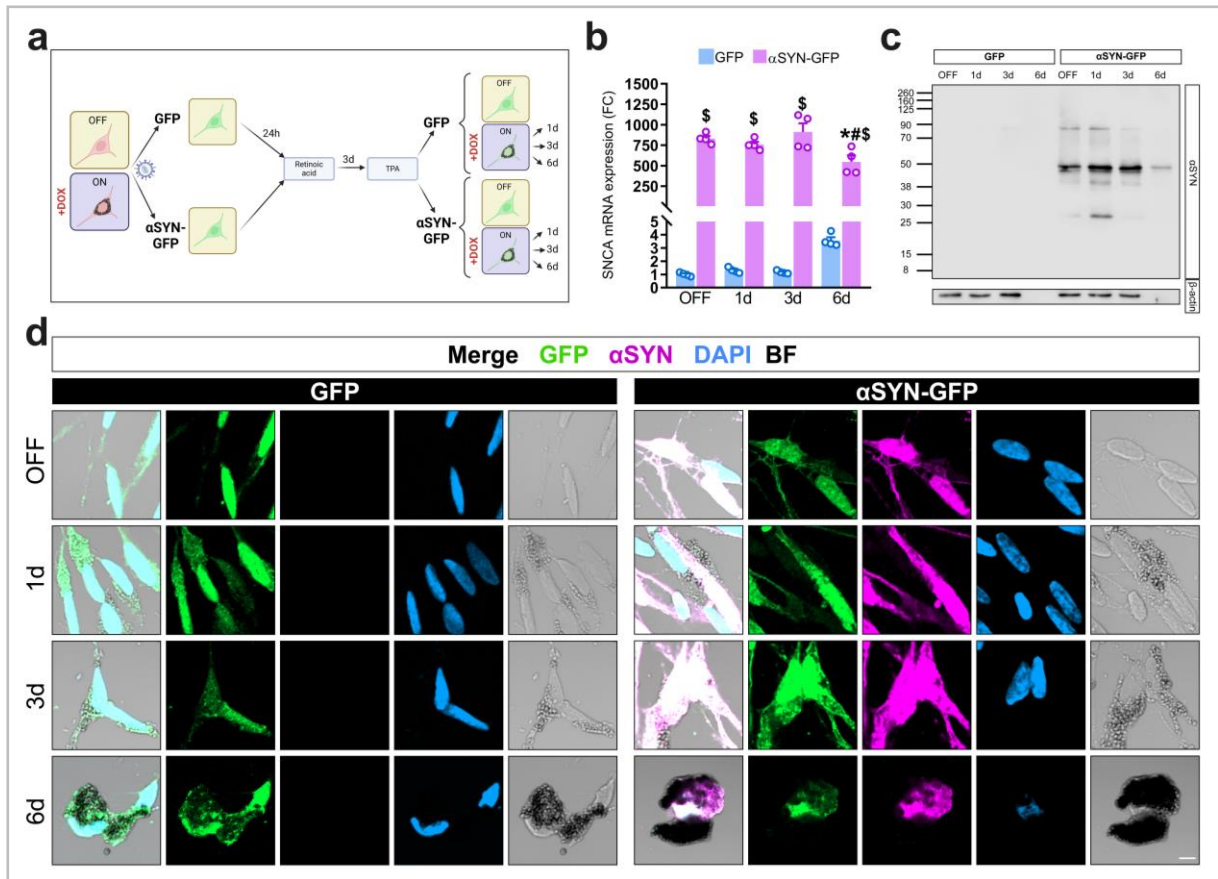


Figure 55. α SYN overexpression in a TYR-inducible TR5TY6 neuroblastoma cell line. (a) Schematic representation of GFP and α SYN-GFP infection and TYR induction protocol. (b) SNCA gene expression normalized to endogenous controls (PPIA and RPLP0) calculated as Fold Change (FC) in GFP and α SYN-GFP cells at OFF, 1, 3 and 6 d. * $p < 0.05$ compared to respective OFF. # $p < 0.05$ compared to α SYN-GFP 3 d. \$ $p < 0.05$ compared to respective GFP. A two-way ANOVA followed by Tukey's post-hoc test was used to assess statistical significance. $n = 4$ replicates per group. (c) α Syn immunoblot of GFP and α SYN-GFP cells for OFF, 1, 3 and 6 d time-points. (d) Representative photomicrographs of GFP and α SYN-GFP cells at OFF, 1, 3 and 6 d. GFP, green; α SYN, magenta; DAPI, blue; NM, dark grey (BF). Scale bar, 5 μ m. Drawing in a was created with Biorender.com.

1.8. Increased intracellular NM levels in α SYN-overexpressing NM-producing cells

To validate in our cellular system the increase of NM levels associated with α SYN overexpression seen in α SYN+TYR-co-injected rats (section 1.2), intracellular NM levels were evaluated in GFP and α SYN-GFP cells at 1, 3 and 6 d. (Figure 56a-e) In both GFP and α SYN-GFP cells, intracellular NM levels progressively increased after TYR induction. Interestingly, α SYN-GFP cells exhibited higher NM levels at 3 and 6 d than GFP cells (Figure 56a-b). Furthermore, the percentage of cytosol occupied by NM was also greater in α SYN-GFP cells than in GFP cells at 3 d (Figure 56d-e). Overall, α SYN overexpression in NM-producing TR5TY6 cells accelerated NM accumulation, mirroring the effects seen in α SYN+TYR-co-injected rats.

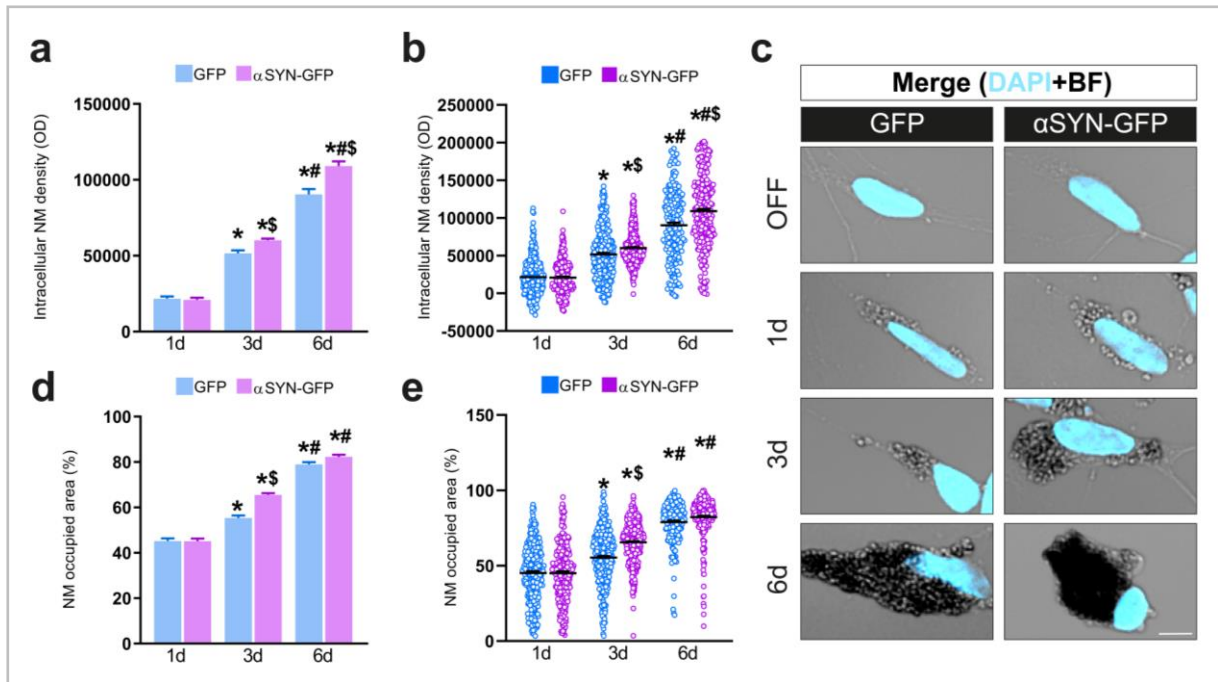


Figure 56. Intracellular NM levels in α SYN-overexpressing NM-producing cells. (a & b) Quantification of intracellular NM levels by OD in GFP and α SYN-GFP cells at OFF, 1, 3 and 6 d time-points. * $p < 0.05$ compared to respective 1 d. # $p < 0.05$ compared to respective 3 d. \$ $p < 0.05$ compared to respective GFP. (c) Representative photomicrographs of non-pigmented and pigmented GFP and α SYN-GFP cells at OFF, 1, 3 and 6 d time-points, respectively. DAPI, blue; NM, dark grey (BF). Scale bar, 5 μ m. (d & e) Percentage of neuronal cytosolic area occupied by NM in GFP and α SYN-GFP cells at OFF, 1, 3 and 6 d. * $p < 0.05$ compared to respective 1 d. # $p < 0.05$ compared to respective 3 d. \$ $p < 0.05$ compared to respective GFP. In all panels, statistical significance was assessed with a two-way ANOVA followed by Tukey's post-hoc test. $n = 186$ -354 cells per group.

1.9. Increased TYR activity and expression levels in α SYN-overexpressing NM-producing cells

Since α SYN-GFP cells demonstrated (i) consistent α SYN overexpression levels and (ii) accelerated NM production, they were deemed as an appropriate model for studying TYR levels and their potential modulation by α SYN. As in TYR- and α SYN+TYR-injected animals, protein TYR levels were subjected to evaluation (Figure 57a-b). In GFP and α SYN-GFP cells, TYR protein levels assessed by immunoblot increased progressively after induction with DOX (Figure 57a). Remarkably, TYR protein expression reached higher levels in α SYN-GFP cells compared to GFP cells at 1 d (Figure 57a), a finding that was qualitatively confirmed by immunocytochemistry (Figure 57b). To determine if increased TYR protein levels in α SYN-GFP cells were associated with increased Tyr function, Tyr enzymatic activity was assessed by adding its substrate L-DOPA to GFP and α SYN-GFP cells at OFF, 1d, 3d and 6d, and measuring the absorbance at 484 nm over 220 min (Figure 57c). The assay was first validated, either by using recombinant Tyr from mushroom, with or without a known Tyr inhibitor (4-Butylresorcinol), or by adding the substrate (L-DOPA) in absence of recombinant Tyr (i.e. PB), as a negative control (Figure 57c, left). TYR enzymatic activity increased continuously over time in both GFP and α SYN-GFP cells following TYR induction with DOX (Figure 57c). As anticipated, GFP OFF cells displayed

negligible TYR activity following the addition of L-DOPA. Surprisingly, however, α SYN-GFP cells exhibited increased TYR activity under OFF conditions (Figure 57c), presumably reflecting already-increased TYR protein levels under basal conditions in α SYN-overexpressing cells (Figure 57a). Following TYR induction, TYR activity was also higher in α SYN-GFP cells at 1 d compared with GFP cells (Figure 57c), in agreement with significantly increased TYR protein levels in these cells (Figure 57a-b). By 3 d, TYR activity in α SYN-GFP cells began to decrease relative to the GFP controls. At 6 d, TYR activity was reduced in both GFP and α SYN-GFP cells, which was probably due to extensive cell loss by that time. To investigate whether the observed increases in TYR protein levels and activity in α SYN-overexpressing cells were linked to an upregulation of TYR gene expression, TYR mRNA expression levels were evaluated in these cells. In α SYN-GFP cells, TYR mRNA levels were increased at 1 and 3 d compared to GFP cells, supporting the notion that α Syn enhances TYR gene expression, and thereby boosting TYR protein levels and activity, which may potentially contribute to increased NM levels in these cells.

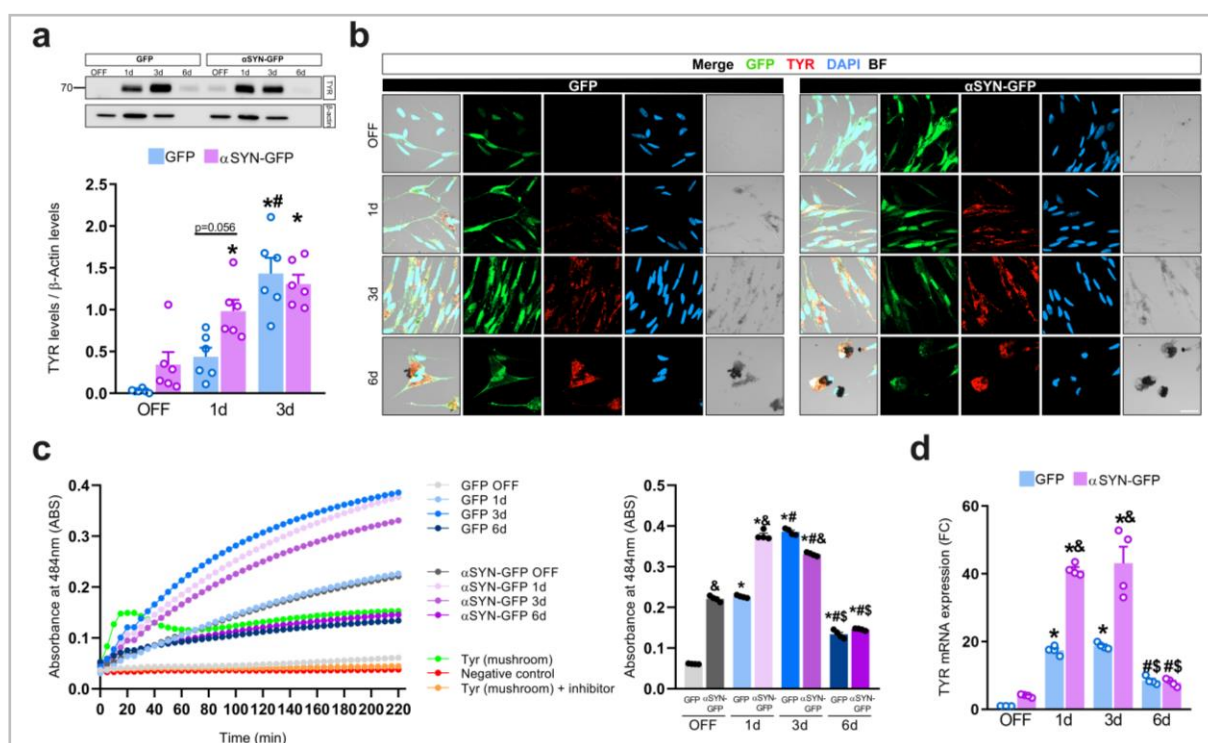


Figure 57. TYR expression and activity in α SYN-overexpressing NM-producing cells. (a) TYR immunoblot in GFP and α SYN-GFP cells at OFF, 1 and 3 d time-points. * p <0.05 compared to respective OFF. # p <0.05 compared to GFP 1 d. Statistical significance was assessed with a two-way ANOVA followed by Tukey's post-hoc test. n =6 replicates per group. (b) Representative photomicrographs of TYR immunolabeling of GFP and α SYN-GFP cells at OFF, 1, 3 and 6 d time-points. GFP, green; TYR, red; DAPI, blue; NM, dark grey (BF). Scale bar, 20 μ m. (c) *Left*, Tyr activity (measured as the absorbance at 484 nm) in GFP and α SYN-GFP cells at OFF, 1, 3 and 6 d time-points; Recombinant Tyr (mushroom), with or without inhibitor, and the negative control are shown for assay validation. *Right*, Tyr activity at 220 min in GFP and α SYN-GFP cells at OFF, 1, 3 and 6 d. * p <0.05 compared to respective OFF. # p <0.05 compared to respective 1 d. \$ p <0.05 compared to respective 3 d. & p <0.05 compared to respective GFP. A two-way ANOVA followed by Tukey's post-hoc test was used to assess statistical significance. n =4 replicates per group. (d) TYR gene expression normalized to endogenous controls (PPIA and RPLP0) calculated as Fold Change (FC) in GFP and α SYN-GFP cells at OFF, 1, 3 and 6 d time-points. * p <0.05 compared to respective OFF. # p <0.05 compared to respective 1 d. \$ p <0.05 compared to respective 3 d. & p <0.05 compared to respective GFP. Statistical significance was assessed with a two-way ANOVA followed by Tukey's post-hoc test. n =4 replicates per group.

2. Chapter II. Impact of NM-associated pathology on α Syn aggregation and propagation in PD

2.1 Experimental design

The intracerebral administration of α SYN PFFs in mice has been used widely as an *in vivo* model of α Syn propagation and pathology^{124,213–219}. To assess whether an oxidative NM-producing environment may accelerate such α Syn propagation and pathology, PD-derived α SYN PFFs were injected into the STR of tgNM and wt mice. While other brain regions, such as the SNpc and the olfactory bulb, have been targeted for PFF injections, the STR offers distinct experimental advantages in that it plays a central role in the nigrostriatal pathway³⁰, it integrates signals essential for movement²²⁰, and it connects extensively with regions such as the cortex, hippocampus, and amygdala²²¹. These features make the STR an effective site for modelling α Syn propagation and PD progression. α SYN PFFs were isolated from a *post-mortem* PD brain and amplified by PMCA by Prof. Melki's group (France). Amplified PD-derived α SYN PFFs were then unilaterally injected into the STR of 3m-old male and female wt and tgNM mice. As a control group, similar injections were performed with BSA in separate wt and tgNM animals. Mice were euthanised at 3.5 and 8mpi (Figure 58). Prior to being euthanised, animals underwent a battery of motor and non-motor tests (Figure 58). An extra group of mice was injected with non-amplified PD-derived α SYN PFFs and euthanised at 3.5 mpi, as an additional control.

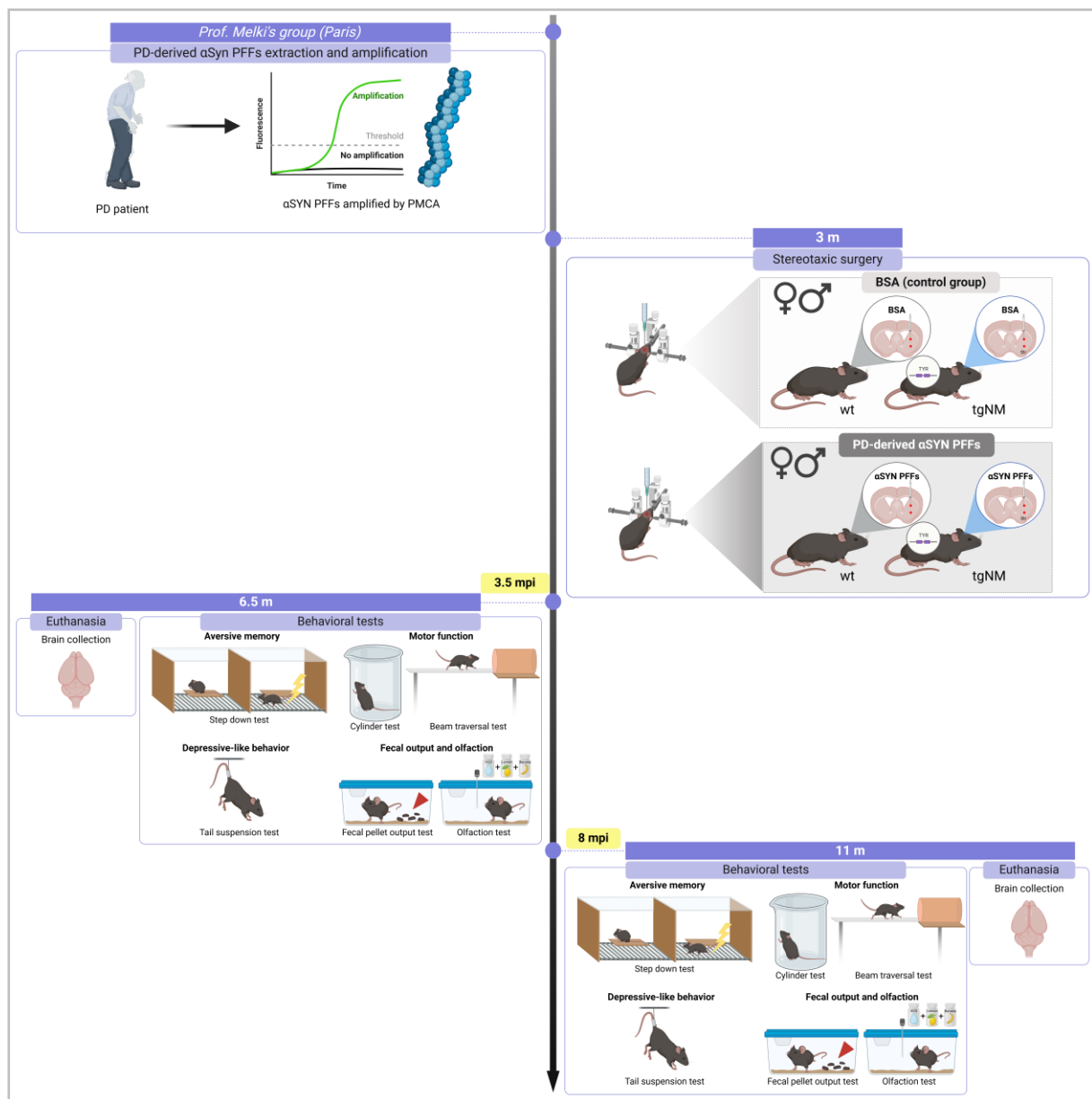


Figure 58. Experimental design of PD-derived αSYN PFFs injections into wt and tgNM animals. αSYN PFFs were isolated from a *post-mortem* PD brain and amplified by PMCA by Prof. Melki's group (France). PD-derived αSYN PFFs and BSA (control) were injected into the STR of 3m-old male/female wt and tgNM mice. Animals were subjected to a battery of motor and non-motor tests as indicated at 3.5 or 8 mpi, after which animals were euthanised. Drawing was created with Biorender.com.

2.2 Local accumulation of endogenous pαSyn in the STR of αSYN PFF-injected wt and tgNM mice

To corroborate whether injecting PD-derived αSYN PFFs into wt and tgNM animals triggers pathological αSyn accumulation at the injection site, striatal sections were immunostained for pαSyn at 3.5 and 8 mpi (Figure 59). At 3.5 mpi, αSYN PFFs induced a notable accumulation of pαSyn in the ipsilateral STR while no detectable pαSyn was observed on the contralateral side (Figure 59a). By 8 mpi, the accumulation of pαSyn in the ipsilateral STR was even more pronounced and a modest pαSyn immunosignal could

also be observed on the contralateral side (Figure 59b). In contrast, no appreciable p α Syn immunosignal was detected in either the ipsilateral or contralateral STR in animals injected with BSA or non-amplified PD-derived α SYN PFFs (Figure 59a-b). Notably, no human-specific α SYN immunosignal was observed at 3.5 mpi or 8 mpi, indicating that the p α Syn accumulation observed in the STR of α SYN PFFs-injected animals corresponds to endogenous mouse α SYN (Figure 59c-d), consistent with previous studies^{174,214,222}.

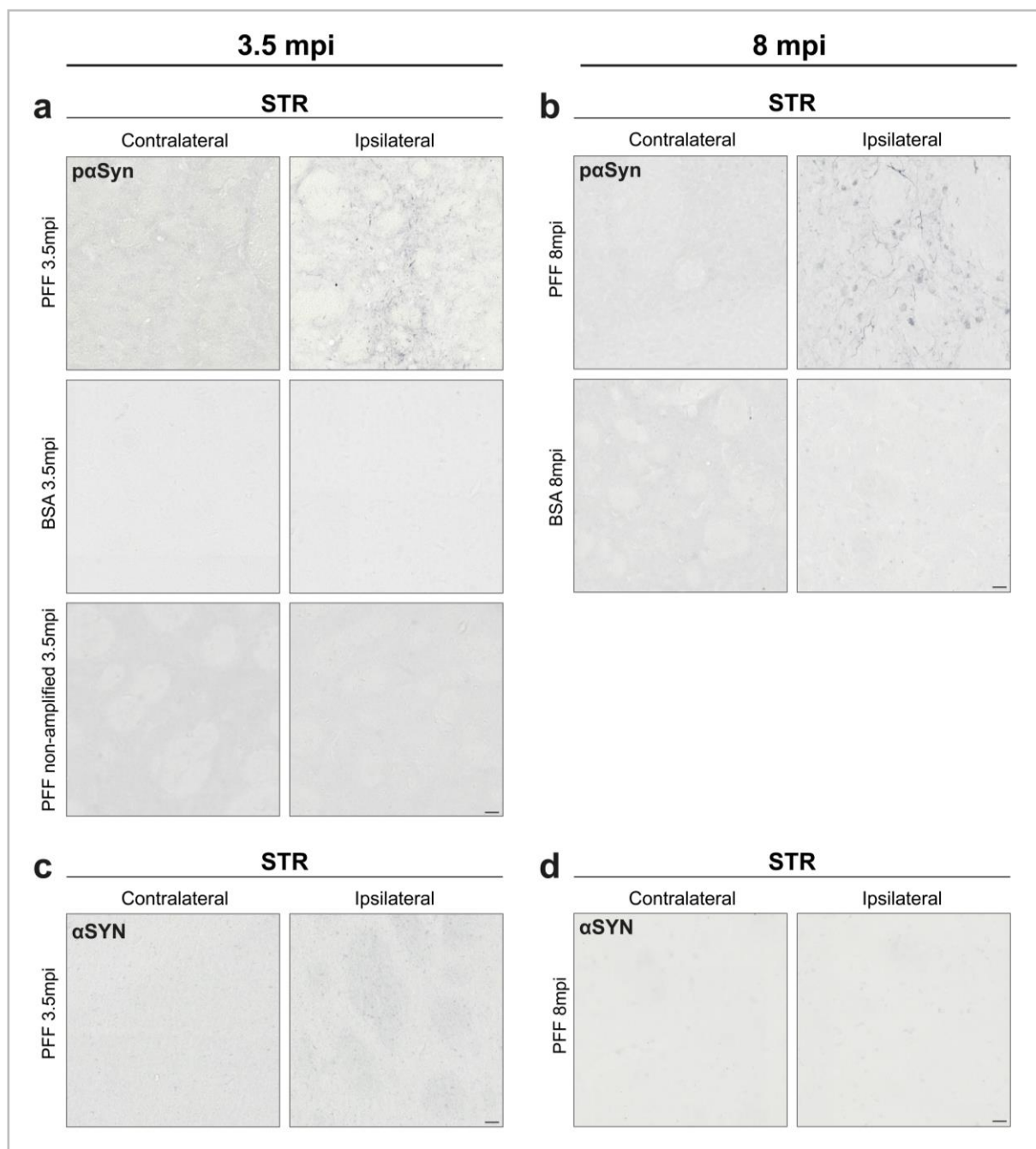


Figure 59. p α Syn and α SYN immunolabeling in the STR of control- and PFF-injected wt and tgNM mice at 3.5 (left) and 8 mpi (right). (a) p α Syn immunostaining in the contralateral (left) and ipsilateral (right) STR in PFF-, BSA- and PFF non-amplified-injected mice at 3.5 mpi. (b) p α Syn immunostaining in the contralateral (left) and ipsilateral (right) STR in PFF-, BSA- and PFF non-amplified-injected mice at 8 mpi. (c) α SYN immunostaining in the contralateral (left) and ipsilateral (right) STR in a PFF-injected mouse at 3.5 mpi. (d) α SYN immunostaining in the contralateral (left) and ipsilateral (right) STR in a PFF-injected mouse at 8 mpi. Similar results were obtained for wt and tgNM mice. Scale bars, 20 μ m.

2.4 Effects of NM-induced oxidative environment on α SYN PFF-induced p α Syn pathology

2.4.1. α SYN PFF-injected wt and tgNM mice at 3,5 mpi

Since p α Syn pathology was observed not only at the injection site but also in projection areas of PFF-injected animals at 3.5 mpi, p α Syn pathology was further characterised and quantified in representative sections encompassing the entire brain of both wt and tgNM animals (Figure 61). Four distinct types of p α Syn-positive structures were identified and quantified: (i) Lewy neurites, (ii) dystrophic Lewy neurites, (iii) aggregates and (iv) p α Syn-positive cells (Figure 61a). Lewy neurites accounted for more than 90% of the p α Syn pathology, followed by dystrophic Lewy neurites, aggregates, and p α Syn-positive cells (Figure 61b-f). At this time-point, most of the p α Syn pathology was concentrated on the ipsilateral side of PFF-injected animals (Figure 61b-g). No significant differences in the extent and type of p α Syn pathology were found between wt and tgNM animals (Figure 61b-g).

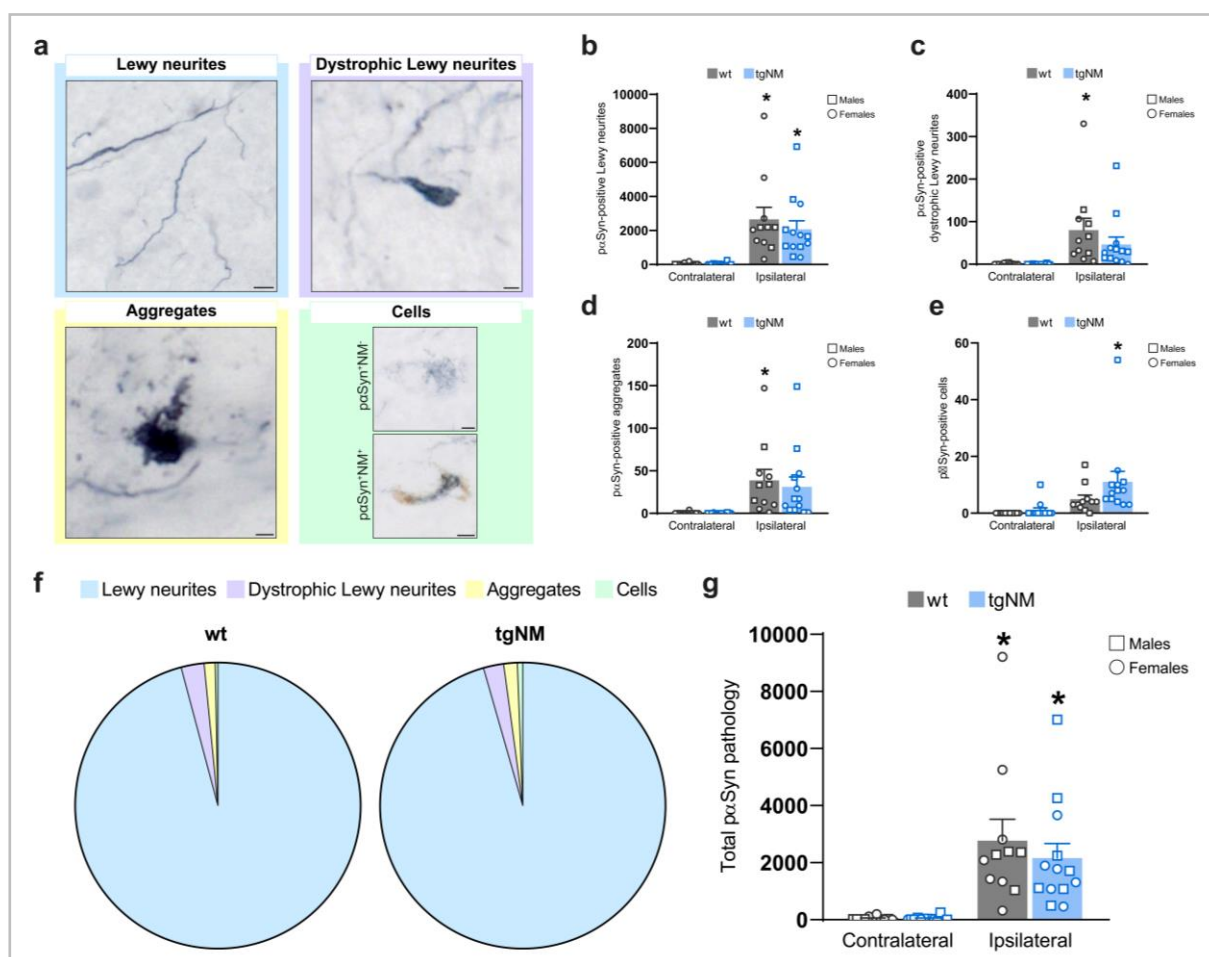


Figure 61. Quantification of the extent and type of p α Syn pathology in PFF-injected wt and tgNM mice at 3.5 mpi. (a) Representative images of the different types of p α Syn-positive structures induced by injected PFF. Scale bars: 5 μ m (Lewy neurites), 2 μ m (dystrophic Lewy neurites), 2 μ m (aggregates), 5 μ m (p α Syn-positive and NM-negative cells), 2 μ m (p α Syn-positive and NM-positive cells). (b-f) Quantification of p α Syn pathology within the entire brain from PFF-injected wt and tgNM animals: (b) p α Syn-positive Lewy neurites. * $p < 0.05$ compared to respective contralateral side; (c) p α Syn-positive dystrophic Lewy neurites. * $p < 0.05$ compared to wt contralateral side. (d) p α Syn-positive aggregates. * $p < 0.05$ compared to wt

contralateral side; (e) p α Syn-positive cells. *p<0.05 compared to tgNM contralateral side. (f) Distribution of the type of p α Syn-positive structures in PFF-injected wt and tgNM animals. (g) Number of total p α Syn structures in PFF-injected wt and tgNM animals. *p<0.05 compared to respective contralateral side. In **b**, **c**, **d**, **e** & **g**, a two-way ANOVA followed by Tukey's post-hoc test were used. n=11-13 animals per group.

To further investigate whether the presence of NM in tgNM animals could influence the anatomical distribution of p α Syn pathology, the latter was also assessed separately across 12 anatomically representative brain regions, from rostral to caudal ([Figure 62](#) and [Figure 63](#)). As with the total p α Syn pathology above, the vast majority of p α Syn-positive structures were restricted to the ipsilateral hemisphere in all regions analysed, with no significant differences observed between wt and tgNM animals ([Figure 62](#)). To better visualize the anatomical distribution of PFF-induced p α Syn pathology, quantification of the latter was normalized to a 0-100% scale and mapped onto coronal mouse brain sections from the Paxinos and Franklin atlas¹⁹⁹, corresponding to the anatomical levels examined ([Figure 63](#)).

Overall, no differences in the extent, type or pattern of PFF-induced p α Syn pathology were observed between wt and tgNM mice at 3.5 mpi. In both groups of animals, p α Syn pathology was primarily localized near the injection site, with limited propagation to rostrally- and caudally-connected regions, such as the PFC and SN.

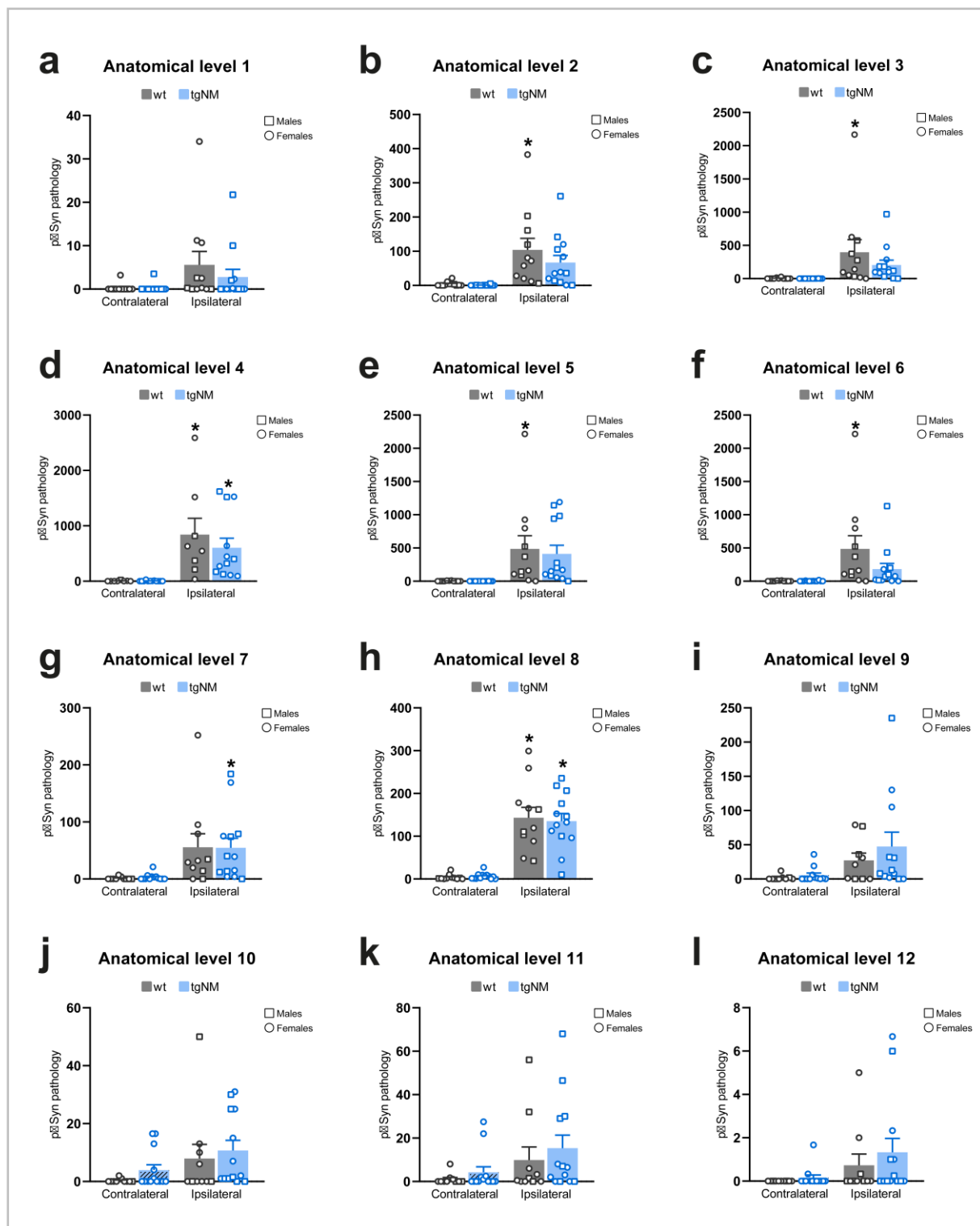


Figure 62. Quantification of total pαSyn pathology throughout the mouse brain in PFF-injected wt and tgNM mice at 3.5 mpi, from anatomical level 1 (a) to 12 (l). Caudal to rostral anatomical levels were defined using the Paxinos and Franklin atlas¹⁹⁹ as shown in Figure 63. *p<0.05 compared to contralateral wt (b, c, e, f), to the respective contralateral side (d, h), or to the contralateral side in tgNM (g). A two-way ANOVA followed by Tukey's post-hoc test were used to assess statistical significance. n=11-13 animals per group.

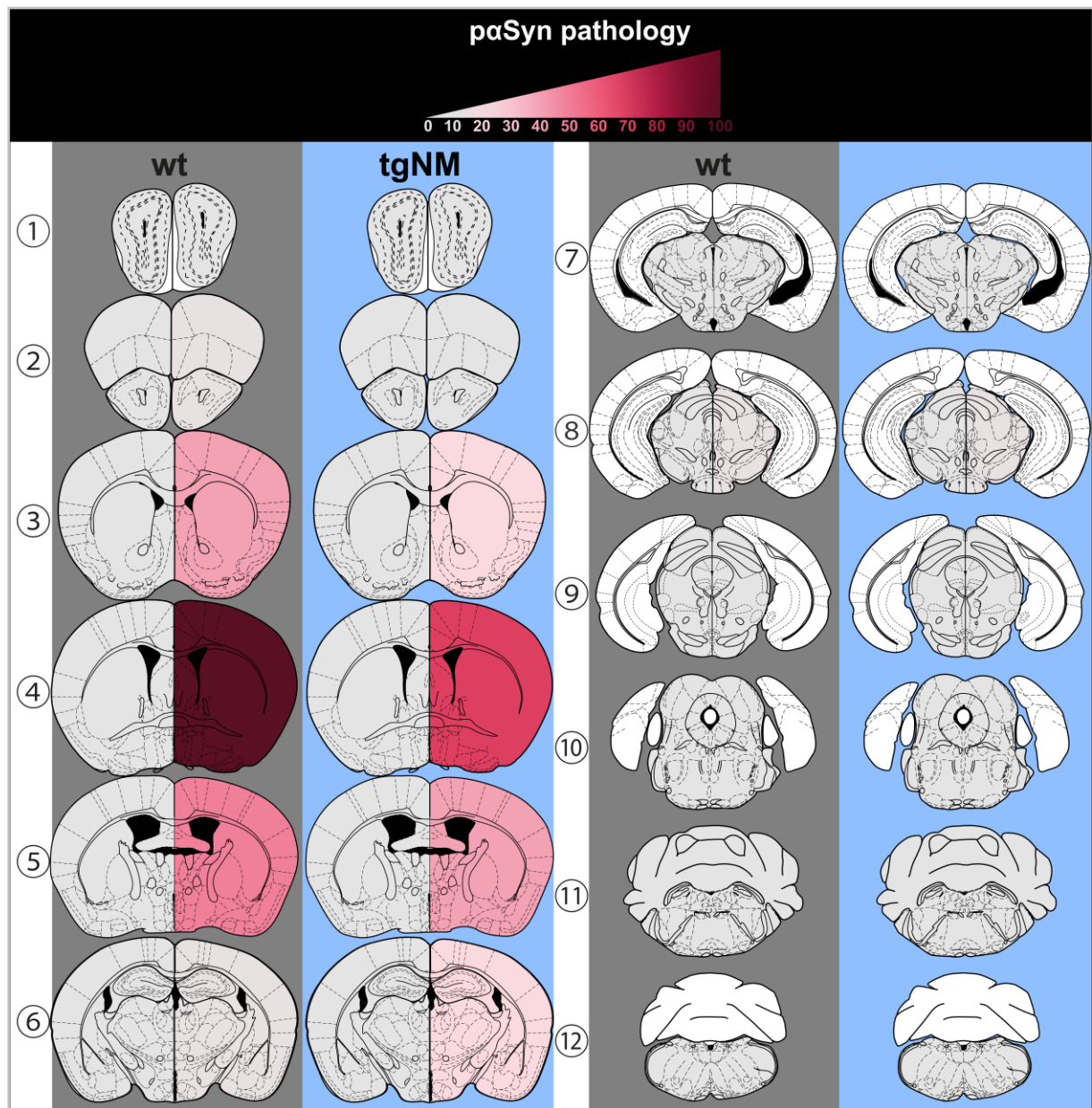


Figure 63. Anatomical distribution of pαSyn pathology in PFF-injected wt and tgNM at 3.5 mpi. pαSyn pathology was mapped from 0% (no pathology) to 100% (highest pathology) onto 12 representative coronal mouse brain sections according to the Paxinos and Franklin atlas¹⁹⁹ in the ipsilateral (*right*) and contralateral (*left*) hemispheres of PFF-injected animals.

2.4.2. α SYN PFF-injected wt and tgNM mice at 8mpi

Since PFF-induced p α Syn pathology was mostly confined to the injection site and its directly interconnected regions at 3.5 mpi, the same representative anatomical brain levels as above (Figure 63) were analysed at 8 mpi, when p α Syn pathology is expected to spread to more distant nuclei^{124,213,223}. Indeed, at this time-point, the extent of p α Syn pathology was so extensive that manual quantification became unfeasible. To address this limitation, a semi-quantitative severity scoring system was developed, whereby p α Syn pathology was categorized from 0 (no pathology) to 5 (massive pathology) (Figure 44, Materials and methods section). All brain nuclei present in each coronal atlas brain section from PFF-injected wt and tgNM animals were quantified using this severity score system.

To identify potential differences between wt and tgNM animals, the scores for contralateral and ipsilateral nuclei were summed across all 12 analysed sections. Similar to findings at the 3.5 mpi time-point, the majority of p α Syn pathology remained predominantly localized to the ipsilateral side (Figure 64). However, by 8 mpi, substantial p α Syn pathology was also observed on the contralateral side (Figure 64). Importantly, no significant differences were detected between wt and tgNM animals across any of the 12 sections analysed (Figure 64).

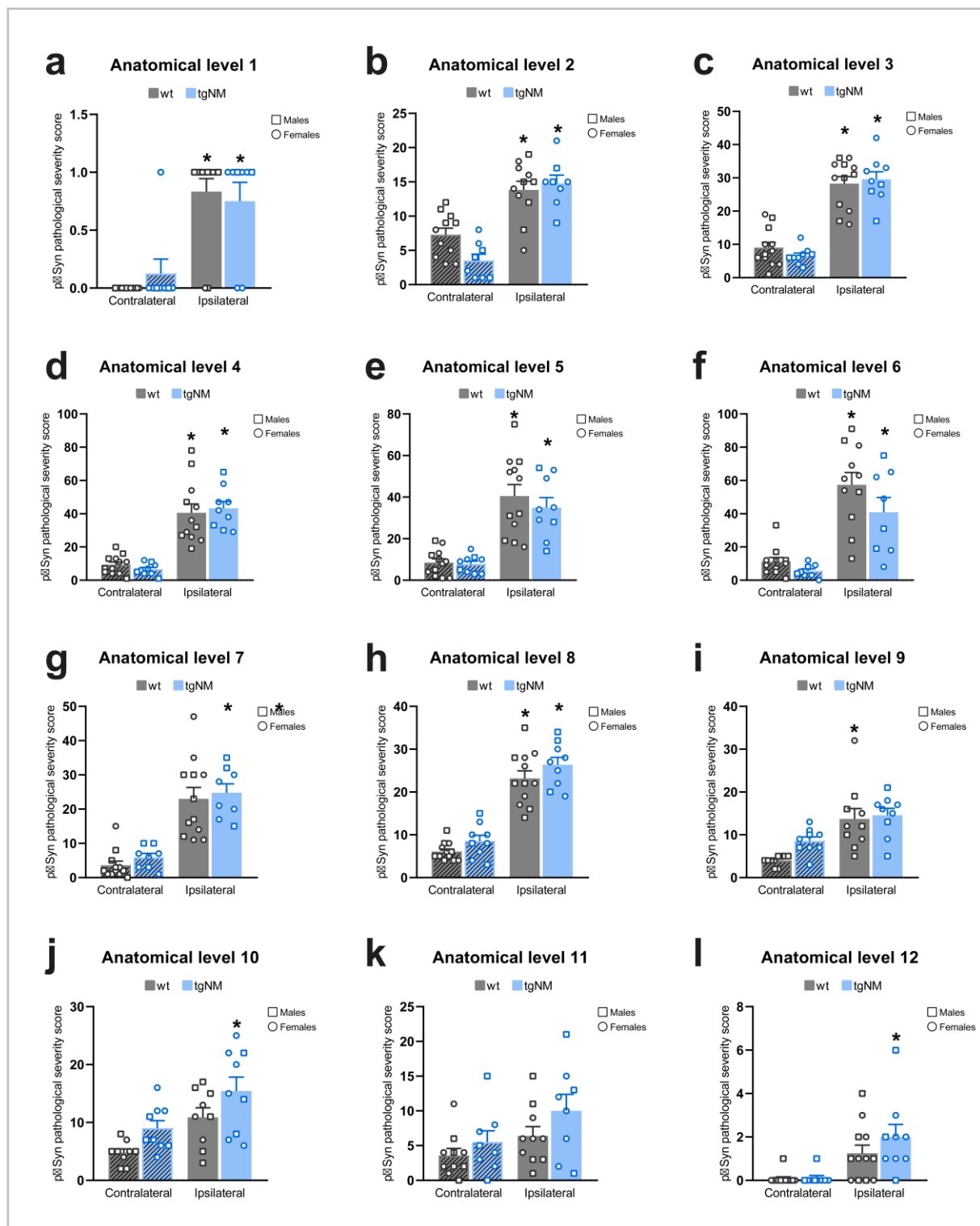


Figure 64. Quantification of total pαSyn pathology throughout the mouse brain in PFF-injected wt and tgNM mice at 8 mpi, from anatomical level 1 (a) to 12 (l). Caudal to rostral anatomical levels were defined using the Paxinos and Franklin atlas¹⁹⁹ as shown in Figure 65. *p < 0.05 compared to the respective contralateral side (a-h), to the wt contralateral side (i), or to the tgNM contralateral side (j). A two-way ANOVA followed by Tukey's post-hoc test were used to assess statistical significance. n=9-12 animals per group.

To better visualize the anatomical distribution of PFF-induced p α Syn pathology, the mean p α Syn pathological severity score from each nucleus was calculated both for wt and tgNM mice and mapped onto coronal mouse brain sections from the Paxinos and Franklin atlas¹⁹⁹, corresponding to the anatomical levels analysed (Figure 65). In both wt and tgNM animals, p α Syn pathology spread to regions anatomically connected to the injection site (Figure 65). More specifically, p α Syn pathology extended from the injection site to rostral areas such as the neocortex, as well as to caudal regions including the globus pallidus, SNpc and substantia nigra pars reticulata (SNpr) as well as the periaqueductal gray. PFF-induced p α Syn pathology followed this expected pattern in wt and tgNM mice, with no significant differences between either group of animals, thus indicating that a NM-producing oxidative environment has no impact on the extent, pattern or distribution of PFF-induced p α Syn pathology up to 8 mpi.

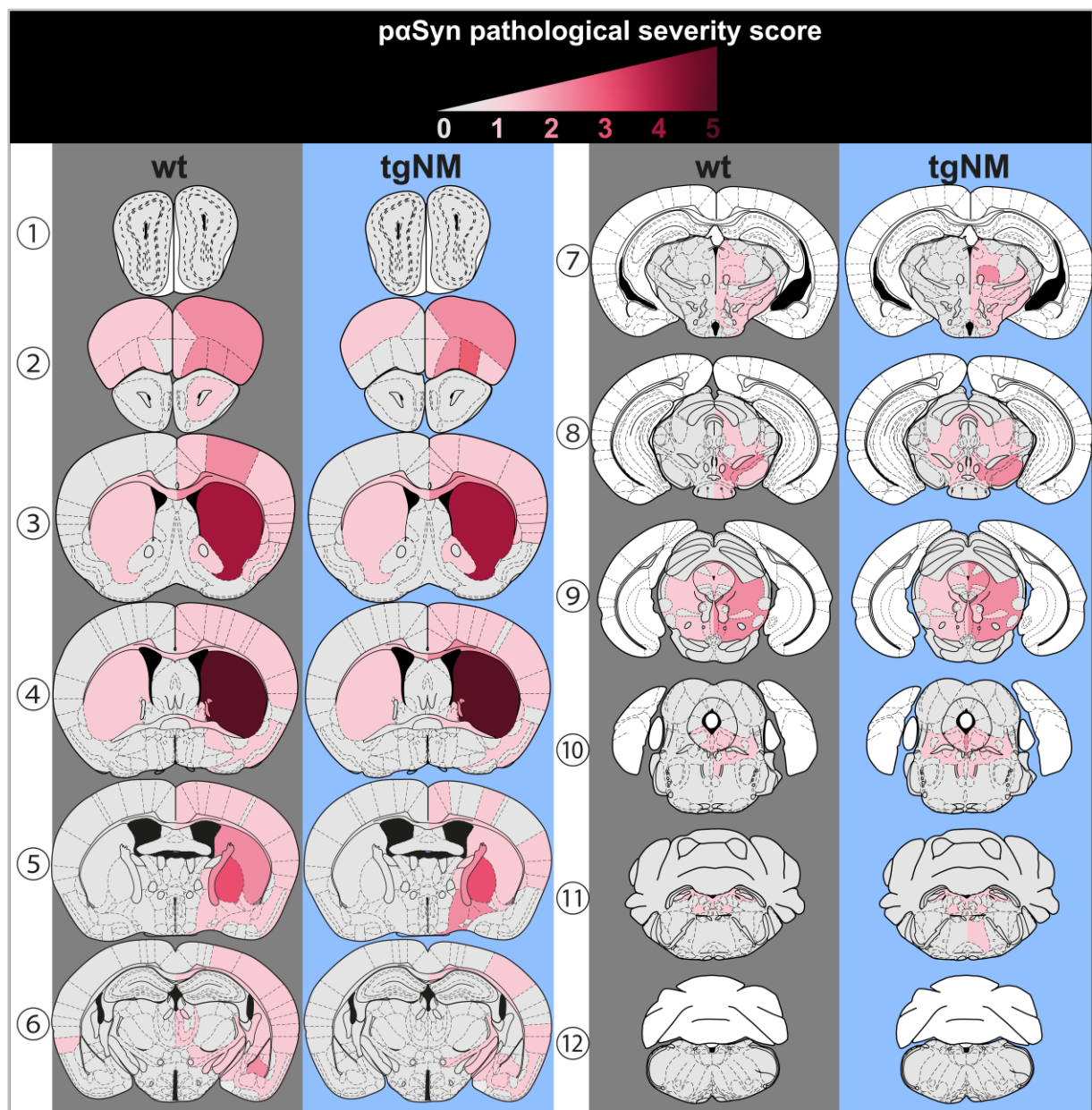


Figure 65. Anatomical distribution of pαSyn pathology in PFF-injected wt and tgNM at 8 mpi. pαSyn pathological severity score mapped in each nucleus from 0 (no pathology) to 5 (highest pathology) onto 12 representative coronal mouse brain sections from the Paxinos and Franklin atlas¹⁹⁹ in the ipsilateral (*right*) and contralateral (*left*) hemispheres of PFF-injected animals.

2.5 Nigrostriatal integrity in α SYN PFF-injected wt and tgNM mice

Previous studies have reported nigrostriatal degeneration associated with p α Syn pathology at 6 m following striatal α SYN PFF injections^{218,223,224}. As noted above, intra-striatal inoculation of PD-derived α SYN PFF resulted in pronounced p α Syn pathology in the nigrostriatal pathway of wt and tgNM mice at 3.5 and 8 mpi. To assess the impact of p α Syn pathology on nigrostriatal integrity, and the influence of NM on the latter, the density of nigrostriatal TH fibers at 3.5 mpi and 8 mpi was quantified by OD in wt and tgNM animals injected with either BSA or α SYN PFFs (Figure 66a). No nigrostriatal dopaminergic denervation was observed in PFF- or BSA-injected wt or tgNM animals, at 3.5 or 8 mpi (Figure 66a).

To further assess the integrity of the nigrostriatal pathway in PFF-injected wt and tgNM mice, the number of SNpc DA neurons was also evaluated in these animals at the latest time-point (8 mpi). Quantification of TH-positive and total DA neurons in the SNpc revealed no significant differences between the ipsilateral and contralateral hemispheres from wt and tgNM animals injected with either BSA or α SYN PFF (Figure 66b, d & f). Similarly, no early signs of neuronal dysfunction such as phenotypic TH downregulation were observed within NM-containing neurons from tgNM mice injected with α SYN PFF compared to BSA-injected animals (Figure 66c).

Furthermore, extracellular NM debris, which is released from dying NM-containing neurons, was also examined in tgNM animals injected with either BSA or α SYN PFF (Figure 66e). In tgNM mice injected with α SYN PFF, there was a modest but significant increase in ipsilateral SNpc extracellular NM debris compared to the contralateral side and to BSA-injected animals (Figure 66e), which is suggestive of an accelerated, incipient neurodegenerative process in these animals.

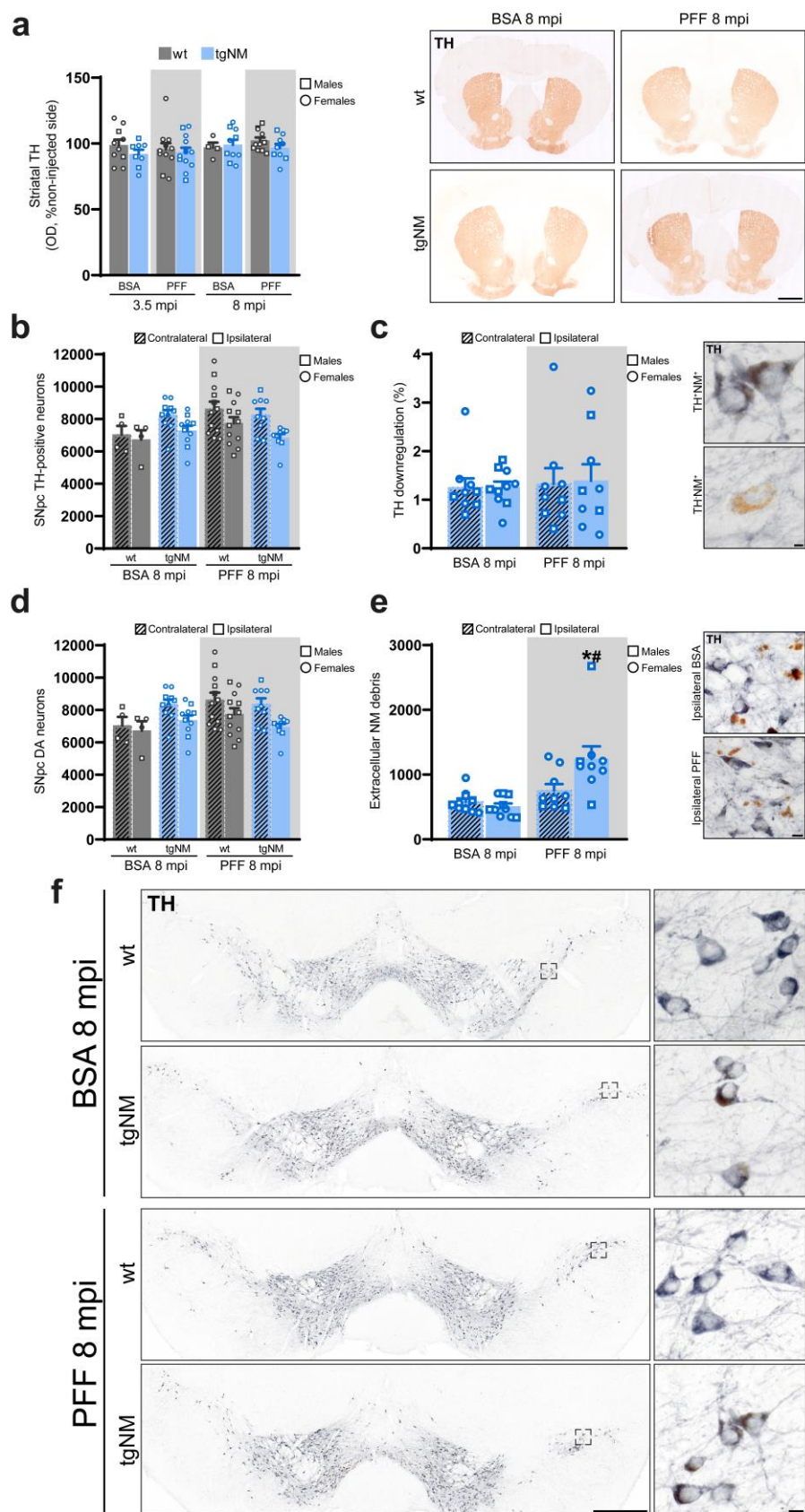


Figure 66. Nigrostriatal integrity in PFF-injected wt and tgNM mice. (a) *Left*, quantification of OD striatal TH fibers in BSA- and PFF-injected wt and tgNM mice at 3.5 and 8 mpi. A three-way ANOVA followed by Tukey's post-hoc test were used to assess statistical significance. $n=4-13$ animals per group. *Right*, representative photomicrographs of striatal TH immunolabeling. Scale bar, 1 mm. (b) Quantification of SNpc TH-positive neurons in BSA- and PFF-injected wt and tgNM mice at 8 mpi. A three-way ANOVA followed by Tukey's post-hoc test were used to assess statistical significance. $n=4-12$ animals per group. (c) *Left*, TH-NM⁺ neurons versus total NM⁺ neurons (including TH⁺NM⁺ and TH-NM⁺ neurons) as an index of TH downregulation in BSA- and α SYN PFF-injected tgNM mice at 8 mpi. A two-way ANOVA followed by Tukey's post-hoc test were used to assess statistical significance. $n=9-10$ animals per group. *Right*, representative photomicrographs of NM⁺TH⁺ neurons (*top*) and NM⁺TH⁻ neuron (*bottom*). Scale bar, 4 μ m. (d) Quantification of SNpc total DA neurons (i.e. independently of the TH phenotype) in BSA- and α SYN PFF-injected wt and tgNM mice at 8 mpi. A three-way ANOVA followed by Tukey's post-hoc test were used to assess statistical significance. $n=4-12$ animals per group. (e) *Left*, quantification of extracellular NM debris in BSA- and PFF-injected tgNM mice at 8 mpi. * $p<0.05$ compared to PFF contralateral side; # $p<0.05$ compared to BSA ipsilateral side. A two-way ANOVA followed by Tukey's post-hoc test were used to assess statistical significance. $n=9-10$ animals per group. *Right*, representative photomicrographs of ipsilateral extracellular NM debris in BSA- and PFF-injected tgNM mice. Scale bar, 10 μ m. (f) Representative photomicrographs of SNpc TH immunolabeling. Scale bars, 500 μ m (*left*) and 10 μ m (*right*).

2.6 Intracellular NM levels in SNpc neurons from α SYN PFF-injected tgNM mice

Given the results in Chapter I of this thesis showing that α SYN overexpression is associated with enhanced intracellular NM accumulation, intracellular NM levels were investigated in both the contralateral and ipsilateral hemispheres of BSA- and α SYN PFF-injected tgNM mice (Figure 67). Remarkably, ipsilateral and contralateral SNpc neurons from α SYN PFF-injected animals exhibited increased intracellular NM levels compared to their BSA-injected counterparts (Figure 67). However, this increase was more pronounced in the ipsilateral hemisphere, which is consistent with a higher α SYN pathological burden in that hemisphere in α SYN PFF-injected animals.

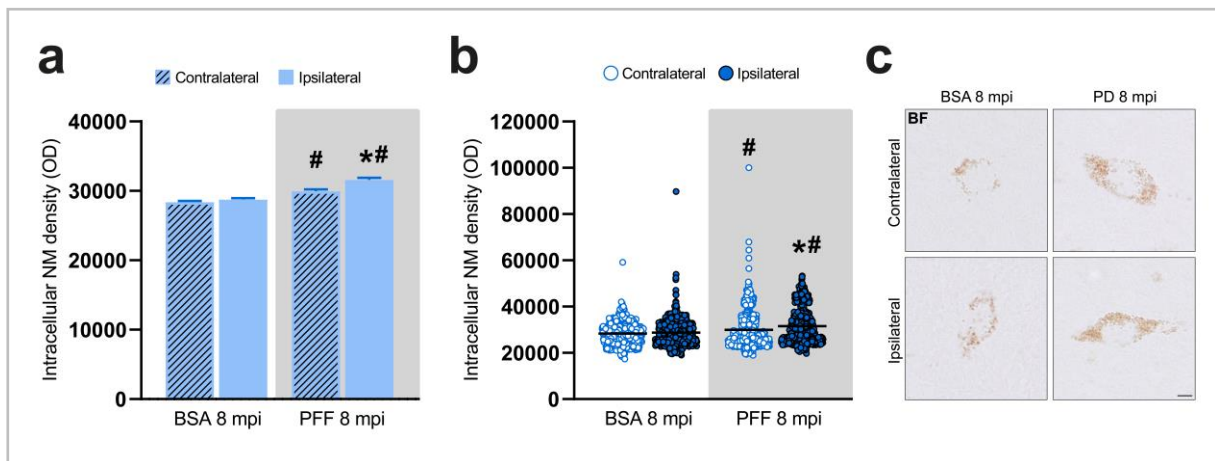


Figure 67. Intracellular NM levels in BSA- and PFF-injected tgNM mice. (a, b) Quantification by OD of intracellular NM levels in contralateral and ipsilateral SNpc neurons from BSA- and PFF-injected TgNM mice at 8 mpi. * $p<0.05$ compared to contralateral PFF. # $p<0.05$ compared to respective BSA. A two-way ANOVA followed by Tukey's post-hoc test were used to assess statistical significance. $n=647-796$ neurons per group. (c) Representative photomicrographs from unstained SNpc brain sections showing neurons containing NM (in brown). Scale bar, 5 μ m.

2.7 Lack of behavioural alterations in α SYN PFF-injected wt and tgNM mice

To determine whether PFF-induced p α Syn pathology in wt and tgNM mice was associated with behavioural alterations, a battery of motor and non-motor tests was carried out in these animals, and results compared to BSA-injected controls at the 3.5 and 8 mpi time-points.

2.7.1. Motor tests

Motor function was evaluated first. Because both BSA and PD-derived α SYN PFFs were unilaterally injected into the right hemisphere, motor asymmetry was assessed by measuring contralateral forepaw use in the cylinder test (Figure 68b-c). Wt and tgNM mice did not exhibit any motor asymmetry, either at baseline or following BSA or PFF injection (Figure 68b). If anything, PFF-injected tgNM animals showed a slightly increased contralateral forepaw use at 8 mpi compared to their BSA-injected control counterparts (Figure 68b). To rule out the influence of external factors that may alter the assessment of motor asymmetry, such as difficulties with cage habituation, the total number of contralateral + ipsilateral forepaw touches during the performance of the cylinder test was also analysed (Figure 68c). No differences were found on this parameter among the experimental groups (Figure 68c). Motor coordination and balance were next evaluated by means of the beam traversal test. At 8 mpi, BSA- and PFF-injected mice were tested using a thicker beam than at 3.5 mpi because of the increased weight of older animals. For this reason, data were plotted separately for each time-point (Figure 68d-i). Results from the first trial (Figure 68d-g), second trial (Figure 68e-h), and the average of both trials (Figure 68f-i) were collected. At 3.5 mpi, tgNM mice needed more time to cross the beam compared to wt animals, regardless of the injected material (Figure 68d, e, f), indicating that this effect is directly linked to the genotype as previously reported¹⁰⁰. However, at 8 mpi, no significant differences were observed between tgNM and wt animals in either the BSA- or PFF-injected groups (Figure 68g, h, i), probably because the thicker beam was easier for the animals to traverse. Overall, these results indicate that PFF-induced p α Syn pathology, including that present in the nigrostriatal system, does not compromise motor function in either wt or tgNM mice at any time-point.

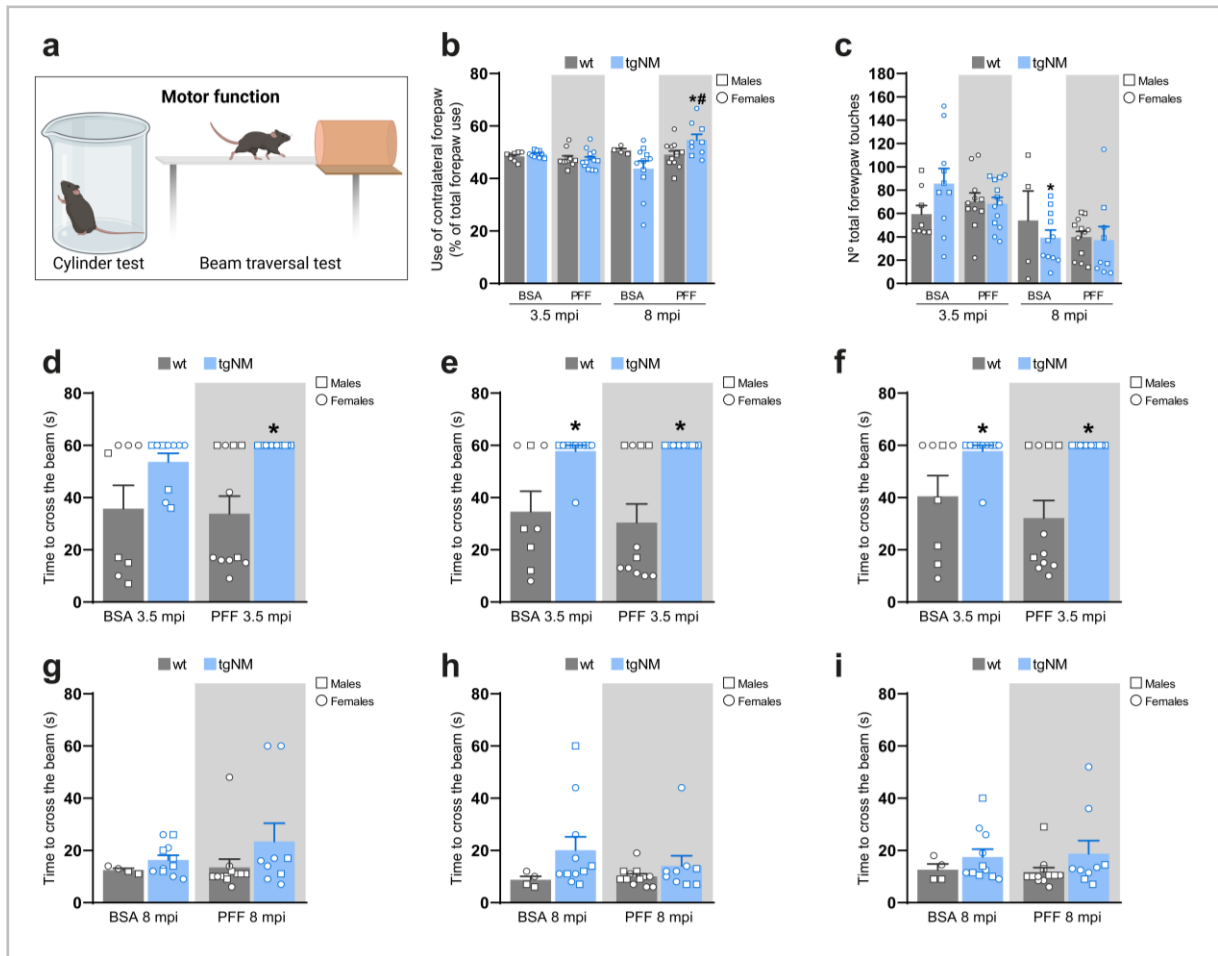


Figure 68. Motor function in BSA- and PFF-injected wt and tgNM mice. (a) Schematic representation of the motor tests performed. (b) Contralateral forepaw use was assessed with the cylinder asymmetry test in BSA- and PFF-injected wt and tgNM mice at 3.5 and 8 mpi. * $p<0.05$ compared to PFF-injected tgNM mice at 3.5 mpi. # $p<0.05$ compared to BSA-injected tgNM mice at 8 mpi. A three-way ANOVA followed by Tukey's post-hoc test were used to assess statistical significance. $n=4-13$ animals per group. (c) Number of total (contralateral + ipsilateral) forepaw touches as assessed with the cylinder asymmetry test in BSA- and PFF-injected wt and tgNM mice at 3.5 and 8 mpi. * $p<0.05$ compared to BSA-injected tgNM mice at 3.5 mpi. A three-way ANOVA followed by Tukey's post-hoc test were used to assess statistical significance. $n=4-13$ animals per group. (d-i) Time spent to cross the beam in the first trial (d-g), second trial (e-h) and the average of both trials (f-i) in BSA- and PFF-injected wt and tgNM mice at 3.5 (d, e, f) and 8 (g, h, i) mpi. * $p<0.05$ compared to PFF-injected wt mice at 3.5 mpi (d) or to respective wt animals (e, f). A two-way ANOVA followed by Tukey's post-hoc test were used to assess statistical significance. In (d, e, f), $n=8-13$ animals per group. In (g, h, i) $n=4-12$ animals per group. Drawing in a was created with Biorender.com.

2.7.2 Non-motor tests

Because two of the most characteristic symptoms of the prodromal phase of PD are constipation and deficits in olfaction, fecal pellet output and olfactory function were assessed in BSA- and PFF-injected wt and tgNM mice at 3.5 and 8 mpi (Figure 69a). Fecal pellet output was assessed by quantifying the number of fecal pellets produced over 1 h (Figure 69b). While tgNM mice showed a trend toward an increased number of total fecal pellets compared to wt animals, regardless of the type of material injected, no significant differences were observed between groups (Figure 69b). To further assess whether the

pattern of fecal deposition differed between groups, the cumulative number of fecal pellets over 1 h was analysed (Figure 69c). All groups exhibited a similar pattern of cumulative fecal pellet output, independently of the genotype and the type of material injected (Figure 69c).

Olfactory function was next evaluated using an olfaction test, in which animals were exposed to water followed by lemon or banana essences (Figure 69a). Olfactory DIs were calculated by subtracting the time spent in smelling water from the time spent smelling either lemon (Figure 69d) or banana essence (Figure 69e). Animals experiencing olfactory difficulties would likely spend similar amounts of time in smelling water and the essences, resulting in a DI close to 0 or even negative value. In contrast, animals with preserved olfactory function would be expected to show a preference for the essences over the water, yielding a positive DI. No significant differences in DI were detected between experimental groups (Figure 69d-e).

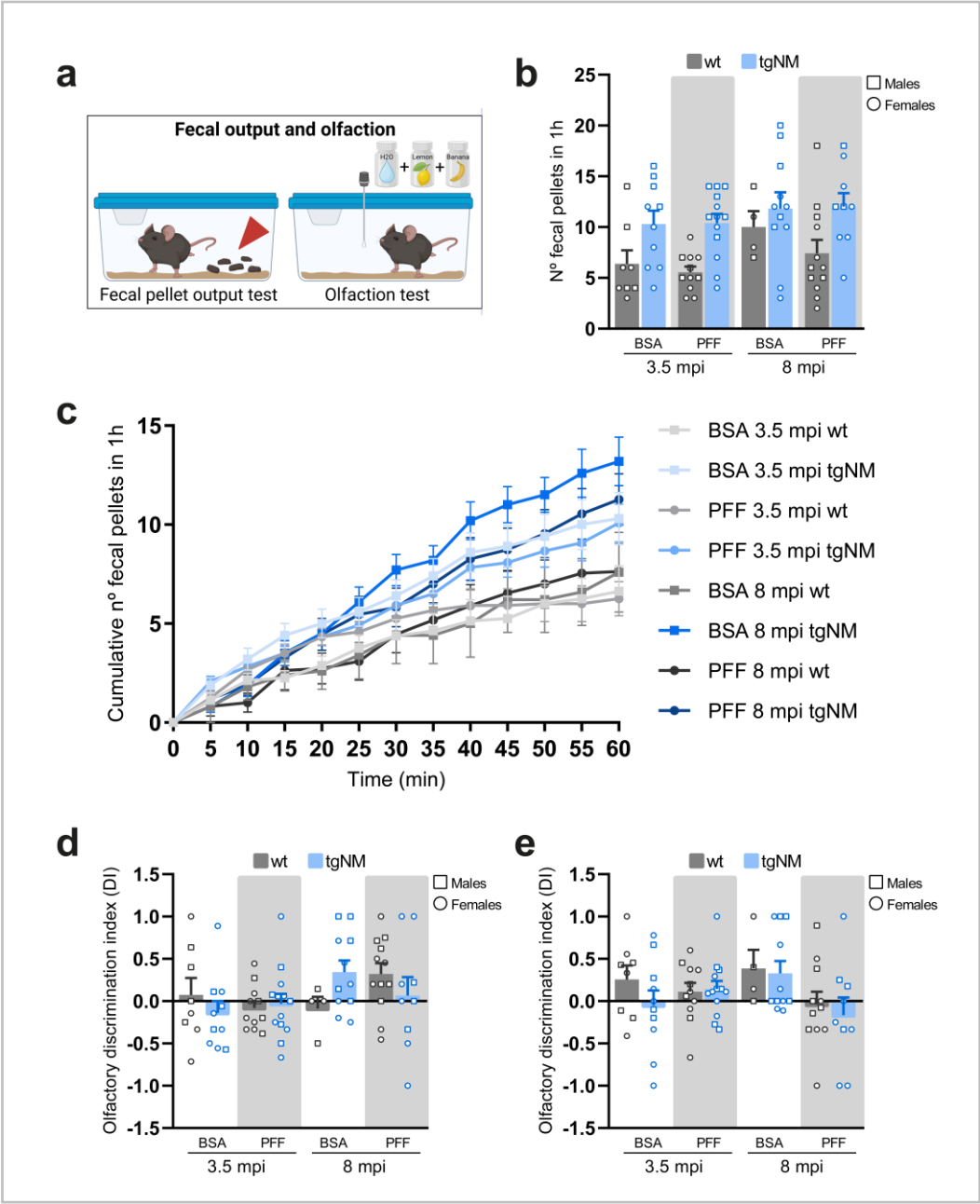


Figure 69. Fecal output and olfactory function in BSA- and PFF-injected wt and tgNM mice. **(a)** Schematic representation of the tests performed. **(b)** Number of fecal pellets produced in 1 h by BSA- and PFF-injected wt and tgNM mice at 3.5 and 8 mpi. A three-way ANOVA followed by Tukey's post-hoc test were used to assess statistical significance. $n=4-13$ animals per group. **(c)** Pattern of cumulative fecal pellets produced in 1 h measured every 5 min in BSA- and PFF-injected wt and tgNM mice at 3.5 and 8 mpi. **(d-e)** Olfactory DI in the lemon **(d)** and banana **(e)** olfaction test calculated by subtracting the time spent in smelling water from the time spent smelling either lemon **(d)** or banana **(e)** essence for BSA- and PFF-injected wt and tgNM mice at 3.5 and 8 mpi. A three-way ANOVA followed by Tukey's post-hoc test were used to assess statistical significance. $n=4-13$ animals per group. Drawing in **a** was created with Biorender.com.

Next, as an index of learning and memory, aversive memory was examined in BSA- and PFF-injected wt and tgNM mice using the step-down test (**Figure 70a**). During a training session, animals were placed on a platform and, upon stepping down onto the grid, they received an electric shock. The next day, in the test session, the latency to step down was recorded to evaluate the learning and memory retention of each group of animals. A longer latency to step down indicates stronger aversive memory, reflecting the animal's ability to associate the platform with the hostile experience from the previous day. No significant differences between groups were observed (**Figure 70b**). Data were also normalized by calculating the ratio of the latency between the test and the training sessions. Again, no differences between groups were observed (**Figure 70c**).

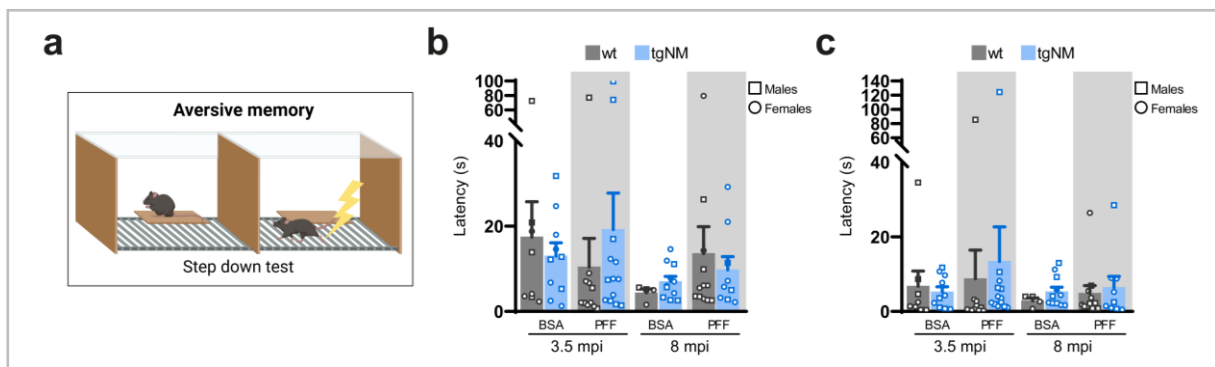


Figure 70. Aversive memory function in BSA- and PFF-injected wt and tgNM mice. **(a)** Schematic representation of the step-down test. **(b-c)** Latency to step down during the test **(b)** and training **(c)** sessions in BSA- and PFF-injected wt and tgNM mice at 3.5 and 8 mpi. A three-way ANOVA followed by Tukey's post-hoc test were used to assess statistical significance. $n=4-13$ animals per group. Drawing in **a** was created with Biorender.com.

α Syn pathology in the dorsal raphe nucleus, a key serotonin-producing region, have been linked to depressive-like behaviour, which is a common feature of PD²²⁵. To investigate a potential depressive-like behaviour induced by α SYN PFF inoculation in wt and tgNM mice, a tail suspension test was performed in these animals (**Figure 71a**). Both wt and tgNM animals exhibited increased latency to the first immobility at 8 mpi compared to the 3.5 mpi time-point (**Figure 71b**). However, no significant differences were observed between groups for the total immobility time (**Figure 71c**).

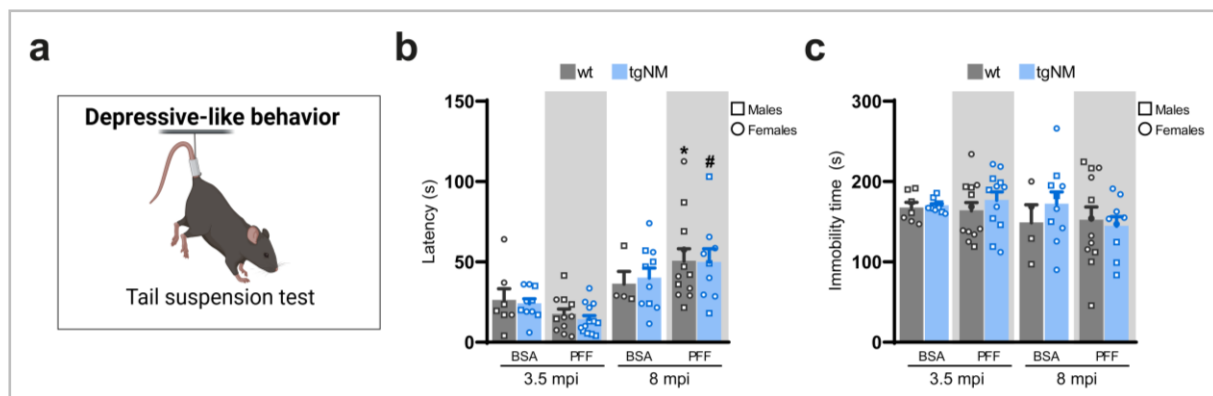


Figure 71. Depressive-like behaviour in BSA- and PFF-injected wt and tgNM mice. (a) Schematic representation of the tail suspension test. (b-c) Latency to the first immobility (b) and total immobility time (c) in BSA- and PFF-injected wt and tgNM mice at 3.5 and 8 mpi. * $p < 0.05$ compared to PFF-injected wt animals at 3.5 mpi. # $p < 0.05$ compared to PFF-injected tgNM mice at 3.5 mpi. A three-way ANOVA followed by Tukey's post-hoc test were used to assess statistical significance. $n = 4-13$ animals per group. Drawing in a was created with Biorender.com.

Summing up the behavioural data, it was found that a unilateral injection of PD-derived α Syn PFFs did not result in motor deficits such as asymmetry, motor balance or coordination impairments, nor in peripheral dysfunction or non-motor alterations, such as constipation, olfaction loss, memory deficits, or depression-like behaviour in either wt or tgNM animals.

Overall, the unilateral inoculation of PD-derived α Syn PFFs into the STR of wt mice induces a local accumulation of endogenous α Syn at the injection site with subsequent spreading of α Syn pathology to anatomically connected rostral and caudal regions. However, this widespread α Syn pathology does not lead to nigrostriatal degeneration or cause any detectable motor or non-motor behavioural alterations. Furthermore, an oxidative environment linked to NM production does not exacerbate PFF-induced α Syn pathology or spread, nor does it result in cell dysfunction, overt nigrostriatal cell loss or behavioural alterations in NM-producing tgNM mice.

DISCUSSION

DISCUSSION

While PD is neuropathologically characterised by the selective loss of NM-accumulating neurons, particularly DA-producing neurons in the SN, along with the presence in affected neurons of α Syn-containing LBs, the exact molecular cascade leading to the pathology remains poorly understood^{10,11,52}. The loss of NM-containing neurons is central to characteristic motor and non-motor symptoms of the disease. At present, PD has no cure and the gold-standard treatment, L-DOPA, often results in long-term adverse effects. As aging is the primary risk factor for PD⁴⁹, the rapid increase in the global aging population has significantly contributed to the rising prevalence of the disease in recent years. Therefore, deciphering the precise mechanism underlying PD has become an urgent priority in global health as such knowledge should facilitate the development of new targeted therapies.

NM pigment, which accumulates naturally with age, plays a protective role by incorporating toxic catecholamine derivatives into its polymer matrix and sequestering harmful metals and compounds⁸⁴. However, excessive NM accumulation can surpass a pathogenic threshold, leading to the release of ROS, disruption of cellular degradation pathways, and interference with endocytic and secretory processes that ultimately impact negatively on neuronal survival. In contrast to humans, most animals, including rodents, do not spontaneously develop NM^{75,98}, making it challenging therefore to investigate its role in PD pathogenesis. To address this limitation, our group developed the first rodent models capable of age-dependent human-like NM production and accumulation within PD-vulnerable neurons^{99,100}. These models, based on the overexpression of TYR, a key enzyme in melanogenesis, demonstrated that progressive intracellular NM accumulation compromises neuronal function when its concentration exceeds a critical threshold, triggering PD-like features in an age-dependent manner. Intriguingly, *post-mortem* analyses of human brains from PD patients and pre-PD individuals reveal that NM levels similarly reach a pathogenic threshold in disease states⁹⁹. Despite these observations, the factors influencing the rate of NM accumulation and accelerating its build-up beyond the pathogenic threshold in PD patients are yet to be elucidated. Identifying these factors is critical, as they may hold the key for novel therapeutic strategies aimed at slowing or preventing disease progression.

α Syn is a widely expressed, multifaceted protein in the CNS, playing essential roles in neuronal health and synaptic plasticity^{103,113}. Under physiological conditions, α Syn exists in a dynamic equilibrium between a soluble, unfolded monomeric form and a membrane-bound state, regulating synaptic vesicle dynamics, neurotransmission and nuclear gene expression¹⁰³. However, under pathological conditions, α Syn undergoes a conformational shift, forming oligomers and amyloid fibrils that aggregate into LBs. These aggregates disrupt synaptic vesicle cycling, impair neurotransmission, and compromise α Syn's nuclear functions, leading to genomic instability and cellular stress^{113–115}. Consistent with its pathological role, aggregated forms of α Syn are consistently elevated in the brain, CSF, blood and skin of PD patients^{62,63,131,136–142,145–147}.

Given α Syn's association with PD, substantial research has focused on elucidating its role in disease onset and progression. While α Syn-based animal models often replicate neurodegeneration and α Syn aggregation, most fail to develop authentic LB pathology¹⁶⁶, a key neuropathological hallmark of PD. Furthermore, connectome-mapping studies and *post-mortem* analyses suggest that the spatial pattern of LB pathology in clinical PD is inconsistent with a simple α Syn propagation model, and the correlation between LB pathology and neuronal death is weak²²⁶. These findings challenge the idea of α Syn as the sole driver of PD pathology. Indeed, while duplications and triplications in the *SNCA* gene cause PD^{10,52,186–188}, other genetic forms of PD, such as those linked to *LRRK2* or *PRKN* mutations, exhibit pure nigrostriatal degeneration without LB formation²²⁷. Additionally, α Syn-targeted vaccine trials in early-stage PD patients have failed to demonstrate disease-modifying effects, despite effectively binding native α SYN in human serum^{160,161}. Collectively, these findings suggest that α Syn pathology may carry out an ancillary role within a broader pathogenic process, such as the one driven by NM accumulation. While α Syn remains a valuable biomarker for PD, its suitability as a primary therapeutic target requires reconsideration.

In the present work, we explored the potential interplay between α Syn and NM in driving PD pathogenesis. Previous findings suggest that α Syn redistributes to the lipid component of NM in early PD stages and is entrapped within NM granules extracted from PD, but not control brains^{175,176}. The elevated levels of both α Syn and NM in SN neurons may predispose these cells to LB formation and degeneration. However, direct experimental investigation of the pathological interaction between α Syn and NM has been hindered by the absence of NM in common laboratory animal models. Using our NM-producing rodent models based on *TYR* overexpression, we demonstrated that *TYR* injection above the SN of α Syn KO mice induces LB-like pathology and nigrostriatal neurodegeneration comparable to that observed in wt mice⁹⁹. These findings suggest that α Syn is dispensable for NM-linked PD pathology, supporting the hypothesis that α Syn acts as an accelerator of PD pathology rather than its primary driver.

α Syn has been shown to propagate across anatomically connected brain regions^{103,148,151,152}. It has been proposed that α Syn pathology may originate in peripheral tissues before spreading to the brain, where it subsequently propagates to other regions^{148,150}. This spreading and accumulation of α Syn have been associated with both motor and non-motor symptoms of PD⁵². While mechanisms and drivers of α Syn propagation have not been fully clarified, oxidative conditions were shown to promote its spreading¹⁸¹. Based on these observations, we hypothesised that an NM-producing oxidative environment would facilitate the spread of α Syn.

Our findings show that the combination of nigral α SYN overexpression in an NM-accumulating context accelerates NM production, enhances α Syn aggregation, induces neuropathological inclusion formation, and triggers nigrostriatal degeneration and neuronophagia. Mechanistic studies revealed that α Syn upregulates *TYR* expression and permeabilises synaptic vesicles, contributing to NM accumulation. However, NM did not exacerbate α Syn pathology when injected with PD patient-derived α SYN PFFs into NM-accumulating transgenic mice, suggesting that NM's role in α Syn spreading may be more nuanced than previously thought.

1. Chapter I. Effects of α SYN overexpression on NM-associated PD pathology

1.1 NM levels

α SYN and TYR co-injected animals showed increased NM production when compared to those injected with TYR alone, demonstrating that increased α Syn levels accelerate NM build-up. Although NM is present in all human brains and increases with age, only a subset of individuals develops PD⁴⁹. Our previous study suggest that PD occurs when a critical pathogenic threshold is surpassed⁹⁹. Supporting this, NM levels exceed this threshold in PD brains and pre-symptomatic cases (i.e., incidental LB disease) but remain below it in age-matched healthy individuals. This implies the presence of factor(s) accelerating NM production in PD patients, driving them to reach the pathogenic threshold earlier. Our results in this thesis suggest that α Syn is a key contributing factor promoting the increased NM accumulation observed in PD pathology.

1.2 α Syn levels and species

While α SYN overexpression in the SNpc of rats induced the accumulation of total α SYN and p α Syn in neurons, α SYN and TYR co-injected animals displayed a reduced number of nigral total α SYN- and p α Syn-positive neurons. Conversely, co-injected rats exhibited increased oligomeric α SYN species. This altered balance between total/phosphorylated α Syn levels and oligomeric α Syn may stem from the pronounced neurodegeneration observed in co-injected animals compared to those injected with α SYN alone. Additionally, consistent with findings in PD *post-mortem* brains and CSF^{131,134-136,138,140,141}, increased aggregated α Syn levels appear to be linked to a reduction in physiological forms of the protein. This could be a consequence of the rapid sequestration of monomeric α Syn into aggregates, which diminishes the availability of its functional forms and drives the pathological progression.

Levels of phosphorylated α Syn at serine 129 are consistently enriched in LBs and detected in *post-mortem* PD brains, CSF, blood and skin samples, demonstrating its association with PD^{109,137,140,145}. While increased p α Syn levels have long been considered an index of pathological α Syn¹²³⁻¹²⁵, emerging evidence highlights its potential physiological roles, adding nuances to this interpretation. Specifically, p α Syn has been shown to (i) act as a protective cellular response to aggregation by facilitating native protein-protein interactions and restoring basal cellular function^{121,122}, (ii) regulate neurotransmitter release homeostasis by promoting synaptic vesicle clustering and limiting vesicle mobility^{121,122} and (iii) be preferentially targeted for degradation via UPS, reducing α Syn levels and favouring the aggregation clearance process¹²⁶. Therefore, further studies are needed to determine whether p α Syn precedes LB formation as part of protective or homeostatic cellular responses or if p α Syn acts as a key contributing factor to disease progression.

In line with previous findings, our results confirm that NM accumulation promotes α Syn aggregation^{99,100,177}. Nevertheless, it remains unclear whether NM binds directly to α Syn to promote its aggregation or if this process is mediated by a secondary factor, such as a

metabolite involved in NM biogenesis. Intriguingly, the α Syn associated with NM granules in PD brains has been found to be protease-resistant, suggesting that during NM biosynthesis, α Syn undergoes cross-linking and becomes irreversibly entrapped within NM granules¹⁷⁶. Oxidative modifications appear to play a pivotal role in this process since they enhance α Syn aggregation and hinder its proteasomal degradation^{228–231}. As NM shifts to a pro-oxidant state, it can release redox-active iron, generating oxidative stress that could further drive α Syn aggregation⁸⁴. Additionally, DA itself can bind to α Syn through oxidation of methionine residues inducing oligomer formation^{230,232}. The highly reactive DA-derived metabolite, DOPAL, also drives α Syn oligomerization by covalent modifications to its lysine residues^{233,234}. Moreover, tyrosine residues in α Syn are substrates for TYR, leading to the formation of reactive quinone species that exacerbate α Syn aggregation²³⁵. Collectively, these findings suggest that NM-associated factors, such as redox-active iron, DA metabolites, and TYR activity, create an oxidative environment that may drive α Syn aggregation, contributing to PD pathogenesis.

1.3 Neuropathological inclusions

In prior studies from this group, it was shown that inclusion body formation in TYR-injected rats peaked before the onset of neurodegeneration, indicating that neurons harbouring these inclusions are more likely to degenerate⁹⁹. Remarkably, α SYN-injected rats did not develop neuropathological inclusions at any of the evaluated time-points, suggesting that NM accumulation is a prerequisite for inclusion body formation. This observation aligns with the well-documented association of classical LBs in melanized neurons described in PD, where LBs are found in close physical association to NM⁸⁸. Moreover, α SYN-injected rats exhibited only a mild striatal denervation and no observable loss of DA neurons in the SNpc. In contrast, LB pathology in TYR-injected animals peaked at 8 w and then diminished, consistent with previous studies⁹⁹. Notably, α SYN+TYR-injected animals displayed more sustained LB pathology, evident at both 8 and 16 w, followed by a decline at 60 w. This prolonged pathology correlated with the heightened neurodegeneration observed in co-injected animals compared to those injected with TYR alone, suggesting that as more neurons exhibited signs of dysfunction, such as LB pathology, an increasing number underwent degeneration. This reinforces the interplay between inclusion formation, neuronal dysfunction, and subsequent degeneration in the context of α SYN and NM interactions.

The intranuclear inclusions – MBs – are confined to pigmented neurons and typically associated with normal aging⁴³. Interestingly, their prevalence is decreased in PD, a reduction that correlates with decreased neuronal density in the SN, suggesting that MB-containing neurons may be more susceptible to degeneration. While α SYN- and TYR-injected animals showed minimal MB formation, α SYN+TYR-co-injected animals displayed significantly increased MB accumulation over time. Given that both NM and MBs are linked to aging, the simultaneous increase in NM levels and MB formation in α SYN+TYR rats suggests that the aging process may be accelerated in these animals. In this regard, exploring and describing a potential senescence phenotype would be appropriate. Consistent with this notion, NM-containing nigral neurons in PD brains exhibit markers of cellular senescence, including increased expression of the pro-

senescence factor p21 and reduced levels of the nuclear membrane protein lamin B1, both hallmark features of senescence²³⁶. Moreover, recent studies have shown that nuclear α Syn accelerates cell senescence and neurodegeneration²³⁷. Overexpression of nuclear α Syn leads to the formation of α Syn-containing nuclear inclusions, upregulation of p21 and induction of senescence-associated secretory phenotype-related genes. Together, these findings highlight a potential link between α Syn pathology, NM accumulation, and cellular senescence, which could play a crucial role in the accelerated aging observed in PD pathology.

1.4 Nigrostriatal degeneration

As stated above, α SYN-injected animals exhibited only modest striatal denervation without any detectable loss of DA neurons in the SNpc, thus aligning with the absence of inclusion body formation in these animals. While most viral vector-mediated α SYN-overexpression models show nigrostriatal degeneration, they fail to reproduce LB pathology^{165,166}. The extent of neurodegeneration varies across studies and is highly dependent on viral titer, serotype, promoters, differences in purification methods, and time post-injection¹⁶⁴. Collectively, these findings underscore the limitations of using α Syn overexpression alone to model PD.

The evident striatal denervation observed in both TYR- and α SYN+TYR-injected animals reveals a clear link between NM accumulation and neurodegeneration. However, α SYN+TYR-co-injected animals exhibited exacerbated striatal denervation at later time-points accompanied by significant DA cell loss in the SNpc when compared to TYR-injected rats. This was further supported by an increased release of extracellular NM from dying neurons followed by its engulfment by macrophages, a process known as neuronophagia. These findings emphasise the exacerbating role of α Syn in NM-associated neurodegeneration.

Summing up all data, α SYN overexpression in NM producing animals accelerated NM production, which likely contributed to enhanced α Syn aggregation and sustained PD-associated neuropathological inclusion formation (Figure 72). As a result, these animals exhibited enhanced neurodegeneration and neuronophagia. These findings underscore the interplay between α Syn and NM in the pathogenesis of PD, accentuating the potential role of NM accumulation in exacerbating neurodegenerative processes.

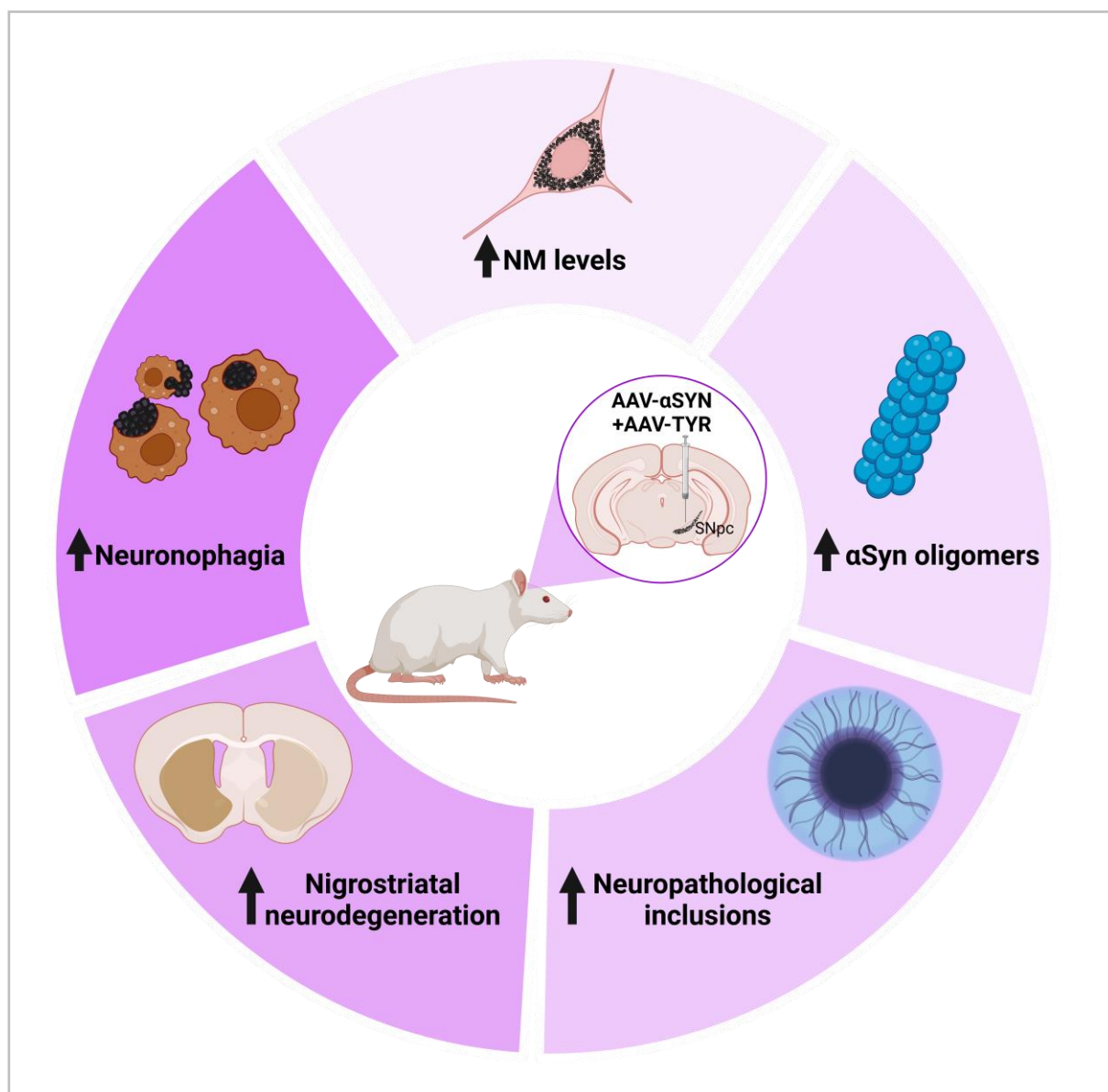


Figure 72. Histopathological features associated with α SYN+TYR co-injection. α SYN overexpression in NM-producing animals increases NM levels, α Syn oligomerization, neuropathological inclusions, nigrostriatal neurodegeneration and neuronophagia. Illustration created with Biorender.com.

1.5 Molecular mechanisms underlying α Syn and NM interplay

Our previous findings in this thesis, indicate that NM production, a by-product of DA metabolism catalysed by TYR in our rat model, is accentuated by mechanisms involving α Syn. To clarify how α Syn enhances NM production, we explored its influence on DA synthesis, vesicular uptake, and oxidative pathways.

In DA neurons, tyrosine is converted to L-DOPA via TH, and L-DOPA is further converted to DA by AADC^{200,238} (Figure 73). Cytosolic DA, which is highly unstable, can be sequestered into synaptic vesicles, metabolized or oxidised. Vesicular DA uptake occurs through VMAT2, enabling DA storage in synaptic vesicles²³⁹. The fusion of synaptic vesicles with the presynaptic membrane, which releases DA into the synaptic cleft, is

facilitated by assembly of the SNARE complex, which includes syntaxin-1 and SNAP-25 on the presynaptic membrane and VAMP2 on the synaptic vesicle¹¹⁰. α Syn directly interacts with VAMP2, stabilizing vesicles and promoting SNARE complex assembly, thereby enhancing synaptic vesicle fusion. After DA release, synaptic vesicles are recycled for subsequent rounds of neurotransmission. DA can also be metabolized into reactive intermediates such as DOPAL and DOPAC, through the actions of monoamine oxidase (MAO) and aldehyde dehydrogenase (ALDH), respectively^{200,238}. These intermediates, along with L-DOPA and DA itself, are prone to oxidation, generating quinones through catalytic reactions involving ferric iron⁴⁶. Quinones can undergo three distinct pathways: (i) conjugation with protein residues, forming quinone-protein adducts; (ii) cyclization, followed by further oxidation and polymerization, leading to the production of eumelanin, and (iii) reaction with L-cysteine or glutathione producing cysteinyl-DA compounds that are subsequently oxidised to pheomelanin. Collectively, these processes lead to the formation of NM⁸².

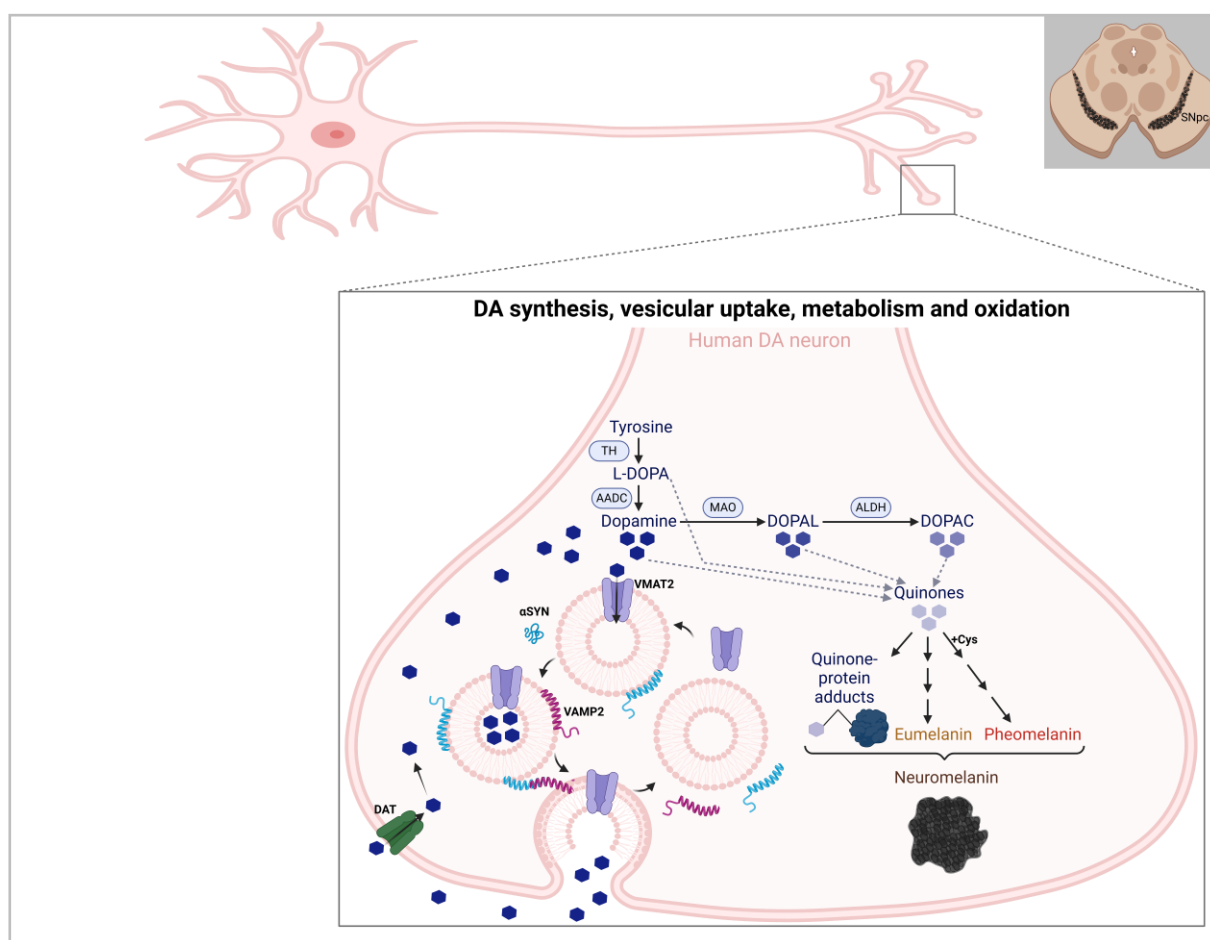


Figure 73. DA synthesis, vesicular uptake, metabolism and oxidation in a schematic human DA neuron. In DA neurons, tyrosine is converted to L-DOPA by TH, and L-DOPA is further converted to DA by AADC. Cytosolic DA, which is highly unstable, is either sequestered into synaptic vesicles, metabolised, or oxidised. Vesicular DA uptake is mediated by VMAT2, enabling DA storage in synaptic vesicles. The fusion of these vesicles with the presynaptic membrane, which triggers DA release into the synaptic cleft, is facilitated by the SNARE complex, which includes VAMP2. α Syn interacts with VAMP2 to stabilize vesicles and enhance SNARE complex assembly, promoting synaptic vesicle fusion. After DA release, synaptic vesicles are recycled for further neurotransmission and extracellular DA can be reincorporated to neurons via DAT. DA is metabolized into intermediates like DOPAL and DOPAC by MAO and ALDH, respectively. These

intermediates, along with DA and L-DOPA, are susceptible to oxidation, producing quinones that can form adducts with proteins or undergo polymerization into eumelanin and pheomelanin pigments, contributing to the formation of NM. Illustration created with Biorender.com.

Although NM synthesis is widely believed to occur via the spontaneous non-enzymatic autooxidation of DA, some evidence challenges this theory, as highlighted in the introduction of this thesis. Indeed, experimentally induced increases in DA or oxidised DA species in rodents, achieved either through chronic L-DOPA treatment^{75,240,241} or by genetically enhancing TH activity^{75,242}, are insufficient to drive NM production. Supporting the notion that NM biosynthesis is under enzymatic regulation, it was previously reported by this group that brain overexpression of TYR, a key enzyme in melanogenesis, in NM-lacking rats led to age-dependent human-like NM production associated with a PD-like phenotype⁹⁹. In this sense, TYR overexpression facilitates the conversion of tyrosine to L-DOPA and drives the DA oxidation pathway, enhancing DA-quinone formation and subsequently promoting NM synthesis^{75,99} (Figure 74).

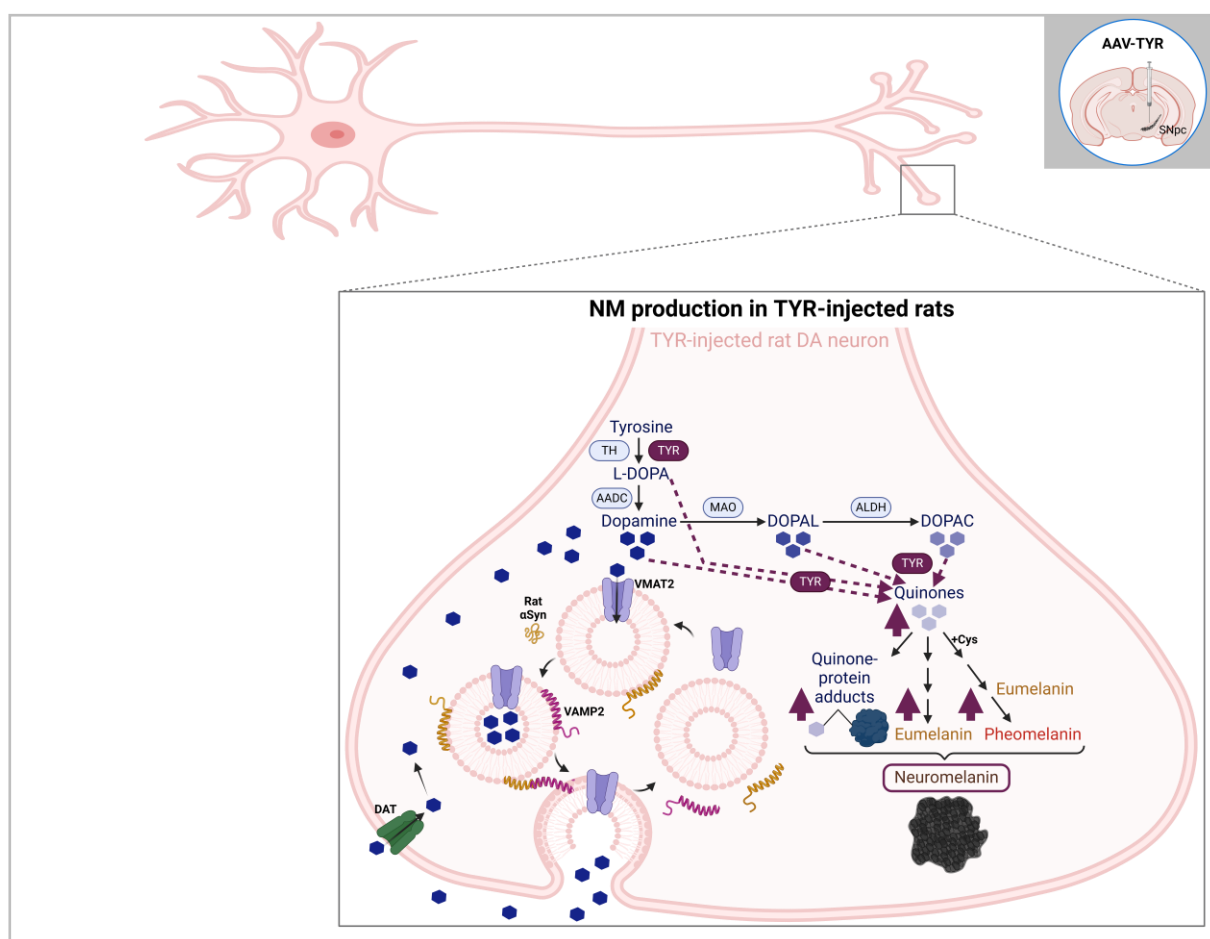
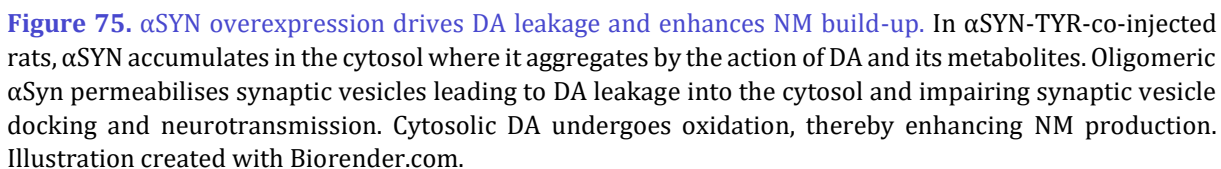


Figure 74. TYR overexpression in rats results in NM production. While rats do not spontaneously produce NM, TYR overexpression enhances the enzymatic conversion of tyrosine to L-DOPA, driving increased DA synthesis and promoting the oxidation of DA and its metabolites, which subsequently increases the formation of reactive quinones. The polymerization of these quinones ultimately results in NM production in these animals. Illustration created with Biorender.com.

In α SYN-overexpressing rats, α Syn accumulates in the cytosol. Under normal conditions, protein clearance mechanisms like autophagy and UPS prevent such accumulation. However, in NM-associated PD contexts, these systems are impaired and oxidative stress from NM production exacerbates protein aggregation. Specifically, α Syn aggregation is promoted by DA^{232,242–246}, DOPAL^{233,234,247}, DOPAC²⁴⁸ and DA-quinones²⁴⁹. In α SYN+TYR overexpressing rats, two synergistic factors converge: TYR drives DA oxidation and NM synthesis, while α Syn accumulation disrupts degradation pathways, further enhancing aggregation through interactions with DA oxidation products. This aligns with our observation of increased α Syn oligomer formation in α SYN+TYR-co-injected animals.

Interestingly, α Syn oligomers are hypothesised to permeabilise synaptic vesicles. In particular, DOPAL-induced α Syn oligomers permeabilise cholesterol, which contains lipid membranes,²³⁴ while α Syn protofibrils form pores that allow the leakage of low-molecular-weight molecules²⁵⁰. Moreover, α Syn overexpression is linked to increased cytosolic catecholamine concentrations¹⁹³. Based on this, we hypothesise that in an oxidative, NM-associated context, α Syn aggregates form pore-like structures in synaptic vesicles, leading to DA leakage into the cytosol. This hypothesis is supported by the reduced vesicular DA uptake observed in α SYN+TYR-injected animals in this thesis. Additionally, while α Syn overexpression alone was associated with increased VAMP2 levels, and the stabilizing of vesicle docking and fusion, α SYN+TYR-injected animals showed reduced VAMP2 levels, suggesting impaired vesicle docking and fusion, consistent with impaired DA vesicular uptake. As cytosolic DA is highly unstable, its oxidation may be promoted in α SYN+TYR animals, further driving NM production. These findings are consistent with the observed increase in NM levels in α SYN+TYR-co-injected animals compared to TYR-injected controls (Figure 75).



On another level, there is an increased reciprocal risk between PD and melanoma^{191,256-260}, a dermatological condition associated with increased melanin production. While TYR

expression levels and protein content are similar between melanocytes derived from pale and dark skin, melanocytes from individuals with darker skin exhibit up to ten times greater TYR activity and melanin content^{261,262}. In melanoma, TYR activity is frequently dysregulated, with some evidence indicating that *TYR* expression is upregulated during tumorigenesis²⁶³, contributing to the elevated melanin production in these cells. However, the regulation of *TYR* expression in melanoma is not uniform, with varying expression levels reported in different melanoma subtypes and stages^{264–266}. Interestingly, α Syn appears to play a pivotal role in this interaction, as it is upregulated in skin biopsies both in PD patients and melanoma cases and has been shown to modulate melanin levels in melanoma cells^{147,189,190,192,209}. Considering these data alongside the ability of α Syn to localize to the nucleus of DA neurons where it may influence transcriptional activity^{114,212}, we hypothesised that α Syn could enhance *TYR* expression, thereby promoting increased NM production in α SYN+TYR-overexpressing rats. Indeed, increased TYR protein levels in α SYN+TYR-co-injected animals as well as increased *TYR* expression, activity and protein levels in α SYN-overexpressing and NM-producing neuroblastoma cells support this hypothesis.

Under physiological conditions, unfolded α Syn is translocated to the nucleus where it regulates gene expression by activating or repressing certain transcription factors¹¹³. However, when α Syn accumulates in the cytosol and undergoes aggregation, it may lose its ability to translocate to the nucleus, thus impairing its normal function in gene regulation. Additionally, aggregation may result in sequestration of key cofactors in the cytosol, preventing their translocation to the nucleus where they are needed for transcriptional regulation. While the precise mechanism by which α Syn promotes *TYR* expression remains unclear, one possibility is that physiological α Syn directly represses *TYR* expression, with its aggregation resulting in a loss-of-function that subsequently leads to TYR activation. Alternatively, aggregated α Syn may sequester a key cofactor responsible for repressing *TYR* expression, thereby indirectly promoting its activation. Taking into account the evidence presented, we propose a model in which α Syn overexpression and aggregation drive TYR activation, ultimately enhancing its expression and activity.

Further to the above, among α Syn's various targets, the transcription factor nuclear receptor-related factor 1 (Nurr1) has garnered attention due to its critical role in the survival and function of DA neurons^{267,268}. Nurr1 regulates the expression of several DA-synthesis-related genes, including TH, DAT and AADC. Notably, Nurr1 and its transcriptional targets are reduced in the SNpc neurons of PD patients exhibiting α Syn inclusions, whereas its levels remain unaltered in SNpc neurons of PD patients without α Syn inclusions²⁶⁹. In the same way, AAV-mediated α Syn transduction downregulates both Nurr1 protein and mRNA²⁷⁰, further linking α Syn pathology with Nurr1 dysregulation. Beyond the CNS, Nurr1 plays important roles in peripheral tissues, where it regulates inflammation and cellular stress²⁷¹. While direct evidence of Nurr1's involvement in *TYR* transcription is lacking, studies have shown that Nurr1 upregulates tyrosinase-related protein-1 (TYRP1) in human melanoma cells²⁷². Additionally, β -catenin, a well-known transcriptional cofactor, is an upstream regulator of Nurr1 and its activity is diminished in both PD and melanoma²⁷³. These connections further support the

epidemiological aforementioned association between PD and melanoma, emphasizing the existence of shared molecular pathways between these conditions.

Summing up the data that have been gathered and analysed, we conclude that α SYN overexpression and oligomerization promote *TYR* upregulation, which exacerbates the DA oxidation pathway in α SYN+TYR-injected animals (Figure 76). Furthermore, DA and DA-derived metabolites enhance α Syn aggregation, which in turn permeabilises synaptic vesicles, facilitating DA leakage into the cytosol and impairing neurotransmission. Subsequently, the unstable cytosolic DA is further oxidised, leading to increased NM production. Overall, the accumulation of aggregated α Syn species, as occurs in PD patients, accelerates NM production, thereby contributing to neuronal dysfunction and neurodegeneration.

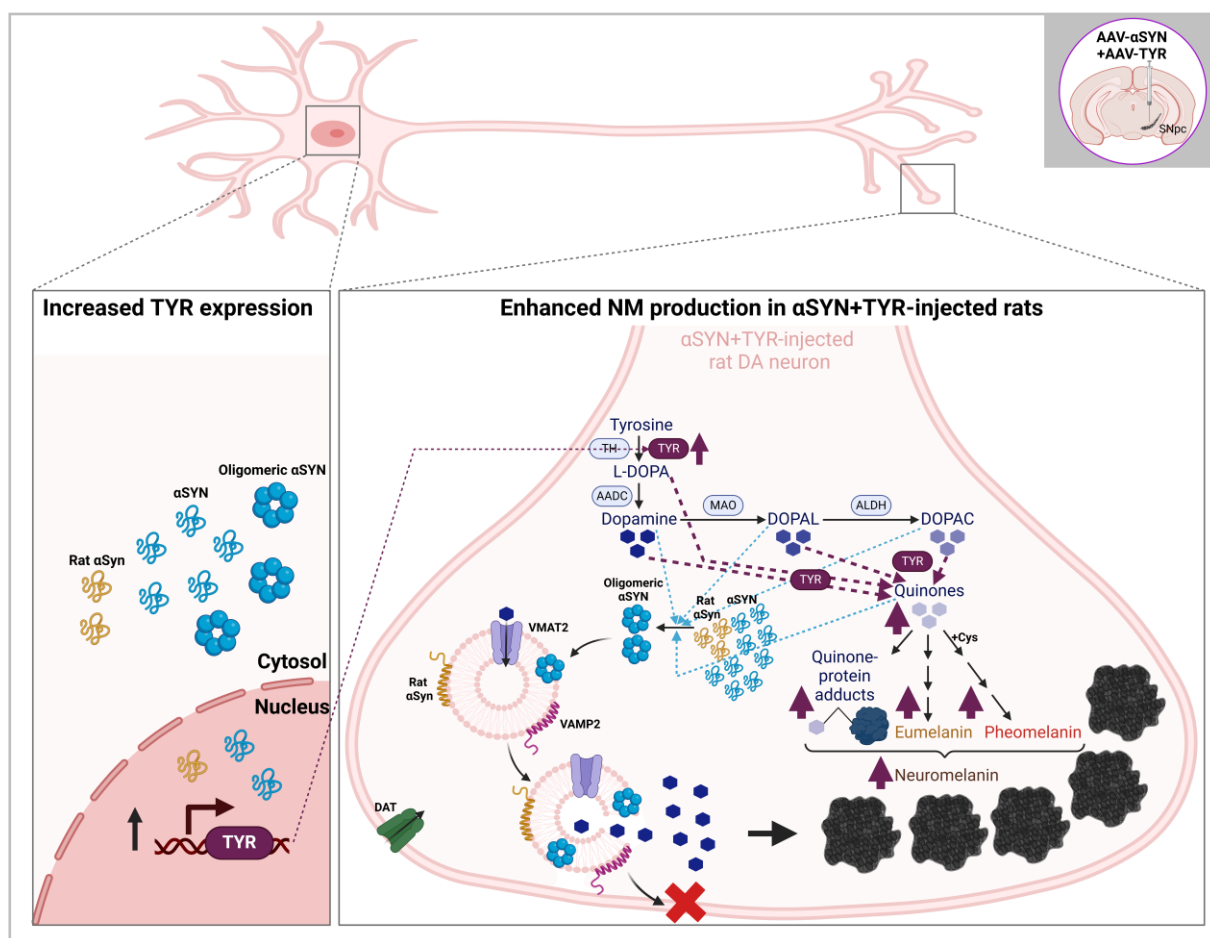


Figure 76. α SYN overexpression promotes *TYR* expression and drives DA leakage, thereby increasing NM production. α Syn accumulation and aggregation in the cytosol upregulates *TYR* expression. However, it remains unclear whether this upregulation occurs through a direct or indirect gene expression regulation mechanism. Increased *TYR* expression boosts DA synthesis and oxidation, further contributing to NM production. Simultaneously, aggregated α Syn permeabilises synaptic vesicles, leading to DA leakage into the cytosol and impairing synaptic vesicle docking and neurotransmission. The excess cytosolic DA undergoes oxidation, enhancing NM production. Illustration created with Biorender.com.

These results emphasise the need to consider additional factors when modelling PD based solely on α Syn. Indeed, α SYN-injected animals did not exhibit clear signs of PD pathology, supporting the view that α Syn may function more as an accelerator than as a primary trigger of PD. While it may appear that this condition is faithfully replicated in α Syn-

injected animals, it is crucial to bear in mind that humans possess NM, a factor absent in rodents. Based on these findings, it is plausible that elevated α Syn levels in *SNCA*-mutated PD patients contribute to the accelerated production of NM, leading to its accumulation beyond the pathogenic threshold that drives PD. Therefore, assessing intracellular NM levels in these patients could yield critical insights into the molecular events contributing to PD pathology.

2. Chapter II. Impact of NM-associated pathology on α Syn aggregation and propagation in PD

2.1 Properties and origins of the injected material

It is widely demonstrated that different α Syn conformations possess unique biochemical and biophysical properties, giving rise to distinct α Synucleinopathies^{155,274,275}. Furthermore, laboratory-derived PFFs generated under varying buffer conditions exhibit diverse α Syn conformations, which in turn have been repeatedly shown to induce distinct pathologies, clinical features, and strain-specific properties. Notably, none of the laboratory-derived PFF conformations reported to date have demonstrated structural homology with α Syn conformations resolved from patients with human LB disease²⁷⁵. Consequently, it remains unclear whether data from synthetic PFFs studies accurately reflect the biological mechanisms of PD or instead represent an artificial disease model driven solely by the specific conformation generated. To address this limitation, many recent studies, including the present work, utilise PFFs generated by seeding the fibrillization reaction with pathogenic α Syn extracted from PD patient samples. This approach aims to clone the α Syn-associated conformation found in PD, thereby enhancing the fidelity of disease modelling and providing insights that are more consistent with the native pathology of PD.

In this study, it was hypothesised that the NM-associated pro-oxidant environment accelerates α Syn pathology and propagation. To evaluate this, we aimed to reproduce mild pathology rather than severe pathology, which would enable the combined effects of NM and α Syn pathology induced by PFFs to be observed. In a previous characterisation study of the PD-derived α Syn PFFs used here, animals received 3.62 μ g of amplified PFFs – supplemented either with PBS or with an AAV encoding A53T α SYN (AAV-A53T α SYN) – by injection into the SNpc¹⁹⁷. Remarkably, α SYN PFFs alone did not cause SNpc cell loss, striatal denervation, or motor asymmetry at 5 mpi. While p α Syn-positive neurons in the SNpc were observed, their numbers were low. However, when α SYN PFFs were combined with AAV-A53T α SYN, animals exhibited significant ipsilateral cell loss, striatal denervation, and evident motor asymmetry, accompanied by high levels of p α Syn-positive neurons. Furthermore, the extent of nigrostriatal cell loss and motor behaviour alterations differed depending on whether the injected α SYN PFFs were derived from PD, DLB or MSA, thus further reinforcing the existence of different α Syn conformations.

Given our interest in studying the combine pathological effects of NM and α Syn, amplified α SYN PFFs alone were used in this study to determine whether their interaction with NM could exacerbate α Syn pathology and neuronal loss.

2.2 α Syn pathology and spreading

Injection of PD-derived amplified α Syn PFFs into mouse STR resulted in local accumulation of p α Syn, consistent with previous studies using the PFF model^{124,218,219,223,224}. It is worth noting that the observed p α Syn was murine, as no human α Syn immunoreactivity was detected, in line with previous findings^{123,174,276}. This observation, coupled with the absence of pathology in α Syn KO mice injected with α Syn PFFs²²⁴, suggests that endogenous α Syn is required for α Syn pathology development. Additionally, it is well established that α Syn pathology induced in the STR by PFF injection propagates in a time-dependent manner to interconnected rostral and caudal brain regions^{124,218,219,223,224}. This pattern of spread was observed in both wt and tgNM animals, further validating the relevance of the model used in this study.

p α Syn pathology was visualised in the form of Lewy neurites, dystrophic Lewy neurites, aggregates, and p α Syn-positive cells. The extent, types and distribution patterns of p α Syn pathology were similar between wt and tgNM animals, revealing that NM accumulation in all catecholaminergic brain areas, along with its associated oxidative stress, did not significantly influence the manifestation or progression of p α Syn pathology. However, these findings contrast with a previous study where the combination of paraquat, a ROS catalyst, and α Syn overexpression in the DMNX enhanced ROS levels, increased oligomeric and fibrillar α Syn species, and accelerated α Syn spreading¹⁸¹. One potential explanation for this is that NM levels in tgNM animals at the assessed time-points may not be high enough to generate sufficient ROS to influence α Syn pathology. Notably, tgNM animals at 11 m of age (8 mpi in this study), exhibit early signs of dysfunction and degeneration in the SNpc. These signs include the formation of LB-like inclusions, TH downregulation, extracellular NM debris, and an associated inflammatory response. However, overt neurodegeneration is not observed in these animals, suggesting that NM levels during this timeframe may remain below the pathogenic threshold required to exacerbate α Syn pathology. While the tgNM model provides a significant advantage by mimicking bilateral NM accumulation across the brain, as observed in humans, a potential next step would be to explore the effects of NM-induced oxidative stress on α Syn propagation more thoroughly. This could be done by injecting α Syn PFFs into the STR and viral vector-mediated TYR overexpression into the SN at varying concentrations, and assessing whether the dose influences NM-associated ROS production and α Syn propagation. In these experiments, p α Syn levels, distribution patterns, and ROS formation should be quantified. If successful, the experiment could be repeated in tgNM animals at longer time-points, where extracellular NM and inflammatory responses are more pronounced and cell loss is more evident. Such studies would help elucidate the role of NM in modulating α Syn pathology and propagation in a model that fully recapitulates brain-wide human NM accumulation and distribution.

2.3 α Synucleinopathy and neurodegeneration

While the α Synucleinopathy induced by the injection of PFFs is well-established and consistently demonstrated, its impact on neurodegeneration has yielded variable outcomes. In this thesis, the intrastriatal injection 1.4 μ g α SYN PFFs did not trigger striatal denervation or DA cell loss in the SNpc at either 3.5 or 8 mpi. Previous studies using intrastriatal PFF injections have reported mixed findings. For example, one study reported that 8 μ g α Syn PFFs induced striatal denervation at 2 and 6 mpi, with associated DA SNpc cell loss at 4 and 6 mpi²²³. Similarly, another study found that 8 μ g α Syn PFFs caused striatal denervation at 1.5, ~4, and ~6 mpi, and SNpc cell loss at ~4 and ~6 mpi²¹⁹. Surprisingly, injections of 8 μ g and 16 μ g induced striatal denervation only at the 8- μ g dose, without causing DA SNpc cell loss²¹⁸. Lastly, 5 μ g α Syn PFFs resulted in significant striatal denervation at 6 mpi but caused minimal DA SNpc cell loss¹²⁴. These findings suggest that striatal denervation precedes SNpc cell loss in this model. Notably, all three studies used mouse-derived α Syn PFFs. The preservation of nigrostriatal integrity observed in the animals evaluated in this thesis may be attributed to factors such as the origin of the PFF material and potential species incompatibility or differences in dosing. The species barrier, however, can likely be ruled out as the observed α Synucleinopathy was endogenous. Additionally, the lack of neurodegeneration in this study cannot be attributed to the time-point assessed, as the longer post-injection time-point used here (8 mpi) would have been sufficient based on previous studies to reveal neurodegeneration if it had occurred^{124,218,223}. While it remains possible that higher PFF doses might induce neurodegeneration, it is important to note that the 1.4 μ g dose used in this study already resulted in substantial α Syn accumulation and widespread distribution. Despite this, the nigrostriatal system remained unaffected, suggesting that even significant α Syn pathology alone may not be sufficient to drive neurodegeneration.

An important consideration is whether α Syn accumulation is inherently pathological, as discussed in section 1.2. A study employing *in vivo* multiphoton microscopy to monitor the conversion of endogenous α Syn into pathological aggregates in α Syn-GFP mice injected with PFFs provides valuable insights²⁷⁷. At 2.5 mpi, α Syn-GFP aggregates were observed forming neuritic inclusions. By 3 mpi, individual neurons near the injection site displayed heterogeneous somatic α Syn-GFP staining. Between 4 and 13 mpi, compact somatic inclusions resembling human Lewy pathology emerged, exhibiting hallmark features such as α Syn, amyloid dye binding, and ubiquitination along with a distinct, compact, "spider-like" morphology. Serial imaging demonstrated a high rate of disappearance among inclusion-bearing neurons, highlighting the selective degeneration of these cells and supporting the pathological role of mature Lewy inclusions. In this thesis, the vast majority of α Syn staining was identified as Lewy neurites, with aggregates representing less than the 2% of the total α Syn pathology in both wt and tgNM. It is therefore possible that these inclusions remain immature and do not yet induce neurodegeneration. To further investigate this possibility, it would be valuable to assess oligomer formation and the presence of mature LB-like inclusions in these animals at both time-points.

As previously stated, tgNM at 3.5 mpi (6.5 m of age) exhibit noradrenergic neurodegeneration and denervation accompanied by autonomic dysfunction¹⁰⁰. By 8 mpi

(11 m of age) both non-motor and motor symptoms emerge alongside DA dysfunction and neuropathological PD-like features such as LB-like pathology, extracellular granules, and neuroinflammation. These findings position tgNM mice as a prodromal PD model where NM accumulation does not yet trigger overt neurodegeneration. We have hypothesised that exposure of NM-vulnerable neurons to specific triggers could accelerate NM-driven processes, ultimately leading to neurodegeneration. At 8 mpi, tgNM animals displayed moderate p α Syn accumulation in the ipsilateral SNpc without accompanying cell loss. These observations suggest that p α Syn accumulation induced by α SYN PFFs, at least at this dose and time-point, is insufficient to provoke significant neurodegeneration in the nigrostriatal system of tgNM animals. It is worth noting that α SYN PFF-injected tgNM animals at 8 mpi showed increased ipsilateral extracellular NM debris, which might suggest early or incipient cell loss. Although this was not the primary focus of this chapter, the evaluation of intracellular NM levels revealed increased NM production following α SYN PFF inoculation, in line with findings presented in the first chapter. While NM production at the evaluated time-point did not influence p α Syn pathology in PFF-injected tgNM animals compared to wt controls, and this p α Syn pathology did not induce overt nigrostriatal cell loss in NM-vulnerable neurons, it seems that p α Syn accumulation enhanced NM production. This, in turn, may have triggered incipient cell loss, as indicated by increased extracellular NM debris.

2.4 Behavioural phenotypes

The behavioural outcomes in α Syn PFF rodent models remain inconsistent and are often contradictory. While some studies report no significant deficits in motor or anxiety-related behaviours following the injection of α Syn PFFs that induce p α Syn accumulation^{197,214,223}, other research has observed mild impairments in motor balance, coordination, grip strength and rotational behaviour^{124,278}. These discrepancies highlight the complexity of α Syn-related pathophysiology and its varied impact on behavioural phenotypes across different experimental approaches. On the other hand, in the tgNM model the bilateral NM accumulation in all catecholaminergic brain nuclei leads to subsequent deficiencies in the associated neurotransmission systems, which induce both motor and non-motor behavioural alterations over time¹⁰⁰. Animals in this model exhibit behavioural impairments characteristic of the prodromal PD, including olfactory deficits and heightened anxiety-related behaviours. Additionally, they display features typical of later PD stages such as impaired motor coordination and balance, deficits in learning and memory and increased depressive-like behaviours.

The unilateral intrastratial injection of α SYN PFFs in both wt and tgNM animals did not result in motor asymmetry or impairments in motor balance and coordination. This aligns with previous studies in which these fibrils were characterised and unilaterally inoculated into the SN of rats. PD-derived α SYN PFF injection in these animals failed to induce motor deficits as assessed by the cylinder test at time-points ranging from 1 w to 5 mpi¹⁹⁷. Similarly, the injection of 16 μ g of mouse PFF (more than 10 times the dose used in this thesis) into the rat STR did not elicit motor deficits for up to 6 mpi²¹⁸. These findings are consistent with the preserved integrity of the nigrostriatal system observed in both wt and tgNM in this study, further supporting the lack of motor deficits in the PFF model.

The observation that pathological α Syn accumulation initiates in the olfactory bulb and the DMNX has led to the hypothesis that PD pathology may originate in the peripheral nervous system synapses and spread to the brain^{10,11,52,279}. This could explain the early non-motor phase of PD, where patients experience anosmia and constipation before the onset of motor symptoms, which emerge when α Syn pathology reaches the SN. Supporting this idea, pathological α Syn has been detected in the peripheral nervous system of PD patients at up to 20 years before diagnosis^{279–282}. However, the “body-first” hypothesis remains controversial. Studies show that ~20-50% of PD patients do not follow the Braak staging scheme, and 7-17% do not exhibit α Syn pathology in the DMNX²⁷⁹. This has prompted the proposal of two distinct LB-disorder phenotypes that may co-exist^{279,283}. The “body-first” phenotype involves early, severe damage to the autonomic peripheral nervous system, with α Syn pathology spreading retrogradely to the medulla and brainstem. In contrast, the “brain-first” phenotype involves early, pronounced damage to the CNS structures, including the SN, with α Syn pathology spreading anterogradely from the CNS to the peripheral nervous system. The present thesis recreates a “brain-first” scenario.

In experimental models, p α Syn accumulation in the CNS has been shown to provoke progressive olfactory deficits and gastrointestinal dysfunction^{214,284}. In this study, animals did not exhibit olfactory impairments, which is consistent with the absence of pathological α Syn deposits in the olfactory bulb. Similarly, since p α Syn spreading did not reach the medulla, it is unlikely that α Syn deposits would propagate through the vagal nerve to the gut, which aligns with the observation that no constipation was evident in the α SYN PFF-injected animals.

The impact of α Syn PFFs on learning and memory behaviour remains controversial. While some studies report preserved learning and memory functions^{213,224}, others demonstrate significant memory deficits²⁸⁵. The amygdala, which is critical for emotional memory formation in aversive experiences²⁸⁶, displayed p α Syn accumulation on the ipsilateral side of both wt and tgNM animals, but the contralateral amygdala was unaffected even at the latter time-point. This may explain the absence of changes in aversive memory performance in these animals.

The nucleus accumbens, which is central to depression-related circuits via connections with the PFC²⁸⁷, also showed ipsilateral p α Syn accumulation in both wt and tgNM animals. However, the contralateral sides were minimally affected, suggesting that ipsilateral p α Syn pathology alone is insufficient to induce pronounced depression-like behaviour, consistent with the lack of significant behavioural alterations observed.

In summary, PD-derived α Syn PFFs injection induced p α Syn pathology and its spread across interconnected brain regions, with similar levels observed in both wt and tgNM animals (Figure 77). However, this accumulation of p α Syn was not associated with neurodegeneration or with the onset of either motor or non-motor behavioural deficits.

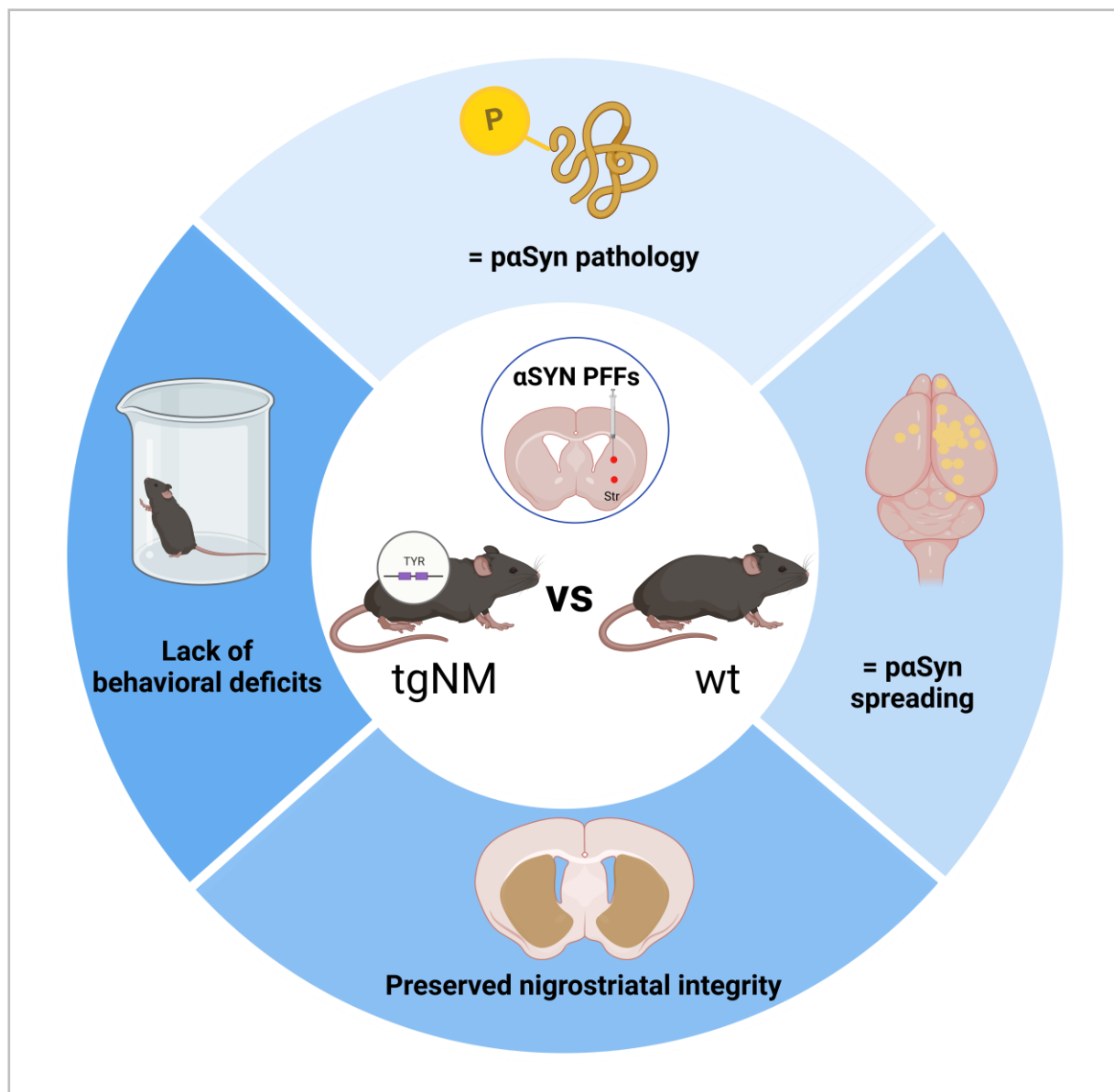


Figure 77. Histopathological features associated with α SYN-PFF-injected tgNM versus wt mice. NM accumulation in tgNM animals did not affect the α Syn pathology induced by PFF injection, as both tgNM and wt animals exhibited comparable levels of p α Syn pathology and spreading. Furthermore, PFF injection did not lead to nigrostriatal neurodegeneration, nor did it induce motor or non-motor behavioural changes in either group. Illustration created with Biorender.com.

3. Contributions of this thesis to PD research

This thesis offers a novel perspective on PD pathophysiology, emphasizing the complex interplay between α Syn and NM in driving disease onset and progression. Although much previous PD research has traditionally focused on α Syn as the primary pathogenic factor, the findings from this work suggest that α Syn acts more as a catalyst of disease processes rather than the principal trigger. Specifically, this study demonstrates that α Syn accumulation and aggregation enhance NM build-up, ultimately contributing to both the initiation and progression of PD. These insights deepen our understanding of PD mechanisms and open new avenues for further exploration and development of therapeutic strategies. From a translational viewpoint, the results presented in this work represent a meaningful step forward in:

- 1. Reconsidering α Syn-based PD models.** This thesis demonstrates that α Syn accumulation alone does not induce PD hallmark traits of cellular dysfunction or overt neurodegeneration. These findings challenge the reliability of α Syn-based models in fully capturing PD pathology and suggest the need for careful consideration when drawing conclusions about mechanisms or therapeutic strategies derived from such models.
- 2. Highlighting the need to incorporate NM in PD-related studies.** The absence of a PD-like phenotype in α SYN-overexpressing rodent models contrasts with the PD phenotype observed in humans carrying *SNCA* duplications or triplications. This divergence may be explained by NM accumulation, as demonstrated by the ability of NM build-up to drive a PD-like phenotype even in α Syn KO mice. These findings emphasise the importance of including NM in experimental models and clinical research to replicate the full complexity of PD.
- 3. Identifying factors driving NM accumulation above the pathogenic threshold.** *Post-mortem* studies of PD patients and pre-PD individuals reveal that intracellular NM levels reach a pathogenic threshold in disease states. The findings presented in this thesis identify α Syn as a driver of accelerated NM accumulation, shedding light on factors that influence NM dynamics and their implications for PD progression.
- 4. Reinforcing α Syn as a valuable biomarker.** Mechanistic studies presented here demonstrate that α Syn accumulation and aggregation accelerate NM production associated with PD. This suggests that α Syn toxicity precedes NM-related PD pathology, and thereby position α Syn as a promising susceptibility and/or diagnostic biomarker.
- 5. Defining α Syn's therapeutic window more precisely.** Despite α Syn's promise as a therapeutic target, α Syn-targeted interventions in early-stage PD have yielded limited success, which is likely a consequence of delayed intervention. By the time PD is clinically diagnosed, substantial neuronal loss has already occurred. This work suggests that the optimal therapeutic window may be during the preclinical

phase, when abnormal α Syn accumulation and aggregation are detectable but before NM levels surpass the pathogenic threshold.

6. **Supporting a potential link between skin and brain pigmentation.** While further research is needed, this thesis adds evidence to the long-standing hypothesis of a connection between pigmentation in the brain and skin. Our findings demonstrate α Syn's modulation of the TYR enzyme, which plays a key role in melanogenesis, suggesting a possible interaction that may hold relevance for both PD and skin pathogenesis.
7. **Raising new questions for PD research.** The findings presented here open new lines of research that could yield critical insights into PD pathogenesis. Key issues include:
 - *The role of TYR in NM synthesis.* Investigating the presence of NM in individuals with the TYR-lacking albinism subtype could clarify TYR's contribution to NM synthesis.
 - *Intracellular NM levels in SNCA-associated genetic PD cases.* Assessing NM levels in SNCA duplication/triplication carriers may further corroborate α Syn's role in accelerating NM production and its contribution to PD pathology.

CONCLUSIONS

CONCLUSIONS

1. Chapter I. Effects of α SYN overexpression on NM-associated PD pathology

1. α SYN overexpression significantly accelerates intracellular NM production.
2. Elevated α SYN levels in NM-producing animals increase α Syn oligomerization and PD-like neuropathological inclusions.
3. α SYN overexpression in NM-accumulating animals exacerbates nigrostriatal neurodegeneration and neuroinflammation.
4. Increased α SYN expression impairs DA vesicular uptake, vesicular docking and neurotransmission in animals synthesizing NM.
5. α SYN overexpression enhances *TYR* gene expression, leading to increased TYR enzymatic activity and protein levels.

2. Chapter II. Impact of NM-associated pathology on α Syn aggregation and propagation in PD

1. NM accumulation in catecholaminergic brain regions of tgNM animals does not exacerbate p α Syn accumulation or its spreading following injection of PD-derived α SYN PFFs.
2. p α Syn pathology induced by the injection of PD-derived α SYN PFFs does not lead to nigrostriatal degeneration *per se*, as observed in wt animals, nor when combined with the NM-mediated oxidative environment in tgNM animals.
3. Injection of PD-derived α SYN PFFs slightly increases NM accumulation.
4. Injection of PD-derived α SYN PFFs does not result in motor or non-motor behavioural changes.

REFERENCES

REFERENCES

1. Parkinson, J. An Essay on the Shaking Palsy. *Sherwood, Neely & Jones (London)* (1817) doi:10.1176/jnp.14.2.223.
2. Charcot, J.-M. De la paralysie agitante. *Oeuvres Complètes (t 1) Leçons sur les maladies du système nerveux* 155–188 (1872).
3. Goetz, C. G. The History of Parkinson's Disease: Early Clinical Descriptions and Neurological Therapies. *Cold Spring Harb Perspect Med* 1, a008862–a008862 (2011).
4. Obeso, J. A. *et al.* Past, present, and future of Parkinson's disease: A special essay on the 200th Anniversary of the Shaking Palsy. *Movement Disorders* 32, 1264–1310 (2017).
5. Blocq, P. O. & Marinesco, G. Sur un cas de tremblement parkinsonien hémiparétique symptomatique d'une tumeur du pédoncule cérébral. *Comptes Rendus Séances Société de Biologie* 5, 105–111 (1893).
6. Parent, M. & Parent, A. Substantia Nigra and Parkinson's Disease: A Brief History of Their Long and Intimate Relationship. *Canadian Journal of Neurological Sciences / Journal Canadien des Sciences Neurologiques* 37, 313–319 (2010).
7. Brissaud, E. Nature et pathogénie de la maladie de Parkinson. *Leçon sur les maladies nerveuses* 1, 188–501 (1895).
8. Lewy, F. J. H. Paralysis agitans. I. Pathologische Anatomie. *Handbuch der Neurologie* 3, 920–933 (1912).
9. Tetriakoff, K. N. Contribution à l'étude de l'anatomie pathologique du locus niger de Soemmering avec quelques déductions relatives à la pathogénie des troubles du tonus musculaire et de la maladie de Parkinson. (University of Paris, 1919).
10. Goedert, M., Spillantini, M. G., Del Tredici, K. & Braak, H. 100 years of Lewy pathology. *Nat Rev Neurol* 9, 13–24 (2013).
11. Kalia, L. V & Lang, A. E. Parkinson's disease. *The Lancet* 386, 896–912 (2015).
12. Carlsson, A. Thirty years of dopamine research. *Adv Neurol* 60, 1–10 (1993).
13. Ehringer, H. & Hornykiewicz, O. Verteilung Von Noradrenalin Und Dopamin (3-Hydroxytyramin) Im Gehirn Des Menschen Und Ihr Verhalten Bei Erkrankungen Des Extrapyramidalen Systems. *Klin Wochenschr* 38, 1236–1239 (1960).
14. Cotzias, G. C., Van Woert, M. H. & Schiffer, L. M. Aromatic Amino Acids and Modification of Parkinsonism. *New England Journal of Medicine* 276, 374–379 (1967).
15. Polymeropoulos, M. H. *et al.* Mutation in the α -Synuclein Gene Identified in Families with Parkinson's Disease. *Science* (1979) 276, 2045–2047 (1997).
16. Spillantini, M. G. *et al.* α -Synuclein in Lewy bodies. *Nature* 388, 839–840 (1997).
17. Lees, A., Eyre, P. & Brown, P. The true face of James Parkinson. *Lancet Neurol* 17, 507 (2018).
18. Hypnosis Motivation Institute. Hypnosis in History. 1882 – Charcot's Salpêtrière School. <https://hypnosis.edu/history/charcots-salpetriere-school>.
19. Fénelon, G. & Walusinski, O. The landmark contributions of Paul Blocq, Georges Marinesco, and Édouard Brissaud in Parkinson's disease. *Rev Neurol (Paris)* 177, 1214–1220 (2021).

20. Lucien Waléry. Bibliothèque Interuniversitaire de Médecine. <http://www.bium.univ-paris5.fr/images/banque/zoom/CIPB0163.jpg>.
21. DGVS. Biography of Friedrich Heinrich Lewy. <https://www.dgvs-gegen-das-vergessen.de/en/biografie/friedrich-fritz-heinrich-lewy/>.
22. Lees, A. J., Selikhova, M., Andrade, L. A. & Duyckaerts, C. The black stuff and Konstantin Nikolaevich Tretiakoff. *Movement Disorders* 23, 777–783 (2008).
23. University of Cambridge. Spillantini Lab. <https://spillantinilab.medschl.cam.ac.uk/professorial-profile>.
24. Google Scholar. Mihael H. Polymeropoulos. <https://scholar.google.com/citations?user=sNmOs24AAAAJ&hl=en>.
25. Parkinson Canada. Dr. Arvid Carlsson—in memoriam (1923-2018). <https://www.parkinson.ca/dr-arvid-carlsson-in-memorial-1923-2018/>.
26. Wolf Foundation. Oleh Hornykiewicz. <https://wolffund.org.il/oleh-hornykiewicz/>.
27. Lasker Foundation. L-Dopa for treating Parkinson's disease. <https://laskerfoundation.org/winners/l-dopa-for-treating-parkinsons-disease/>.
28. Bernheimer, H., Birkmayer, W., Hornykiewicz, O., Jellinger, K. & Seitelberger, F. Brain dopamine and the syndromes of Parkinson and Huntington Clinical, morphological and neurochemical correlations. *J Neurol Sci* 20, 415–455 (1973).
29. Hornykiewicz, O. Biochemical aspects of Parkinson's disease. *Neurology* 51, (1998).
30. Dauer, W. & Przedborski, S. Parkinson's Disease. *Neuron* 39, 889–909 (2003).
31. Jankovic, J. Parkinson's disease: clinical features and diagnosis. *J Neurol Neurosurg Psychiatry* 79, 368–376 (2008).
32. Gibb, W. R. G., Scott, T. & Lees, A. J. Neuronal inclusions of Parkinson's disease. *Movement Disorders* 6, 2–11 (1991).
33. Pollanen, M. S., Dickson, D. W. & Bergeron, C. Pathology and Biology of the Lewy Body. *J Neuropathol Exp Neurol* 52, 183–191 (1993).
34. Volpicelli-Daley, L. A. *et al.* Formation of α -synuclein Lewy neurite-like aggregates in axons impedes the transport of distinct endosomes. *Mol Biol Cell* 25, 4010–4023 (2014).
35. Ingelsson, M. Alpha-Synuclein Oligomers—Neurotoxic Molecules in Parkinson's Disease and Other Lewy Body Disorders. *Front Neurosci* 10, (2016).
36. Spillantini, M. G., Crowther, R. A., Jakes, R., Hasegawa, M. & Goedert, M. α -Synuclein in filamentous inclusions of Lewy bodies from Parkinson's disease and dementia with Lewy bodies. *Proceedings of the National Academy of Sciences* 95, 6469–6473 (1998).
37. Serpell, L. C., Berriman, J., Jakes, R., Goedert, M. & Crowther, R. A. Fiber diffraction of synthetic α -synuclein filaments shows amyloid-like cross- β conformation. *Proceedings of the National Academy of Sciences* 97, 4897–4902 (2000).
38. Neupane, S., De Cecco, E. & Aguzzi, A. The Hidden Cell-to-Cell Trail of α -Synuclein Aggregates. *J Mol Biol* 435, 167930 (2023).
39. Shahmoradian, S. H. *et al.* Lewy pathology in Parkinson's disease consists of crowded organelles and lipid membranes. *Nat Neurosci* 22, 1099–1109 (2019).
40. Bartels, T. A traffic jam leads to Lewy bodies. *Nat Neurosci* 22, 1043–1045 (2019).

41. Kuusisto, E., Parkkinen, L. & Alafuzoff, I. Morphogenesis of Lewy Bodies: Dissimilar Incorporation of α -Synuclein, Ubiquitin, and p62. *J Neuropathol Exp Neurol* 62, 1241–1253 (2003).
42. Limanaqi, F. *et al.* Promiscuous Roles of Autophagy and Proteasome in Neurodegenerative Proteinopathies. *Int J Mol Sci* 21, 3028 (2020).
43. Woulfe, J. Nuclear bodies in neurodegenerative disease. *Biochimica et Biophysica Acta (BBA) - Molecular Cell Research* 1783, 2195–2206 (2008).
44. Abbott, R. D. *et al.* Marinesco bodies and substantia nigra neuron density in Parkinson's disease. *Neuropathol Appl Neurobiol* 43, 621–630 (2017).
45. Zecca, L. *et al.* Neuromelanin can protect against iron-mediated oxidative damage in system modeling iron overload of brain aging and Parkinson's disease. *J Neurochem* 106, 1866–1875 (2008).
46. Zucca, F. A. *et al.* Interactions of iron, dopamine and neuromelanin pathways in brain aging and Parkinson's disease. *Prog Neurobiol* 155, 96–119 (2017).
47. Tansey, M. G. *et al.* Inflammation and immune dysfunction in Parkinson disease. *Nat Rev Immunol* 22, 657–673 (2022).
48. Trist, B. G., Hare, D. J. & Double, K. L. Oxidative stress in the aging substantia nigra and the etiology of Parkinson's disease. *Aging Cell* 18, (2019).
49. Balestrino, R. & Schapira, A. H. V. Parkinson disease. *Eur J Neurol* 27, 27–42 (2020).
50. Deliz, J. R., Tanner, C. M. & Gonzalez-Latapi, P. Epidemiology of Parkinson's Disease: An Update. *Curr Neurol Neurosci Rep* 24, 163–179 (2024).
51. World Health Organization. Parkinson disease. <https://www.who.int/news-room/fact-sheets/detail/parkinson-disease> (2023).
52. Poewe, W. *et al.* Parkinson disease. *Nat Rev Dis Primers* 3, 17013 (2017).
53. Kouli, A., Torsney, K. M. & Kuan, W.-L. Parkinson's Disease: Etiology, Neuropathology, and Pathogenesis. in *Parkinson's Disease: Pathogenesis and Clinical Aspects* 3–26 (Codon Publications, 2018). doi:10.15586/codonpublications.parkinsonsdisease.2018.ch1.
54. Day, J. O. & Mullin, S. The Genetics of Parkinson's Disease and Implications for Clinical Practice. *Genes (Basel)* 12, 1006 (2021).
55. Perinán, M. T. *et al.* Effect Modification between Genes and Environment and Parkinson's Disease Risk. *Ann Neurol* 92, 715–724 (2022).
56. Yamashita, K. Y., Bhoopatiraju, S., Silvergate, B. D. & Grossberg, G. T. Biomarkers in Parkinson's disease: A state of the art review. *Biomark Neuropsychiatry* 9, 100074 (2023).
57. Pilotto, A. *et al.* Biofluid Markers and Tissue Biopsies Analyses for the Prodromal and Earliest Phase of Parkinson's Disease. *J Parkinsons Dis* 14, S333–S344 (2024).
58. Yoo, D. *et al.* Diagnostic value of α -synuclein seeding amplification assays in α -synucleinopathies: A systematic review and meta-analysis. *Parkinsonism Relat Disord* 104, 99–109 (2022).
59. Fernandes Gomes, B. *et al.* α -Synuclein seed amplification assay as a diagnostic tool for parkinsonian disorders. *Parkinsonism Relat Disord* 117, 105807 (2023).
60. Siderowf, A. *et al.* Assessment of heterogeneity among participants in the Parkinson's Progression Markers Initiative cohort using α -synuclein seed amplification: a cross-sectional study. *Lancet Neurol* 22, 407–417 (2023).

61. Wang, Z. *et al.* Skin α -Synuclein Aggregation Seeding Activity as a Novel Biomarker for Parkinson Disease. *JAMA Neurol* 78, 30 (2021).
62. Groveman, B. R. *et al.* Rapid and ultra-sensitive quantitation of disease-associated α -synuclein seeds in brain and cerebrospinal fluid by α Syn RT-QuIC. *Acta Neuropathol Commun* 6, 7 (2018).
63. Okuzumi, A. *et al.* Propagative α -synuclein seeds as serum biomarkers for synucleinopathies. *Nat Med* 29, 1448–1455 (2023).
64. Okuzumi, A. *et al.* α -Synuclein Seeding Assay Using RT-QuIC. in 3–16 (2021). doi:10.1007/978-1-0716-1495-2_1.
65. Nagatsu, T. *et al.* The role of tyrosine hydroxylase as a key player in neuromelanin synthesis and the association of neuromelanin with Parkinson's disease. *J Neural Transm* 130, 611–625 (2023).
66. Verbeek, M. M. & Bloem, B. R. An emerging biomarker for dopaminergic cell loss. *Nat Aging* 3, 1180–1182 (2023).
67. Tan, Y.-Y., Jenner, P. & Chen, S.-D. Monoamine Oxidase-B Inhibitors for the Treatment of Parkinson's Disease: Past, Present, and Future. *J Parkinsons Dis* 12, 477–493 (2022).
68. Kin, K., Yasuhara, T., Kameda, M. & Date, I. Animal Models for Parkinson's Disease Research: Trends in the 2000s. *Int J Mol Sci* 20, 5402 (2019).
69. Dovonou, A. *et al.* Animal models of Parkinson's disease: bridging the gap between disease hallmarks and research questions. *Transl Neurodegener* 12, 36 (2023).
70. He, S., Ru, Q., Chen, L., Xu, G. & Wu, Y. Advances in animal models of Parkinson's disease. *Brain Res Bull* 215, 111024 (2024).
71. Vila, M. *et al.* α -Synuclein Up-Regulation in Substantia Nigra Dopaminergic Neurons Following Administration of the Parkinsonian Toxin MPTP. *J Neurochem* 74, 721–729 (2000).
72. Bové, J., Prou, D., Perier, C. & Przedborski, S. Toxin-induced models of Parkinson's disease. *NeuroRX* 2, 484–494 (2005).
73. Chia, S. J., Tan, E.-K. & Chao, Y.-X. Historical Perspective: Models of Parkinson's Disease. *Int J Mol Sci* 21, 2464 (2020).
74. FEDOROW, H. *et al.* Neuromelanin in human dopamine neurons: Comparison with peripheral melanins and relevance to Parkinson's disease. *Prog Neurobiol* 75, 109–124 (2005).
75. Vila, M. Neuromelanin, aging, and neuronal vulnerability in Parkinson's disease. *Movement Disorders* 34, 1440–1451 (2019).
76. Dimitri Agamanolis. Chapter 9 DEGENERATIVE DISEASES. <https://neuropathology-web.org/chapter9/chapter9dPD.html> (2023).
77. Sulzer, D. & Surmeier, D. J. Neuronal vulnerability, pathogenesis, and Parkinson's disease. *Movement Disorders* 28, 715–724 (2013).
78. Halliday, G. M., Leverenz, J. B., Schneider, J. S. & Adler, C. H. The neurobiological basis of cognitive impairment in Parkinson's disease. *Movement Disorders* 29, 634–650 (2014).
79. Bogerts, B. A brainstem atlas of catecholaminergic neurons in man, using melanin as a natural marker. *Journal of Comparative Neurology* 197, 63–80 (1981).
80. Zhang, X. T. *et al.* Molecular cloning and expression analysis of *tyr* and *tyrp1* genes in normal and albino yellow catfish *Tachysurus fulvidraco*. *J Fish Biol* 92, 979–998 (2018).

81. Ito, S. & Wakamatsu, K. Chemistry of Mixed Melanogenesis—Pivotal Roles of Dopaquinone †. *Photochem Photobiol* 84, 582–592 (2008).
82. Sulzer, D. *et al.* Neuromelanin detection by magnetic resonance imaging (MRI) and its promise as a biomarker for Parkinson's disease. *NPJ Parkinsons Dis* 4, 11 (2018).
83. Sulzer, D. *et al.* Neuromelanin biosynthesis is driven by excess cytosolic catecholamines not accumulated by synaptic vesicles. *Proceedings of the National Academy of Sciences* 97, 11869–11874 (2000).
84. Zucca, F. A. *et al.* Neuromelanin of the Human Substantia Nigra: An Update. *Neurotox Res* 25, 13–23 (2014).
85. Halliday, G. M. *et al.* Evidence for specific phases in the development of human neuromelanin. *J Neural Transm* 113, 721–728 (2006).
86. Zecca, L. *et al.* The absolute concentration of nigral neuromelanin, assayed by a new sensitive method, increases throughout the life and is dramatically decreased in Parkinson's disease. *FEBS Lett* 510, 216–220 (2002).
87. DUFFY, P. E. & TENNYSON, V. M. PHASE AND ELECTRON MICROSCOPIC OBSERVATIONS OF LEWY BODIES AND MELANIN GRANULES IN THE SUBSTANTIA NIGRA AND LOCUS CAERULEUS IN PARKINSON'S DISEASE. *J Neuropathol Exp Neurol* 24, 398–414 (1965).
88. Braak, E. *et al.* α -Synuclein immunopositive Parkinson's disease-related inclusion bodies in lower brain stem nuclei. *Acta Neuropathol* 101, 195–201 (2001).
89. Moreno-García, A., Kun, A., Calero, M. & Calero, O. The Neuromelanin Paradox and Its Dual Role in Oxidative Stress and Neurodegeneration. *Antioxidants* 10, 124 (2021).
90. Giguère, N., Burke Nanni, S. & Trudeau, L.-E. On Cell Loss and Selective Vulnerability of Neuronal Populations in Parkinson's Disease. *Front Neurol* 9, (2018).
91. Mann, D. M. A. & Yates, P. O. The effects of ageing on the pigmented nerve cells of the human locus caeruleus and substantia nigra. *Acta Neuropathol* 47, 93–97 (1979).
92. Chu, Y. & Kordower, J. H. Age-associated increases of α -synuclein in monkeys and humans are associated with nigrostriatal dopamine depletion: Is this the target for Parkinson's disease? *Neurobiol Dis* 25, 134–149 (2007).
93. Beach, T. G. *et al.* Marked microglial reaction in normal aging human substantia nigra: correlation with extraneuronal neuromelanin pigment deposits. *Acta Neuropathol* 114, 419–424 (2007).
94. Kordower, J. H. *et al.* Disease duration and the integrity of the nigrostriatal system in Parkinson's disease. *Brain* 136, 2419–2431 (2013).
95. Masato, A., Plotegher, N., Boassa, D. & Bubacco, L. Impaired dopamine metabolism in Parkinson's disease pathogenesis. *Mol Neurodegener* 14, 35 (2019).
96. Panneton, W. M., Kumar, V. B., Gan, Q., Burke, W. J. & Galvin, J. E. The Neurotoxicity of DOPAL: Behavioral and Stereological Evidence for Its Role in Parkinson Disease Pathogenesis. *PLoS One* 5, e15251 (2010).
97. Goldstein, D. S. *et al.* Catechols in post-mortem brain of patients with Parkinson disease. *Eur J Neurol* 18, 703–710 (2011).
98. Barden, H. & Levine, S. Histochemical observations on rodent brain melanin. *Brain Res Bull* 10, 847–851 (1983).
99. Carballo-Carbajal, I. *et al.* Brain tyrosinase overexpression implicates age-dependent neuromelanin production in Parkinson's disease pathogenesis. *Nat Commun* 10, 973 (2019).

100. Laguna, A. *et al.* Modelling human neuronal catecholaminergic pigmentation in rodents recapitulates age-related neurodegenerative deficits. *Nat Commun* 15, 8819 (2024).
101. Gonzalez-Sepulveda, M. *et al.* *In vivo* reduction of age-dependent neuromelanin accumulation mitigates features of Parkinson's disease. *Brain* 146, 1040–1052 (2023).
102. Maroteaux, L., Campanelli, J. & Scheller, R. Synuclein: a neuron-specific protein localized to the nucleus and presynaptic nerve terminal. *The Journal of Neuroscience* 8, 2804–2815 (1988).
103. Burré, J., Sharma, M. & Südhof, T. C. Cell Biology and Pathophysiology of α -Synuclein. *Cold Spring Harb Perspect Med* 8, a024091 (2018).
104. Lashuel, H. A., Overk, C. R., Oueslati, A. & Masliah, E. The many faces of α -synuclein: from structure and toxicity to therapeutic target. *Nat Rev Neurosci* 14, 38–48 (2013).
105. Holec, S. A. M., Liu, S. L. & Woerman, A. L. Consequences of variability in α -synuclein fibril structure on strain biology. *Acta Neuropathol* 143, 311–330 (2022).
106. Lavedan, C. The Synuclein Family. *Genome Res* 8, 871–880 (1998).
107. Human Protein Atlas [proteinatlas.org](https://www.proteinatlas.org/ENSG00000145335-SNCA/tissue). Synuclein alpha protein expression overview. <https://www.proteinatlas.org/ENSG00000145335-SNCA/tissue>.
108. Bernal-Conde, L. D. *et al.* Alpha-Synuclein Physiology and Pathology: A Perspective on Cellular Structures and Organelles. *Front Neurosci* 13, (2020).
109. Bell, R. & Vendruscolo, M. Modulation of the Interactions Between α -Synuclein and Lipid Membranes by Post-translational Modifications. *Front Neurol* 12, (2021).
110. Gao, V., Briano, J. A., Komer, L. E. & Burré, J. Functional and Pathological Effects of α -Synuclein on Synaptic SNARE Complexes. *J Mol Biol* 435, 167714 (2023).
111. Perez, R. G. *et al.* A Role for α -Synuclein in the Regulation of Dopamine Biosynthesis. *The Journal of Neuroscience* 22, 3090–3099 (2002).
112. Wu, B. *et al.* Phosphorylation of α -synuclein upregulates tyrosine hydroxylase activity in MN9D cells. *Acta Histochem* 113, 32–35 (2011).
113. Somayaji, M., Lanseur, Z., Choi, S. J., Sulzer, D. & Mosharov, E. V. Roles for α -Synuclein in Gene Expression. *Genes (Basel)* 12, 1166 (2021).
114. Surguchov, A. α -Synuclein and Mechanisms of Epigenetic Regulation. *Brain Sci* 13, 150 (2023).
115. Sharma, M. & Burré, J. α -Synuclein in synaptic function and dysfunction. *Trends Neurosci* 46, 153–166 (2023).
116. Nemani, V. M. *et al.* Increased Expression of α -Synuclein Reduces Neurotransmitter Release by Inhibiting Synaptic Vesicle Reclustering after Endocytosis. *Neuron* 65, 66–79 (2010).
117. Fouke, K. E. *et al.* Synuclein Regulates Synaptic Vesicle Clustering and Docking at a Vertebrate Synapse. *Front Cell Dev Biol* 9, (2021).
118. Stöckl, M. T., Zijlstra, N. & Subramaniam, V. α -Synuclein Oligomers: an Amyloid Pore? *Mol Neurobiol* 47, 613–621 (2013).
119. Desplats, P. *et al.* α -Synuclein Sequesters Dnmt1 from the Nucleus. *Journal of Biological Chemistry* 286, 9031–9037 (2011).
120. Yoon, Y.-S. *et al.* Senescence and impaired DNA damage responses in alpha-synucleinopathy models. *Exp Mol Med* 54, 115–128 (2022).

121. Parra-Rivas, L. A. *et al.* Serine-129 phosphorylation of α -synuclein is an activity-dependent trigger for physiologic protein-protein interactions and synaptic function. *Neuron* 111, 4006-4023.e10 (2023).
122. Mor, D. E. Keeping neuronal activity in check: a novel role for α -synuclein serine-129 phosphorylation in the healthy brain. *Trends Biochem Sci* 49, 382–383 (2024).
123. Volpicelli-Daley, L. A. *et al.* Exogenous α -Synuclein Fibrils Induce Lewy Body Pathology Leading to Synaptic Dysfunction and Neuron Death. *Neuron* 72, 57–71 (2011).
124. Luk, K. C. *et al.* Intracerebral inoculation of pathological α -synuclein initiates a rapidly progressive neurodegenerative α -synucleinopathy in mice. *Journal of Experimental Medicine* 209, 975–986 (2012).
125. Ma, M.-R., Hu, Z.-W., Zhao, Y.-F., Chen, Y.-X. & Li, Y.-M. Phosphorylation induces distinct alpha-synuclein strain formation. *Sci Rep* 6, 37130 (2016).
126. Kawahata, I., Finkelstein, D. I. & Fukunaga, K. Pathogenic Impact of α -Synuclein Phosphorylation and Its Kinases in α -Synucleinopathies. *Int J Mol Sci* 23, 6216 (2022).
127. Yamada, M., Mizuno, Y. & Mochizuki, H. Parkin Gene Therapy for α -Synucleinopathy: A Rat Model of Parkinson's Disease. *Hum Gene Ther* 16, 262–270 (2005).
128. Zhang, J., Li, X. & Li, J.-D. The Roles of Post-translational Modifications on α -Synuclein in the Pathogenesis of Parkinson's Diseases. *Front Neurosci* 13, (2019).
129. Sagredo, G. T., Tanglay, O., Shahdadpuri, S., Fu, Y. & Halliday, G. M. α -Synuclein levels in Parkinson's disease – Cell types and forms that contribute to pathogenesis. *Exp Neurol* 379, 114887 (2024).
130. Kim, C. & Lee, S. Controlling the mass action of α -synuclein in Parkinson's disease. *J Neurochem* 107, 303–316 (2008).
131. Calabresi, P. *et al.* Alpha-synuclein in Parkinson's disease and other synucleinopathies: from overt neurodegeneration back to early synaptic dysfunction. *Cell Death Dis* 14, 176 (2023).
132. Solano, S. M., Miller, D. W., Augood, S. J., Young, A. B. & Penney, J. B. Expression of α -synuclein, parkin, and ubiquitin carboxy-terminal hydrolase L1 mRNA in human brain: Genes associated with familial Parkinson's disease. *Ann Neurol* 47, 201–210 (2000).
133. Chiba-Falek, O., Lopez, G. J. & Nussbaum, R. L. Levels of alpha-synuclein mRNA in sporadic Parkinson disease patients. *Movement Disorders* 21, 1703–1708 (2006).
134. Kingsbury, A. E. *et al.* Alteration in α -synuclein mRNA expression in Parkinson's disease. *Movement Disorders* 19, 162–170 (2004).
135. Miwa, H., Hiwatani, Y. & Kondo, T. Drug discarding: A problematic therapeutic event in Parkinson's disease. *Movement Disorders* 22, 293–293 (2007).
136. de Boni, L. *et al.* Brain region-specific susceptibility of Lewy body pathology in synucleinopathies is governed by α -synuclein conformations. *Acta Neuropathol* 143, 453–469 (2022).
137. Swirski, M. *et al.* Evaluating the relationship between amyloid- β and α -synuclein phosphorylated at Ser129 in dementia with Lewy bodies and Parkinson's disease. *Alzheimers Res Ther* 6, 77 (2014).
138. Roberts, R. F., Wade-Martins, R. & Alegre-Abarrategui, J. Direct visualization of alpha-synuclein oligomers reveals previously undetected pathology in Parkinson's disease brain. *Brain* 138, 1642–1657 (2015).
139. Bargar, C. *et al.* Streamlined alpha-synuclein RT-QuIC assay for various biospecimens in Parkinson's disease and dementia with Lewy bodies. *Acta Neuropathol Commun* 9, 62 (2021).

140. Du, T. *et al.* Biomarkers and the Role of α -Synuclein in Parkinson's Disease. *Front Aging Neurosci* 13, (2021).
141. Kapsali, I., Brinia, M.-E. & Constantinides, V. C. Cerebrospinal Fluid Total, Phosphorylated and Oligomeric A-Synuclein in Parkinson's Disease: A Systematic Review, Meta-Analysis and Meta-Regression Study. *Biomedicines* 12, 2266 (2024).
142. Shahnawaz, M. *et al.* Discriminating α -synuclein strains in Parkinson's disease and multiple system atrophy. *Nature* 578, 273–277 (2020).
143. Wang, N., Gibbons, C. H., Lafo, J. & Freeman, R. α -Synuclein in cutaneous autonomic nerves. *Neurology* 81, 1604–1610 (2013).
144. Gibbons, C. H., Garcia, J., Wang, N., Shih, L. C. & Freeman, R. The diagnostic discrimination of cutaneous α -synuclein deposition in Parkinson disease. *Neurology* 87, 505–512 (2016).
145. Gibbons, C. H. *et al.* Skin Biopsy Detection of Phosphorylated α -Synuclein in Patients With Synucleinopathies. *JAMA* 331, 1298 (2024).
146. Mazzetti, S. *et al.* α -Synuclein oligomers in skin biopsy of idiopathic and monozygotic twin patients with Parkinson's disease. *Brain* 143, 920–931 (2020).
147. Wang, Z. *et al.* Skin α -Synuclein Aggregation Seeding Activity as a Novel Biomarker for Parkinson Disease. *JAMA Neurol* 78, 30 (2021).
148. Braak, H. *et al.* Staging of brain pathology related to sporadic Parkinson's disease. *Neurobiol Aging* 24, 197–211 (2003).
149. Braak, H., Rüb, U., Gai, W. P. & Del Tredici, K. Idiopathic Parkinson's disease: possible routes by which vulnerable neuronal types may be subject to neuroinvasion by an unknown pathogen. *J Neural Transm* 110, 517–536 (2003).
150. Heras-Garvin, A. & Stefanova, N. From Synaptic Protein to Prion: The Long and Controversial Journey of α -Synuclein. *Front Synaptic Neurosci* 12, (2020).
151. Kordower, J. H., Chu, Y., Hauser, R. A., Freeman, T. B. & Olanow, C. W. Lewy body-like pathology in long-term embryonic nigral transplants in Parkinson's disease. *Nat Med* 14, 504–506 (2008).
152. Li, J.-Y. *et al.* Lewy bodies in grafted neurons in subjects with Parkinson's disease suggest host-to-graft disease propagation. *Nat Med* 14, 501–503 (2008).
153. Choi, Y. R., Park, S. J. & Park, S. M. Molecular events underlying the cell-to-cell transmission of α -synuclein. *FEBS J* 288, 6593–6602 (2021).
154. Brás, I. C. & Outeiro, T. F. Alpha-synuclein spreading mechanisms in Parkinson's disease: The role of membrane receptors. in 1–63 (2021). doi:10.1016/bs.irmvd.2021.08.002.
155. Just, M. K. *et al.* Alpha-Synuclein Strain Variability in Body-First and Brain-First Synucleinopathies. *Front Aging Neurosci* 14, (2022).
156. Bousset, L. *et al.* Structural and functional characterization of two alpha-synuclein strains. *Nat Commun* 4, 2575 (2013).
157. Wojewska, M. J., Otero-Jimenez, M., Guijarro-Nuez, J. & Alegre-Abarrategui, J. Beyond Strains: Molecular Diversity in Alpha-Synuclein at the Center of Disease Heterogeneity. *Int J Mol Sci* 24, 13199 (2023).
158. Malfertheiner, K., Stefanova, N. & Heras-Garvin, A. The Concept of α -Synuclein Strains and How Different Conformations May Explain Distinct Neurodegenerative Disorders. *Front Neurol* 12, (2021).

159. Rodger, A. T., ALNasser, M. & Carter, W. G. Are Therapies That Target α -Synuclein Effective at Halting Parkinson's Disease Progression? A Systematic Review. *Int J Mol Sci* 24, 11022 (2023).
160. Lang, A. E. *et al.* Trial of Cinpanemab in Early Parkinson's Disease. *New England Journal of Medicine* 387, 408–420 (2022).
161. Pagano, G. *et al.* Trial of Prasinezumab in Early-Stage Parkinson's Disease. *New England Journal of Medicine* 387, 421–432 (2022).
162. Jensen, P. H., Schlossmacher, M. G. & Stefanis, L. Who Ever Said It Would Be Easy? Reflecting on Two Clinical Trials Targeting α -Synuclein. *Movement Disorders* 38, 378–384 (2023).
163. Alarcón-Arís, D. *et al.* Anti- α -synuclein ASO delivered to monoamine neurons prevents α -synuclein accumulation in a Parkinson's disease-like mouse model and in monkeys. *EBioMedicine* 59, 102944 (2020).
164. Björklund, A. & Mattsson, B. The AAV- α -Synuclein Model of Parkinson's Disease: An Update. *J Parkinsons Dis* 14, 1077–1094 (2024).
165. Recasens, A., Ulusoy, A., Kahle, P. J., Di Monte, D. A. & Dehay, B. In vivo models of alpha-synuclein transmission and propagation. *Cell Tissue Res* 373, 183–193 (2018).
166. Gómez-Benito, M. *et al.* Modeling Parkinson's Disease With the Alpha-Synuclein Protein. *Front Pharmacol* 11, (2020).
167. Lu, J., Sun, F., Ma, H., Qing, H. & Deng, Y. Comparison between α -synuclein wild-type and A53T mutation in a progressive Parkinson's disease model. *Biochem Biophys Res Commun* 464, 988–993 (2015).
168. Koprach, J. B., Johnston, T. H., Reyes, M. G., Sun, X. & Brotchie, J. M. Expression of human A53T alpha-synuclein in the rat substantia nigra using a novel AAV1/2 vector produces a rapidly evolving pathology with protein aggregation, dystrophic neurite architecture and nigrostriatal degeneration with potential to model the pathology of Parkinson's disease. *Mol Neurodegener* 5, 43 (2010).
169. Phan, J.-A. *et al.* Early synaptic dysfunction induced by α -synuclein in a rat model of Parkinson's disease. *Sci Rep* 7, 6363 (2017).
170. Ulusoy, A. *et al.* Caudo-rostral brain spreading of α -synuclein through vagal connections. *EMBO Mol Med* 5, 1119–1127 (2013).
171. Pinto-Costa, R., Harbachova, E., La Vitola, P. & Di Monte, D. A. Overexpression-Induced α -Synuclein Brain Spreading. *Neurotherapeutics* 20, 83–96 (2023).
172. Visanji, N. P. *et al.* α -Synuclein-Based Animal Models of Parkinson's Disease: Challenges and Opportunities in a New Era. *Trends Neurosci* 39, 750–762 (2016).
173. Chung, H. K., Ho, H.-A., Pérez-Acuña, D. & Lee, S.-J. Modeling α -Synuclein Propagation with Preformed Fibril Injections. *J Mov Disord* 12, 139–151 (2019).
174. Recasens, A. *et al.* Lewy body extracts from Parkinson disease brains trigger α -synuclein pathology and neurodegeneration in mice and monkeys. *Ann Neurol* 75, 351–362 (2014).
175. Halliday, G. M. *et al.* α -Synuclein redistributes to neuromelanin lipid in the substantia nigra early in Parkinson's disease. *Brain* 128, 2654–2664 (2005).
176. Fasano, M., Giraudo, S., Coha, S., Bergamasco, B. & Lopiano, L. Residual substantia nigra neuromelanin in Parkinson's disease is cross-linked to α -synuclein. *Neurochem Int* 42, 603–606 (2003).

177. Chocarro, J. *et al.* Neuromelanin accumulation drives endogenous synucleinopathy in non-human primates. *Brain* 146, 5000–5014 (2023).
178. Blesa, J., Trigo-Damas, I., Quiroga-Varela, A. & Jackson-Lewis, V. R. Oxidative stress and Parkinson's disease. *Front Neuroanat* 9, (2015).
179. Spencer, J. P. E. *et al.* Conjugates of Catecholamines with Cysteine and GSH in Parkinson's Disease: Possible Mechanisms of Formation Involving Reactive Oxygen Species. *J Neurochem* 71, 2112–2122 (1998).
180. Chakrabarti, S. & Bisaglia, M. Oxidative Stress and Neuroinflammation in Parkinson's Disease: The Role of Dopamine Oxidation Products. *Antioxidants* 12, 955 (2023).
181. Musgrove, R. E. *et al.* Oxidative stress in vagal neurons promotes parkinsonian pathology and intercellular α -synuclein transfer. *Journal of Clinical Investigation* 129, 3738–3753 (2019).
182. Han, D., Zheng, W., Wang, X. & Chen, Z. Proteostasis of α -Synuclein and Its Role in the Pathogenesis of Parkinson's Disease. *Front Cell Neurosci* 14, (2020).
183. Pivtoraiko, V. N., Stone, S. L., Roth, K. A. & Shacka, J. J. Oxidative Stress and Autophagy in the Regulation of Lysosome-Dependent Neuron Death. *Antioxid Redox Signal* 11, 481–496 (2009).
184. Gründemann, J., Schlaudraff, F., Haeckel, O. & Liss, B. Elevated α -synuclein mRNA levels in individual UV-laser-microdissected dopaminergic substantia nigra neurons in idiopathic Parkinson's disease. *Nucleic Acids Res* 36, e38 (2008).
185. Sánchez-Danés, A. *et al.* Disease-specific phenotypes in dopamine neurons from human iPS-based models of genetic and sporadic Parkinson's disease. *EMBO Mol Med* 4, 380–395 (2012).
186. Ibáñez, P. *et al.* Causal relation between α -synuclein locus duplication as a cause of familial Parkinson's disease. *The Lancet* 364, 1169–1171 (2004).
187. Chartier-Harlin, M.-C. *et al.* α -synuclein locus duplication as a cause of familial Parkinson's disease. *The Lancet* 364, 1167–1169 (2004).
188. Singleton, A. B. *et al.* α -Synuclein Locus Triplication Causes Parkinson's Disease. *Science* (1979) 302, 841–841 (2003).
189. Manne, S. *et al.* Blinded <sc>RT-QuIC</sc> Analysis of <sc> α -Synuclein</sc> Biomarker in Skin Tissue From Parkinson's Disease Patients. *Movement Disorders* 35, 2230–2239 (2020).
190. Rodriguez-Leyva, I. *et al.* The Presence of Alpha-Synuclein in Skin from Melanoma and Patients with Parkinson's Disease. *Mov Disord Clin Pract* 4, 724–732 (2017).
191. Ye, Q., Wen, Y., Al-Kuwari, N. & Chen, X. Association Between Parkinson's Disease and Melanoma: Putting the Pieces Together. *Front Aging Neurosci* 12, (2020).
192. Pan, T., Zhu, J., Hwu, W.-J. & Jankovic, J. The Role of Alpha-Synuclein in Melanin Synthesis in Melanoma and Dopaminergic Neuronal Cells. *PLoS One* 7, e45183 (2012).
193. Mosharov, E. V. *et al.* α -Synuclein Overexpression Increases Cytosolic Catecholamine Concentration. *The Journal of Neuroscience* 26, 9304–9311 (2006).
194. Monzani, E. *et al.* Dopamine, Oxidative Stress and Protein–Quinone Modifications in Parkinson's and Other Neurodegenerative Diseases. *Angewandte Chemie International Edition* 58, 6512–6527 (2019).
195. Zolotukhin, S. *et al.* Recombinant adeno-associated virus purification using novel methods improves infectious titer and yield. *Gene Ther* 6, 973–985 (1999).

196. Piedra, J. *et al.* Development of a Rapid, Robust, and Universal PicoGreen-Based Method to Titer Adeno-Associated Vectors. *Hum Gene Ther Methods* 26, 35–42 (2015).
197. Van der Perren, A. *et al.* The structural differences between patient-derived α -synuclein strains dictate characteristics of Parkinson's disease, multiple system atrophy and dementia with Lewy bodies. *Acta Neuropathol* 139, 977–1000 (2020).
198. Paxinos, G. & Watson, C. *The Rat Brain In Stereotaxic Coordinates*. (Academic Press, United States of America, 1982).
199. Paxinos, G. & Franklin, K. B. J. *The Mouse Brain in Stereotaxic Coordinates*. (Academic Press, United States of America, 2004).
200. Gonzalez-Sepulveda, M. *et al.* Validation of a Reversed Phase UPLC-MS/MS Method to Determine Dopamine Metabolites and Oxidation Intermediates in Neuronal Differentiated SH-SY5Y Cells and Brain Tissue. *ACS Chem Neurosci* 11, 2679–2687 (2020).
201. Goldstein, D. S. *et al.* Determinants of buildup of the toxic dopamine metabolite <sc>DOPAL</sc> in Parkinson's disease. *J Neurochem* 126, 591–603 (2013).
202. Yan, C., Jiang, J., Yang, Y., Geng, X. & Dong, W. The function of VAMP2 in mediating membrane fusion: An overview. *Front Mol Neurosci* 15, (2022).
203. Takamori, S. *et al.* Molecular Anatomy of a Trafficking Organelle. *Cell* 127, 831–846 (2006).
204. Burré, J., Sharma, M. & Südhof, T. C. Systematic Mutagenesis of α -Synuclein Reveals Distinct Sequence Requirements for Physiological and Pathological Activities. *The Journal of Neuroscience* 32, 15227–15242 (2012).
205. Lou, X., Kim, J., Hawk, B. J. & Shin, Y.-K. α -Synuclein may cross-bridge v-SNARE and acidic phospholipids to facilitate SNARE-dependent vesicle docking. *Biochemical Journal* 474, 2039–2049 (2017).
206. Agarwal, A. *et al.* VAMP2 regulates phase separation of α -synuclein. *Nat Cell Biol* 26, 1296–1308 (2024).
207. Stefanovic, A. N. D., Stöckl, M. T., Claessens, M. M. A. E. & Subramaniam, V. α -Synuclein oligomers distinctively permeabilize complex model membranes. *FEBS J* 281, 2838–2850 (2014).
208. Musteikytė, G. *et al.* Interactions of α -synuclein oligomers with lipid membranes. *Biochimica et Biophysica Acta (BBA) - Biomembranes* 1863, 183536 (2021).
209. Matsuo, Y. & Kamitani, T. Parkinson's Disease-Related Protein, α -Synuclein, in Malignant Melanoma. *PLoS One* 5, e10481 (2010).
210. Huang, P., Yang, X.-D., Chen, S.-D. & Xiao, Q. The association between Parkinson's disease and melanoma: a systematic review and meta-analysis. *Transl Neurodegener* 4, 21 (2015).
211. Bose, A., Petsko, G. A. & Eliezer, D. Parkinson's Disease and Melanoma: Co-Occurrence and Mechanisms. *J Parkinsons Dis* 8, 385–398 (2018).
212. Davidi, D. *et al.* α -Synuclein Translocates to the Nucleus to Activate Retinoic-Acid-Dependent Gene Transcription. *iScience* 23, 100910 (2020).
213. Masuda-Suzukake, M. *et al.* Prion-like spreading of pathological α -synuclein in brain. *Brain* 136, 1128–1138 (2013).
214. Rey, N. L. *et al.* Widespread transneuronal propagation of α -synucleinopathy triggered in olfactory bulb mimics prodromal Parkinson's disease. *Journal of Experimental Medicine* 213, 1759–1778 (2016).

215. Karampetsou, M. *et al.* Phosphorylated exogenous alpha-synuclein fibrils exacerbate pathology and induce neuronal dysfunction in mice. *Sci Rep* 7, 16533 (2017).
216. Okuzumi, A. *et al.* Rapid dissemination of alpha-synuclein seeds through neural circuits in an in-vivo prion-like seeding experiment. *Acta Neuropathol Commun* 6, 96 (2018).
217. Henderson, M. X. *et al.* Spread of α -synuclein pathology through the brain connectome is modulated by selective vulnerability and predicted by network analysis. *Nat Neurosci* 22, 1248–1257 (2019).
218. Patterson, J. R. *et al.* Time course and magnitude of alpha-synuclein inclusion formation and nigrostriatal degeneration in the rat model of synucleinopathy triggered by intrastriatal α -synuclein preformed fibrils. *Neurobiol Dis* 130, 104525 (2019).
219. Thomsen, M. B. *et al.* PET imaging reveals early and progressive dopaminergic deficits after intrastriatal injection of preformed alpha-synuclein fibrils in rats. *Neurobiol Dis* 149, 105229 (2021).
220. Kravitz, A. V. & Kreitzer, A. C. Striatal Mechanisms Underlying Movement, Reinforcement, and Punishment. *Physiology* 27, 167–177 (2012).
221. Groenewegen, H. J. The Basal Ganglia and Motor Control. *Neural Plast* 10, 107–120 (2003).
222. Uemura, N. *et al.* α -Synuclein aggregates amplified from patient-derived Lewy bodies recapitulate Lewy body diseases in mice. *Nat Commun* 14, 6892 (2023).
223. Paumier, K. L. *et al.* Intrastriatal injection of pre-formed mouse α -synuclein fibrils into rats triggers α -synuclein pathology and bilateral nigrostriatal degeneration. *Neurobiol Dis* 82, 185–199 (2015).
224. Luk, K. C. *et al.* Pathological α -Synuclein Transmission Initiates Parkinson-like Neurodegeneration in Nontransgenic Mice. *Science* (1979) 338, 949–953 (2012).
225. Miquel-Rio, L. *et al.* Human α -synuclein overexpression in mouse serotonin neurons triggers a depressive-like phenotype. Rescue by oligonucleotide therapy. *Transl Psychiatry* 12, 79 (2022).
226. Surmeier, D. J., Obeso, J. A. & Halliday, G. M. Selective neuronal vulnerability in Parkinson disease. *Nat Rev Neurosci* 18, 101–113 (2017).
227. Lang, A. E. & Espay, A. J. Disease Modification in Parkinson's Disease: Current Approaches, Challenges, and Future Considerations. *Movement Disorders* 33, 660–677 (2018).
228. Paxinou, E. *et al.* Induction of α -Synuclein Aggregation by Intracellular Nitritative Insult. *The Journal of Neuroscience* 21, 8053–8061 (2001).
229. Krishnan, S. *et al.* Oxidative Dimer Formation Is the Critical Rate-Limiting Step for Parkinson's Disease α -Synuclein Fibrillogenesis. *Biochemistry* 42, 829–837 (2003).
230. Leong, S. L. *et al.* Formation of dopamine-mediated α -synuclein-soluble oligomers requires methionine oxidation. *Free Radic Biol Med* 46, 1328–1337 (2009).
231. Alvarez-Castelao, B., Goethals, M., Vandekerckhove, J. & Castaño, J. G. Mechanism of cleavage of alpha-synuclein by the 20S proteasome and modulation of its degradation by the RedOx state of the N-terminal methionines. *Biochimica et Biophysica Acta (BBA) - Molecular Cell Research* 1843, 352–365 (2014).
232. Lee, H.-J. *et al.* Dopamine promotes formation and secretion of non-fibrillar alpha-synuclein oligomers. *Exp Mol Med* 43, 216 (2011).
233. Burke, W. J. *et al.* Aggregation of α -synuclein by DOPAL, the monoamine oxidase metabolite of dopamine. *Acta Neuropathol* 115, 193–203 (2008).

234. Plotegher, N. *et al.* DOPAL derived alpha-synuclein oligomers impair synaptic vesicles physiological function. *Sci Rep* 7, 40699 (2017).
235. Tessari, I. *et al.* The Reaction of α -Synuclein with Tyrosinase. *Journal of Biological Chemistry* 283, 16808–16817 (2008).
236. Riessland, M. *et al.* Loss of SATB1 Induces p21-Dependent Cellular Senescence in Post-mitotic Dopaminergic Neurons. *Cell Stem Cell* 25, 514–530.e8 (2019).
237. Du, T. *et al.* Nuclear alpha-synuclein accelerates cell senescence and neurodegeneration. *Immunity & Ageing* 21, 47 (2024).
238. Meiser, J., Weindl, D. & Hiller, K. Complexity of dopamine metabolism. *Cell Communication and Signaling* 11, 34 (2013).
239. German, C. L. *et al.* Regulation of the Dopamine and Vesicular Monoamine Transporters: Pharmacological Targets and Implications for Disease. *Pharmacol Rev* 67, 1005–1024 (2015).
240. Burbulla, L. F. *et al.* Dopamine oxidation mediates mitochondrial and lysosomal dysfunction in Parkinson's disease. *Science* (1979) 357, 1255–1261 (2017).
241. Murer, M. G. *et al.* Chronic levodopa is not toxic for remaining dopamine neurons, but instead promotes their recovery, in rats with moderate nigrostriatal lesions. *Ann Neurol* 43, 561–575 (1998).
242. Mor, D. E. *et al.* Dopamine induces soluble α -synuclein oligomers and nigrostriatal degeneration. *Nat Neurosci* 20, 1560–1568 (2017).
243. Lee, H.-J. *et al.* Dopamine promotes formation and secretion of non-fibrillar alpha-synuclein oligomers. *Exp Mol Med* 43, 216 (2011).
244. Moussa, C. E.-H., Mahmoodian, F., Tomita, Y. & Sidhu, A. Dopamine differentially induces aggregation of A53T mutant and wild type α -synuclein: Insights into the protein chemistry of Parkinson's disease. *Biochem Biophys Res Commun* 365, 833–839 (2008).
245. Jethva, P. N., Kardani, J. R. & Roy, I. Modulation of α -synuclein aggregation by dopamine in the presence of MPTP and its metabolite. *FEBS J* 278, 1688–1698 (2011).
246. Outeiro, T. F. *et al.* Dopamine-Induced Conformational Changes in Alpha-Synuclein. *PLoS One* 4, e6906 (2009).
247. Masato, A. *et al.* DOPAL initiates α Synuclein-dependent impaired proteostasis and degeneration of neuronal projections in Parkinson's disease. *NPJ Parkinsons Dis* 9, 42 (2023).
248. Palazzi, L. *et al.* Structural Features and Toxicity of α -Synuclein Oligomers Grown in the Presence of DOPAC. *Int J Mol Sci* 22, 6008 (2021).
249. Bisaglia, M. *et al.* Dopamine quinones interact with α -synuclein to form unstructured adducts. *Biochem Biophys Res Commun* 394, 424–428 (2010).
250. Volles, M. J. & Lansbury, P. T. Vesicle Permeabilization by Protofibrillar α -Synuclein Is Sensitive to Parkinson's Disease-Linked Mutations and Occurs by a Pore-like Mechanism. *Biochemistry* 41, 4595–4602 (2002).
251. Miranda, M., Botti, D., Bonfigli, A., Ventura, T. & Arcadi, A. Tyrosinase-like activity in normal human substantia nigra. *General Pharmacology: The Vascular System* 15, 541–544 (1984).
252. Greggio, E. *et al.* Tyrosinase exacerbates dopamine toxicity but is not genetically associated with Parkinson's disease. *J Neurochem* 93, 246–256 (2005).

253. Xu, Y. *et al.* Tyrosine mRNA is expressed in human substantia nigra. *Molecular Brain Research* 45, 159–162 (1997).
254. Grønskov, K., Ek, J. & Brøndum-Nielsen, K. Oculocutaneous albinism. *Orphanet J Rare Dis* 2, 43 (2007).
255. Foley, J. M. & Banter, D. On the Nature of Pigment Granules in the Cells of the Locus Coeruleus and Substantia Nigra. *J Neuropathol Exp Neurol* 17, 586–598 (1958).
256. Gao, X., Simon, K. C., Han, J., Schwarzschild, M. A. & Ascherio, A. Genetic determinants of hair color and parkinson's disease risk. *Ann Neurol* 65, 76–82 (2009).
257. Gao, X., Simon, K. C., Han, J., Schwarzschild, M. A. & Ascherio, A. Family history of melanoma and Parkinson disease risk. *Neurology* 73, 1286–1291 (2009).
258. Olsen, J. H. *et al.* Atypical cancer pattern in patients with Parkinson's disease. *Br J Cancer* 92, 201–205 (2005).
259. Lubbe, S. J. *et al.* Rare variants analysis of cutaneous malignant melanoma genes in Parkinson's disease. *Neurobiol Aging* 48, 222.e1–222.e7 (2016).
260. Bertoni, J. M. Increased Melanoma Risk in Parkinson Disease. *Arch Neurol* 67, 347 (2010).
261. Iozumi, K., Hoganson, G. E., Pennella, R., Everett, M. A. & Fuller, B. B. Role of Tyrosinase as the Determinant of Pigmentation in Cultured Human Melanocytes. *Journal of Investigative Dermatology* 100, 806–811 (1993).
262. Jin, W., Stehbens, S. J., Barnard, R. T., Blaskovich, M. A. T. & Ziora, Z. M. Dysregulation of tyrosinase activity: a potential link between skin disorders and neurodegeneration. *Journal of Pharmacy and Pharmacology* 76, 13–22 (2024).
263. Aris, M. *et al.* MART-1- and gp100-Expressing and -Non-Expressing Melanoma Cells Are Equally Proliferative in Tumors and Clonogenic In Vitro. *Journal of Investigative Dermatology* 132, 365–374 (2012).
264. Hofbauer, G. F. L., Kamarashev, J., Geertsen, R., Böni, R. & Dummer, R. Tyrosinase immunoreactivity in formalin-fixed, paraffin-embedded primary and metastatic melanoma: frequency and distribution. *J Cutan Pathol* 25, 204–209 (1998).
265. Boyle, J. L., Haupt, H. M., Stern, J. B. & Mulhaupt, H. A. B. Tyrosinase Expression in Malignant Melanoma, Desmoplastic Melanoma, and Peripheral Nerve Tumors. *Arch Pathol Lab Med* 126, 816–822 (2002).
266. Plaza, J. A., Suster, D. & Perez-Montiel, D. Expression of Immunohistochemical Markers in Primary and Metastatic Malignant Melanoma: A Comparative Study in 70 Patients Using a Tissue Microarray Technique. *Applied Immunohistochemistry & Molecular Morphology* 15, 421–425 (2007).
267. Al-Nusaif, M., Yang, Y., Li, S., Cheng, C. & Le, W. The role of NURR1 in metabolic abnormalities of Parkinson's disease. *Mol Neurodegener* 17, 46 (2022).
268. Decressac, M., Volakakis, N., Björklund, A. & Perlmann, T. NURR1 in Parkinson disease—from pathogenesis to therapeutic potential. *Nat Rev Neurol* 9, 629–636 (2013).
269. Chu, Y. *et al.* Nurr1 in Parkinson's disease and related disorders. *J Comp Neurol* 494, 495–514 (2006).
270. Decressac, M. *et al.* α -Synuclein-Induced Down-Regulation of Nurr1 Disrupts GDNF Signaling in Nigral Dopamine Neurons. *Sci Transl Med* 4, (2012).

271. O'Kane, M. *et al.* Increased Expression of the Orphan Nuclear Receptor NURR1 in Psoriasis and Modulation following TNF- α Inhibition. *Journal of Investigative Dermatology* 128, 300–310 (2008).
272. Watanuki, Y. *et al.* Involvement of Nurr-1/Nur77 in corticotropin-releasing factor/urocortin1-induced tyrosinase-related protein 1 gene transcription in human melanoma HMV-II cells. *Mol Cell Endocrinol* 370, 42–51 (2013).
273. Guttuso, T. High lithium levels in tobacco may account for reduced incidences of both Parkinson's disease and melanoma in smokers through enhanced β -catenin-mediated activity. *Med Hypotheses* 131, 109302 (2019).
274. Holec, S. A. M. & Woerman, A. L. Evidence of distinct α -synuclein strains underlying disease heterogeneity. *Acta Neuropathol* 142, 73–86 (2021).
275. Woerman, A. L. & Luk, K. C. Are Preformed Fibrils a Model of Parkinson's Disease? *J Parkinsons Dis* 14, 1095–1103 (2024).
276. Luk, K. C. *et al.* Exogenous α -synuclein fibrils seed the formation of Lewy body-like intracellular inclusions in cultured cells. *Proceedings of the National Academy of Sciences* 106, 20051–20056 (2009).
277. Osterberg, V. R. *et al.* Progressive Aggregation of Alpha-Synuclein and Selective Degeneration of Lewy Inclusion-Bearing Neurons in a Mouse Model of Parkinsonism. *Cell Rep* 10, 1252–1260 (2015).
278. Gordon, R. *et al.* Inflammasome inhibition prevents α -synuclein pathology and dopaminergic neurodegeneration in mice. *Sci Transl Med* 10, (2018).
279. Borghammer, P. & Van Den Berge, N. Brain-First versus Gut-First Parkinson's Disease: A Hypothesis. *J Parkinsons Dis* 9, S281–S295 (2019).
280. Stokholm, M. G., Danielsen, E. H., Hamilton-Dutoit, S. J. & Borghammer, P. Pathological α -synuclein in gastrointestinal tissues from prodromal <scp>P</scp> arkinson disease patients. *Ann Neurol* 79, 940–949 (2016).
281. Shannon, K. M., Keshavarzian, A., Dodiya, H. B., Jakate, S. & Kordower, J. H. Is alpha-synuclein in the colon a biomarker for premotor Parkinson's Disease? Evidence from 3 cases. *Movement Disorders* 27, 716–719 (2012).
282. Hilton, D. *et al.* Accumulation of α -synuclein in the bowel of patients in the pre-clinical phase of Parkinson's disease. *Acta Neuropathol* 127, 235–241 (2014).
283. Horsager, J. *et al.* Brain-first versus body-first Parkinson's disease: a multimodal imaging case-control study. *Brain* 143, 3077–3088 (2020).
284. Wang, X.-J. *et al.* Autonomic ganglionic injection of α -synuclein fibrils as a model of pure autonomic failure α -synucleinopathy. *Nat Commun* 11, 934 (2020).
285. Guo, Q. *et al.* α -Synuclein decoy peptide protects mice against α -synuclein-induced memory loss. *CNS Neurosci Ther* 29, 1547–1560 (2023).
286. Maren, S. & Quirk, G. J. Neuronal signalling of fear memory. *Nat Rev Neurosci* 5, 844–852 (2004).
287. Song, J. & Kim, Y. Animal models for the study of depressive disorder. *CNS Neurosci Ther* 27, 633–642 (2021).